ISNTT2017

International School and Symposium on Nanoscale Transport and phoTonics

Program & Abstract

November 13-17, 2017

NTT Atsugi R&D Center

International School and Symposium on Nanoscale Transport and phoTonics

* ISNTT2017 *

November 13 (Mon.) – 17 (Fri.), 2017

NTT Basic Research Laboratories (Atsugi R&D Center, JAPAN)

- **Organizing Committee**

  Tetsuomi SOGAWA (NTT BRL director)
  Akira FUJIWARA (NTT) **Co-chair**
  Hiroshi YAMAGUCHI (NTT)
  Koji MURAKI (NTT)
  Hideki GOTOH (NTT)

- **Advisory Committee**

  Per DELSING (Chalmers Univ. of Tech.)
  Yoshiro HIRAYAMA (Tohoku Univ.)
  Johan E. MOOIJ (TU Delft)
  Junsaku NITTA (Tohoku Univ.)
  Koichi SEMBA (NICT)
  Seigo TARUCHA (Univ. of Tokyo)
  Yasuhiro TOKURA (Univ. of Tsukuba)

- **Program Committee**

  Shiro SAITO (NTT) **Chair**
  Akira FUJIWARA (NTT)
  Hiroshi YAMAGUCHI (NTT)
  Koji MURAKI (NTT)
  Takehiko TAWARA (NTT)
  Kenichi SASAKI (NTT)
  William John MUNRO (NTT) **BRL School**

- **Steering Committee**

  Kiyoshi KANISAWA (NTT) **Chair**
  Haruki SANADA (NTT) **Vice-chair**
  Norio KUMADA (NTT) **Treasurer**
  Hajime OKAMOTO (NTT) **BRL School**

* Floor Map of Atsugi R&D Center *

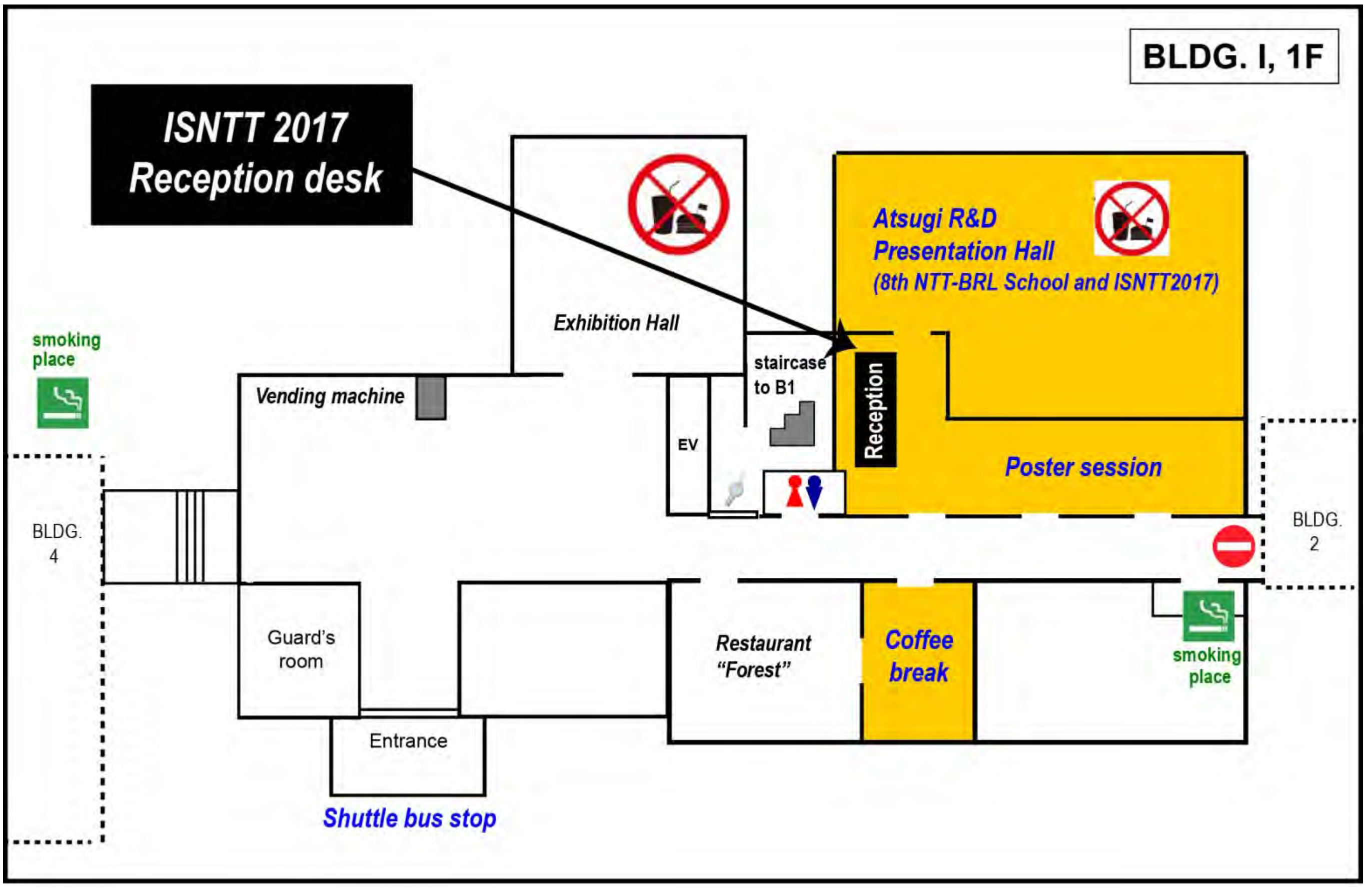

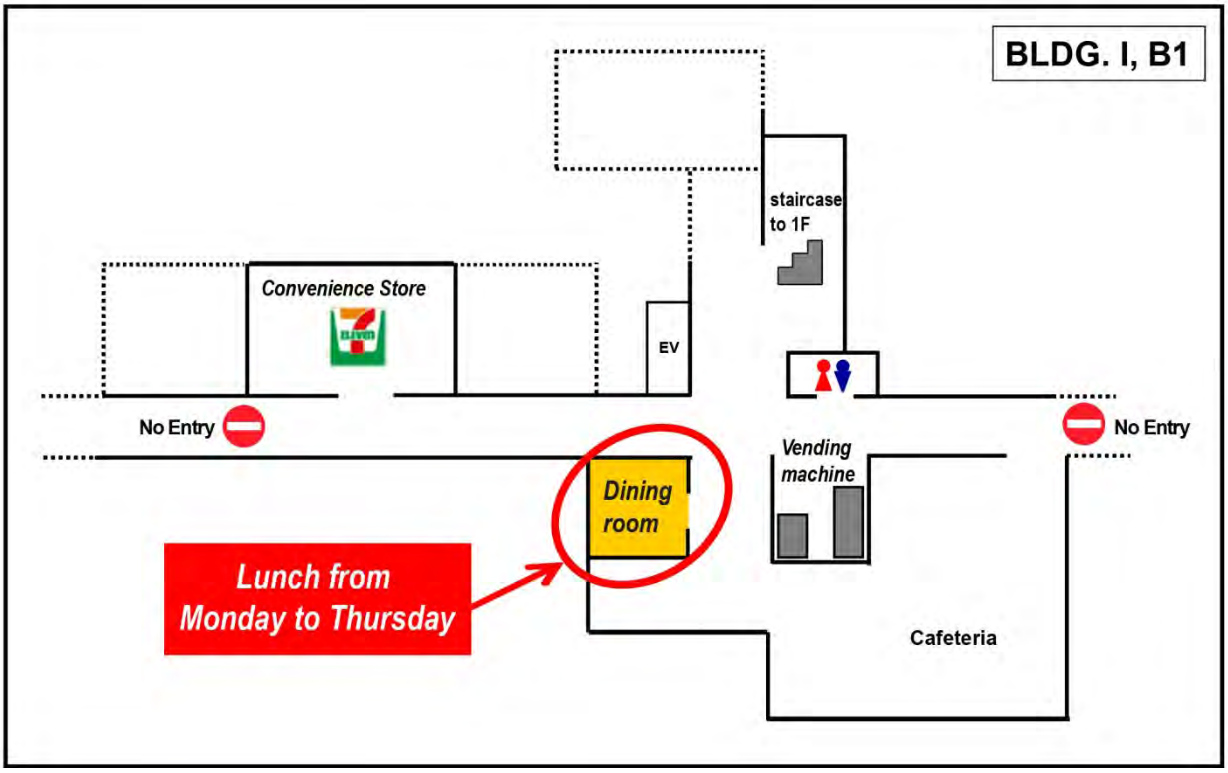

* Timetable of the shuttle bus *

Morning
Rembrandt Hotel Atsugi ⇒NTT Atsugi R&D Center

Nov. 13 (Mon)	Nov. 14 (Tue)	Nov. 15 (Wed)	Nov. 16 (Thu)	Nov. 17 (Fri)
-	8:30	8:00	8:00	8:00
9:10	8:40	8:20	8:20	8:20
10:00	9:40	9:20	9:20	9:20
13:00	9:50	9:40	9:40	9:40

Evening
NTT Atsugi R&D Center ⇒ Hon-Atsugi Sta. ⇒ Rembrandt Hotel Atsugi

Nov. 13 (Mon)	Nov. 14 (Tue)	Nov. 15 (Wed)	Nov. 16 (Thu)	Nov. 17 (Fri)
17:30	18:00	18:00	18:30	13:10
17:45	19:00	19:00	18:45	13:20
19:45	19:50	19:50		14:30
20:15	20:20	20:20		

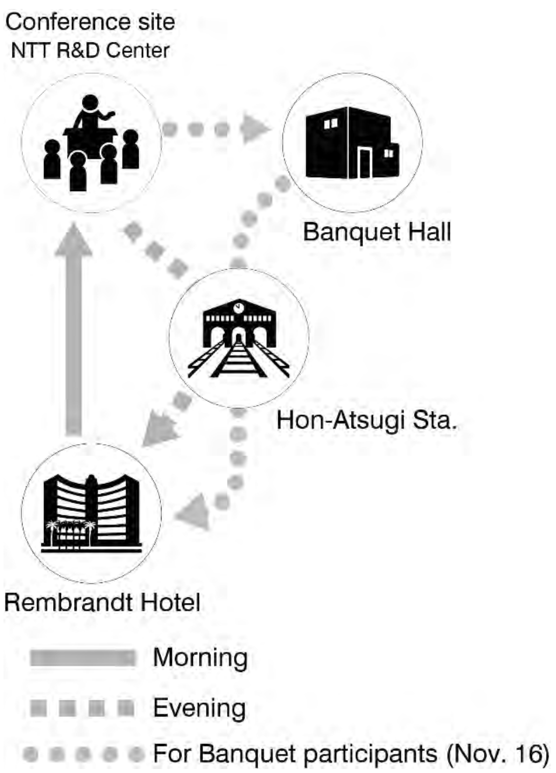

For Banquet participants

Nov. 16 (Thu)	
NTT ⇒ Banquet Hall	Banquet Hall ⇒Hon-Atsugi Sta.⇒Rembrandt Hotel Atsugi
18:05	
18:10	
18:25	
	20:50
	21:00

* Public bus from Hon-Atsugi station *

Local Bus (Kanachu Bus): 厚 44
Take No.44 bus from the bus terminal Pole 9 and
get off at “Tsushin kenkyujo mae” (通信研究所前)
Fare: 320Yen

Atsugi Bus Terminal ⇒ NTT Atsugi R&D Center		NTT Atsugi R&D Center ⇒ Atsugi Bus Terminal	
8	12 37	17	24 39 59
9	05 37	18	19 39 59
10	17 52	19	19 49
11	20 50	20	19 49
12	47	21	14

* Public bus from Aiko-Ishida station *

Local Bus (Kanachu Bus): 愛 17, 18, 19, 21
Take No. 17, 18, 19, or 21the bus from Pole 4 and
get off at “Tsushin kenkyujo mae” (通信研究所前)
Fare: 260Yen

Aiko-ishida Sta. ⇒ NTT Atsugi R&D Center		NTT Atsugi R&D Center ⇒ Aiko-ishida Sta.	
8	02 05 08 11 14 17 20 23 27 31 35 39 43 47 51 57	17	01 10 21 30 40 41 50 51
9	03 09 19 29 39 49 59	18	01 10 11 15 21 30 31 41 51
10	05 15 20 28 58	19	01 11 21 31 41 51
11	10 28 35 50 58	20	01 11 23 35 46
12	10 30 50	21	06 26 46

* Map of Hon-Atsugi Area *

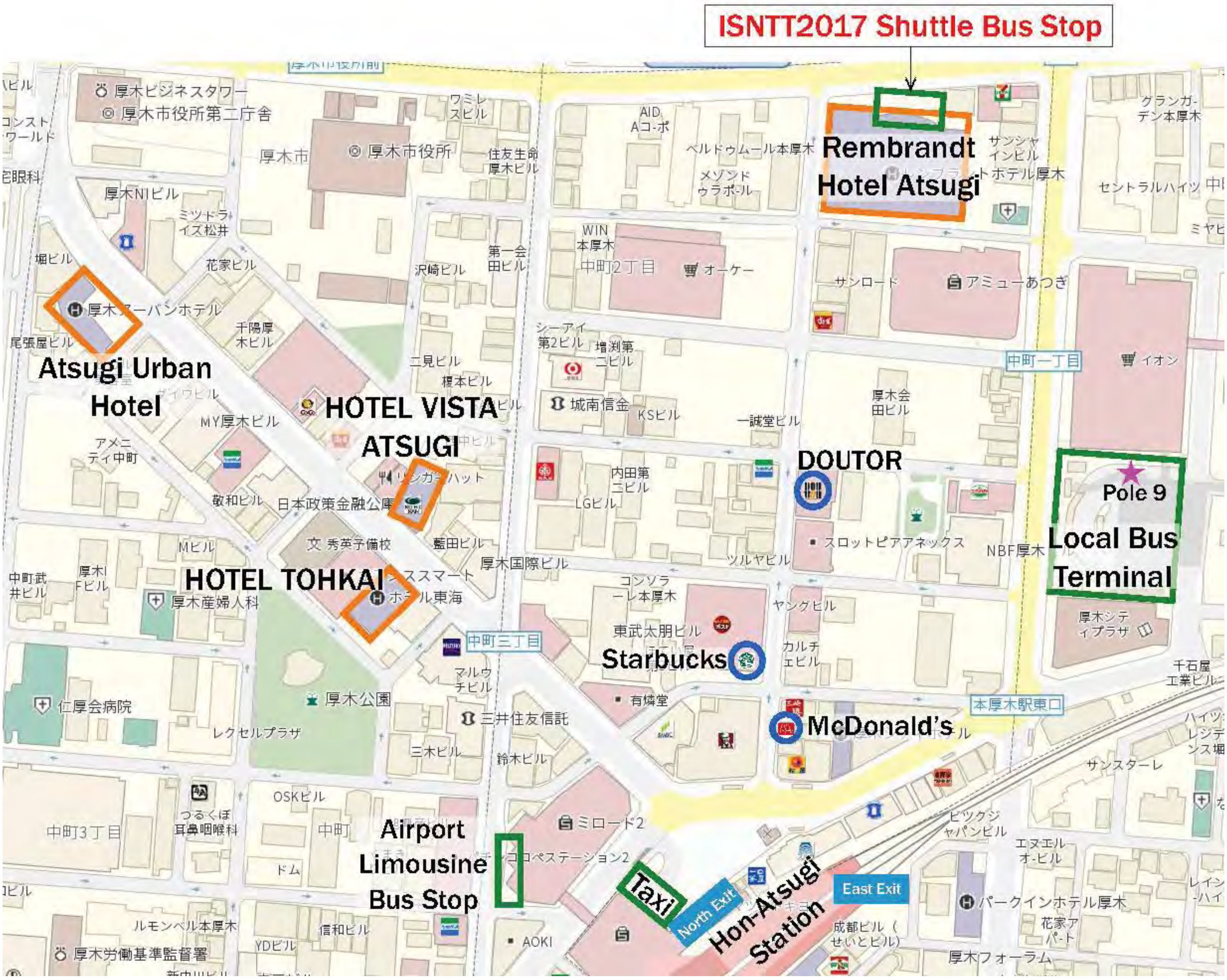

- **Free Wi-Fi spot in Hon-Atsugi area (please buy one drink at least)>**
  "**McDonald's**", "**Starbucks**", and "**DOUTOR**" coffee shops, symbols marked with circle, are the free Wi-Fi spot in Hon-Atsugi area, but please buy at least one drink.
- **Free Shuttle bus will stop at Rembrandt Hotel Atsugi>**
  It will be about 5-10 minutes from each hotels and the station by walking.

  Rembrandt Hotel Atsugi
  ADDRESS: 2-13-1, Naka-cho, Atsugi-shi, Kanagawa, 243-0018
  Intl TEL: +81-46-221-0001
- **How to get to NTT by using the local buses>**
  The Local Bus Terminal for the public buses is located at the east side of Hon-Atsugi station. Be sure that it will take about 30 minutes from Hon-Atsugi station to NTT. Look for "**Pole 9**" at the bus terminal, take "Atsu 44 (**厚 44**)" bus bound for "Morinosato (**森の里**)", and get off at "Tsushin-Kenkyujo-mae (**通信研究所前**)".

November 13th (Monday)

Registration
(Open from 9:30 AM)

8th NTT-BRL School
(open for all ISNTT participants)

Opening Remarks
(10:00 - 10:30)

Short Break
(10:30 - 10:45)

Lecture 1

10:45 **The ABC's of Quantum Computation**
Prof. Kae Nemoto
National Institute of Informatics (NII)

NTT-BRL School Photo
(12:15 - 12:30)

Lunch Time
(12:30 - 13:45)

Lecture 2

13:45 **Hybrid Quantum Systems Using Collective Excitations in Solid**
Prof. Yasunobu Nakamura
Research Center for Advanced Science and Technology (RCAST), The University of Tokyo

Coffee Break
(15:15 - 15:45)

Lecture 3

15:45 **Coherent Ising Machine for Solving Complex Optimization Problems**
Dr. Hiroki Takesue
NTT Basic Research Laboratories

Welcome Reception
(17:30 - 19:30)

November 14th (Tuesday)

Registration
(Open from 9:00 AM)

ISNTT2017 Symposium

Opening Remarks
(9:40 - 10:00)

Session 1		
Tu-01	10:00	Serge Haroche (Keynote)
Coffee Break (11:00 - 11:30)		
Session 2: Optomechanics		
Tu-02	11:30	Alejandro Fainstein (Invited)
Tu-03	12:00	Amirhossein Ghadimi
Tu-04	12:20	Anton Frisk Kockum
ISNTT2017 Symposium Photo (12:40 - 12:50)		
Lunch Time (12:50 - 14:00)		
Session 3: Quantum State Manipulation in Superconducting Systems		
Tu-05	14:00	William D. Oliver (Invited)
Tu-06	14:30	Maika Takita (Invited)
Tu-07	15:00	Kazuki Koshino
Tu-08	15:20	Yasunobu Nakamura
Coffee Break (15:40 - 16:10)		
Session 4: Unconventional Superconducting Junctions		
Tu-09	16:10	Fabrizio Nichele (Invited)
Tu-10	16:40	Ana Monteiro
Tu-11	17:00	Taketomo Nakamura
Tu-12	17:20	Rais Shaikhaidarov
Poster Session I (17:40 - 19:30)		

November 15th (Wednesday)

Session 5: Strongly Coupled Systems		
We-01	9:00	Junichiro Kono (Invited)
We-02	9:30	Mauro Cirio
We-03	9:50	Fumiki Yoshihara
We-04	10:10	Kosuke Kakuyanagi
Coffee Break (10:30 - 11:00)		
Session 6: Semiconductor-based Quantum Devices and Technologies		
We-05	11:00	Xiao Mi (Invited)
We-06	11:30	Takashi Kobayashi
We-07	11:50	Sergey Shevchenko
We-08	12:10	Michael Zudov
Lunch Time (12:30 - 14:00)		
Session 7: Nanophotonics and Nano Structures		
We-09	14:00	Benjamin Sussman (Invited)
We-10	14:30	Feng Tian
We-11	14:50	Yin Yin
We-12	15:10	Xiao Hu (Invited)
Coffee Break (15:40 - 16:10)		
We-13	16:10	Julian Klein
We-14	16:30	Michael Mounaix
We-15	16:50	Nicolas Clement
We-16	17:10	Katsuhiko Ariga (Invited)
Poster Session II (17:40 - 19:30)		

November 16th (Thursday)

Session 8: Single-electron Devices and Physics		
Th-01	9:00	Jukka P. Pekola (Invited)
Th-02	9:30	Rolf J. Haug (Invited)
Th-03	10:00	Kensaku Chida
Th-04	10:20	Rubén Seoane Souto
Coffee Break (10:40 - 11:10)		
Session 9: Spin-orbit Interactions and Spin Transport		
Th-05	11:10	Yoji Kunihashi
Th-06	11:30	Andrea Hofmann
Th-07	11:50	Takase Shimizu
Th-08	12:10	Paul Seifert
Th-09	12:30	Yukio Takahashi
Lunch Time (12:50 - 14:00)		
Session 10: Nanomechanics and Phononics		
Th-10	14:00	Adrian Bachtold (Invited)
Th-11	14:30	Joseph Losby (Invited)
Th-12	15:00	Xueyong Yuan
Th-13	15:20	Ryuichi Ohta
Coffee Break (15:40 - 16:10)		
Th-14	16:10	Donghun Lee
Th-15	16:30	Laszlo Daniel Toth
Th-16	16:50	Toshimasa Fujisawa (Invited)
Th-17	17:20	Hubert J. Krenner (Invited)
Bus Transfer (17:50 - 18:40)		
BANQUET (18:40 - 20:40)		

November 17th (Friday)

Session 11: Topological Phases and Phase Transitions in 2D Systems		
Fr-01	9:00	Tauno Palomaki (Invited)
Fr-02	9:30	Hiroshi Irie
Fr-03	9:50	John Nicholas Moore
Coffee Break (10:10 - 10:40)		
Session 12: Superconducting Hybrid Systems		
Fr-04	10:40	Atsushi Noguchi (Invited)
Fr-05	11:10	Maria Ekström
Fr-06	11:30	Sebastian de Graaf
Fr-07	11:50	Rangga Budoyo
Fr-08	12:10	Xiaobo Zhu (Invited)
CLOSING (12:40 - 12:50)		

* Instruction of presentation and poster *

Oral presentation instructions

The time allotted to each oral presentation is:
- Keynote papers 60 min including 5 min discussion
- Invited papers 30 min including 5 min discussion
- Contributed papers 20 min including 5 min discussion

Oral presentations will be given using an LCD projector. All speakers are asked to bring BOTH their own computers AND presentation files copied in USB memories, just in case of trouble. The display settings available for our LCD projector are shown in the following table.

Resolution	Refresh rate
1920 x 1080	60Hz
1280 x 800	60Hz
1280 x 768	60Hz
1280 x 720	60Hz
1024 x 768	70Hz
	75Hz
	85Hz
	100Hz
800 x 600	60Hz
	75Hz
	85Hz
	100Hz
	20Hz

We have prepared VGA(DE-15/HD-15) and HDMI(DVI) cables for the projector. Please be sure to bring conformable adaptor if you use Macintosh.

Poster presentation instructions

Boards, 90cm wide and 180cm high, will be available for poster presentation.

The title of the paper, the authors and their affiliations should be clearly displayed at the top of the board. Material for fixing the poster to the board (pins or magnets) will be provided. Please set up posters before the session begins and keep on display for full conference days.

Student Poster Award

ISNTT2017 will have a Student Poster Award!
The award will be given to a limited number of students who give outstanding presentations at the poster sessions held on Tuesday and Wednesday. The selection will be based on the technical content, appearance, graphic excellence, and presentation quality. The award winners will be presented during the Banquet on Thursday.

November 13th, Monday

8th NTT-BRL School

10:00 - 10:30	**Opening Remarks**
10:30 - 10:45	**Short Break**
10:45 - 12:15	**Lecture 1**

The ABC's of Quantum Computation

Prof. Kae Nemoto

National Institute of Informatics (NII)

12:15 - 12:30	**8th NTT-BRL School Photo**
12:30 - 13:45	**Lunch Time**
13:45 - 15:15	**Lecture 2**

Hybrid Quantum Systems Using Collective Excitations in Solid

Prof. Yasunobu Nakamura

Research Center for Advanced Science and Technology (RCAST),

The University of Tokyo

15:15 - 15:45	**Coffee Break**
15:45 - 17:15	**Lecture 3**

Coherent Ising Machine for Solving Complex Optimization Problems

Dr. Hiroki Takesue

NTT Basic Research Laboratories

17:30 - 19:30	**Welcome Reception**

November 14th, Tuesday

ISNTT2017 Symposium

9:40 - 10:00	**Opening Remarks**

Session 1

10:00 - 11:00
Tu-01 : **Quantum Metrology with Schrödinger Cats**
(Keynote) S. Haroche
Laboratoire Kastler Brossel, Collège de France

11:00 - 11:30	**Coffee Break**

Session 2: Optmechanics

11:30 - 12:00
Tu-02 : **Extremely High Frequency Cavity Optomechanics**
(Invited) A. Fainstein
Comisión Nacional de Energia Atómica (CNEA),
Consejo Nacional de Investigaciones Cientificas y Técnicas (CONICET)

12:00 - 12:20
Tu-03 : **Toward a Phononic Crystal Nano-string with a Quality Factor of One Billion**
A. Ghadimi, S. Fedorov, N. J. Engelsen, M. Breyhi, R. Schilling, H. Shutz, D. J. Wilson, and T. J. Kippenberg
Ecole Polytechnique Federale de Lausanne (EPFL)

12:20 - 12:40
Tu-04 : **The Fully Quantized Dynamical Casimir Effect – Vacuum Casimir-Rabi Oscillations in Optomechanical Systems**
V. Macrì, A. Ridolfo, O. Di Stefano, A. F. Kockum, F. Nori, and S. Savasta
RIKEN

12:40 - 12:50	**ISNTT2017 Symposium Photo**

12:50 - 14:00	**Lunch Time**

Session 3: Quantum State Manipulation in Superconducting Systems

14:00 - 14:30
Tu-05 : **Quantum Engineering of Superconducting Qubits**
(Invited) W. D. Oliver
Massachusetts Institute of Technology

14:30 - 15:00
Tu-06 : **Towards Fault-tolerant Quantum Computing Using Superconducting Qubits**
(Invited) M. Takita
IBM

15:00 - 15:20
Tu-07 : **Tunable Quantum Gate Between a Superconducting Atom and a Propagating Microwave Photon**
K. Koshino, K. Inomata, Z. R. Lin, Y. Tokunaga, T. Yamamoto, and Y. Nakamura
College of Liberal Arts and Sciences, Tokyo Medical and Dental University

15:20 - 15:40
Tu-08 : **Quantum Non-demolition Detection of an Itinerant Microwave Photon Using an Entangling Gate with a Superconducting Qubit**
S. Kono, Y. Tabuchi, A. Noguchi, R. Yamazaki, K. Koshino, and Y. Nakamura
Research Center for Advanced Science and Technology (RCAST),
The University of Tokyo

15:40 - 16:10	**Coffee Break**

Session 4: Unconventional Superconducting Junctions

16:10 - 16:40
Tu-09 : **Majorana Modes in InAs/Al Two-dimensional Heterostructures**
(Invited) F. Nichele
University of Copenhagen

16:40 - 17:00
Tu-10 : **Tunable Josephson Junctions and Superconducting Quantum Interference in an Interfacial Superconductor**
A. M. R. V. L. Monteiro, D. J. Groenendijk, N. Manca, E. Mulazimoglu, S. Goswami, R. Wölbing, D. Koelle, R. Kleiner, Y. Blanter, L. M. K. Vandersypen, and A. D. Caviglia
Kavli Institute of Nanoscience

17:00 -17:20
Tu-11 : **Finite Supercurrent in Nb/(In, Fe)As/Nb Junctions**
T. Nakamura, L. D. Anh, Y. Hashimoto, S. Ohya, M. Tanaka, and S. Katsumoto
The University of Tokyo

17:20 - 17:40
Tu-12 : **Charge Quantum Interference Device**
R. Shaikhaidarov, S. E. de Graaf, S. T. Scacel, T. Höenigl-Decrinis, V. A. Antonov, E. V. Il'ichev, and O. V. Astafiev
Royal Holloway University of London

17:40 - 19:30	Poster Session I

November 15th, Wednesday

Session 5: Strongly Coupled Systems

9:00 - 9:30
We-01 : **Polaritons Beyond The Rotating Wave Approximation**
(Invited) J. Kono
Rice University

9:30 - 9:50
We-02 : **Probing the Dressed Structure of the Light-matter Ground State in the Ultra-strong Coupling Regime**
M. Cirio, N. Lambert, S. De Liberato, K. Debnath, and F. Nori
Riken

9:50 - 10:10
We-03 : **Twists of Qubit Energies in Deep-strongly-coupled Qubit-oscillator Circuits**
F. Yoshihara, T. Fuse, Z. Ao, S. Ashhab, K. Kakuyanagi, S. Saito, T. Aoki, and K. Semba
National Institute of Information and Communications Technology

10:10 - 10:30
We-04 : **A Coupling Between a Lamped Element Resonator and 4300 Superconducting Flux Qubits Ensemble**
K. Kakuyanagi, Y. Matsuzaki, C. Déprez, H. Toida, K. Semba, H. Yamaguchi, W. J. Munro, and S. Saito
NTT Basic Research Laboratories

10:30 - 11:00	**Coffee Break**

Session 6: Semiconductor-based Quantum Devices and Technologies

11:00 - 11:30
We-05 : **Strong-Coupling Silicon Charge and Spin Qubits to Microwave Photons**
(Invited) X. Mi
Princeton University

11:30 - 11:50
We-06 : **Long Spin Coherence of Acceptor Atoms in Mechanically Strained Silicon**
T. Kobayashi, J. van der Heijden, J. Salfi, C. Chua, M. G. House, B. C. Johnson, J. C. McCallum, H. Riemann, N. Abrosimov, P. Becker, H.-J. Pohl, M. Y. Simmons, and S. Rogge
University of New South Wales, Tohoku University

11:50 - 12:10
We-07 : **Multi-level Landau-Zener-Stückelberg-Majorana Transitions in a Silicon-based Single-electron Interferometer**
S. N. Shevchenko, A. Chatterjee, S. Barraud, R. Otxoa, F. Nori, J. J. L. Morton, and M. F. Gonzalez-Zalba
B. Verkin Institute for Low Temperature Physics and Engineering

12:10 - 12:30
We-08 : **Quantum Hall Stripes in Tilted Magnetic Fields**
M. A. Zudov, Q. Shi, Q. Qian, G. C. Gardner, J. D. Watson, and M. J. Manfra
University of Minnesota

12:30 - 14:00	**Lunch Time**

Session 7: Nanophotonics and Nano Structures

14:00 - 14:30
We-09 : **Quantum Processing with Phonons**
(Invited) B. Sussman
National Research Council Canada

14:30 - 14:50
We-10 : **Spontaneous Emission Enhanced by Purcell Effect in a Set of Optomechanical Cavities**
F. Tian, H. Sumikura, E. Kuramochi, M. Takiguchi, M. Ono, H. Taniyama, A. Shinya, and M. Notomi
NTT Basic Research Laboratories

14:50 - 15:10
We-11 : **Optoplasmonic Rolled-up-microtube Cavities**
Y. Yin and O. G. Schmidt
Leibniz Institute for Solid State and Materials Research Dresden (IFW Dresden)

15:10 - 15:40
We-12 : **Towards Nano Topological Photonics**
(Invited) X. Hu
National Institute for Materials Science

15:40 - 16:10 **Coffee Break**

16:10 - 16:30
We-13 : **Electric-field Switchable Second-harmonic Generation in Bilayer MoS_2 by Inversion Symmetry Breaking**
J. Klein, J. Wierzbowski, A. Steinhoff, M. Florian, M. Rösner, F. Heimbach, K. Müller, F. Jahnke, T. O. Wehling, J. J. Finley, and M. Kaniber
Walter Schottky Institut und Physik Department

16:30 - 16:50
We-14 : **Spatio-temporal Coherent Control of Light Transport in Disordered Materials**
M. Mounaix, S. Gigan
Laboratoire Kastler Brossel, ENS, CNRS, UPMC

16:50 - 17:10
We-15 : **Estimation of π- π Electronic Couplings from Current Measurements**
J.Trasobares, J. Rech, T. Jonckheere, T. Martin, O. Aleveque, E. Levillain, V. Diez-Cabanes, Y. Olivier, J. Cornil, J. P. Nys, R. Sivakumarasamy, K. Smaali, P. Leclere, A. Fujiwara, D. Theron, D. Vuillaume, and N. Clement
NTT Basic Research Laboratories

17:10 - 17:40
We-16 : **Challenges for Nanocar and Molecular Machine by nm-size Tip Approach and cm-level Hand Motion**
(Invited) K. Ariga
National Institute for Materials Science

17:40 - 19:30 **Poster Session II**

November 16th, Thursday

Session 8: Single-electron Devices and Physics

9:00 - 9:30
Th-01 : **Stochastic Thermodynamics in Superconducting and Hybrid Circuits**
(Invited) J. P. Pekola
Aalto University School of Science

9:30 - 10:00
Th-02 : **Shot Noise and Feedback in Single-electron Tunneling through Quantum Dots**
(Invited) R. J. Haug
University of Hannover

10:00 - 10:20
Th-03 : **Power Generation with Maxwell's Demon in a Silicon Nanodevice**
K. Chida, K. Nishiguchi, and A. Fujiwara
NTT Basic Research Laboratories

10:20 - 10:40
Th-04 : **Quench Dynamics in Superconducting Nanojuncions: Metastability and Dynamical Phase Transitions**
R. Souto, A. Martín-Rodero, and A. L. Yeyati
Autonomous university of Madrid

10:40 - 11:10	**Coffee Break**

Session 9: Spin-orbit Interactions and Spin Transport

11:10 - 11:30
Th-05 : **Drift-induced Enhancement of Cubic Dresselhaus Spin-orbit Interaction in Two-dimensional Electron Gas**
Y. Kunihashi, H. Sanada, Y. Tanaka, H. Gotoh, K. Onomitsu, K. Nakagawara, M. Kohda, J. Nitta, and T. Sogawa
NTT Basic Research Laboratories

11:30 - 11:50
Th-06 : **Anisotropy and Suppression of Spin-orbit Interaction in GaAs Double Quantum Dots**
A. Hofmann, V. F. Maisi, T. Krähenmann, C. Reichl, W. Wegscheider, K. Ensslin, and T. Ihn
ETH Zürich

11:50 - 12:10
Th-07 : **Detecting Non-local Spin Signal through Electron Interaction**
T. Shimizu, Y. Hashimoto, S. Sugumaran, A.Endo, T. Nakamura, and S. Katsumoto
The University of Tokyo

12:10 - 12:30
Th-08 : **Spin Hall Photoconductance and Ultrafast Helicity-dependent Currents in Topological Insulators**
P. Seifert, C. Kastl, K. Vaklinova, S. Ganichev, K. Kern, M. Burghard, and A. W. Holleitner
Walter Schottky Institut , TU Munich

12:30 - 12:50
Th-09 : **Observation of Full Spin-Orbit Polarization in a Band-Inverted InAs/InGaSb Composite Quantum Well at Zero Magnetic Field**
Y. Takahashi, H. Irie, T. Akiho, K. Onomitsu, and K. Muraki
NTT Basic Research Laboratories

12:50 - 14:00 **Lunch Time**

Session 10: Nanomechanics and Phononics

14:00 - 14:30
Th-10 : **Electro-mechanical Resonators Based on Graphene**
(Invited) A. Bachtold
The Institute of Photonic Sciences

14:30 - 15:00
Th-11 : **Broadband Nanomechanical Torque Magnetometry**
(Invited) J. E. Losby
University of Alberta

15:00 - 15:20
Th-12 : **Reorientation of Quantization Axis for Quantum Dot through High Variable Uniaxial Stress**
X.Yuan, F. Weihausen-Brinkmann, J. Martín-Sánchez, G. Piredda, V. Krapek, Y. Huo, H. Huang, O. G. Schmidt, J. Edlinger, G. Bester, R. Trotta, and A. Rastelli
Johannes Kepler University Linz, Institute of Semiconductor and Solid State Physics

15:20 - 15:40
Th-13 : **Coherent Coupling of Dark and Bright Excitons in a Mechanical Resonator**
R. Ohta, H. Okamoto, T. Tawara, H. Gotoh, and H. Yamaguchi
NTT Basic Research Laboratories

15:40 - 16:10 **Coffee Break**

16:10 - 16:30
Th-14 : **Spins and Mechanics in Diamond Quantum Systems**
D. Lee, K. Lee, J. Cady, and A. Jayich
Korea University

16:30 - 16:50
Th-15 : **Dissipation as a Resource for Quantum-limited Amplification and Nonreciprocal Devices in Superconducting Circuit Optomechanics**
L. D. Toth, N. R. Bernier, A. Nunnenkamp, A. K. Feofanov, and T. J. Kippenberg
Ecole Polytechnique Federale de Lausanne (EPFL)

16:50 - 17:20
Th-16 : **Double Quantum Dot Coupled with a Phonon Resonator**
(Invited) T. Fujisawa
Tokyo Institute of Technology

17:20 - 17:50
Th-17 : **Acoustic Control of Light and Matter on a Chip**
(Invited) H. J. Krenner
University of Augsburg

17:50 - 18:40 **Bus Transfer**

18:40 - 20:40 **Banquet**

November 17th, Friday

Session 11: Topological Phases and Phase Transitions in 2D Systems

9:00 - 9:30
Fr-01 : **Edge Conduction in Monolayer WTe_2**
(Invited) T. Palomaki
University of Washington

9:30 - 9:50
Fr-02 : **Electric-field Driven Topological Phase Transition in $InAs/In_xGa_{1-x}Sb$ Composite Quantum Wells**
H. Irie, T. Akiho, K. Suzuki, F. Couëdo, K. Onomitsu, and K. Muraki
NTT Basic Research Laboratories

9:50 - 10:10
Fr-03 : **First-order Phase Transition of Quantum Hall Skyrmions Observed by Photoluminescence Microscopy**
J. N. Moore, J. Hayakawa, H. Iwata, T. Mano, T. Noda, and G. Yusa
Tohoku University

10:10 - 10:40	**Coffee Break**

Session 12: Superconducting Hybrid Systems

10:40 - 11:10
Fr-04 : **Qubit-assisted Transduction for a Detection of Surface Acoustic Waves Near the Quantum Limit**
(Invited) A. Noguchi
The University of Tokyo

11:10 - 11:30
Fr-05 : **Efficient Unidirectional Transduction Between Electrical Microwaves and Surface Acoustic Waves and Routing of Propagating Microwave Phonons at the Quantum Level**
M. K. Ekström, T. Aref, J. Runeson, J. Björck, I. Boström, H. Sanada, G. Andersson, B. Suri, and P. Delsing
Chalmers University of Technology

11:30 - 11:50
Fr-06 : **Reducing 1/f Noise in Quantum Devices by Surface Spin Desorption**
S. E. de Graaf, L. Faoro, J. Burnett, A. Adamyan, A. Y. Tzalenchuk, S. E. Kubatkin, T. Lindstrom, and A. V. Danilov
National Physical Laboratory

11:50 - 12:10
Fr-07 : **Effects of Phonon-Bottleneck in Spin Relaxation of Er:YSO**
R. P. Budoyo, K. Kakuyanagi, H. Toida, Y. Matsuzaki, I. Mahboob, W. J. Munro, H. Yamaguchi, and S. Saito
NTT Basic Research Laboratories

12:10 - 12:40
Fr-08 : **Progress on Superconducting Multi-qubits System**
(Invited) X. Zhu
University of Science and Technology of China

12:40 - 12:50	**Closing**

Poster Session I (November 14th, Tuesday)

PTu01 : **Energy Detuning Control of a Superconducting Flux Qubit Using Microwave Irradiation**
H. Toida, T. Ohrai, Y. Matsuzaki, K. Kakuyanagi, H. Yamaguchi, and S. Saito
NTT Basic Research Labolatories

PTu02 : **Superconducting Flux Qubits Embedded in a 3D Cavity**
S. Saito, I. Mahboob, H. Toida, Y. Matsuzaki, K. Kakuyanagi, W. J. Munro, Y. Nakamura, and H. Yamaguchi
NTT Basic Research Labolatories

PTu03 : **Excitons in Capacitively Coupled Chains of Small Josephson Junctions**
H. Shimada, K. Matsudo, C. Ishida, H. Murai, and Y. Mizugaki
The University of Electo-Communications

PTu04 : **A 3D JPA**
I. Mahboob, H. Toida, K. Kakuyanagi, Y. Nakamura, and S. Saito
NTT Basic Research Labolatories

PTu05 : **Quantum Dynamics of a Josephson Junction-Driven Cavity Mode System in the Presence of Voltage Bias Noise**
H. Wang, M. P. Blencowe, A. D. Armour, and A. J. Rimberg
Dartmouth College

PTu06 : **Realization of a Nanowire Superinductance**
D. Niepce, J. Burnett, and J. Bylander
Chalmers University of Technology

PTu07 : **Coherent Emission of a Continuously Driven Three-level Artificial Atom**
I. Antonov, R. Shaikhaidarov, T. Honigl-Decrinis, V. N. Antonov, and O.V. Astafiev
Royal Holloway, University of London

PTu08 : **Coupling a Superconducting Qubit to Light Using Hybrid Qubit-Quantum Dot Nanostructures**
V. E. Elfving, S. Das, and A. S. Sørensen
University of Copenhagen

PTu09 : **Giant Lamb Shift Observed in Deep-strongly-coupled Superconducting Qubit-oscillator Circuit**
Z. Ao, F. Yoshihara, T. Fuse, S. Ashhab, K. Kakuyanagi, S. Saito, T. Aoki, and K. Semba
Waseda University

PTu10 : **Parity Symmetry and Selection Rules in a Qubit-Harmonic Oscillator Coupled System**
T. Fuse, F. Yoshihara, S. Ashhab, K. Kakuyanagi, S. Saito, and K. Semba
National Institute of Information and Communications Technology (NICT)

PTu11 : **Parity-preserving Light-matter System Mediates Effective Two-body Lnteractions**
T. H. Kyaw, S. Allende, L.-C. Kwek, and G. Romero
Centre for Quantum Technologies

PTu12 : **Superradiance with Local Phase-breaking Effects**
N. Shammah, N. Lambert, F. Nori, and S. De Liberato
RIKEN Center for Emergent Matter Science (CEMS)

PTu13 : **Non-Markovian Effect of Energy Flow**
R. Tezuka, and C. Uchiyama
University of Yamanashi

PTu14 : **Upper Bound on the Two-way Assisted Private Capacity of Various Quantum Channels**
K. Tsuji, and Y. Tokura
University of Tsukuba

PTu15 : **Two-way Quantum Computer**
A. Takemura, and Y. Tokura
University of Tsukuba

PTu16 : **Effects of Strong Atom-cavity Coupling on the Entanglement Dynamics of Two Atoms**
S. Kato, R. Suzuki, K. Yoshida, and Y. Tokura
University of Tsukuba

PTu17 : **Multi-mode Quantum Rabi Model and Superluminal Signalling**
C. S. Muñoz, F. Nori, and S. De Liberato
RIKEN Center for Emergent Matter Science (CEMS)

PTu18 : **State Preparation and Lifetime Measurements through Spectral Hole Burning in $^{167}Er^{3+}:Y_2SiO_5$**
M. I. Jspeert, M. Hiraishi, T. Tawara, K. Shimizu, H. Omi, S. Adachi, and H. Gotoh
NTT Basic Research Labolatories

PTu19 : **Cooperatively Coupled Motion with Superradiant and Subradiant Atoms**
K.-T. Lin, and G.-D. Lin
National Taiwan University

PTu20 : **Scalable Quantum Computing with an Ion Crystal Stabilized by Tweezers and Sympathetic Cooling**
Y.-C. Shen, and G.-D. Lin
National Taiwan University

PTu21 : **Atom Interferometry with the Sr Optical Clock Transition Inside an Optical Guide**
T. Takahashi, T. Akatsuka, and H. Katori
The University of Tokyo

PTu22 : **Efficient Single-Photon Coupling between an Optical Nanofiber and a Diamond Nanowire**
Y. Yonezu, K. Wakui, K. Furusawa, M. Takeoka, K. Semba, and T. Aoki
Waseda University

PTu23 : **Field and Temperature Dependent cavity Coupling for Highly Sensitive On-chip Spin Detection**
G. Franco, M. Martens, L. Chen, A. Zabalo, N. Dalal, and I. Chiorescu
Florida State University , The National High Magnetic Field Laboratory

PTu24 : **Non-unitary Transformation of the Square Root of Density Matrices**
K. Asai, and Y. Tokura
University of Tsukuba

PTu25 : **Spin Resonance beyond the Rotating Wave Approximations**
K. Yokohama, and Y. Tokura
University of Tsukuba

PTu26 : **Toward Coherent Feedback Control in Quantum Transport in Magnetic Field**
R. Suzuki, S. Kato, K. Yoshida, and Y. Tokura
University of Tsukuba

PTu27 : **Role of Density on Microwave Photoresistance in 2D Electron Gas**
X. Fu, M. D. Borisov, Q. Shi, Q. A. Ebner, M. A. Zudov, Q. Qian, J. D. Watson, and M. J. Manfra
University of Minnesota

PTu28 : **Fine Structure of Microwave-induced Resistance Oscillations**
Q. Shi, M. A. Zudov, I. A. Dmitriev, K. W. Baldwin, L. N. Pfeiffer, and K. W. West
University of Minnesota

PTu29 : **Dispersion Engineering of a PPLN Waveguide for the Generation of Spectrally-pure Photon Pairs**
A. Bergeot, T. Kashiwazaki, and N. Matsuda
NTT Basic Research Labolatories

PTu30 : **Shaped Microwave Pulses for Measuring Hybrid Quantum Devices**
A. Keyser, S. de Graaf, M. Oxborrow, and T. Lindström
National Physical Laboratory, Imperial College London

PTu31 : **Characterization of Low Loss Microstrip Resonators as a Building Block for Circuit QED in a 3D Waveguide**
D. Zoepfl, P. R. Muppalla, C. M. F. Schneider, S. Kasemann, S.Partel, and G. Kirchmair
University of Innsbruck

PTu32 : **Probing the Spectral Density of the Surface Electromagnetic Fields through Scattering of Waveguide Photons**
G.-Y. Chen
National Chung Hsing University

PTu33 : **Slow Microwave Propagation Guided by One-dimensional Left-handed Metamaterials**
Y.-H. Chang, V. C. Silalahi, and W. Kuo
National Chung Hsing University

PTu34 : **Optical Characterization of VLSI Graphene NEMS**
S. Houri, S. Cartamil-Bueno, P. G. Steeneken, and H. S. J. van der Zant
NTT Basic Research Labolatories

PTu35 : **Acoustically Modulated Single-photon Sources**
P. L. J. Helgers, K. Biermann, H. Sanada, Y. Kunihashi, and P. V. Santos
Paul-Drude-Institut für Festkörperelektronik

PTu36 : **Efficiency Bounds on Quantum Thermoelectric Heat Engine with Broken Time-reversal Symmetry: the Role of Inelastic Processes**
K. Yamamoto, O. Entin-Wohlman, A. Aharony, and N. Hatano
The University of Tokyo

PTu37 : **Evanescently-coupled Optomechanical Device with a GaAs Optical Disk- Mechanical Beam Structure**
M. Asano, R. Ohta, H. Okamoto, T. Tawara, H. Gotoh, and H. Yamaguchi
NTT Basic Research Labolatories

PTu38 : **Coarse-grain Molecular Dynamics Simulation of Vertical Lamellar Phase of Diblock Copolymer in a Thin Film**
T. Yamaguchi, H. Tanaka, N. Clement, and A. Fujiwara
NTT Basic Research Labolatories

PTu39 : **Theory of a Carbon-nanotube Polarization Switch**
K. Sasaki
NTT Basic Research Labolatories

PTu40 : **Structure-dependent Optical and Electrical Transport Properties of Ni-doped ZnO Nanorods by Spray Pyrolysis**
G. E. Patil and G. H. Jain
KKHA Arts, SMGL Commerce & SPHJ Science College

PTu41 : **Parity-dependent Shot Noise in a Superconductor-nanowire Quantum Dot**
K. Takase, Y. Ashikawa, G. Zhang, K. Tateno, Y. Okazaki, and S. Sasaki
NTT Basic Research Labolatories

PTu42 : **Giant Gate Control of Rashba Spin-orbit Interaction in a Gate-all-around InAs/InP Core-shell Nanowire**
K. Takase, D. Ibrahimagic, K. Tateno, and S. Sasaki
NTT Basic Research Labolatories

PTu43 : **Telecom-band Light Emitting Diodes Based on Bottom-up InAs/InP Heterostructure**
G. Zhang, M. Takiguchi, K. Tateno, T. Tawara, M. Notomi, and H. Gotoh
NTT Basic Research Labolatories

PTu44 : **Probing Photonic States in 1D Space using Quantum Wave Mixing**
T. Hoenigl-Decrinis, A. Yu. Dmitriev, R. Shaikhaidarov, V. N. Antonov, and O. Astafiev
Royal Holloway, University of London, National Physical Laboratory (NPL)

PTu45 : **Electrical Control of a Quantum Non-linearity in a Nano-photonic Waveguide**
D. Hallett, A. Foster, B. Royall, D. Hurst, P. Kok, E. Clarke, M. S. Skolnick, and L. R. Wilson
University of Sheffield

PTu46 : **Evaluation of 2*f*-to-3*f* Self-referencing Interferometer Using Dual-pitch PPLN Ridge Waveguides**
K. Hara, K. Hitachi, A. Ishizawa, T. Nishikawa, and H. Gotoh
NTT Basic Research Labolatories

PTu47 : **Valley-contrasting Eigenmodes in Photonic Crystals with Triangular Lattice**
T. Yoda, and M. Notomi
Tokyo Institute of Technology, NTT Basic Research Laboratories

PTu48 : **Integrated Optics in 3C Silicon Carbide**
F. Martini, and A. Politi
University of Southampton

PTu49 : **$CsPbBr_3$-perovskite Nanowire-induced Nanocavities in SiN Photonic Crystals**
S. Sergent, M. Takiguchi, T. Tsuchizawa, J. Chen, Y. Fu, H. Taniyama, E. Kuramochi, S. Jin, and M. Notomi
NTT Basic Research Labolatories

Poster Session II (November 15th, Wednesday)

PWe01 : **Spin Diffusion Dynamics Under Spin-orbit Magnetic Field in Undoped GaAs Quantum Wells**
H. Sanada, Y. Kunihashi, Y. Tanaka, H. Gotoh, K. Onomitsu, M. Kohda, J. Nitta, and T. Sogawa
NTT Basic Research Labolatories

PWe02 : **Spin Chain Applications for Quantum Information Processing**
M. P. Estarellas, I. D'Amico, and T. P. Spiller
York Center for Quantum Technologies

PWe03 : **Geometric Phase Switching in Circular and Polygonal Mesoscopic Rings**
H. Saarikoski, A. Reynoso, D. Frustaglia, J.-P. Baltanás, M. Kohda, and J. Nitta
RIKEN Center for Emergent Matter Science (CEMS)

PWe04 : **Diffusion-suppressed Drift-spin Dynamics in GaAs Quantum Wells**
Y. Tanaka, Y. Kunihashi, H. Sanada, H. Gotoh, K. Onomitsu, M. Kohda, J. Nitta, and T. Sogawa
NTT Basic Research Labolatories

PWe05 : **In-plane Spin-filtering with Rashba-Dresselhaus Interaction**
Y. Hashimoto, X. Yao, Y. Iwasaki, T. Nakamura, and S. Katsumoto
Institute for Solid State Physics, The University of Tokyo

PWe06 : **Evaluation of Spin Orbit Interaction by Weak Anti-localization Measurement in Copper Nitride System**
R. Enoki, H. Gamou, S. Karube, M. Kohda, Y. Kunihashi, H. Sanada, and J. Nitta
Tohoku University

PWe07 : **Spin-current Induced Mechanical Torque in a Chiral Molecular Junction**
N. Sasao, H. Okada, and Y. Utsumi
Mie University

PWe08 : **Spin-orbit Semimetal $SrIrO_3$ in the Two-dimensional Limit**
D. J. Groenendijk, C. Autieri, J. Girovsky, M. C. Martinez-Velarte, N. Manca, G. Mattoni, A. M. R. V. L. Monteiro, N. Gauquelin, J. Verbeeck, A. F. Otte, M. Gabay, S. Picozzi, and A. D. Caviglia
Delft University of Technology

PWe09 : **Strain-induced Dirac State Shift in Topological Insulator Bi_2Se_3 Nanowires**
C. Schindler, C. Wiegand, J. Sichau, L. Tiemann, K. Nielsch, R. Zierold, and R. Blick
University of Hamburg

PWe10 : **Disorder-induced Dephasing in Backscattering-free Quantum Transport**
C. Gneiting and F. Nori
RIKEN Center for Emergent Matter Science (CEMS)

PWe11 : **Probing Helicity and the Topological Origins of Helicity Via Non-local Hanbury-Brown and Twiss Correlations**
A. Mani and C. Benjamin
National Institute of Science Education & Research (NISER)

PWe12 : **Topological Classification of Single-wall Carbon Nanotubes**
R. Okuyama, W. Izumida, and M. Eto
Keio University

PWe13 : **Conduction Impedance Effects in Atomically Thin Materials**
N. J. Townsend, I. Amit, T. J. Octon, J. D. Mehew, F. Reale, C. Mattevi, C. D. Wright, M. F. Craciun, and S. Russo
University of Exeter

PWe14 : **Electronic Properties of Laser-Patterned 2H/1T' Interface in Exfoliated Multilayer $MoTe_2$**
K. Sakanashi, K. Kamiya, H. Ouchi, T. Yamanaka, P. Krueger, K. Miyamoto, T. Omatsu, J. P. Bird, and N. Aoki
Chiba University

PWe15 : **Influence of Metal Contacts on Metal-insulator Transition in Molybdenum Disulfide Field Effect Transistors**
T. Iwabuchi, K. Arai, and Y. Shimazu
Yokohama National University

PWe16 : **A Simulation of Two-Dimensional Crystal Heterostructure Solar Cells Quantum Efficiency**
P. Pashaei, G. Allegretto, and P. Servati
Quantum Matter Institute (QMI), University of British Columbia

PWe17 : **Enhanced Optical Activity of Atomically Thin $MoSe_2$ Proximal to Nanoscale Plasmonic Slot-waveguides**
M. Blauth, G. Mélen, M. Prechtl, O. Hartwig, J. Harms, M. Kaniber, and J. J. Finley
Walter Schottky Institut

PWe18 : **Engineering Coherent Color Centers in Two Dimensional Materials**
H. Songyan, M. D. Birowosuto, U. Saleem, T. H. T. Edwin, and W. Hong
Nanyang Technological University

PWe19 : **Ultrafast All Optical Modulation in Graphene-loaded Plasmonic Waveguides**
M. Hata, M. Ono, H. Sumikura, K. Nozaki, E. Kuramochi, and M. Notomi
Tokyo Institute of Technology, NTT Basic Research Labolatories

PWe20 : **Excitation Power Dependence of Nonequilibrium Carrier Relaxation Dynamics in Graphene**
Y. Hasegawa, K. Oguri, K. Kato, T. Nishikawa, and H. Gotoh
NTT Basic Research Labolatories

PWe21 : **Modulating Plasmons in Graphene by Substrate Modification**
M. Takamura, N. Kumada, S. Wang, and K. Kumakura
NTT Basic Research Labolatories

PWe22 : **Effects of Interaction on Charge Fractionalization in Tomonaga-Luttinger Liquids**
P. Brasseur, N. H. Tu, Y. Sekine, K. Muraki, M. Hashisaka, T. Fujisawa, and N. Kumada
NTT Basic Research Labolatories

PWe23 : **Evolution of Graphene Alignment on Recrystallizing Polycrystalline Cu-foil for Chemical Vapor Deposition Growth**
Y. Ogawa, S, Suzuki, H, Hibino, and K, Kumakura
NTT Basic Research Labolatories

PWe24 : **SIMPLE – Single Ion Multispecies Positioning at Low Energy – A Single Ion Implanter for Quantum Technologies**
N. Cassidy, R. Webb, R. Curry, P. Blenkinsopp, I. Brown, T. Adams, B. Murdin, L. Antwis, and D. Cox
University of Surrey

PWe25 : **Effects of Strain and Electric Filed on Single Erbium Ions in Silicon Nano-transistors**
G. Hu, Q. Zhang, G. G. de Boo, M. Rancic, B. C. Johnson, J. C. McCallum, J. Du, M. J. Sellars, C. Yin, and S. Rogge
University of New South Wales

PWe26 : **Mechanism of Single-electron Pumping via a Single-trap Level in Silicon**
G. Yamahata, S. P. Giblin, M. Kataoka, T. Karasawa, and A. Fujiwara
NTT Basic Research Labolatories

PWe27 : **Dependence of Threshold Voltages on Temperature Observed in Random Arrays of Au Nanoparticles**
M. Moriya, M. Moribayashi, K. Matsumoto, H. T. T. Tran, H. Shimada, Y. Kimura, A. Hirano-Iwata, and Y. Mizugaki
The University of Electro-Communications

PWe28 : **Fluctuations of Information Content and the Local Particle Number Superselection in a Quantum Conductor**
Y. Utsumi
Mie University

PWe29 : **Enhancement of the Impact Ionization Rate in Direct Gap Semiconductors Driving the Fast I-MOS Nanotransistors**
A. N. Afanasiev, A. A. Greshnov, and G. G Zegrya
Ioffe Institute

PWe30 : **High Fidelity Readout and Error Correction of Single Electron Pump**
H. Tanaka, G. Yamahata, and A. Fujiwara
NTT Basic Research Labolatories

PWe31 : **Quantum Interference and Single Electron Transport in CVD Graphene Nanoribbon**
J.-H. Chen, Y.-L. Zhong, L.-J. Li, and C.-D. Chen
Chung Yuan Christian University

PWe32 : **Gate-based Dispersive Readout of a Classical-quantum CMOS Single-electron Memory Cell**
S. Schaal, S. Barraud, J. J. L. Morton, and M. F. Gonzalez-Zalba
Hitachi Cambridge Laboratory

PWe33 : **Landau-Zener-Stückelberg Interference in a Charge Qubit of a One-electron Double Quantum Dot**
T. Ota, K. Hitachi, and K. Muraki
NTT Basic Research Labolatories

PWe34 : **Tuning Hole Spin Physics in InAs Quantum Dot Molecules**
A. Lin, M. Doty, and G. Bryant
University of Maryland, NIST

PWe35 : **In-plane Nuclear Field Formation in Individual InAlAs Quantum Dots: Role of Nuclear Quadrupole Effects**
S. Yamamoto, R. Matsusaki, R. Kaji, and S. Adachi
Hokkaido University

PWe36 : **Evaluations of the Electron g-factor Anisotropy and Fluctuation of the Overhauser Field in Single Quantum Dots**
R. Matsusaki, S. Yamamoto, R. Kaji, and S. Adachi
Hokkaido University

PWe37 : **Electrical Transport in Low Dimensional Systems Fabricated in a (110) GaAs Quantum Well**
T. Nakagawa, R. Fukai, Y. Sakai, H. Kiyama, J. Ritzmann, A. Ludwig, A. D. Wieck, and A. Oiwa
Osaka University

PWe38 : **Electrical Properties of Quinoidal Dipyranylidene Derivative and its Use as a Hole Transport Layer in Perovskite Solar Cells**
M. Courté, S. Chao, and D. Fichou
Nanyang Technological University

PWe39 : **Ferroelectricity and Leakage Current Behavior Investigation for $HfZrO_4$ Film with Al_2O_3 Interlayers**
P. C. Han, C. H. Wu, and E. Y. Chang
National Chiao Tung University

PWe40 : **Transport Properties of Spray Deposited Lead Telluride Films**
A. B. Gite, V. B. Gaikwad, S. R. Jadkar, G. H. Jain, and H. M. Pathan
SNJB KKHA Arts, SMGL Comm and SPHJ Sci College chandwad Nashik

PWe41 : **Fluctuation of Exergy Efficiency in Quantum Transport**
H. Okada, and Y. Utsumi
Mie University

PWe42 : **Study of Single Electron Wavepacket Propagation in Quantum Hall Edge States High Above the Fermi Energy**
N. Johnson, J. D. Fletcher, C. Emary, S. Ryu, H.-S. Sim, P. See, J. P. Griffiths, G. A. C. Jones, I. Farrer, D. A. Ritchie, M. Pepper, T. J. B. M. Janssen, and M. Kataoka
NTT Basic Research Labolatories

PWe43 : **Effect of Gate Voltage Sweep on Integer Quantum Hall Transport Properties of InAs Quantum Wells**
T. Akiho, H. Irie, K. Onomitsu, and K. Muraki
NTT Basic Research Labolatories

PWe44 : **Excess Conductance in Quantum Hall Edge Transport Driven by Andreev Reflection**
M. Onizaki, Y. Hashimoto, T. Nakamura, and S. Katsumoto
The University of Tokyo

PWe45 : **Detection Limitation of Resistively-detected NMR (RD-NMR) in Quantum Point Contact (QPC)**
A. Noorhidayati, M. H. Fauzi, M. F. Sahdan, S. Maeda, K. Sato, K. Nagase, and Y. Hirayama
Tohoku University

PWe46 : **Nonlinear Quantum Transport in MgZnO/ZnO Heterostructures**
Q. Shi, J. Falson, M. A. Zudov, Y Kozuka, A. Tsukazaki, M. Kawasaki, K. von Klitzing, and J. Smet
University of Minnesota

PWe47 : **Hall Field-induced Resistance Oscillations in a Tunable-density Wide GaAs/AlGaAs Quantum Well**
M. A. Zudov, I. A. Dmitriev, B. Friess, Q. Shi, V. Umansky, K. von Klitzing, and J. Smet
University of Minnesota

PWe48 : **A Double-gate Delay Line for Edge Magneto Plasmons**
C. J. Lin, M. Hashisaka, K. Muraki, and T. Fujisawa
Tokyo Institute of Technology

PWe49 : **Effects of Two-Dimensional Electron System on the Coupling between Edge Channels on Opposite Sides of a Hall Bar**
N. H. Tu, Y. Sekine, K. Muraki, M. Hashisaka, T. Fujisawa, and N. Kumada
NTT Basic Research Labolatories

PWe50 : **Shot-noise Signature of Quantum Many-body Correlation in a Non-equilibrium Regime of a Microscopic Integer Quantum Hall State**
M. Hashisaka, K. Muraki, and T. Fujisawa
NTT Basic Research Labolatories

Oral Session Abstract

Quantum metrology with Schrödinger cats

Serge Haroche

Laboratoire Kastler Brossel, Collège de France, Paris, France

Quantum systems can be prepared in superposition of states with different classical attributes, called "Schrödinger cat (SC) states". The high sensitivity of these states to perturbations makes quantum systems prepared in SC states ideal probes for precise measurements. My research team has studied light and matter SC states. The former are superposition of classical microwave fields stored in a high Q superconducting cavity containing N photons on average and assuming two different phases at the same time [1]. The latter are superposition of Rydberg atomic states associated to a large angular momentum J, simultaneously pointing in two different directions [2]. These SC states can be represented by their Wigner function in a plane phase (microwave field SC) or on a Bloch sphere (Rydberg atom SC). These functions present two Gaussian features associated to the classical components of the superposition with narrow interference fringes between these Gaussian components (see Fig.1). When a perturbation is applied to the system (addition of a small microwave field in the cavity or small change of the electric field applied to the Rydberg atom), the SC Wigner functions are shifted. The shift is easier to observe on the narrow fringes than on the broader classical Gaussian components. When classical features are observed, the sensitivity to the perturbation scales as $1/\sqrt{N}$ or $1/\sqrt{J}$ which corresponds to the standard quantum limit (SQL). When the fringes are detected, the sensitivity increases and can reach the Heisenberg limit (scaling as 1/N or 1/J). Using quantum interferometer set-ups, we have shown that SC states can be effectively used to detect tiny microwave field [3] or static electric field variations [4], with a sensitivity going beyond the SQL and nearing the Heisenberg limit. In the case of electric field measurements, our method can detect with one atom in 200 nanoseconds a field change of 200μV/cm, i.e. the electric field of a single electron at a distance of 270 micrometers. I will describe these experiments and discuss possible applications to the study of electric charge fluctuations in mesoscopic systems (quantum dots or carbon nanotubes). Generalization to the measurement of small magnetic fields will also be described.

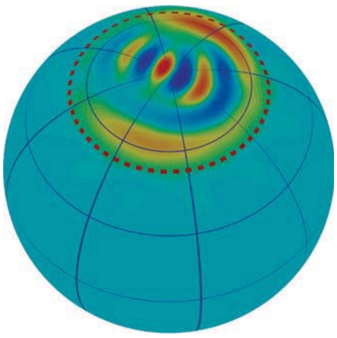

Figure 1: Wigner function of Rydberg atom SC state represented on its Bloch sphere (from ref. [2]).

[1] S. Deléglise, I. Dotsenko, C. Sayrin, J. Bernu, M. Brune, J-M. Raimond and S. Haroche, Nature, **455**, 510 (2008).
[2] A. Signoles, A. Facon, D. Grosso, I. Dotsenko, S. Haroche, J-M. Raimond, M. Brune and S. Gleyzes, Nature Physics, 10, **715** (2014).
[3] M. Penasa,S. Gerlich, T. Rybarczyk, V. Métillon, M. Brune, J-M. Raimond, S. Haroche, L. Davidovich and I. Dotsenko, Phys.Rev.A **94**, 022313 (2016).
[4] A. Facon, E-K. Dietsche, D. Grosso, S. Haroche, J-M. Raimond, M. Brune and S. Gleyzes, Nature, 535, **262** (2016).

Extremely high frequency cavity optomechanics

S. Anguiano[1], V. Villafañe[1], P. Sesin[1], P. Soubelet[1], A. E. Bruchhausen[1], I. Favero[2], F. R. Lamberti[2,3], L. Lanco[3], I. Sagnes[3], A. Lemaître[3], N. D. Lanzillotti-Kimura[3], P. Senellart[3], and A. Fainstein[1]

[1] *Centro Atómico Bariloche & Instituto Balseiro, C.N.E.A., CONICET, 8400 San Carlos de Bariloche, Río Negro, Argentina*
[2] *Matériaux et Phénomènes Quantiques, Université Paris Diderot, CNRS-UMR 7162, Sorbonne Paris Cité,10 rue Alice Domon et Léonie Duquet, 75013 Paris, France*
[3] *Centre de Nanosciences et de Nanotechnologies, C.N.R.S., Université Paris-Sud, Université Paris-Saclay, C2N Marcoussis, 91460 Marcoussis, France*

Strong confinement, in all dimensions, and high mechanical frequencies are highly desirable for quantum optomechanical applications. We describe GaAs/AlAs micropillar cavities that fully confine not only photons but also extremely high frequency (> 20 GHz) acoustic phonons. A strong increase of the optomechanical coupling upon reducing the pillar size is observed, together with room-temperature optical and mechanical Q-factors in the range 10^3 and 10^4, respectively, leading to record Q-frequency products of 10^{14} [1].

The study of these ultra-high frequency optomechanical resonators requires the use of purposely-designed spectroscopic and time-resolved optical techniques. We address the role of radiation pressure, electrostriction, photothermal and optoelectronic forces in this context, and show that optoelectronic forces involving real carrier photoexcitation and deformation potential interaction is the strongest mechanism of light-to-sound transduction when exciting with pulsed lasers close to the GaAs optical gap [2].

A new concept of quantum well photoelastic comb for the efficient coupling of NIR cw laser light to mechanical resonances at hundreds of GHz is also demonstrated in Raman-type ultra-high resolution experiments. This new approach is exploited to evidence the tailored transfer of spectral weight from the fundamental mechanical breathing mode at ~20 GHz to modes at 180-230 GHz, corresponding to the 9th and 11th mechanical overtone of the light-sound cavities. The wavelength dependence of the optomechanical coupling further proves the role of resonant photoelastic (electrostrictive) interaction, highlighting the potentiality to access ultra-strong dispersive coupling regimes [3].

These hybrid optomechanical semiconductor resonators can integrate quantum emitters or polariton condensates, opening exciting perspectives at the interface with nonlinear and quantum optics.

[1] A. Anguiano *et al*, Phys. Rev. Lett. **118**, 263901 (2017).
[2] V. Villafañe *et al*, arXiv:1709.08987 [physics.optics](2017).
[3] B. Jusserand *et al*, Phys. Rev. Lett. **115**, 267402 (2015).

TOWARD A PHONONIC CRYSTAL NANOSTRING WITH A QUALITY FACTOR OF ONE BILLION

A. Ghadimi*, S. Fedorov, N. J. Engelsen, M. Breyhi, R. Schilling,
H. Shutz, D. J. Wilson, T. J. Kippenberg
Ecole Polytechnique Federale de Lausanne (EPFL), Lausanne, Switzerland

Nanomechanical resonators are exquisite sensors of mass, force, and charge, and have recently emerged as a potential quantum technology. Central to these applications is the realization of resonator designs which simultaneously minimize effective mass and maximize quality factor. Recently it has been shown [1] that periodic micropatterning of a stressed thin film can lead to exceptionally high quality/mass flexural-mechanical modes through a combination of mode localization and dissipation dilution [2]. Here we apply this strategy to doubly clamped nanobeams made of high stress silicon nitride, and show that, using a strikingly simple corrugation pattern, unprecedented room temperature quality-frequency products of $4*10^{14}$ Hz are accessible, highlighted by a 1.5 megahertz mode with a quality factor of 250 million. In conjunction with their picogram effective masses, the string-like resonators we study are capable of thermal force sensitivities of 10 $aN/\sqrt{Hz}$ and dozens of oscillations within the thermal decoherence time at room temperature. Silicon nitride has low optical loss, enabling integration with high finesse optical cavities. We thus anticipate that devices similar to ours will have a significant impact on the field of cavity optomechanics. We also envision them playing an important role in future sensing technologies, ranging from high-speed AFM to hybrid quantum sensors based on doped crystalline materials.

***Submitting author:** A. Ghadimi, EPFL University, 1015 Lausanne, Station 3, EPFL-SB-IPHYS-LPQM1, PHD3-315, Tel: +41786355123; E-mail: amir.ghadimi@epfl.ch

[1] Y. Tsaturyan, A. Barg, E. S. Polzik, and A. Schliesser, arXiv preprint arXiv:1608.00937 (2016).
[2] Q. P. Unterreithmeier, T. Faust, and J. P. Kotthaus, Phys. Rev. Lett. 105, 027205 (2010).

The fully quantized dynamical Casimir effect – vacuum Casimir-Rabi oscillations in optomechanical systems

Vincenzo Macrì[1,2], Alessandro Ridolfo[2], Omar Di Stefano[2], Anton Frisk Kockum[2], Franco Nori[2,3], and Salvatore Savasta[1,2]

[1] *Dipartimento di Scienze Matematiche e Informatiche, Scienze Fisiche e Scienze della Terra, Università di Messina, I-98166 Messina, Italy*
[2] *Center for Emergent Matter Science, RIKEN, Saitama 351-0198, Japan*
[3] *Physics Department, The University of Michigan, Ann Arbor, Michigan 48109-1040, USA*

By rapidly changing a boundary condition for the electromagnetic field, e.g., by moving a mirror very quickly, fluctuations in the quantum vacuum can be converted into real photons. This is known as the dynamical Casimir effect, the first experimental demonstration of which was realized only a few years ago, using superconducting circuits. In most theoretical studies treating the dynamical Casimir effect, the trajectory of the mirror is classical. In this work [1], we instead use a fully quantum-mechanical description of both the cavity field and the oscillating mirror in an optomechanical setup (Fig. 1). We do not linearize the dynamics, nor do we adopt any parametric or perturbative approximation.

By numerically diagonalizing the full optomechanical Hamiltonian, we show that the resonant generation of photons from the vacuum is determined by a ladder of mirror-field Rabi splittings, and that vacuum Casimir-Rabi oscillations can occur. We also study the case where the mirror is coherently driven. We find that, for strong optomechanical coupling, a resonant production of photons out from the vacuum can be observed even for mechanical frequencies below the cavity frequency. Since high mechanical frequencies, which are hard to achieve experimentally, were thought to be imperative for realizing the dynamical Casimir effect, this result removes a major obstacle for its experimental observation in a conventional optomechanical setup.

[1] V. Macrì, A. Ridolfo, O. Di Stefano, A. F. Kockum, F. Nori, and S. Savasta, arXiv:1706.04134 (2017).

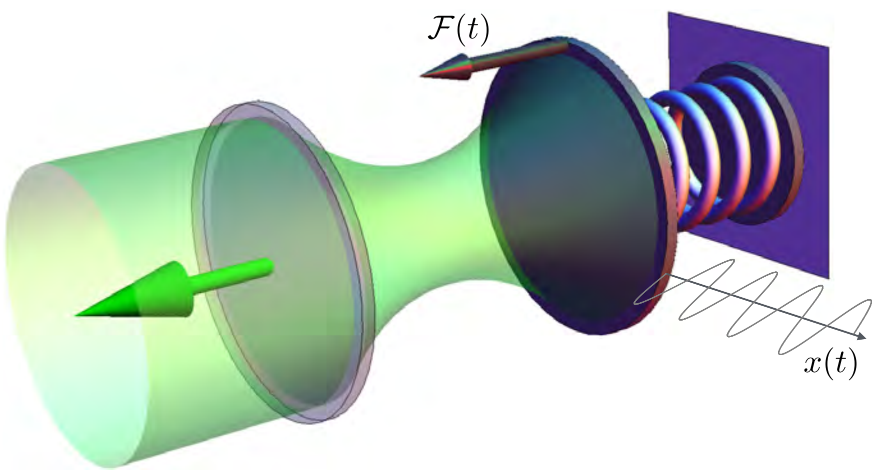

Figure 1: The optomechanical system we consider for the fully quantized dynamical Casimir effect. The mechanical vibrations of the mirror to the right can be converted into photons that leak out (green arrow) from the cavity formed by the two mirrors.

Quantum Engineering of Superconducting Qubits

William D. Oliver [1,2,3]

[1] *Research Laboratory of Electronics, MIT, Cambridge, MA 02139*
[2] *Department of Physics, MIT, Cambridge, MA 02139*
[3] *MIT Lincoln Laboratory, Lexington, MA 02420*

Superconducting qubits are coherent artificial atoms assembled from electrical circuit elements and microwave optical components. Their lithographic scalability, compatibility with microwave control, and operability at nanosecond time scales all converge to make the superconducting qubit a highly attractive candidate for the constituent logical elements of a quantum information processor.

In this talk, we revisit the design, fabrication, and control of the superconducting flux qubit [1]. By adding a high-Q capacitor, we dramatically improve its reproducibility, anharmonicity, and coherence, achieving T_1 = 55 μs and T_2 = 90 μs. We identify quasiparticles as a leading cause of temporal variability in the T_1. We introduce and demonstrate a stochastic control technique that effectively pumps away these quasiparticles and thereby stabilizes and improves T_1 [2].

[1] F. Yan et al., Nature Communications **7**, 12964 (2016).
[2] S. Gustavsson et al., Science **354**, 1573 (2016).

Towards Fault-tolerant Quantum Computing using Superconducting Qubits

Maika Takita

IBM T.J. Watson Research Center, Yorktown Heights, NY 10598, USA

Recent advances in materials and design of superconducting qubits has allowed the realization of quantum processors with multiple qubits and high coherence. Although the implementation of a fully fault-tolerant architecture is still far away, existing devices with five to seven physical qubits present a platform for testing both fault-tolerant state preparations of a small quantum code and short-depth circuits for studying near-term applications. The smallest code that detects a general error requires four data qubits. With one additional qubit as a syndrome qubit, we can study the [[4,2,2]] code and prepare one of its logical qubits fault-tolerantly. In the first part of my talk, I will present how these logical states are prepared and discuss how errors are detected. I will compare the results between logical qubits that are prepared fault-tolerantly and not. I will also compare the lifetimes of these qubits with each data qubit [1]. Finally, I will present a hardware efficient approach to addressing electronic structure problems of small molecules on existing quantum hardware. This approach enabled the largest molecular simulation on a quantum processor to date, using up to six qubits for estimating the lowest energy state of beryllium hydride (BeH_2) [2].

[1] M. Takita, A.W. Cross, A.D. Córcoles, J.M. Chow, J.M. Gambetta, *arXiv preprint* arXiv:1705.09259 (2017).
[2] A. Kandala, A. Mezzacapo, K. Temme, M. Takita, M. Brink, J.M. Chow, J.M. Gambetta, *Nature* 549, 242-246 (2017).

Tunable quantum gate between a superconducting atom and a propagating microwave photon

K. Koshino[1], **K. Inomata**[2,3], **Z. R. Lin**[2], **Y. Tokunaga**[4], **T. Yamamoto**[2,5], **Y. Nakamura**[2,6]

[1]*College of Liberal Arts and Sciences, Tokyo Medical and Dental University*
[2]*RIKEN Center for Emergent Matter Science*
[3]*National Institute of Advanced Industrial Science and Technology*
[4]*NTT Secure Platform Laboratories, NTT Corporation*
[5]*IoT Device Research Laboratories, NEC Corporation*
[6]*Research Center for Advanced Science and Technology, The University of Tokyo*

We propose a new scheme for implementing deterministic two-qubit gates between a superconducting atom and a propagating microwave photon [1]. In the proposed device, a driven superconducting atom is coupled to a waveguide photon via a resonator [Fig. 1(a)]. The atomic qubit is encoded on its two lowest levels, and the photon qubit is encoded on its carrier frequencies. The gate operation completes deterministically upon reflection of a photon, and the gate type is continuously variable (including SWAP, $\sqrt{\text{SWAP}}$, and Identity gates) through *in situ* control of the drive field to the atom. Using a propagating photon as a flying qubit, we can execute various gate operations between remote superconducting atoms, such as the entanglement generation and the qubit-state transfer [Fig. 1(b)]. The present scheme provides a communication channel between distant clusters of superconducting qubits and thus widens the potential of quantum computation in superconducting devices.

This work was partly supported by JSPS KAKENHI (Grants No. 16K05497, No. 26220601, and No. 15K17731) and JST ERATO (Grant No. JPMJER1601).

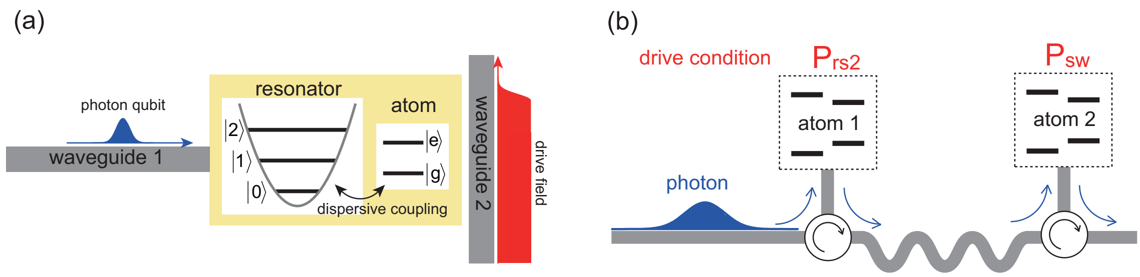

Figure 1: (a) Schematic of the tunable atom-photon quantum gate. We input a photon qubit through waveguide 1 and drive the superconducting atom through waveguide 2. The quantum-gate operation completes deterministically upon reflection of the photon. We can realize various types of quantum gate by changing the drive condition. (b) Schematic of the circuit for entanglement generation. Superconducting atoms 1 and 2 are cascaded by circulators. A resonant input photon deterministically generates entanglement between remote superconducting atoms.

[1] K. Koshino, K. Inomata, Z. R. Lin, Y. Tokunaga, T. Yamamoto, and Y. Nakamura, Physical Review Applied **7**, 064006 (2017).

Quantum non-demolition detection of an itinerant microwave photon using an entangling gate with a superconducting qubit

S. Kono[1], Y. Tabuchi[1], A. Noguchi[1],
R. Yamazaki[1], K. Koshino[2], Y. Nakamura[1,3]

[1]*Research Center for Advanced Science and Technology (RCAST), The University of Tokyo, Meguro-ku, Tokyo 153-8904, Japan*
[2]*College of Liberal Arts and Sciences, Tokyo Medical and Dental University, Ichikawa, Chiba 272-0827, Japan*
[3]*Center for Emergnent Matter Science (CEMS), RIKEN, Wako, Saitama 351-0198, Japan*

Photon detection is an elementary tool for measurement and control of light. In the optical domain, it has been applied in a wide range of fields, such as quantum sensing, quantum cryptography, and distributed quantum computation. On the other hand, the technical advancement of Rydberg atoms and superconducting quantum circuits has enabled measurement and manipulation of microwave photons which have energy much smaller than that of optical photons [1,2]. However, these techniques are realized in a cavity quantum electrodynamics system, where a controllable "atom" interacts with photons confined in a cavity.

Here, we experimentally demonstrate a quantum non-demolition (QND) detection of an itinerant single microwave photon using an entanglement with a superconducting qubit. When an itinerant photon is reflected by a cavity coupled with a superconducting qubit in the strong dispersive regime, it interacts dispersively with the qubit through the cavity mode. It is possible to control the interaction strength by tuning the resonance frequency and bandwidth of the cavity, so that the qubit deterministically acquires the phase flip after the photon is reflected. With a single-shot measurement of the phase flip of the qubit, the presence of the single photon is detected without destroying it.

In the experiment, we use a transmon qubit mounted at the center of a 3D superconducting cavity that is connected to a 1D transmission line. We evaluate the quantum efficiency and the dark count probability of our detection scheme using a weak coherent pulse as the input state. To verify the QND property, we characterize the reflected pulse mode by using conditional quantum state tomography based on the outcome of the qubit readout. We find an itinerant single photon in the reflected pulse mode in a heralded way, although the input pulse is in a classical coherent state. We also confirm that the interaction corresponds to an entangling gate between the reflected photon and the qubit, which indicates our scheme is applicable to construct a quantum network between localized superconducting qubits.

[1] J. M. Raimond, M. Brune, and S. Haroche, Rev. Mod. Phys. **73**, 565 (2001).
[2] Max Hofheinz *et al.,* Nature **459**, 546 (2009).

Majorana modes in InAs/Al two-dimensional heterostructures

Fabrizio Nichele [1], Henri J. Suominen [1], Morten Kjaergaard [1], Asbjorn Drachmann [1], Alexander M. Withicar [1], Eoin C.T. O'Farrel [1], Antonio Fornieri [1], Javad Shabani [2], Chris Palmstrom [2], Tian Wang [3], Geoffrey C. Gardner [3], Candince Thomas [3], Anthony T. Hatke [3], Michael J. Manfra [3], Karsten Flensberg [1], Charles M. Marcus [1]

[1] *Center for Quantum Devices and Station Q Copenhagen, Niels Bohr Institute, University of Copenhagen, Universitetsparken 5, 2100 Copenhagen, Denmark*
[2] *California NanoSystems Institute, University of California, Santa Barbara, CA 93106, USA*
[3] *Department of Physics and Astronomy and Station Q Purdue, Purdue University, West Lafayette, Indiana 47907 USA*

There is growing interest in material systems that both support Majorana zero modes (MZMs), relevant for topological quantum computing, and can be fabricated to provide branched, complex, and scalable geometries. Emerging as zero-energy states in one-dimensional semiconductors with induced superconductivity, Zeeman coupling, and spin-orbit interaction, MZMs have been tentatively identified in individual InSb or InAs nanowires, including recently realized epitaxial hybrids. Future tests of non-Abelian statistics will likely involve braiding or interferometric measurement, requiring branched or looped geometries, challenging to realize using individual nanowires or mechanically assembled nanowires networks.
I will present investigations of hybrid superconductor/semiconductor devices based on a planar InAs heterostructure strongly coupled to a thin layer of epitaxial Al [1]. By top-down lithography and gating, we define one dimensional wires, expected to hold MZMs in a large magnetic field [2]. Characterization of the wires indicate a hard superconducting gap, ballistic tunneling probes and in-plane critical fields up to 3 T. In the presence of an in-plane magnetic field aligned along the wires, zero energy states robust in field emerge out of coalescing Andreev bound states. The observed ZBPs are consistent with theory for Majorana modes, including a peak conductance that is proportional to tunnel coupling, saturates at the conductance quantum, decreases as expected with field-dependent gap, and collapses onto a simple scaling function in the dimensionless ratio of temperature and tunnel coupling [3].

[1] J. Shabani, M. Kjaergaard, H. J. Suominen, Y. Kim, F. Nichele, K. Pakrouski, T. Stankevic, R. M. Lutchyn, P. Krogstrup, R. Feidenhans'l, S. Kraemer, C. Nayak, M. Troyer, C. M. Marcus, C. J. Palmstrøm. Phys. Rev. B **93** 155402 (2016)
[2] H. J. Suominen, M. Kjaergaard, J. Shabani, C. J. Palmstrøm, C. M. Marcus, F. Nichele. arXiv: 1703.03699
[3] F. Nichele, A.C.C. Drachmann, A.M. Whiticar, E.C.T. O'Farrell, H.J. Suominen, A. Fornieri, T. Wang, G.C. Gardner, C. Thomas, A.T. Hatke, P. Krogstrup, M.J. Manfra, K. Flensberg, C.M. Marcus. Phys. Rev. Lett. *In press.*

Tunable Josephson Junctions and Superconducting Quantum Interference in an interfacial superconductor

A.M.R.V.L. Monteiro[1], D. J. Groenendijk[1], N. Manca[1], E. Mulazimoglu[1], S. Goswami[1], R. Wölbing[2], D. Koelle[2], R. Kleiner[2], Ya. Blanter[1], L.M.K. Vandersypen[1], and A. D. Caviglia[1]

[1] *Kavli Institute of Nanoscience, Delft University of Technology, Delft, Netherlands.*
[2] *Physikalisches Institut and CQ Center for Quantum Science in LISA+, Eberhard Karls Universität Tübingen, Tübingen, Germany.*

The two-dimensional superconductor hosted at the interface between the complex oxides lanthanum aluminate (LAO) and strontium titanate (STO) has several intriguing properties that set it apart from conventional superconductors. Most notably, its critical temperature (T_c) can be tuned by field-effect, revealing a dome-shaped phase diagram reminiscent of high T_c superconductors. To date, experiments with oxide interfaces have measured quantities which probe only the magnitude of the superconducting order parameter and are not sensitive to its phase.

Here, we perform phase-sensitive measurements by realizing the first superconducting quantum interference devices (SQUIDs) at the LAO/STO interface. We employ two distinct approaches for the creation and control of Josephson junctions: (i) combination of lateral confinement and local side gating [1] and (ii) local top-gating [2]. In particular, the gate-defined SQUIDs are unique in that the entire device is made from a single superconductor with purely electrostatic interfaces between the superconducting reservoir and the weak link. Our observation of robust quantum interference opens up a new pathway to understand the nature of superconductivity at oxide interfaces.

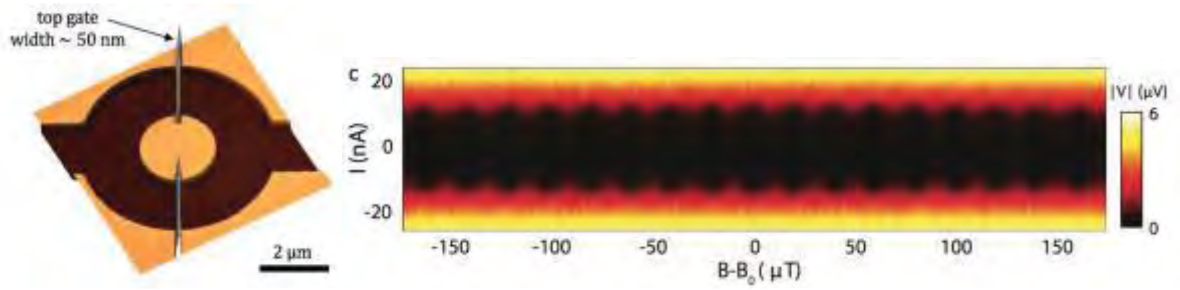

Figure 1 Left: AFM image of an electrostatically defined SQUID. Right: 2D plot showing SQUID oscillations with the top gates optimally tuned.

[1] A.M.R.V.L. Monteiro, D.J. Groenendijk, N. Manca, E. Mulazimoglu, S. Goswami, Ya. Blanter, L.M.K. Vandersypen, and A.D. Caviglia, Nano Lett. **17**, 715 (2017).

[2] Goswami, E. Mulazimoglu, A.M.R.V.L. Monteiro, R.Wölbing, D. Koelle, R. Kleiner, Y. M. Blanter, L.M.K. Vandersypen, A.D. Caviglia, Nature Nanotech. **11**, 861 (2016).

Finite Supercurrent in Nb/(In, Fe)As/Nb Junctions

T. Nakamura [1], L. D. Anh[2], Y. Hashimoto [1], S. Ohya [2,3], M. Tanaka [2,3] and S. Katsumoto [1,3]

[1]*Institute for Solid State Physics, The University of Tokyo*
[2]*Depertment of Electrical Engineering and Information Systems., The University of Tokyo*
[3]*Center for Spintronics Research Network, The University of Tokyo*

Superconductor/ferromagnet/superconductor (SFS) junctions exhibit attractive phenomena like π-junction [1] and triplet Cooper pairs [2]. It is an interesting challenge to use a ferromagnetic semiconductor (FMS) as an F-layer though many of FMSs are *p*-type and good contacts to superconductors are difficult to be formed. Here we adopt an FMS (In,Fe)As, in which Fe atoms work only as local moments. Hence, with doping Be during low-temperature MBE growth, (In,Fe)As is n-type (electron concentration ~10^{19} cm^{-3}), because Be atoms at interstitial sites in (In,Fe)As work as double donors [3]. Thus, (In,Fe)As is expected to have very low Schottky barrier as well as an *n*-type InAs.

We fabricated SFS junctions by depositing Nb superconducting electrodes onto the surface of an MBE grown (In,Fe)As film with Fe concentration of 6%. The Curie temperature is 120 K. The gaps of Nb strips along [-110] are 0.6, 0.8, 1.0 and 1.2 μm as shown in the inset of Fig.1. Figure 1 displays the differential resistance of the junctions at zero external magnetic fields as a function of bias current. All the junctions exhibit a resistance dip at the zero-bias, and several junctions show zero resistance manifesting a supercurrent in the ferromagnetic (In,Fe)As. As shown in Fig. 2, the critical current Ic oscillates against the magnetic fields ***H***, indicating that the Josephson effect forms an interference loop at the junction without a direct contact of the Nb electrodes. The I_c become maximum at around +20 Oe, even though both the applied field ***H*** and the magnetization ***M*** are positive and the sum ***H***+***M*** is much larger than the flux quantum. The magnetic hysteresis and other behaviors are consistently explained by ferromagnetic properties of (In,Fe)As.

[1] T. Kontos *et al*., Phys. Rev. Lett. **89**, 137007 (2002).
[2] R. S. Keizer *et al*. Nature **439**, 825 (2006).
[3] P. N. Hai, *et al*., Appl. Phys. Lett. **101**, 182403 (2012).

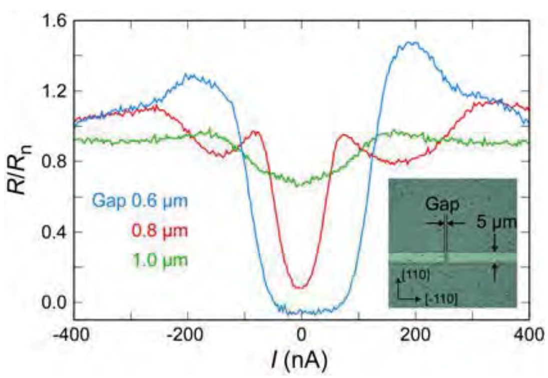

Fig.1 Bias dependence of the differential resistance for three junctions at 60 mK without applying field.

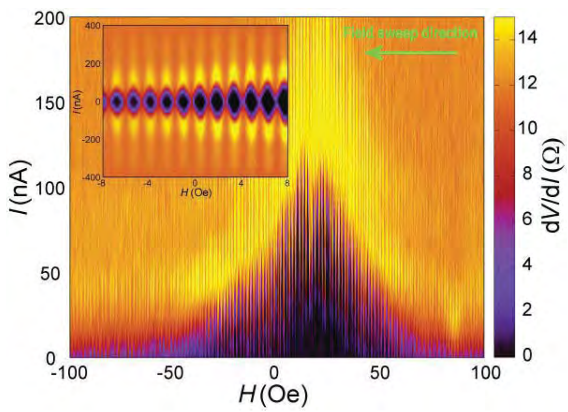

Fig.2 Differential resistance map of the junction with gap of 0.6 μm at 60 mK. Inset is an enlargement around 0 Oe.

Charge Quantum Interference Device

R. Shaikhaidarov [1,2], S. E. de Graaf [3], S. T. Scacel [4], T. Hoenigl-Decrinis[1,3], V. A. Antonov [1,2], E.V. Il'ichev [5,6], and O. V. Astafiev [1,2,3]

[1] *Royall Holloway University of London, Egham, Surrey, TW20 0EX, UK*
[2] *Moscow Institute of Physics and Technology, 141700, Dolgoprudny, Moscow region, Russia*
[3] *Nationa Physical Laboratory, Hampton Road, Teddington, Middlesex, TW11 0LW, UK*
[4] *Physikalisches Institut, Karlsruhe Institute of Technology, D-76128 Karlsruhe, Germany*
[5] *Leibniz Institute of Photonic Technology, P.O. box 100232, D-07702 Jena, Germany*
[6] *Russian Quantum Center, National University of Science and Technology MISIS, Moscow 119049, Russia*

Coherent Quantum Phase Slip (CQPS) effect has been demonstrated in loops of highly disordered InO and NbN thin films. The loops have constrictions, which work as tunnel barriers for magnetic fluxes and make possible coherent tunneling of magnetic fluxes in and out of the loop [1, 2]. We demonstrate Charge Quantum Interference Device (CQUID) – dual to a SQUID – in the NbN loops with two constrictions [3]. In that case flux tunneling becomes sensitive to a charge on an island between constrictions [4].

In the CQUID flux coherently tunnels across two narrow constrictions in a continuous superconductor. The constrictions are connected in series and the wider region between constrictions capacitively coupled to a gate electrode. The charge induced by gate potential controls the interference of phase slip amplitudes with period *2e*. The CQUID is implemented in a highly inductive NbN loop embedded in $\lambda/2$ superconducting resonator made of the same material. The resonator allows for direct readout of the energy spectrum of the device by dispersive microwave spectroscopy.

We perform energy level spectroscopy as a function of magnetic field for different values of gate electrode potentials. We also monitor response of energy levels due to induced charge on the island when magnetic field is fixed. We observe oscillations with period corresponding to *2e*. At each value of gate voltage we see two spectroscopy lines. These lines are shifted by exactly half period.

We demonstrate control of the interference of coherent quantum phase slip amplitudes in a charge quantum interference device CQUID. Oscillations shifted by half period represent charge parity shift on the island.

[1] Astafiev, O. V., Ioffe, L. B., Kafanov, S., Pashkin, Yu. A, Arutyonov, K. Yu., Shahar, D., Cohen, O., and Tsai, J.S., Nature (London) **484**, 355-358 (2012).
[2] Peltonen, J. T. Z. H. Peng, Yu. P. Korneeva, B. M. Voronov, A. A. Korneev, A. V. Semenov, G. N. Gol'tsman, J. S. Tsai, and O. V. Astafiev, Phys Rev. B **94**, 180508(R) (2016).
[3] S. E. de Graaf at al. to be published.
[4] Aharonov, Y., and Casher A., Phys. Rev. Lett. 53, 319-321 (1984).

Polaritons Beyond The Rotating Wave Approximation

Xinwei Li,[1] Motoaki Bamba,[2] and Junichiro Kono[1,3,4,*]

[1] *Department of Electrical & Computer Engineering, Rice University, Houston, TX, U.S.A.*
[2] *Department of Material Engineering Science, Osaka University, Osaka, Japan*
[3] *Department of Physics & Astronomy, Rice University, Houston, TX, U.S.A.*
[4] *Department of Materials Science & NanoEngineering, Rice University, Houston, TX, U.S.A.*
**Email: kono@rice.edu Website: http://kono.rice.edu/*

Understanding and controlling the dynamics of a two-level system resonantly driven by an ac field constitutes one of the most basic requirements for diverse modern technology, including nuclear magnetic resonance, laser diodes, and quantum computation. However, the seemingly simple Schrödinger equation for a two-level system in the presence of a resonant ac field cannot be solved exactly unless one adopts the rotating wave approximation, which neglects the counter-rotating component of the applied ac field. When the field becomes sufficiently strong, this approximation breaks down, leading to a finite ac-field-intensity-dependent resonance-frequency shift known as the Bloch-Siegert (BS) shift [1].

Here, we report the *vacuum* BS shift, which is induced by the ultrastrong coupling of electrons with the counter-rotating component of the vacuum fluctuation field inside a high-quality-factor (Q) terahertz (THz) cavity [2]. Specifically, electron cyclotron resonance (CR) in a Landau-quantized ultrahigh-mobility two-dimensional electron gas in a GaAs quantum well coupled ultrastrongly with vacuum photons in a THz photonic crystal cavity with $Q \sim 10^3$ [3]. In this Landau-polariton system, we simultaneously achieved an ultrahigh g/ω_0 (0.36) and an ultrahigh cooperativity $C \equiv 4g^2/\kappa\gamma = 3513$, where g is the light-matter coupling rate, ω_0 is the resonance frequency, and κ (γ) is the photon (matter) decay rate. Using a linearly polarized THz probe, i.e., a 50%-50% mixture of CR-active (CRA) and CR-inactive (CRI) circularly polarized radiation, we identified the vacuum BS shift. We clearly distinguished it from the other unique signature of the ultrastrong coupling regime, i.e., the photon-field self-interaction effect due to the A^2 (or diamagnetic) terms in the Hamiltonian. We demonstrated that the vacuum BS shift *only appears in the CRI mode dispersion* through the counter-rotating coupling of CRI radiation and electrons. This observation represents a unique manifestation of a strong-field phenomenon without a strong field.

[1] F. Bloch and A. Siegert, Phys. Rev. **57**, 522 (1940).
[2] X. Li et al., unpublished.
[3] Q. Zhang, M. Lou, X. Li, J. L. Reno, W. Pan, J. D. Watson, M. J. Manfra, and J. Kono, Nat. Phys. **12**, 1005 (2016).

Probing the dressed structure of the light-matter ground state in the ultra-strong coupling regime

M. Cirio[1], N. Lambert[1], S. De Liberato[2], K. Debnath[3], and F. Nori[1,4]

[1] *CEMS, RIKEN, Wako-shi, Saitama 351-0198, Japan*
[2] *School of Physics and Astronomy, University of Southampton, Southampton SO17 1BJ, United Kingdom*
[3] *Ecole Polytechnique Federale de Lausanne (EPFL), CH-1015 Lausanne, Switzerland*
[4] *Department of Physics, University of Michigan, Ann Arbor, Michigan 48109-1040, USA*

When the interaction strength between matter and the radiation field confined in a cavity becomes a sensible fraction of the bare energy of the system, hybridization properties become relevant. For example, in this ultra-strong coupling regime, the expected number of photons present in the light-matter ground state is non-zero. When matter can be modelled as a two level system, since the ground state has minimal amount of energy, these "virtual" photons cannot be spontaneously emitted into extra-cavity radiation.
Different theoretical ideas, mainly based on non-adiabatic modulations of the light-matter interaction strength, have been proposed to induce such an emission (as, for example, in [1, 2, 3]). Following this line of research, in [4], we show that an electric current flowing through a system in the ultra-strong coupling regime can induce emission of extra-cavity radiation, i.e., electroluminescence. While standard electroluminescence relies on the population of excited states followed by spontaneous emission, the process we describe extracts bound photons from the dressed ground state and it has peculiar features that unequivocally distinguish it from usual electroluminescence.
However, while they probe the presence of virtual photons in the system, methods based non-adiabatic modulations of the light-matter interaction destroy all internal coherences present in the dressed ground state. It is then relevant to find new ways to probe the structure of the light-matter ground state which do not rely on a fast modulation of the coupling (which might also be challenging to realize) and are not invasive. In [5] (see [6] for a parallel theoretical proposal) we show that, utilizing a time-dependent opto-mechanical interaction, a mechanical probe can provide an amplified measurement of the virtual photons dressing the quantum ground state of an ultra strongly-coupled light-matter system while minimally disturbing it.

[1] C. Ciuti, G. Bastard and I. Carusotto, Phys. Rev. B **72**, 115303 (2005).
[2] S. De Liberato, D. Gerace, I. Carusotto, and C. Ciuti, Phys. Rev. A **80**, 053810 (2009).
[3] R. Stassi, A. Ridolfo, O. Di Stefano, M. J. Hartmann, and S. Savasta, Phys. Rev. Lett. **110**, 243601 (2013).
[4] M. Cirio, S. De Liberato, N. Lambert, F. Nori, Phys. Rev. Lett. **116**, 113601 (2016).
[5] M. Cirio, K. Debnath, N. Lambert, F. Nori, Phys. Rev. Lett. **119**, 053601 (2017).
[6] J. Lolli, A. Baksic, D. Nagy, V. E. Manucharyan, and C. Ciuti, Phys. Rev. Lett. **114**, 183601 (2015).

Twists of qubit energies in deep-strongly-coupled qubit-oscillator circuits

F. Yoshihara [1], T. Fuse [1], Z. Ao [1,2], S. Ashhab [3], K. Kakuyanagi [4], S. Saito [4], T. Aoki [2], and K. Semba [1]

[1] *National Institute of Information and Communications Technology, Koganei, Japan*
[2] *Depertment of Applied Physics, Waseda University, Tokyo, Japan*
[3] *Qatar Environment & Energy Research Institute, Doha, Qatar*
[4] *NTT Basic Research Laboratories, Atsugi, Japan*

The interaction between an atom and an electromagnetic field inside a cavity has played a crucial role in the development of our understanding of light-matter interaction and is a central part of various quantum technologies. The electromagnetic field inside a cavity renormalizes transition energies of an atom, by the Lamb shift and the ac Stark shift. The Lamb shift was first observed in a hydrogen atom. In circuit-QED experiments, the photon-number-dependent light shift (the ac Stark plus Lamb shifts) of the atom transition frequency was observed about ten years ago [1, 2].

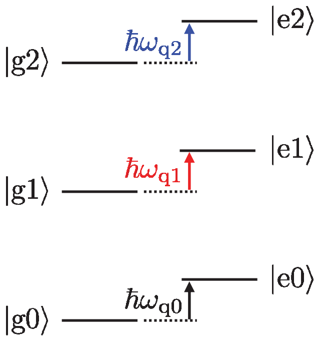

Fig. 1: energy levels of a qubit-oscillator circuit. g (e) indicates the ground (excited) state of a qubit, and 0, 1, 2 indicate the vacuum, 1-photon, and 2-photon states of an oscillator, respectively. ω_{qi} is the renormalized qubit transition frequency with *i*-photon in the oscillator.

The radiative shifts of an atom for large values of g/ω is expected to show interesting behaviors, where g is the coupling constant between an atom and an electromagnetic field in a cavity and ω is the resonance frequency of the cavity. The Lamb (n = 0) and n-photon ac Stark shifts can be described as $\omega_{qn}/\Delta = \exp[-2(g/\omega)^2]L_n[(2g/\omega)^2]/L_n(0)$ in the limit of $\Delta \ll \omega$ [3], where ω_{qn} is the photon-number-dependent renormalized qubit transition frequency (Fig. 1), Δ is the transition frequency of a non-interacting atom, and L_n is the Laguerre polynomials. ω_{qn} has n zero points, reflecting the nature of Laguerre polynomials (Fig. 2). Crossing the zero points, ω_{qn} changes its sign and the qubit energies "twist".

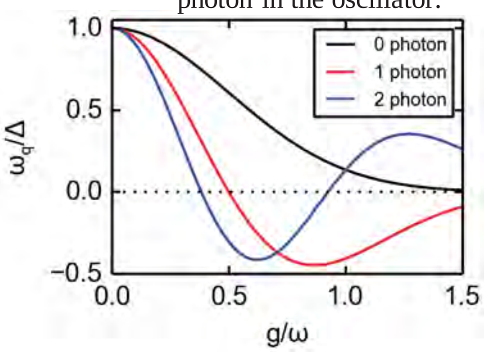

Fig.2: renormalized qubit transition frequencies

To explore the parameter range with large values of g/ω (~ 1.0), we use circuits of a superconducting flux qubit deep strongly coupled to an LC oscillator, where g is comparable to or larger than both Δ and ω [4]. The measured transition-energy spectra of the coupled circuits were fit by the Rabi model Hamiltonian $H_{Rabi} = \hbar\omega(a^\dagger a + 1/2) + \hbar(\Delta\sigma_x + \varepsilon\sigma_z)/2 + \hbar g(a + a^\dagger)\sigma_z$ [$a^\dagger$ (a): photon creation (annihilation) operator, σ_z (σ_x): qubit Pauli matrix, ħε: qubit's energy bias] and the circuit parameters, ω, Δ, and g, were obtained. The energies of the energy eigenstates up to the fifth excited states were obtained from measurements of five transition frequencies. In the presentation, experimentally observed Lamb and (1-photon and 2-photon) ac Stark shifts for g/ω ranging from 0.86 to 1.18 will be presented.

[1] D. I. Schuster et al., Nature **445**, 515 (2007).
[2] A. Fragner et al., Science **322**, 1357 (2008).
[3] S. Ashhab and Franco Nori, Phys. Rev. A **81**, 042311 (2010).
[4] F. Yoshihara, T. Fuse et al., Nature Phys. **13**, 44 (2017).

A coupling between a lamped element resonator and 4300 superconducting flux qubits ensemble

K. Kakuyanagi[1], Y. Matsuzaki[1], C. Déprez[1], H. Toida[1], K. Semba[2], H. Yamaguchi[1], W. J. Munro[1], and S. Saito[1]

[1]NTT Basic Research Laboratories, 3-1, Morinosato-Wakamiya, Kanagawa 243-0198, Atsugi, Japan
[2]National Institute of Information and Communication Technology, 4-2-1, Nukui-Kitamachi, Koganei, Tokyo 184-8795, Japan

A coupling between a resonator and an ensemble of two level systems has been considered as essential for quantum information processing [1]. Especially, this system can, in principle, provide a powerful experimental tool to observe new physical phenomena [2].

A superconducting qubit is an artificial two level system. Since the superconducting qubit is an artificial atom to have a large degree of freedom of design, it is easy to control the coupling energy and qubit energy. We can control energy bias of superconducting flux qubit by applying external magnetic field while we can control the gap energy by changing the size of Josephson junction of superconducting flux qubit. The coherent coupling between the resonator and flux-qubit ensemble would be a suitable candidate for the controllable quantum simulator, if realized. So we aimed to observe such a coherent coupling between them.

We fabricated a lamped element LC resonator and 4300 superconducting flux qubits. Each superconducting flux qubit has a shared edge with a line inductor (Fig. 1). So, the resonator is robust against unwanted broken Josephson junctions that some of the superconducting flux qubits could contain. It is expected that the behavior of the coupling should strongly depend on the detuning between resonator energy and qubit gap energy. So we prepared several samples whose averaged gap energy is different, and measured microwave transmission properties of lamped element LC resonator. When we measured the sample whose averaged gap energy is larger than resonator energy, we observed a large dispersive frequency shift in the spectrum, and this indicates a collective enhancement of the coupling from the flux qubit ensemble. From the measurement on the other sample where the gap energy is smaller than the resonator energy, the dispersive shift becomes much smaller, which could be explained by thermalisation of the flux qubits. We succeeded to reproduce these results by our theoretical model. Our results are relevant to realize a practical quantum simulator [3].

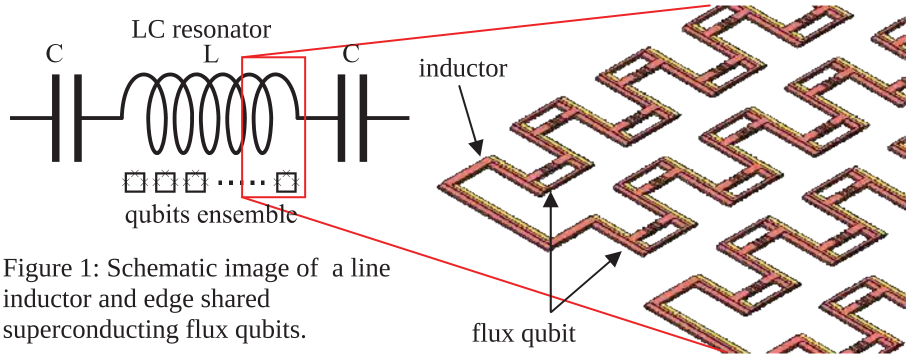

Figure 1: Schematic image of a line inductor and edge shared superconducting flux qubits.

[1] Z.-L. Xiang, S. Ashhab, J. You, and F. Nori, Rev. Mod. Phys. 85, 623 (2013).
[2] N. Lambert, Y. N. Chen, R. Johansson, and F. Nori, Phys.Rev. B 80, 165308 (2009).
[3] K. Kakuyanagi, Y. Matsuzaki, C. Déprez, H. Toida, K. Semba, H. Yamaguchi, W. J. Munro, and S. Saito, Phys. Rev. Lett. 117, 210503 (2016)

Strong-Coupling Silicon Charge and Spin Qubits to Microwave Photons

X. Mi[1], M. Benito[2], S. Putz[1], D. M. Zajac[1], J. M. Taylor[3,4,5], G. Burkard[2], and J. R. Petta[1]

[1] *Department of Physics, Princeton University, Princeton, NJ 08544, USA*
[2] *Department of Physics, University of Konstanz, D-78464 Konstanz, Germany*
[3] *Joint Quantum Institute/University of Maryland, College Park, Maryland 20742, USA*
[4] *Joint Center for Quantum Information and Computer Science/NIST, College Park, Maryland 20742, USA*
[5] *Research Center for Advanced Science and Technology, The University of Tokyo, Meguro-ku, Tokyo, Japan*

Coherent coupling of single electrons in Si gate-defined quantum dots to microwave photons provides a scalable pathway toward long-range entanglement, a necessary step for constructing large-scale spin-based quantum processors. We achieve the strong-coupling regime of light-matter interaction using both the charge and spin states of a single electron in a Si gate-defined double quantum dot. A strong charge-photon coupling is facilitated by an exceptionally low charge dephasing rate of 2.6 MHz possible in our hybrid device. We induce a strong spin-photon coupling by spin-charge hybridization in the presence of a magnetic field gradient, which enables spin-photon coupling rates above 10 MHz. Furthermore, we take advantage of this coupling to perform quantum non-demolition readout of a single-spin qubit using its dispersive interaction with the microwave cavity. Lastly, I will demonstrate the capability of the hybrid quantum device for high resolution valley states spectroscopy and present our group’s realization of a fast CNOT gate using two exchange-coupled single-spin qubits. Together, these results constitute major advances toward building a large-scale silicon quantum computer.

Acknowledgements

Research sponsored by ARO grant No. W911NF-15-1-0149, the Gordon and Betty Moore Foundation's EPiQS Initiative through Grant GBMF4535, and NSF DMR-1409556. Devices were fabricated in the Princeton University Quantum Device Nanofabrication Laboratory.

Long spin coherence of acceptor atoms in mechanically strained silicon

T. Kobayashi[1,2], J. van der Heijden[1], J. Salfi[1], C. Chua[1], M. G. House[1], B. C. Johnson[3], J. C. McCallum[3], H. Riemann[4], N. Abrosimov[4], P. Becker[5], H.-J. Pohl[6], M. Y. Simmons[1] and S. Rogge[1]

[1] *CQC2T, School of Physics, University of New South Wales, NSW 2052, Australia*
[2] *Department of Physics, Tohoku University, Sendai 980-8578, Japan*
[3] *CQC2T, School of Physics, University of Melbourne, VIC 3010, Australia*
[4] *Leibniz-Institut für Kristallzüchtung, 12489 Berlin, Germany*
[5] *PTB Braunschweig, 38116 Braunschweig, Germany*
[6] *VITCON Projectconsult GmbH, 07745 Jena, Germany*

Electron spins on shallow donors in isotopically purified ^{28}Si have demonstrated a robust coherence not only in a high-quality crystal [1] but in a field-effect-transistor structure as well [2]. This is the result of the scarcity of magnetic noise from nuclear spins due to the isotopically enriched environment in combination with the isolation from electric noise due to the lack of electric dipole moment of the electron spin in silicon. This last hallmark, however, is not compatible with long-range interaction between qubits, which is highly demanded for scalable quantum information architectures. In terms of long-range interaction, a qubit defined by a hole spin trapped by an acceptor atom in silicon is more attractive because of their intrinsic electric dipole moment. However, question of how decoherence is induced by the electric dipole moment has not been addressed yet. Here, we present measurements of the coherence time measured by spin echo decay T_{2SE} and the spin-lattice relaxation time T_1 of boron spins in mechanically strained ^{28}Si, showing a T_{2SE} in the same order of magnitude as phosphorus spins.

We carry out paramagnetic resonance measurements of a ^{28}Si:B sample (99.99+-% ^{28}Si with boron concentration of 1.0-1.5 x 10^{15} cm^{-3}) subjected to biaxial tensile stress. The T_{2SE} is near millisecond (Fig **a** red plots), which is in the same order of magnitude as phosphorus spins ^{28}Si. Yet, the T_1 (~5 ms) much shorter than donors implies the finite electric dipole moment of acceptor spins (Fig **b** red plots). Dynamical decoupling improves the coherence time up to 9 ms, which is nearly limited by T_1. A mechanically relaxed ^{28}Si:B sample shows T_{2SE} and T_1 one order of magnitude smaller than the strained sample (grey plots in Figs **a** and **b**), indicating that, to obtain robust coherence, the modification of the acceptor states by strain is crucial. Our results indicate the potential of acceptor spins in silicon as a solid-state qubit with robust coherence and long-range interaction.

[1] A. M. Tryshkin, et. al., Nature Materials **11**, 143-147 (2012).
[2] Y. Muhonen et al., Nature Nanotechnology **9**, 986-991 (2014).

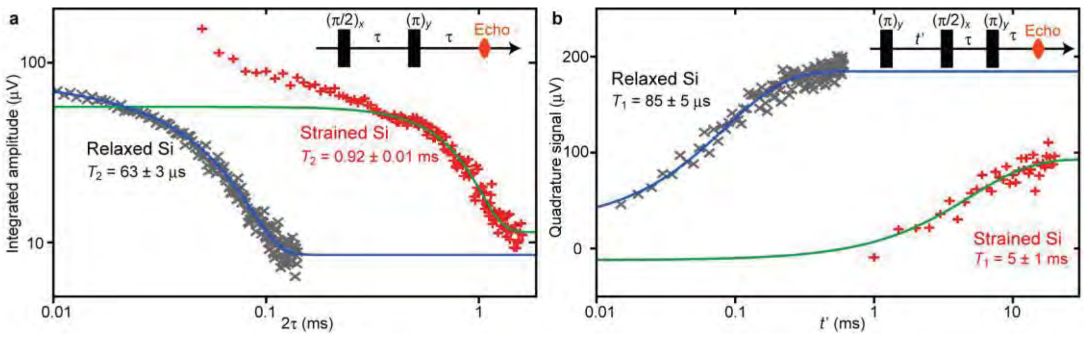

Figure **a** Hahn echo decays to measure T_2. **b** Inversion-recovery measurements of T_1.

Multi-level Landau-Zener-Stückelberg-Majorana transitions in a silicon-based single-electron interferometer

Sergey N. Shevchenko[1,2,3], **Anasua Chatterjee**[4], **Sylvain Barraud**[5], **Rubén Otxoa**[6,7], **Franco Nori**[1,8], **John J. L. Morton**[4,9], **and M. Fernando Gonzalez-Zalba**[6]

[1] *Center for Emergent Matter Science, RIKEN, Wako-shi, Saitama, Japan*
[2] *B. Verkin Institute for Low Temperature Physics and Engineering, Kharkov, Ukraine*
[3] *V. Kazarin Kharkov National University, Kharkov, Ukraine*
[4] *London Centre for Nanotechnology, University College London, London, United Kingdom*
[5] *CEA/LETI-MINATEC, CEA-Grenoble, Grenoble, France*
[6] *Hitachi Cambridge Laboratory, J. J. Thomson Avenue, Cambridge, United Kingdom*
[7] *Donostia International Physics Center, Donostia-San Sebastian, Spain*
[8] *Physics Department, University of Michigan, Ann Arbor, MI, USA*
[9] *Dept. of Electronic & Electrical Engineering, University College London, United Kingdom*

A driven quantum system experiences Landau-Zener-Stückelberg-Majorana (LZSM) transitions between its eigenstates [1]. When its coherence allows, this can include double-passage and multiple-passage interference [1,2]. Such processes for mesoscopic systems display quantum effects on macroscopic scales. Moreover, the LZSM fringes are useful for defining the parameters of the quantum system, as well as the parameters of its interaction with the environment, such as relaxation and coherence times.

An interesting element of quantum technologies is a charge qubit realized using a silicon-nanowire field-effect transistor. We recently demonstrated coherent charge oscillations in such transistor-based qubit [3]. In this system, at low temperatures, electrons are localized in the two top-most corners of the transistors due to the “corner effect” forming a double quantum dot (DQD). Such charge qubit is manipulated via the gate voltages by both dc signals, which control the energy level distance, and ac signals, which control the level occupation probabilities. In the low-driving-amplitude regime, only two states are relevant with an excess electron either in the left or in the right dot, denoted as 10 and 01 states. The charge state of this DQD modifies the resonant state of a coupled electrical resonator, which allows probing the DQD charge configuration. This is done by the qubit’s state dependent “quantum” capacitance that loads the resonator.

Under a stronger driving, additional energy levels, coming from the interaction of the qubit with a fermionic sea, are involved in the process. For our field-effect transistor, this involves the 00, 10, 01, and 11 charge states [4]. We demonstrate that in such a multi-level system several LZSM regimes may be realized. Depending on the driving parameters, one of the four regimes is considered, which we term as incoherent, double-passage, multi-passage, and multi-level incoherent regimes. Our report is devoted to the theoretical and experimental realization of those regimes in a silicon-based single-electron DQD. Such an interferometer displays rich physics and presents a four-in-one quantum device, implemented using the well-established metal-oxide semiconductor silicon technology.

[1] S.N. Shevchenko et al., Landau-Zener-Stuckelberg interferometry, Phys. Rep. **492**, 1 (2010).
[2] D. M. Berns et al., Coherent quasiclassical dynamics of a persistent current qubit, Phys. Rev. Lett. **97**, 150502 (2006).
[3] M. F. Gonzalez-Zalba et al., Gate-sensing coherent charge oscillations in a silicon field-effect transistor, Nano Lett. **16**, 1614 (2016).
[4] A. Chatterjee et al., A silicon-based single-electron interferometer coupled to a fermionic sea, in preparation.

Quantum Hall stripes in tilted magnetic fields

Michael A. Zudov[1], **Qianhui Shi**[1], **Qi Qian**[2], **Geoff C. Gardner**[3], **John D. Watson**[2], and **Michael J. Manfra**[2,3,4]

[1] *School of Physics and Astronomy, Univ. of Minnesota, Minneapolis, MN 55455, USA*
[2] *Department of Physics and Astronomy and Birck Nanotechnology Center, Purdue Univ., West Lafayette, Indiana 47907, USA*
[3] *School of Materials Engineering and School of Electrical and Computer Engineering, Purdue Univ., West Lafayette, Indiana 47907, USA*
[4] *Station Q Purdue, Purdue Univ., West Lafayette, Indiana 47907, USA*

It is well established that quantum Hall stripes (QHS) [1] in GaAs quantum wells are usually aligned along [110] crystal direction, for yet unknown reason, and that an in-plane magnetic field $B_{||}$ can reorient them perpendicular to it [2]. Here, we report the results showing that this "standard" picture is incomplete.

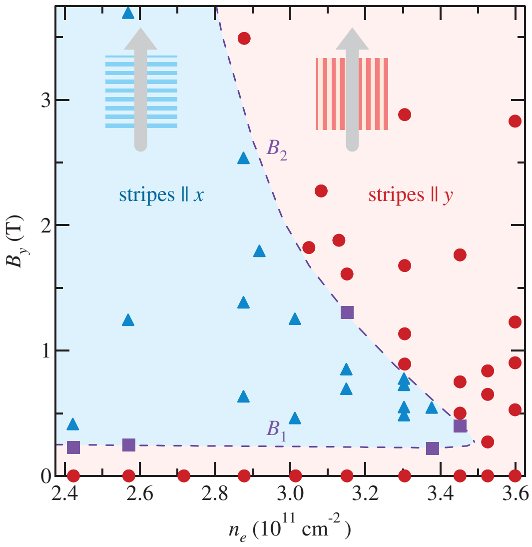

Figure 1: QHS orientation vs n_e and $B_{||} = B_y$ at $\nu = 9/2$. Triangles (circles) mark orientation perpendicular (parallel) to $B_{||}$. Squares mark isotropic states.

First, we show [3] that $B_{||}$ needed to reorient QHS depends on the filling factor ν within a given Landau level, giving rise to orthogonally-oriented QHS near and away from half-filling. Second, we present evidence [4] for a new symmetry breaking mechanism which ultimately aligns QHS *parallel* to $B_{||}$ and for a nontrivial coupling between the native and external symmetry breaking fields, which has not been theoretically considered. Finally, we demonstrate [5] that this mechanism sensitively depends on the carrier density n_e; as shown in Fig. 1, at $\nu = 9/2$ we detect one, two, and zero $B_{||}$-induced reorientations at low, intermediate, and high n_e, respectively. Our analysis suggests that screening might play an important role in determining stripe orientation providing guidance to future studies.

[1] A. A. Koulakov, M. M. Fogler, and B. I. Shklovskii, Phys. Rev. Lett. **76**, 499 (1996); M. P. Lilly, K. B. Cooper, J. P. Eisenstein, L. N. Pfeiffer, and K. W. West, Phys. Rev. Lett. **82**, 394 (1999); R. R. Du, D. C. Tsui, H. L. Stormer, L. N. Pfeiffer, K. W. Baldwin, and K. W. West, Solid State Commun. **109**, 389 (1999).

[2] W. Pan, R. R. Du, H. L. Stormer, D. C. Tsui, L. N. Pfeiffer, K. W. Baldwin, and K. W. West, Phys. Rev. Lett. **83**, 820 (1999); M. P. Lilly, K. B. Cooper, J. P. Eisenstein, L. N. Pfeiffer, and K. W. West, Phys. Rev. Lett. **83**, 824 (1999); T. Jungwirth, A. H. MacDonald, L. Smrcka, and S. M. Girvin, Phys. Rev. B **60**, 15574 (1999).

[3] Q. Shi, M. A. Zudov, J. D. Watson, G. C. Gardner, and M. J. Manfra, Phys. Rev. B **93**, 121404(R) (2016).

[4] Q. Shi, M. A. Zudov, J. D. Watson, G. C. Gardner, and M. J. Manfra, Phys. Rev. B **93**, 121411(R) (2016).

[5] Q. Shi, M. A. Zudov, Q. Qian, J. D. Watson, and M. J. Manfra, Phys. Rev. B **95**, 161303(R) (2017).

Quantum Processing with Phonons

Ben Sussman

Quantum Photonics Program
National Research Council, Canada
Ben.Sussman@nrc.ca

The fragility of the quantum state is a challenge facing all quantum technologies. Great efforts have been undertaken to mitigate the deleterious effects of decoherence by isolating quantum systems, for example, by cryogenically cooling and isolating in vacuum. State-of-the-art decoherence times are now measured in hours. An alternative approach we have been developing is to build quantum technologies that execute on ultrafast timescales—as short as femtoseconds—such that operations can be completed before decoherence overwhelms unitarity.

Until recently, most photonic approaches to quantum technologies have leveraged phenomena in atoms, ions, and micro-structured solid-state systems. In contrast, vibrations in molecules and bulk phonons have an array of attributes not available in these substrates, offering potential for exploitation in quantum technology platforms. We have explored a number of ultrafast systems, including molecular hydrogen and bulk diamond for quantum processing.

Like a classical memory, an essential component for quantum technologies is a quantum memory. Quantum memories can absorb single photons and release them on demand at a variable delay [1]. The short reset times – picosecond and nanosecond for diamond and hydrogen, respectively – can be useful in a wide range of emerging applications where high-bandwidth is required. We will discuss some of our development of quantum memories based on hydrogen and bulk diamond, as well as applications that these systems are suitable for including: quantum random number generation for secure cryptographic key generation [2], single-photon frequency conversation for device hybridization and multiplexing [3], and ultrafast slow-light for networking [4].

[1] Heshami, K., England, D. G., Humphreys, P. C., Bustard, P. J., Acosta, V. M., Nunn, J., & Sussman, B. J. (2016). Quantum memories: emerging applications and recent advances. *Journal of Modern Optics*, 1-24.

[2] Bustard, P. J., England, D. G., Nunn, J., Moffatt, D., Spanner, M., Lausten, R., & Sussman, B. J. (2013). Quantum random bit generation using energy fluctuations in stimulated Raman scattering. *Optics express*, 21(24), 29350-29357.

[3] Fisher, K. A., England, D. G., MacLean, J. P. W., Bustard, P. J., Resch, K. J., & Sussman, B. J. (2016). Frequency and bandwidth conversion of single photons in a room-temperature diamond quantum memory. *Nature communications*, 7.

[4] Bustard, P. J., Heshami, K., England, D. G., Spanner, M., & Sussman, B. J. (2016). Raman-induced slow-light delay of THz-bandwidth pulses. *Physical Review A*, 93(4), 043810.

Spontaneous emission enhanced by Purcell effect in a set of optomechanical cavities

Feng Tian [1,2], Hisashi Sumikura [1,2], Eiichi Kuramochi [1,2], Masato Takiguchi [1,2], Masaaki Ono [1,2], Hideaki Taniyama [1,2], Akihiko Shinya [1,2] and Masaya Notomi [1,2]

[1] *NTT Basic Research Laboratories*
[2] *NTT Nanophotonics Center*

Purcell effect describes the enhancement of spontaneous emission (SE) rate by a cavity environment [1]. It has been reported that the SE from dopants in silicon (Si) is speeded up by Purcell effect, where copper isoelectronic centres (Cu-IECs) are doped into Si photonic crystal (PhC) cavity [2]. The L3 PhC cavity is used in previous study, while in this paper, double coupled nanobeam PhC cavities are adopted for the SE enhancement. Both two types of cavities possess good coupling between dopants and cavity modes, but double coupled nanobeam PhC cavities, an typical optomechanical configuration [3,4], have mechanical degree of freedom strongly interacting with cavity modes, so they can potentially enable the optomechanical control of the SE process.

Figure 1(a) and (b) show the global view of the device and the detailed cavities, respectively. The cavities' central region is empty for reserving large amount of dopants, and the PhC mirror segments in both sides are gradually tapered to the central region for less scattering loss. Cavities' even mode is shown in Fig. 1(c), which has much larger optomechanical interaction. The fundamental in-plane mechanical mode is simulated in Fig. 1(d) and the measured corresponding resonance is shown in Fig. 1(e). There are two devices, one has cavity modes detuned from zero-phonon line (ZPL) (Fig. 2(a)) while the other's even mode coincides with ZPL (Fig. 2(b)). It is clear that the SE is drastically enhanced in the Fig. 2(b). Besides, the decay rate measured in Fig. 2(c) is as fast as that in Ref. 2.

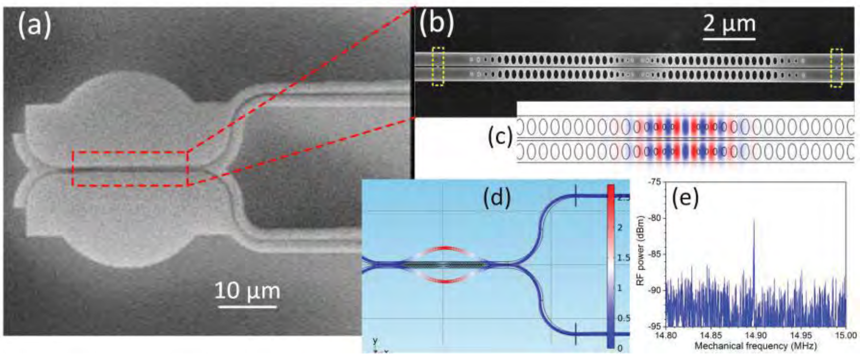

Fig. 1(a) Global view SEM image of the device. (b) Close-up SEM image of the coupled nanobeam cavities. (c) FDTD simulated cavities' even mode. (d) FEM simulated fundamental in-plane mechanical mode. (e) Measured mechanical resonance corresponding to mode in (d).

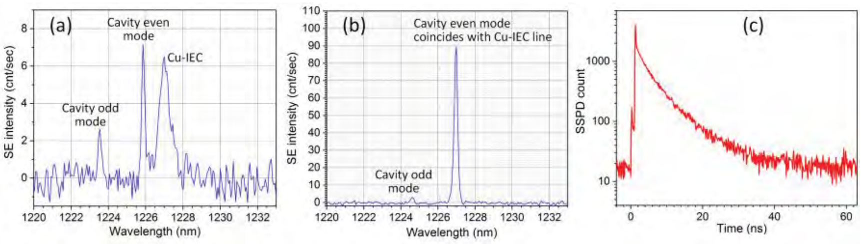

Fig. 2(a) PL spectrum of the device, where two coupled cavity modes and ZPL of Cu-IECs are observed. (b) The even mode coincides with ZPL and the SE intensity is drastically enhanced. (c) Fast SE decay rate.

[1] E. M. Purcell, Phys. Rev. **69**, 681 (1946).
[2] H. Sumikura, E. Kuramochi, H. Taniyama, and M. Notomi, Sci. Rep. **4**, 5040 (2014).
[3] M. Eichenfield, R. Camacho, J. Chan, K. J. Vahala, and O.Painter, Nature **459**, 550-555 (2009).
[4] F. Tian, H. Sumikura, E. Kuramochi, H. Taniyama, M. Takiguchi, and M. Notomi, Opt. Express **24**, 28039-28055 (2016).

Optoplasmonic rolled-up-microtube cavities

Yin Yin and Oliver G. Schmidt

Leibniz Institute for Solid State and Materials Research Dresden, Germany

Optical whispering-gallery-mode (WGM) microcavities, which are of importance for the study of light-matter interactions and applications such as optical sensing and communications, have gained considerable interest in recent years [1]. Combination of the dielectric WGM microcavities with noble metal layers, consists the optoplasmonic cavities, giving rise to the coupling between resonant light and surface plasmons [2, 3]. In contrast to the pure photonic modes in WGM microcavities, hybrid photon-plasmon modes in optoplasmonic microcavities preserve the high-quality resonances and possess enhanced plasmon-type field localized at the metal layer which are promising for the enhanced light-matter interactions and sensing applications.

To push the light-plasmon coupling to a limit, the microtube cavities fabricated by rolled-up tech are the suitable platforms which benefit from the strong evanescent field supported by the ultra-thin cavity wall [4]. In this presentation, the hybrid modes with different plasmon-types of evanescent field in the optoplasmonic microtube cavities are firstly discussed [5]. The basic physical mechanism for the generation of plasmon-type field is comprehensively investigated based on an effective potential approach. In particular, when the cavity wall becomes ultra-thin, the plasmon-type field can be greatly enhanced, and the hybrid modes are identified as strong photon-plasmon hybrid modes which are experimentally demonstrated in the metal-coated rolled-up-microtube cavities [6]. By designing a metal nanocap onto the rolled-up-microtube cavities, angle-dependent tuning of hybrid photon-plasmon modes are realized, in which transverse electric (*TE*) and transverse magnetic (*TM*) polarized modes exhibit inverse tuning trends due to the polarization match/mismatch [7]. And a novel sensing scheme is proposed relying on the intensity ratio change of *TE* and *TM* modes instead of conventionally used mode shift. In addition, localized surface plasmon resonances coupled to resonant light is explored by designing a vertical metal nanogap on rolled-up-microtube cavities. Selective coupling of high-order axial modes is demonstrated depending on spatial-location of the metal nanogap [8]. A modified quasi-potential well model based on perturbation theory is developed to explain the selective coupling mechanism.

These researches systematically explore the design of optoplasmonic microtube cavities and the mechanism of photon-plasmon coupling therein, providing a novel platform for the study of both fundamental and applied physics such as the enhanced light-matter interactions, topology optics and label-free sensing [9, 10].

[1] K. J. Vahala, **Nature** 424, 839 (2003)
[2] B. Min *et al.*, **Nature** 457, 455 (2009)
[3] Y-F. Xiao *et al.*, **Phys. Rev. Lett.** 105, 153902 (2010)
[4] O. G. Schmidt *et al.*, **Nature** 410, 168 (2001)
[5] Y. Yin *et al.*, **Phys. Rev. A** 94, 013832 (2016)
[6] Y. Yin *et al.*, **Phys. Rev. B** 92, 241403(R) (2015)
[7] Y. Yin *et. al.*, **ACS Photonics** 4, 736 (2017)
[8] Y. Yin *et. al.*, **Phys. Rev. Lett.** 116, 253904 (2016)
[9] Y. Yin *et. al.*, **Laser Photon. Rev.** 11, 1600219 (2017)
[10] L. B. Ma *et. al.*, **Nat. Commun.** 7, 10983 (2016)

Towards nano topological photonics

Xiao HU

International Center for Materials Nanoarchitectonics (WPI-MANA)
National Institute for Materials Science (NIMS), Tsukuba, Japan

Honeycomb lattice plays an extremely important role in fostering topology physics as known from the Haldane model and the Kane-Mele model [1]. Recently, we propose a way to achieve all-dielectric topological photonics starting from honeycomb structure. We identify a pseudospin degree of freedom in electromagnetic (EM) modes hosted by honeycomb lattice, which can be explored for establishing topological EM states with time-reversal symmetry [2]. We demonstrate theoretically the nontrivial topology in terms of photonic band inversions and indices of C_2 symmetry at high-symmetry points in Brillouin zone. I will show recent experimental results of microwaves which confirm our theory [3]. The idea can also be applied for other bosonic systems such as phonons as well as electronic systems [4, 5]. Recent progresses and perspectives of the present approach will be discussed.

[1] H.-M. Weng, R. Yu, X. Hu, X. Dai and Z. Fang, Adv. Phys. vol. 64, 227 (2015).
[2] L.-H. Wu and X. Hu: Phys. Rev. Lett. vol. 114, 223901 (2015).
[3] Y.-T. Yang, J.-H. Jiang, X. Hu and Z.-H. Hang: arXiv.1610.07780.
[4] L.-H. Wu and X. Hu: Sci. Rep. vol. 6, 24347 (2016).
[5] T. Kariyado and X. Hu: arXiv.1607.08706.

Electric-field switchable second-harmonic generation in bilayer MoS_2 by inversion symmetry breaking

J. Klein,[1] J. Wierzbowski,[1] A. Steinhoff,[2] M. Florian,[2] M. Rösner,[2,3] F. Heimbach,[4] K. Müller[1], F. Jahnke,[2] T. O. Wehling,[2,3] J. J. Finley,[1] and M. Kaniber[1]

[1]*Walter Schottky Institut und Physik Department, Technische Universität München, Am Coulombwall 4, 85748 Garching, Germany*
[2]*Institut für Theoretische Physik, Universität Bremen, P.O. Box 330 440, 28334 Bremen, Germany*
[3]*Bremen Center for Computational Materials Science, Universität Bremen, 28334 Bremen, Germany*
[4]*Lehrstuhl für Physik funktionaler Schichtsysteme, Physik Department E10, Technische Universität München, James-Frank-Straße 1, 85748 Garching Germany*

We present electric-field switchable second-harmonic generation in the 2H-stacked bilayer transition metal dichalcogenide (TMDC) MoS_2 [1]. The second order susceptibility and, hence, the nonlinear conversion efficiency is tuned by applying large electric fields, perpendicular to the basal plane to controllably break macroscopic inversion symmetry of the crystal. This is achieved using Si(n)-SiO_2-TMDC-Al_2O_3-metal micro-capacitor devices that facilitate application of static electric fields up to $|F| = 2.6$ MVcm^{-1} to electrically isolated flakes, while facilitating optical access (fig 1a) [2]. Upon exciting bilayer regions of mechanically exfoliated MoS_2 using ~ 70 fs duration pulses tuned between 1.24 – 1.47 eV, we observe strong electric-field tunable second-harmonic signal that varies according to $(F-F_0)^2$, where F_0 is the electric field for which local inversion symmetry is re-established (fig 1b). The spectral dependence of the electric-field-induced SHG signal is shown to reflect the local bandstructure and wave function admixture. Furthermore, it exhibits particularly strong tunability below the C-resonance, in good agreement with density functional theory calculations. We show that the field-induced second-harmonic generation relies on the interlayer coupling in the bilayer. Our findings strongly suggest that the strong tunability of the electric-field-induced second-harmonic generation signal in bilayer TMDCs may find applications in miniaturized electrically switchable nonlinear devices.

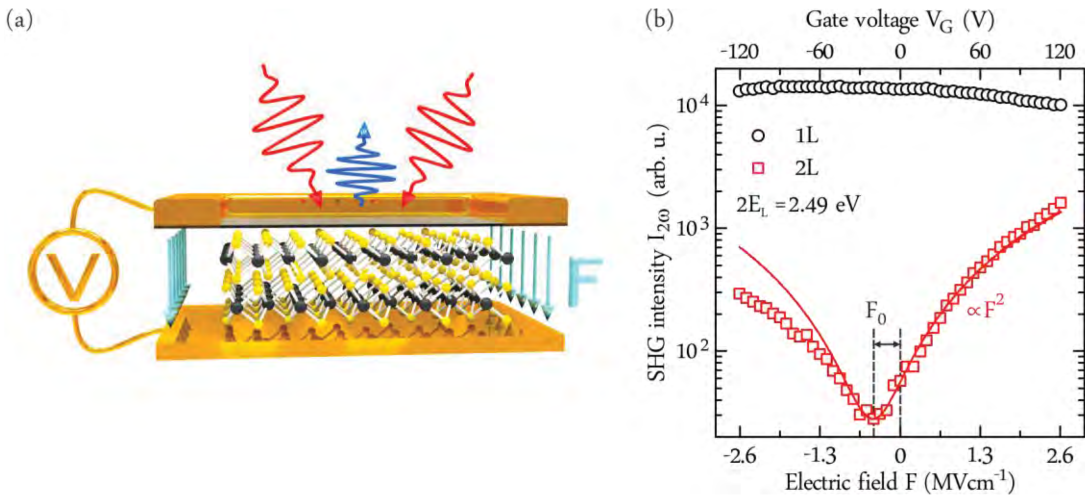

Figure 1: (a) Schematic illustration of the bilayer embedded in the microcapacitor device. (b) Electric-field (voltage) dependent SHG signal of mono- and bilayer MoS_2

[1] Klein *et al.*, Nano Lett. **17**, 392-398 (2017)
[2] Klein and Wierzbowski *et al.*, Nano Lett. **16**, 1554-1559 (2016)

Spatio-temporal coherent control of light transport in disordered materials

M. Mounaix[1], **S. Gigan**[1]

[1]*Laboratoire Kastler Brossel, ENS-PSL, CNRS, UPMC, Paris, France*

Phase and amplitude information of coherent light are seemingly lost during propagation through nanoscale disordered photonic materials, mainly because of multiple scattering events. Nonetheless, light scattering is deterministic: transmitted light through the material can be controlled using a spatial light modulator, under illumination of a monochromatic coherent beam [1]. For instance, light can be focused in arbitrary spatial position with the measurement of an operator, the transmission matrix [2]. However, if the laser is broadband, such as an ultrashort pulse of light (duration $\sim$ 100 fs), the scattering medium responds differently for the different spectral components of the pulse. This complex spatio-spectral/temporal coupling of light by the medium results in a temporal broadening of the pulse (average duration $\sim$ 1 ps - 10 ps) [3].

In this work, we extend the previous monochromatic control of light to the broadband regime. By measuring either the transmission matrix of the medium, composed of ZnO nanobeads randomly distributed, for all the spectral components of the pulse [3], or for all the arrival times of transmitted photons [4], we can coherently manipulate transmitted light both in space and time. We exploit these operators to achieve spatio-temporal focusing of the output pulse at any arbitrary space and time position. The pulse is recompressed almost its Fourier-limited time-width, and it is spatially diffraction-limited. We also generate more sophisticated spatio-temporal profiles such as pump-probe pulse.

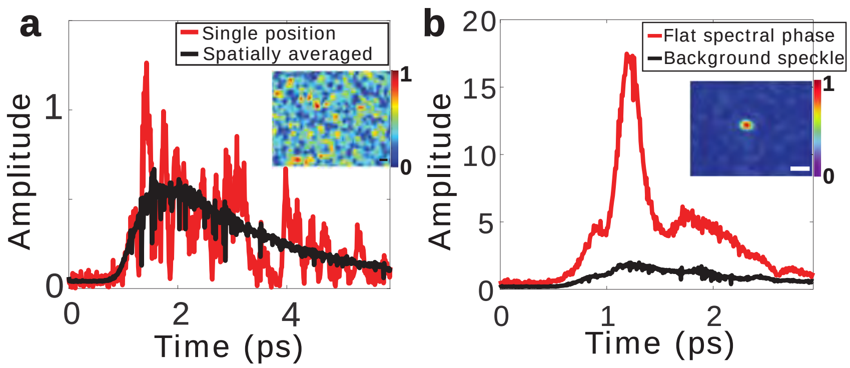

Figure 1: **(a)** Temporal profile of light through ZnO nanobeads randomly distributed. Naturally, the pulse is temporally stretched (red). The averaged signal has an exponential decay (black). **(b)** The output pulse can be spatially focused, and temporally compressed to its initial duration (red) via adjusting its spectral phase. Inset: CCD image.

This deterministic control of light opens perspectives in coherent control in disordered media. Its extension to quantum system [5] enables control of two-photon interference: it paves the way for future photonic devices for quantum computing, and communication.

[1] S. Rotter and S. Gigan, Rev. Mod. Phys., **89**, 015005, (2017)
[2] S. Popoff et al, Phys. Rev. Lett., **104**, 100601, (2010)
[3] M. Mounaix et al., Phys. Rev. Lett., **116**, 253901, (2016)
[4] M. Mounaix et al., Phys. Rev. A, **94**, 041802 (R), (2016)
[5] H. Defienne et al., Sci. Adv., **2**, e1501054, (2016)

Estimation of π-π Electronic Couplings from Current Measurements

J. Trasobares [1], J. Rech [2] T. Jonckheere [2], T. Martin[2], O. Aleveque[3], E. Levillain[3], V. Diez-Cabanes[4], Y. Olivier[4], J. Cornil[4], J.P. Nys[1], R. Sivakumarasamy[1], K. Smaali[1], P. Leclere[4], A. Fujiwara[5], D. Theron[1], D. Vuillaume[1] and N. Clement[5]

[1] *Institute of Electronics, Microelectronics and Nanotechnology, CNRS, Univ. of Lille, Avenue Poincaré, BP60069, 59652, Villeneuve d'Ascq France*
[2] *Aix Marseille Univ., Universite de Toulon, CNRS, CPT, 163 Avenue de Luminy, 13288 Marseille cedex 9, France*
[3] *Université d'Angers, CNRS UMR 6200, Laboratoire MOLTECH-Anjou, 2 bd Lavoisier, 49045 Angers cedex, France*
[4] *Laboratory for Chemistry of Novel Materials, University of Mons, Place du Parc 20, B-7000 Mons, Belgium*
[5] *NTT Basic Research Laboratories, 3-1, Morinosato Wakamiya, Atsugi-shi, kanagawa, 243-0198, Japan*

The π-π interactions between organic molecules are among the most important parameters for optimizing the transport and optical properties of organic transistors, light-emitting diodes, and (bio-) molecular devices. Despite substantial theoretical progress, direct experimental measurement of the π-π electronic coupling energy parameter t has remained an old challenge due to molecular structural variability and the large number of parameters that affect the charge transport. Here, we propose a study of π-π interactions from electrochemical and current measurements on a large array of ferrocene-thiolated gold nanocrystals [1]. We confirm the theoretical prediction that t can be assessed from a statistical analysis of current histograms [2]. The extracted value of $t \approx 35$ meV is in the expected range based on our density functional theory analysis. Furthermore, the t distribution is not necessarily Gaussian and could be used as an ultrasensitive technique to assess intermolecular distance fluctuation at the sub-angström level. The present work establishes a direct bridge between quantum chemistry, electrochemistry, organic electronics, and mesoscopic physics, all of which were used to discuss results and perspectives in a quantitative manner.

[1] J. Trasobares et al., *Nanolett.* **17**, 3215 (2017).
[2] M.G. Reuter, et al. *Nano Lett.* **12**, 2243 (2012)

Challenges for nanocar and molecular machine by nm-size tip approach and cm-level hand motion

Katsuhiko Ariga[1,2] **and Waka Nakanishi**[1]

[1] *WPI-MANA, National Institute for Materials Science (NIMS)*
[2] *Graduate School of Frontier Sciences, The University of Tokyo*

Manipulation of ultrasmall functional objects, nanocars and molecular machines, is considered as an ultimate technical goal of nanotechnology. Motional regulations of nano-objects have been performed using nm-size tip approach. In fact, we had world-wide competition of nanocars on the based on scanning tunneling microscope technology.[1-3]

Unlike the above-mentioned common-sense approach, we have been proposing a novel methodology, hand-operating nanotechnology,[4,5] where molecular orientation, organization and even functions in nanometer-scale can be operated by our macroscopic operation such as human-hand-level motions. This concept can be realized at dynamic two-dimensional medium such as thin films at the air-water interface because this medium possess both features of bulk and molecular dimension. For example, we successfully manipulated molecular machines at the air-water interface upon bulk (10-100 cm size) motion of the entire monolayer and realized “capture and release” of aqueous guest molecules using molecular machine, steroid cyclophane (Figure right). In addition, mechanically controlled chiral recognition of amino acid and discrimination of nucleosides by the supramolecular monolayer was successfully demonstrated.

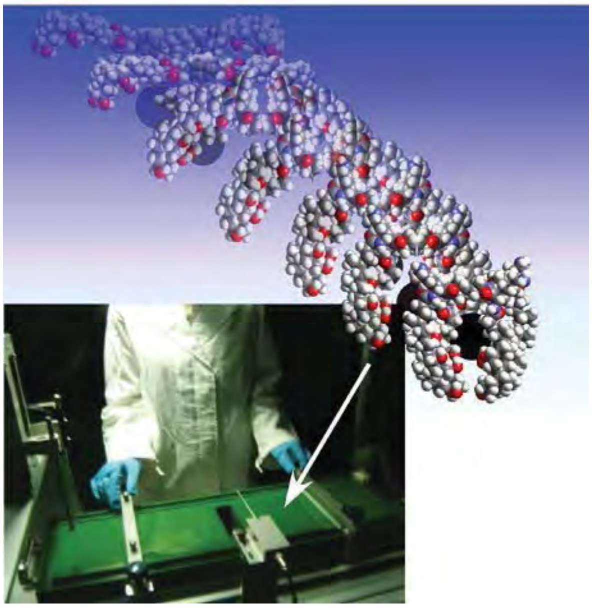

These examples demonstrate our new concept, manual nanotechnology so-called, hand-operating nanotechnology, with which we can manually control nano/molecular phenomena and functions by macroscopic mechanical force such as hand motions. Using hands for functional operation would be most environmentally friendly and least energy consuming technology.

[1] D. Castelvecchi, Nature **544**, 278 (2017). Drivers gear up for world’s first nanocar race: Chemists will navigate molecular wagons along a tiny golden track.
[2] Y. Shirai *et al.*, Jpn. J. Appl. Phys. **55**, 1102A2 (2016). Driving nanocars and nanomachines at interfaces: From concept of nanoarchitectonics to actual use in world wide race and hand operation.
[3] W.-H. Soe *et. al.*, ACS Nano in press DOI: 10.1021/acsnano.7b05314. Conformation manipulation and motion of a double paddle molecule on an Au(111) surface.
[4] K. Ariga *et al.*, Polym. J. **48**, 371 (2016). What are emerging concepts and challenges in NANO?: Nanoarchitectonics, hand-operating nanotechnology, and mechanobiology.
[5] K. Ariga *et al.*, Chem. Mater. **26**, 519 (2014). Bridging the difference to the billionth-of-a-meter length scale: How to operate nanoscopic machines and nanomaterials by using macroscopic actions.

Stochastic Thermodynamics in Superconducting and Hybrid Circuits

Jukka P. Pekola

Low Temperature Laboratory, Aalto University, 00076 Aalto, Finland

I present first experiments on stochastic thermodynamics based on controlling and measuring transport of single electrons in nanoscale circuits [1]. Common fluctuation relations can be verified in these systems with high accuracy thanks to statistics in a large number of experiments. Two types of Maxwell demons, a Szilard engine and an autonomous Maxwell demon, have been realized, where information is used to extract heat from a bath [2,3]. Our current efforts aim at realizing a single microwave photon detector and quantum heat engines based on superconducting quantum circuits [4,5]. Preliminary experiments will be presented.

[1] O.-P. Saira, Y. Yoon, T. Tanttu, M. Möttönen, D.V. Averin, and J.P. Pekola, *Test of Jarzynski and Crooks fluctuation relations in an electronic system*, Phys. Rev. Lett. **109**, 180601 (2012).
[3] J. P. Pekola, *Towards quantum thermodynamics in electronic circuits*, Nature Physics **11**, 118 (2015).
[2] J. V. Koski, A. Kutvonen, I. M. Khaymovich, T. Ala-Nissila, and J. P. Pekola**,** *On-chip Maxwell's demon as an information-powered refrigerator*, Phys. Rev. Lett. **115**, 260602 (2015).
[4**]** S. Gasparinetti, K. L. Viisanen, O.-P. Saira, T. Faivre, M. Arzeo, M. Meschke, and J. P. Pekola**,** *Fast electron thermometry towards ultra-sensitive calorimetric detection***,** Phys. Rev. Applied **3**, 014007 (2015).
[5] B. Karimi and J. P. Pekola, *Otto refrigerator based on a superconducting qubit: Classical and quantum performance*, Phys. Rev. B **94**, 184503 (2016).

Shot Noise and Feedback in Single-Electron Tunneling through Quantum Dots

Rolf J. Haug

Institut für Festkörperphysik, Leibniz Universität Hannover, Germany

Electronic transport through quantum dots, i.e. quasi zero-dimensional systems in semiconductors, is governed by single-electron tunneling and Coulomb interactions. In studying shot noise in tunneling through quantum dots one has access to correlations in these systems in a variety of ways. In applying ultrasensitive noise and correlation measurements deep insight into the quantum mechanical properties of the systems studied is obtained. Such electron transport experiments with quantum dots can be performed in very similar ways to experimental arrangements in quantum optics. So, e.g. electron pairs can be generated on demand and the splitting and partitioning of these electron pairs can be investigated [1]. Another scheme often applied in quantum optics is the usage of feedback to influence the quantum mechanical states. Recently, we were successfully applying feedback control in experiments with quantum dots and we showed that the full counting statistics of such systems can be strongly influenced [2,3]. We were able to demonstrate that in this way one can generate an extremely stable electrical current. In addition we analyzed shot noise in single-electron tunneling in a variety of different ways to acquire further knowledge about single-electron tunneling through quantum dots.

[1] N. Ubbelohde, F. Hohls, V. Kashcheyevs, T. Wagner, L. Fricke, B. Kästner, K. Pierz, H.W. Schumacher, R.J. Haug; Nature Nanotech. 10, 46 (2015).

[2] T. Wagner, P. Strasberg, J.C. Bayer, E.P. Rugeramigabo, T. Brandes, R.J. Haug; Nature Nanotech. 12, 218 (2017).

[3] T. Wagner, J.C. Bayer, E.P. Rugeramigabo, R.J.Haug; Phys. Status Solidi B 254, 1600701 (2017).

Power generation with Maxwell's demon in a silicon nanodevice

Kensaku Chida, Katsuhiko Nishiguchi and Akira Fujiwara
NTT Basic Research Laboratories, Morinosato-Wakamiya, Atsugi, 243-0198, Japan

Maxwell's demon is an entity that can perform a feedback operation based on observations at the level of thermal fluctuation and convert information into energy [1]. Improvements in experimental techniques have enabled researchers to accomplish the feedback operation in their laboratories [2, 3]. In this study, we demonstrated power generation with Maxwell's demon in a silicon nanodevice in one of the most natural ways [4].

Our device is made on a silicon-on-insulator wafer and consists of a single-electron box (SEB) that is electrostatically defined by gate electrodes of two transistors, G1 and G2, and a detector with single-electron sensitivity, which can detect thermal fluctuation in the SEB at the single-electron level [5]. The SEB connects to the source (S) and drain (D) through G1 and G2, respectively (Fig.1). The electron transition rates between the S(D) and SEB is tuned by the voltage applied to G1(G2). The number of electrons in the SEB is monitored in real time at a frequency of about 14 Hz by measuring current through the detector (I_{det}). Based on the observation, we open and close G1 and G2 alternately as shown in Fig. 2. All the measurements were performed at room temperature.

By repeating the protocol in Fig. 2, we rectify the thermal motion of electrons from the S to D, to generate electrical power. When the source-drain bias voltage V_{SD} is ~ 30 mV, the generated power shows the maximum value of 0.5 zW and the information-to-energy conversion efficiency of 18%. Those values are reasonably reproduced by Monte-Carlo simulation, which provides the maximum power and efficiency of 0.7 zW and 24%, respectively. This consistency indicates that silicon nanodevices are an ideal platform for studying Maxwell's demon. Moreover, the simulation shows that the power output increases as the detector becomes faster. However, to increase the efficiency, we should also consider the protocol. In the protocol in this study, measurements without feedback operation wasted information and decreased efficiency. To reduce the waste, a protocol like the one for the Szilard engine is preferred, namely one that can thoroughly use the information and in which the feedback operation performed after each measurement.

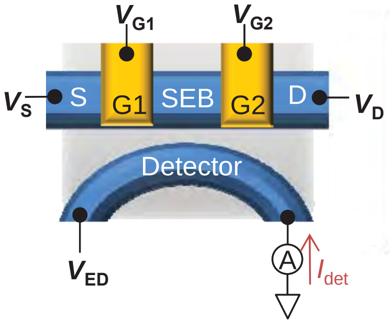

Fig. 1. Schematic illustration of our device.

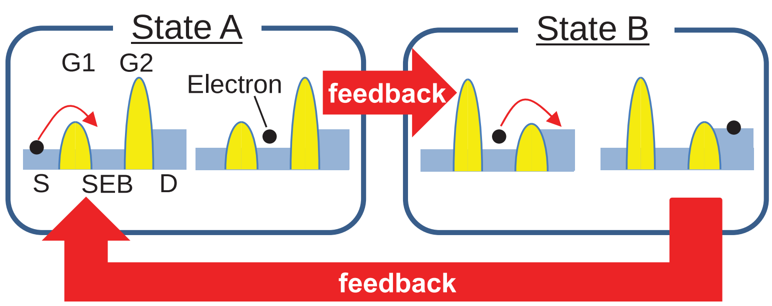

Fig. 2. Schematic illustration of Maxwell's demon operation to rectify thermal motion of electrons.

[1] For example, J. M. R. Parrondo, J. Horowitz, and T. Sagawa, Nat. Phys. **11**, 131 (2015), and references therein. [2] For example, S. Ciliberto, Phys. Rev. X **7**, 021051 (2017); A. Rex, Entropy **19**, 240 (2017). [3] J. V. Koski *et al.*, Proc. Natl. Acad. Sci. **111**, 13786 (2014); J. V. Koski *et al.*, Phys. Rev. Lett. **113**, 030601 (2014); J. V. Koski *et al.*, Phys. Rev. Lett. **115**, 260602 (2015); K. Chida *et al.*, Appl. Phys. Lett. **107**, 073110 (2015); A. Hofmann *et al.*, Phys. Rev. B **93**, 035425 (2016); T. Wagner *et al.*, Nat. Nanotechnol. **12**, 218 (2017). [4] K. Chida *et al.*, Nat. Commun. **8**, 15301 (2017). [5] K. Nishiguchi *et al.*, Nanotechnology **25**, 275201 (2014).

Quench dynamics in superconducting nanojuncions: metastability and dynamical phase transitions

R Seoane Souto, A. Martín-Rodero and A. Levy Yeyati

Departamento de Fsica Terica de la Materia Condensada, Condensed Matter Physics Center (IFIMAC) and Instituto Nicols Cabrera, Universidad Autnoma de Madrid E-28049 Madrid, Spain

The shot noise and the higher order cumulants contain valuable information about interactions and quantum correlations between electrons in nanodevices. While these studies have traditionally been restricted to the stationary case, recent technological advances in the direction of the single electron detection have attracted an increasing interest in the time resolved full counting statistics (FCS). On the other hand, superconducting nanodevices are of central interest as building blocks in quantum technologies. In this kind of devices, an unexplained excess of quasiparticles has been observed, which set the limit for possible applications. In superconducting atomic junctions these quasiparticles can decay to the Andreev bound states, giving rise to long lived odd parity states [1].

In this presentation I will focus in the dynamics of the charge transfer through nanojunctions coupled to superconducting electrodes. Under rather general conditions, the system gets trapped in a metastable state, characterized by a non-equilibrium population of the Andreev bound states. Although the trapped quasiparticles lead to a peculiar time dynamics, the quantum state of the system cannot be inferred from the evolution of the single particle observables. Instead, the information provided by the full counting statistics is needed to fully characterize the state [2, 3].

Finally, I will also demonstrate that the evolution of the roots of the FCS generating function, recently measured experimentally for the first time in a superconducting nanojunction [4], contain all the information about the system transport properties. Their evolution also allows to identify dynamical quantum phase transitions, much in the same way as the Lee Yang zeros of the partition function are connected to phase transitions in the equilibrium mechanics [5]. I will also discuss when a simplified description of the system dynamics based on the dominant zeros is possible and the kind of information that can be obtained from the lower current cumulants.

[1] M. Zgirski, L. Bretheau, Q. Le Masne, H. Pothier, D. Esteve, and C. Urbina, Phys. Rev. Lett. **106**, 257003 (2011).

[2] R. S. Souto, A. Martn-Rodero, and A. L. Yeyati, Phys. Rev. Lett. **117**, 267701 (2016).

[3] R. S. Souto, A. Martn-Rodero, and A. L. Yeyati, arXiv:1707.01844 (2017).

[4] K. Brandner, V. F. Maisi, J. P. Pekola, J. P. Garrahan and C. Flindt, Phys. Rev. Lett. **118**, 180601 (2017).

[5] C. N. Yang and T. D. Lee, Phys. Rev. 87, 404 (1952). T. D. Lee and C. N. Yang, Phys. Rev. **87**, 410 (1952).

Drift-induced enhancement of cubic Dresselhaus spin-orbit interaction in two-dimensional electron gas

Y. Kunihashi[1], H. Sanada[1], Y. Tanaka[1], H. Gotoh[1], K. Onomitsu[1], K. Nakagawara[2], M. Kohda[2], J. Nitta[2], and T. Sogawa[1]

[1] *NTT Basic Research Laboratories, NTT Corporation, Atsugi, Japan*
[2] *Department of Materials Science, Tohoku University, Sendai, Japan*

The electrical control of spin dynamics by using spin-orbit effective magnetic fields is one of the fundamental technologies for future spintronics devices. In previous studies, it has been demonstrated that only the Rashba spin-orbit interaction (SOI) is controlled by a gate electric field in III-V semiconductor heterostructures. Here, we show the experimental demonstration of electrically-controlled Dresselhaus SOI by application of in-plane electric field for electron spins laterally drifting in a GaAs quantum well. The strengths of SOI were quantitatively estimated from spin precession periods measured by using spatially resolved Kerr rotation microscopy. The in-plane electric field dependence of the spin precession frequency for steadily drifting spins reveals that the strength of a cubic Dresselhaus SOI is varied by an in-plane electric field induced change in the momentum distribution in an electron system. Our achievement will provide a new way to control electron spins with the cubic Dresselhaus SOI and will be of great importance as regards a further understanding of spin transport dynamics.

The drift transport of electron spins optically injected into a GaAs quantum well was detected as spatially oscillating Kerr rotation signals θ_K at $T = 8$ K. In Fig. 1, the spatial profile of drifting spins in [1-10] direction show the velocity-dependent shift of the precession phase that becomes clearer with increasing pump-probe distance. The spatial frequency of the spin precession was extracted by fitting the experimental data to a model function $\theta_K = A\exp(-d/l_{SO})\cos(k_{SO}d)$, where d is the distance from the pump position, l_{SO} is the spin decay length and k_{SO} is the wavenumber that represents the spatial frequency of the spin precession. k_{SO} decreases monotonically with increases in drift velocity v_d for all crystallographic directions, indicating that the effective magnetic fields are weakened by applying in-plane electric fields. The experimentally observed drift velocity dependence of k_{SO} cannot be explained by the presence of a k-linear SOI, since the k_{SO} originating from the k-linear SOI is constant for the drift velocity [1]. A model developed for drifting spins with a heated electron distribution characterized by electron temperature T_e suggests that the in-plane electric field enhances the cubic Dresselhaus SOI, which cancels out the total effective magnetic fields and qualitatively explains the experimental result [2].

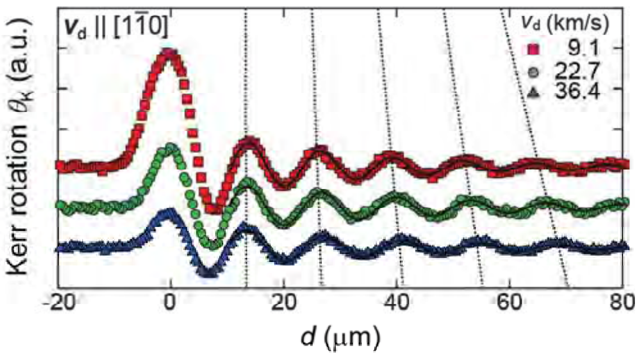

Fig. 1 Spatial distribution of spins drifting in the [1-10] direction at v_d = 9.1, 22.7 and 36.4 km/s. Solid lines are fitted to the data using the model function. Dotted lines are guides for the eye to indicate the spatial shift of the local maxima of the oscillating signals.

This work was supported by JSPS KAKENHI Grant Numbers JP15H05699 and JP16H03821.

[1] Y. Kunihashi *et al*., Nat. Comm. **7**, 10722 (2016).
[2] Y. Kunihashi *et al*., Phys. Rev. Lett. (accepted)

Anisotropy and Suppression of Spin-orbit Interaction in GaAs Double Quantum Dots

A. Hofmann[1], V. F. Maisi[1], T. Krähenmann[1], C. Reichl[1], W. Wegscheider[1], K. Ensslin[1], and T. Ihn[1]

[1] *Solid State Physics Laboratory, ETH Zürich - 8093 Zürich Switzerland*

We measure the anisotropy of spin–orbit interaction (SOI) using real-time charge detection of single electrons tunneling between different states of GaAs/AlGaAs-based double quantum dots (DQDs). The strength of the SOI depends on the crystallographic direction of the electron tunneling, and on the relative alignment between the tunneling direction and the spin quantization axis. In the DQD, the tunneling direction is defined by the main axis of the device, and the spin quantization axis is chosen by the direction of an external in-plane magnetic field. This set-up allows us to control the strength of the spin-orbit interaction and leads to spin lifetimes of 10 s.

We fabricate two DQDs on a GaAs heterostructure, one with its main axis along the [110] crystal axis [shown in Fig. 1(a)], and another one with the main axis rotated by 90 degrees, i.e. along [$\bar{1}$10]. By applying suitable gate voltages to metallic top-gates, each DQD is brought into a configuration where two electrons reside in the device, and tunneling to the source and drain is suppressed. Using a charge detector, we distinguish between two resonant charge states: one state where both electrons reside in the right quantum dot, $(0, 2)$, and one state where each dot is occupied by a single electron, $(1, 1)$. It has been shown [2] that in this configuration, the Pauli spin blockade [1] can be used to measure the strength of the spin-orbit interaction experienced by tunneling electrons.

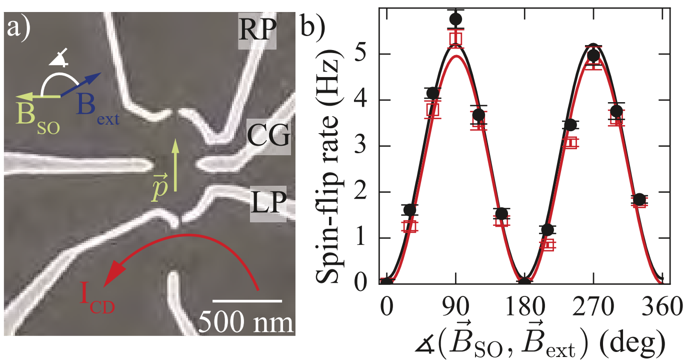

Figure 1: (a) SEM image of one of the DQDs. (b) Anisotropy and suppression of spin-flip tunneling

We use the two DQDs for measuring the different strength of the SOI experienced by electrons moving along distinct crystallographic axes. We find that the SOI induces spin-flips for electrons moving along [110], and that the SOI vanishes for an electron moving along [$\bar{1}$10]. For a given tunneling direction, we vary the strength of the experienced SOI by changing the alignment between the tunneling direction and spin-quantization axis by means of rotating the direction of the applied in-plane field. We find a sinusoidal dependence on the relative angle between the two directions.

At high magnetic fields, in the absence of the incoherent spin-relaxation processes within single dots, we measure the anisotropy of spin-flip tunneling rates between two energetically resonant quantum states. In this way, the spin-orbit interaction can be turned from on to almost completely off, as shown in Fig. 1(b).

[1] K. Ono et al, Science **23**, 1313 (2002).
[2] V. F. Maisi, et al, PRL **116**, 136803 (2016) and T. Fujita, et al, PRL **117**, 206802 (2016)
[3] presented work: A. Hofmann, et al, arXiv:1612.06199 (2016)

Detecting non-local spin signal through electron interaction

Takase Shimizu, Y. Hashimoto, S. Sugumaran, A.Endo, T. Nakamura and S. Katsumoto

Institute for Solid State Physics, University of Tokyo, Kashiwa, Chiba 277-8581
E-mail: takase@issp.u-tokyo.ac.jp

The quantum Hall edge states (QHESs) are known to have high quantum coherence, which property has been utilized to, *e.g.* electron Mach-Zehnder interferometer [1] while control of electron spins with orbital motion via spin-orbit interaction (SOI) has been reported. Naturally, control of spins with such a high coherence is expected when the QHESs are combined with SOI. Due to the electron correlation, QHESs show spin separation at comparatively low fields (quantum Hall ferromagnets). Hence the spin precessions in QHESs can be viewed as, in a sense, the transition between the edge states. Here we show an example of such control through non-adiabatic transport.

Figure 1 shows the gates configuration fabricated onto a two-dimensional electron system (2DES) in an AlGaAs/GaAs heterostructure. In the system we can expect small but finite Rashba-type SOI. The sample was cooled down to 60 mK and magnetic field up to 7 T was applied. In the regions below the two side-gates, the electron concentration was reduced to the filling factor $\nu=1$. Then in this sample configuration, when the filling in the 2DES without gate is m, we have two separation points and two meeting points of 1 and $m-1$ edge states. When there is a sharp corner in the electron orbit at the meeting points, the electron spin may experience non-adiabatic transition with the change in the direction of the effective magnetic field by SOI and be thrown into coherence (Rabi) oscillation between QHESs due to the chirality of them [2]. The oscillation is nothing but a spin precession. In Fig.2, the non-local resistances measured in the configuration in Fig.1 are plotted as a function of the center gate (gate15) voltage for $m=3$ and 4. Both show spin precession signals, the latter of which is much more regular due to the interaction between the QHESs. In this sense, $m=2$ is expected to be the best for the observation and the result there will also be presented in the symposium.

[1] Y. Ji, *et al.*, Nature **422**, 415 (2003).
[2] T. Nakajima, K.-T. Lin and S. Komiyama, AIP Conf. Proc. **1566**, 301 (2013).

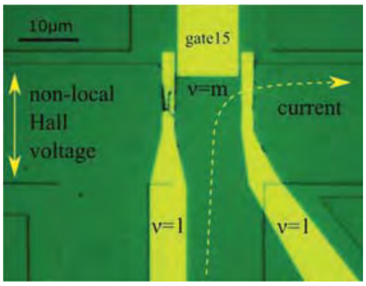

Fig. 1 Optical micrograph of the sample, which shows the gates and the terminal configuration. The regions below the side gates are tuned to ν=1. The broken line with an arrow indicates the current path and the line with arrows at the both ends indicates the voltage for the non-local resistance measurement.

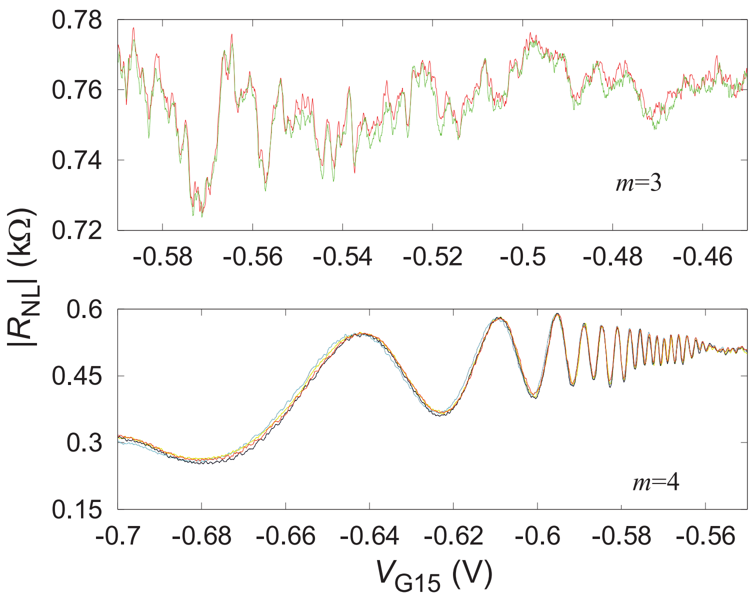

Fig. 2 Non-local resistances measured in the configuration in Fig.1 as a function of the center gate voltage for the filling $m=3$ and 4. Different colored lines demonstrate the reproducibility.

Spin Hall photoconductance and ultrafast helicity-dependent currents in topological insulators

P. Seifert[1], C. Kastl[1], K. Vaklinova[2], S. Ganichev[3], K. Kern[2,4], M. Burghard[2], and A.W. Holleitner[1]

[1] *Walter Schottky Institut and Physics-Department, TU Munich, Germany*
[2] *Max-Planck-Institut für Festkörperforschung, Stuttgart, Germany*
[3] *Terahertz Center, University of Regensburg, D-93040 Regensburg, Germany*
[4] *Institut de Physique, Ecole Polytechnique Fédérale de Lausanne, Lausanne, Switzerland*

Three-dimensional topological insulators constitute a fascinating class of materials with a strong spin-orbit coupling exhibiting non-trivial, gapless states on the surface and insulating bulk states [1-4]. In revealing the optoelectronic dynamics in the whole range from femto- to microseconds, we demonstrate that the long surface lifetime of Bi_2Te_2Se-nanowires allows to access the respective surface states by a pulsed photoconduction scheme even at room temperature [5]. Moreover, we highlight how to access ultrafast helicity-dependent surface currents in the topological insulators within the spin-relaxation lifetime of the investigated topological insulators [2,4].

Moreover, we show that the symmetry of helicity-dependent photocurrents in Bi_2Te_2Se-platelets can be broken by extrinsic and intrinsic anisotropies within the circuits [6,7]. In particular, we observe a helical, bias-dependent photoconductance at the lateral edges of topological Bi_2Te_2Se platelets for perpendicular incidence of light, indicative of spin accumulation induced by a transversal spin Hall effect in the bulk states of the Bi_2Te_2Se platelets [7]. Our results open the avenue for two-dimensional, topological materials as active modules in optoelectronic high-frequency and on-chip THz-circuits [4].

We acknowledge financial support by the ERC grant NanoREAL and the DFG priority program SPP1666 on “topological insulators”.

[1] J. W. McIver, et al. *Nature Nano* 7, 96 (2012).
[2] C. Kastl, et al. *Nature Comm.* 6, 6617 (2015).
[3] C. Kastl, et al. *2D Materials* 2, 024012 (2015).
[4] C. Kastl, et al. *IEEE J. Sel. Topics Quantum Electron.* 23, 8700305 (2017).
[5] P. Seifert, et al. *Nano Letters* 17, 973 (2017).
[6] P. Seifert, et al. *Symmetry and Topology Concepts in Reference Module in Chemistry, Molecular Sciences and Chemical Engineering, Elsevier,* ISBN 9780124095472 (2017).
[7] P. Seifert, et al. arXiv:1708.00283, under review (2017).

Observation of Full Spin-Orbit Polarization in a Band-Inverted InAs/InGaSb Composite Quantum Well at Zero Magnetic Field

Yukio Takahashi [1], **Hiroshi Irie** [1], **Takafumi Akiho** [1], **Koji Onomitsu**[1], **Koji Muraki** [1]

[1] *NTT Basic Research Laboratories, NTT Corporation, Japan*

A composite quantum well (CQW) comprising an InAs/(In)GaSb junction turns into a 2D topological insulator in the band-inverted regime [1]. Besides the robustness of its helical edge states, this system possesses a unique feature of large spin splitting in the bulk bands that arises from the spin-orbit (SO) interaction and the inversion asymmetry of the heterostructure [1]. Recently, magnetotransport in this system has shown that, over a range of gate voltage, only one of the spin-split bands resides at the Fermi level [2], which was ascribed to the large SO splitting and then interpreted as a hallmark of the full SO polarization at zero magnetic field. However, theory shows that, under a finite magnetic field, there can be energy regions where only Landau levels originating from a single spin branch exist, without breaking the inversion symmetry [3]. Therefore, in order to prove the full SO polarization at zero magnetic field, an alternative method that does not require magnetic fields is necessary.

Here, we experimentally probe the spin degeneracy (g_s) of the bulk states at zero magnetic field by capacitance measurements, which detect a change in g_s as that in the quantum-capacitance (C_q) contribution to the total capacitance [see the equivalent circuit in Fig. 1(a)]. The sample studied is a large Hall bar comprising an InAs (10.9 nm)/$In_{0.25}Ga_{0.75}Sb$ (5.9 nm) CQW with AlSb barrier layers. The capacitance between the front gate and the CQW was measured using a capacitance bridge at a temperature of 0.25 K and frequency of 600 Hz.

Figure 1(b) displays the front-gate bias (V_{FG}) dependence of the capacitance, together with the total density of states (DOS) obtained by 8-band $\boldsymbol{k\cdot p}$ calculations (inset). The capacitance takes a minimum around V_{FG} = 0 V, reflecting the lower DOS inside the hybridization gap. The most striking observations are the clear jumps in the capacitance around $V_{FG} = -1.3$ and +0.7 V, where the capacitance shows a slight increase before it drops, forming shoulder-like structures. Comparison with the calculated DOS confirms that these structures originate from the van Hove singularities at the edge of the spin-orbit split bands. Hence, the observed jumps can be attributed to changes in DOS across the regions with different g_s. Our observations thus present the first experimental demonstration of the full SO polarization at zero magnetic field, for the bulk states of the present system.

This work was supported by JSPS KAKENHI Grant No. JP15H05854.

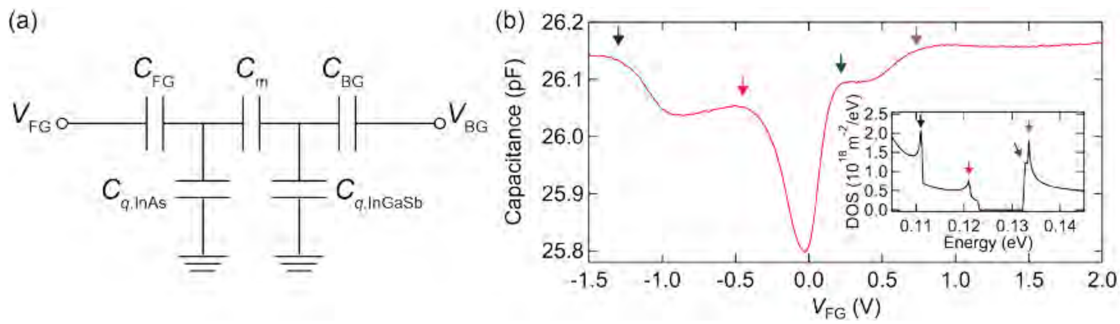

Fig.1: (a) Equivalent circuit model of the InAs/InGaSb CQW. C_{FG}, C_m, and C_{BG} are geometrical capacitances. $C_{q,InAs(InGaSb)}$ is a quantum capacitance arising from the InAs (InGaSb) layer. (b) V_{FG} dependence of the capacitance. An inset shows the calculated DOS for a strained InAs(11 nm)/$In_{0.25}Ga_{0.75}Sb$(6 nm) QW. Arrows indicate structures related to the van Hove singularity.

[1] C. Liu *et al.*, Phys. Rev. Lett. **100**, 236601 (2008).
[2] T. Akiho *et al.*, Appl. Phys. Lett. **109**, 192105 (2016); F. Nichele *et al.*, Phys. Rev. Lett. **118**, 016801 (2017).
[3] S.-B. Zhang *et al.*, Phys. Rev. B **90**, 115305 (2014).

Electro-mechanical resonators based on graphene

Adrian Bachtold [1]

[1] *ICFO, Castelldefels Barcelona, Spain*

When a graphene layer is suspended over a circular hole, the graphene vibrates as a music drum. However, such a graphene drum has an extremely small mass. Another difference is the quality factor Q, which becomes extremely large in graphene resonators at cryogenic temperature (Q above 1 million). Because of this combination of low mass and high quality factor, the motion is enormously sensitive to external forces. Here, we couple the graphene resonator to a superconducting cavity via the radiation pressure interaction. The superconducting cavity allows us to transduce the graphene motion with unprecedented sensitivity. We sideband cool the graphene motion to an average phonon occupation that approaches the quantum ground-state [1]. We show that the graphene resonator is a fantastic force sensor with a sensitivity approaching the fundamental limit imposed by thermo-mechanical noise. We find that energy decays in a way that has thus far never been observed nor predicted [2]. As the energy of a vibrational mode freely decays, the rate of energy decay switches abruptly to lower values, in stark contrast to what happens in the paradigm of a system directly coupled to an environmental bath. Our finding is related to the hybridization of the measured mode with other modes of the resonator. Our work opens up new possibilities to manipulate vibrational states, engineer hybrid states with mechanical modes at completely different frequencies, and to study the collective motion of this highly tunable system.

[1] P. Weber, J. Guttinger, A. Noury, J. Vergara-Cruz & A. Bachtold. Nature Communications **7**, 12496 (2016).
[2] J. Guettinger, A. Noury, P. Weber, A. M. Eriksson, C. Lagoin, J. Moser, C. Eichler, A. Wallraff, A. Isacsson, A. Bachtold, Nature Nanotechnology **12**, 631 (2017).

Broadband nanomechanical torque magnetometry

Joseph E. Losby[1,2], Fatemeh Fani Sani[1,2], Marcelo Wu[2,3], Paul E. Barclay[2,3], and Mark R. Freeman[1,2]

[1]*Department of Physics, University of Alberta, Edmonton, Alberta, Canada*
[2]*National Institute for Nanotechnology, Edmonton, Alberta, Canada*
[3]*Physics & Astronomy, University of Calgary, Calgary, Alberta, Canada*

Nanomechanical torque magnetometry is a highly sensitive probe of magnetostatic responses in nanoscale specimens, having nanometer- and 0.1 eV-scale resolution of position-dependent energy landscapes in spin textures [1]. In this method, a nanomagnet is affixed to a compliant mechanical sensor and angular momentum, from an induced change of magnetic torque, is transferred to the mechanical system. This results in a small mechanical twist that can be read out optically.

Recently, nanomechanical torque detection has been extended to magnetic AC susceptibility as well as spin resonance spectroscopy [2]. Here, the magnetic torque arising from the transverse component of a precessing dipole moment is used as a signal mixer and converted to a mechanical deflection. A key feature of torque magnetometry is broadband detection (to DC), allowing for simultaneous optomechanical readout of spin resonances and equilibrium magnetization.

An overview and demonstrations of broadband nanomechanical torque magnetometry will be presented, as well as efforts to further enhance its sensitivity through integration of mechanics with resonant photonic cavities [3] for emerging applications towards a nanomechanical lab-on-a-chip for magnetism.

The authors are very grateful for support from NSERC, CRC, AITF, and NINT.

[1] J.A.J. Burgess et al., Science **339**, 1051 (2013).
[2] J.E. Losby et al., Science, **350**, 198 (2015).
[3] M. Wu et al., Nature Nanotechnol., **12**, 127 (2017).

Reorientation of quantization axis for quantum dot through high variable uniaxial stress

Xueyong Yuan*[1], Fritz Weihausen-Brinkmann[2], Javier Martín-Sánchez[1], Giovanni Piredda[3], Vlastimil Krapek[4], Yongheng Huo[1,5], Huiying Huang[1], Oliver G. Schmidt[5], Johannes Edlinger[3], Gabriel Bester[2], Rinaldo Trotta[1], Armando Rastelli*[1],

[1] *Institute of Semiconductor and Solid State Physics, Johannes Kepler University Linz, Altenbergerstraße 69, 4040, Linz, Austria*
[2] *Institut für Physikalische Chemie, Universität Hamburg, Grindelallee 117, 20146 Hamburg, Germany*
[3] *Forschungszentrum Mikrotechnik, FH Vorarlberg, Hochschulstraße 1, 6850 Dornbirn, Austria*
[4] *Central European Institute of Technology, Brno University of Technology, Purkynova 123, 61200 Brno, Czech Republic*
[5] *Institute for Integrative Nanosciences, IFW Dresden, Helmholtzstraße 20, 01069 Dresden, Germany*

A novel micro-machined piezoelectric actuators featuring geometrical strain amplification is developed to explore the optical properties of GaAs quantum dots subject to variable uniaxial tension up to mechanical fracture. First of all, due to the modification of band gap from the stress, the emission energy of an exciton confined in a GaAs "artificial atom" can be continuously shifted by more than 100 meV. This strain-induced shift overcompensates the confinement energies, leading to emission well below the bandgap of GaAs, and this is the largest reported so far for piezoelectric-semiconductor devices. Second, valence band mixing leads to dramatic changes in the optical selection rules for excitonic transitions: one light component emitted from the sample surface becomes fully polarized perpendicular to the pulling direction while initially forbidden vertically polarized transitions become bright. By exploiting hole mixing and a wedge-waveguide geometry we are able to observe the whole transition process of neutral exciton under variable uniaxial stress without resorting to the magnetic field. Under the high tension stress effect, two new bright states displace the old ones, which indicates a new quantization axis should be chosen. These results show a promising route to tailor the polarization properties of single-photons emitted by epitaxial quantum dots and allow us to test the reliability of state-of-the-art methods (**k·p** and empiricial pseudopotential) under extreme conditions. Furthermore, QDs with this uniaxial stress strategy was predicted possess high indistinguishability and efficient coupling to guided mode, will be a competitive candidate to photonic circuits.

Contact: xueyong.yuan@jku.at or armando.rastelli@jku.at

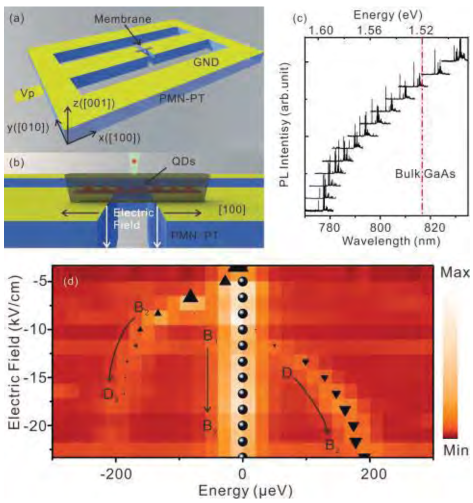

Coherent coupling of dark and bright excitons in a mechanical resonator

R. Ohta[*], H. Okamoto, T. Tawara, H. Gotoh, and H. Yamaguchi

NTT Basic Research Laboratories, NTT Corporation
3-1 Morinosato Wakamiya, Atsugi-shi, Kanagawa 243-0198, Japan
*ota.ryuichi@lab.ntt.co.jp

Dark excitons are optically inactive electron-hole pairs which form long-lived two level systems in solid-state platforms. Although they are of great interest in quantum information and spintronic applications, read and write to the dark excitons are technically challenging, which requires precisely designed pulse sequences and intermediate states [1]. The coherent coupling to the bright excitons breaks the parity of the dark excitons and activates their optical accessibility, which has been demonstrated with strong magnetic and electric fields [2]. Here, we demonstrate the dynamic coupling of dark and bright bound excitons using vibrational strain in a mechanical resonator. In-plane strain field breaks the crystal symmetries and causes the coherent coupling without external fields. This electromechanical approach provides rapid control of the coupling and is compatible with present semiconductor-based device architecture, which will open the way to integrate quantum memories on chip.

The mechanical resonator was fabricated with 37-μm-length, 20-μm-width, and 600-nm-thickness using $Al_{0.3}Ga_{0.7}As/GaAs$ heterostructure, and is schematically shown in the inset of Fig. 1. Dark and bright bound excitons are formed in the GaAs layer, whose energies can be periodically modified by the mechanical motion via deformation potentials. Figure 1 shows the exciton energies with the mechanical motion calculated with $\boldsymbol{k} \cdot \boldsymbol{p}$ theory. The dark exciton in heavy-hole (HH) band and the bright exciton in light-hole (LH) band are coupled by the vibrational strain. The strain effects of exciton energies were investigated by stroboscopic PL measurements, where a phase-locked pump pulse is periodically applied with the relative phase to the mechanical oscillation (Fig. 2(a)). Figure 2(b) shows measured PL spectra at the various phase with drive voltage of 12 mV_{pp}. The vibrational strain causes the anti-crossings between dark exciton in HH band and bright exciton in LH band around phase of $\pi/2$ and $3\pi/2$. Dashed lines in Fig. 2(b) indicate the calculated peak energies from $\boldsymbol{k} \cdot \boldsymbol{p}$ theory. Good agreement with the calculation confirms the coupling of dark and bright bound excitons using the dynamic strain of the mechanical resonator.

This work is partly supported by MEXT KAKENHI (No. JP15H05869, JP16H01057)

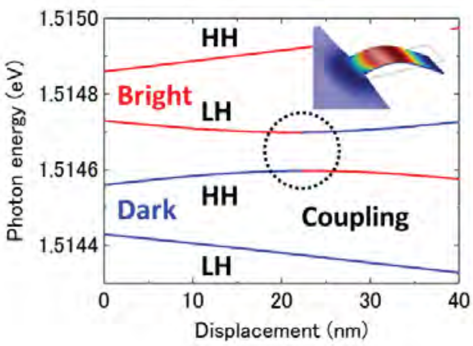

Fig.1: Calculated bound exciton energies in the vibrating GaAs resonator. Inset shows the schematic image of the mechanical resonator and its strain distribution.

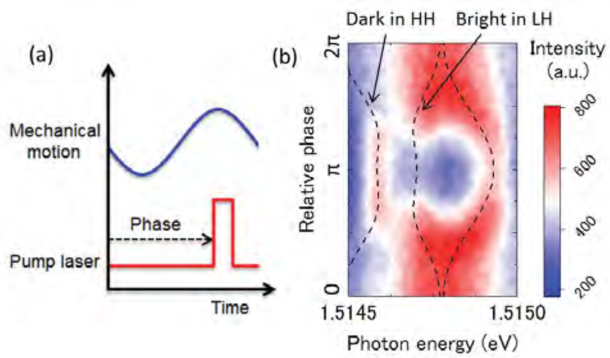

Fig.2: (a) Schematic image of stroboscopic PL measurement. (b) PL spectra from dark and bright bound excitons. Dashed lines are eigen energies of excitons calculated with $\boldsymbol{k} \cdot \boldsymbol{p}$ theory.

[1] E. Poem *et al*, Nat. Phys. **6,** 993 (2010).
[2] M. Bayer *et al*, Phys. Rev. **B 61,** 7273 (2000).

Spins and mechanics in diamond quantum systems

Donghun Lee[1,2], Kenny Lee[1], Jeff Cady[1] and Ania Jayich[1]

[1] *Department of Physics, University of California at Santa Barbara, USA*
[2] *Department of Physics, Korea University, Seoul, South Korea*

There has been rapidly growing interest in hybrid mechanical systems where high quality mechanical oscillators are coupled to two-level systems[1,2]. Such hybrid systems can provide new methods to quantum control of mechanical objects, transduction of quantum information between distinct quantum systems and high precision quantum sensing[1,2].

In this talk, we will present diamond-based quantum devices in which a diamond mechanical oscillator is coupled to embedded atom-like defect centers. Nitrogen-vacancy (NV) defect centers in diamond are solid-state spin-qubits possessing remarkable quantum properties applicable to various fields including quantum information science and quantum sensing. Using strain associated with the resonator's mechanical motion, we will demonstrate coherent mechanical control of NV's spin and optical properties[3,4]. We will also discuss future aspects of spin-mechanical hybrid systems such as strain-mediated long-range spin-spin interaction, indistinguishable photon generation and ground state phonon cooling[2].

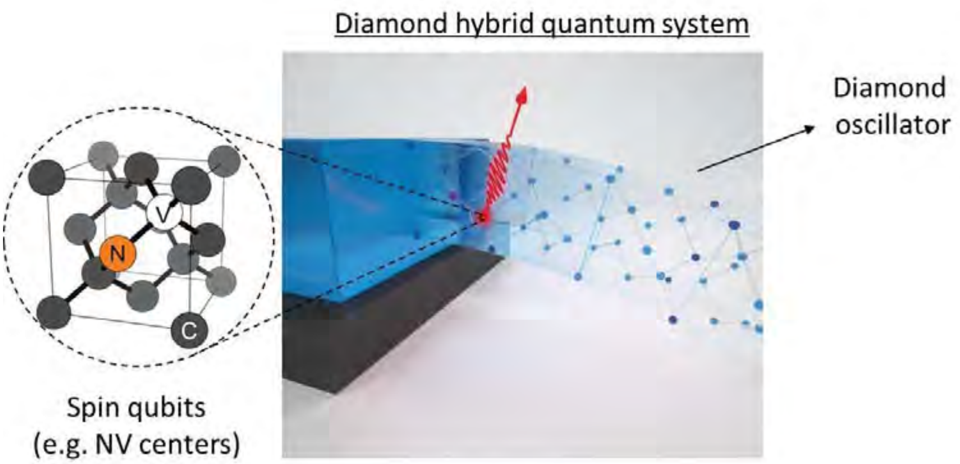

Figure: Schematics of diamond hybrid quantum systems where spin qubits (e.g. NV centers) coupled to the motion of diamond mechanical resonator via strain

[1] P. Treutlein *et al.*, Cavity Optomechanics, Springer pp 327-351 (2014).
[2] D. Lee*, K. Lee* *et al.*, J. Opt. **19** 033001 (2017).
[3] P. Ovartchaiyapong et al., Nat. Comms. **5** 4429 (2014).
[4] K. Lee*, D. Lee* *et al.*, Phys. Rev. Appl. **6** 034005 (2016).

Dissipation as a resource for quantum-limited amplification and nonreciprocal devices in superconducting circuit optomechanics

L. D. Tóth[1], **N. R. Bernier**[1], **A. Nunnenkamp**[2], **A. K. Feofanov**[1], **T. J. Kippenberg**[1]

[1]*Institute of Physics, École Polytechnique Fédérale de Lausanne (EPFL), CH-1015 Lausanne, Switzerland*
[2]*Cavendish Laboratory, University of Cambridge, Cambridge CB3 0HE, United Kingdom*

Isolation of a system from its environment is often desirable, from precision measurements to control of individual quantum systems; however, dissipation can also be a useful resource. Remarkably, engineered dissipation enables the preparation of quantum states of atoms, ions or superconducting qubits as well as their stabilization. This is achieved by a suitably engineered coupling to a dissipative cold reservoir formed by electromagnetic modes. Breaking from this paradigm, we realize a dissipative, cold reservoir for microwave photons using a ground-state-cooled mechanical oscillator [1]. Coupling to this engineered mechanical reservoir enables to manipulate the microwave photons in a superconducting microwave circuit. This corresponds to dynamical backaction control of a microwave field [2], enabling observation of stimulated emission and maser operation. Moreover, the reservoir can function as a useful quantum resource. We evidence this by employing the engineered cold reservoir to implement a large gain (above 40 dB) phase preserving microwave amplifier that operates 0.87 quanta above the limit of added noise imposed by quantum mechanics. Engineered mechanical dissipation can extend the toolbox of quantum manipulation techniques of the microwave field.

Dissipation can also form an essential ingredient for building cavity-based nonreciprocal devices [3], which are ubiquitous in radar and radio-frequency communication systems as well as are indispensable in the readout chains of superconducting quantum circuits. These devices commonly rely on magnetically biased ferrite materials, which are bulky, lossy and require large magnetic fields. Therefore, there has been significant interest in magnetic-field-free on-chip alternatives, such as those recently implemented using the Josephson nonlinearity. We realise reconfigurable nonreciprocal transmission between two microwave modes using purely optomechanical interactions in a superconducting electromechanical circuit [4]. We analyse the isolation, transmission and the noise properties of this nonreciprocal circuit. Finally, we show how quantum-limited circulators can be realized with the same principle. The technology can be fabricated on-chip and does not require any external magnetic field to operate, and is hence fully compatible with superconducting quantum circuits. All-optomechanically-mediated nonreciprocity can also be extended to implement directional amplifiers [5], and it forms the basis towards realising topological states of light and sound.

[1] L. D. Tóth, N. R. Bernier, A. Nunnenkamp, A. K. Feofanov, T. J. Kippenberg, Nat. Phys. **13**, 789–793 (2017).
[2] L. D. Tóth, N. R. Bernier, A. K. Feofanov, T. J. Kippenberg, Phys. Lett. A (2017). In Press. https://doi.org/10.1016/j.physleta.2017.05.045
[3] A. Metelmann, A. A. Clerk, Phys. Rev. X **5**, 021025 (2017).
[4] N. R. Bernier, L. D. Tóth, A. Koottandavida, M. Ioannou, D. Malz, A. Nunnenkamp, A. K. Feofanov, T. J. Kippenberg, arXiv:1612.08223 (2017). To appear in Nat. Commun.
[5] D. Malz, L. D. Tóth, N. R. Bernier, A. K. Feofanov, T. J. Kippenberg, A. Nunnenkamp, arXiv:1705.00436 (2017).

Double quantum dot coupled with a phonon resonator

Toshimasa Fujisawa

Department of Physics, Tokyo Institute of Technology, Tokyo, Japan.

An electron-phonon hybrid system can be formed in a double quantum dot (DQD) with a surface-acoustic-wave (SAW) phonon resonator, where novel phonon dressed electronic states are expected to appear [1]. While boson dressed qubit states are often investigated by spectroscopy on bosons, we have demonstrated spin-flip (SF) phonon assisted tunneling (PnAT) in the Pauli spin-blockade regime for investigating Rabi splitting and phonon dressed electronic states [2].

We have fabricated an electron-phonon hybrid device in an AlGaAs/GaAs heterostructure with periodic surface metallization for a SAW phonon resonator. Figure 1(a) illustrates the SF PnAT process in the presence of coherent piezoelectric potential wave with the amplitude $\tilde{\varepsilon}$ at frequency f ~ 3 GHz in the resonator [1]. In the Pauli spin blockade regime at zero magnetic field, the DQD is prepared in a triplet state (1,1)T, one electron in each dot, with finite energy spacing $-\varepsilon$ (~ hf) to the singlet state (0,2)S on the right dot. The phonon field induces weak SF PnAT from (1,1)T to (0,2)S with a spin-flip mechanism associated with the inhomogeneous nuclear spin fluctuations. This is energetically allowed when the singlet state is located hf above (1,1)T. Figure 1(b) shows how the Rabi splitting Δ_1 shows up in phonon dressed singlet states; no splitting (Δ_1 ~ 0) in a weak field ($\alpha = \tilde{\varepsilon}/hf$ ~ 0) but finite Δ_1 (> 0) in a strong field (α > 0). Since SF PnAT takes place at $E = hf$, the condition ε_{SF} for SF PnAT changes from $\varepsilon_{SF} \sim hf$ at $\alpha \sim 0$ to $\varepsilon_{SF} < hf$ at $\alpha \gtrsim 1$. Therefore, one can study Rabi splitting by observing the conditions for SF PnAT peaks. Figure 1(c) shows the experimental current profile as a function of ε. As the phonon field is increased with the RF voltage V_{IDT} on the interdigital transducer, two SF PnAT current peaks appear. These conditions are close to $\varepsilon = \pm hf$ (13 μeV) at small V_{IDT}, and shift to lower values at larger V_{IDT}. Strikingly, the peaks are finally merged into a single peak at $\varepsilon \sim 0$. This is consistent with numerical simulations of SF PnAT in Fig. 1(d). In this way, the Rabi splitting can be studied with SF-PnAT spectroscopy.

We acknowledge JSPS KAKENHI (JP15K13271 and JP26247051) and TokyoTech Nanotechnology Platform.

[1] J. C. H. Chen et al., Sci. Rep. 5, 15176 (2015).
[2] Y. Sato et al., Phys. Rev. B 96, 115416 (2017).

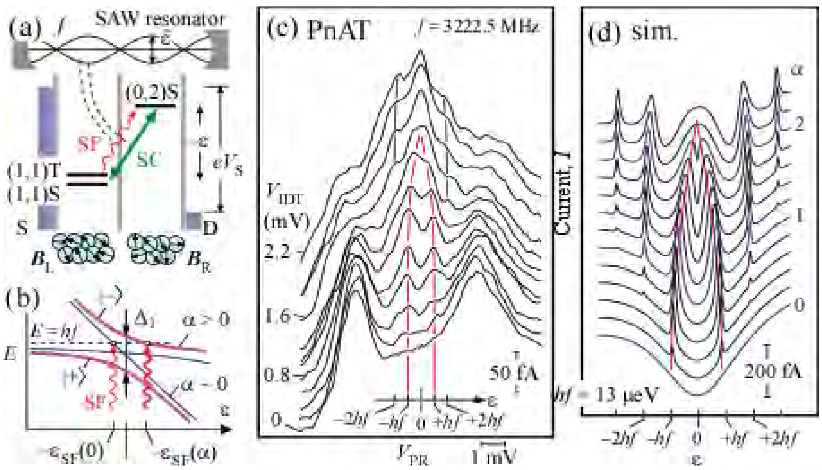

Fig. 1. (a) A DQD coupled to a SAW resonator. (b) The energy diagram for phonon dressed states. (c) Measured current profiles for PnAT processes at $\varepsilon = nhf$. (c) Calculated current profiles, which reproduce the measurement.

Acoustic Control of Light and Matter on a Chip

Hubert J. Krenner[1,2]

[1] *Experimental Physics 1, University of Augsburg, 86159 Augsburg, Germany*
[2] *Nanosystems Initiative Munich (NIM), 80799 Munich, Germany*

Today, physicists control different types of quantum states with unprecedented precision. However, no individual, isolated approach meets all the stringent criteria for applications in future quantum technologies. Hybrid quantum systems aim to combine complementary strengths of different single systems, while at the same time avoiding individual shortcomings. For the realization of such hybrid quantum architectures, mechanical excitations stand out. They interact strongly with literally any other quantum system and, most excitingly, can be routed in the form of a surface acoustic wave (SAW) over millimeter distances with ultra-low dissipation.

In my presentation, I will give an overview on our recent advances on the control of optically active quantum dots by SAWs and their coupling to photonic crystal nanocavities. I will demonstrate the dynamic acoustic field of a SAW modulates both the sharp optical transition of a quantum dot [1] and the high quality factor optical mode of the nanocavity [2] at gigahertz frequencies. Both effects can be combined to achieve dynamic switching of the light-matter interaction and trigger the emission of single photons from the system at precisely defined time during the acoustic cycle [3]. This precisely regulated single photon generation arises from a modulation of the Purcell-effect by the SAW. This scheme can readily be extended to entangling quantum gates employing acoustically-driven Landau-Zener transitions [4].

[1] F. J. R. Schülein, E. Zallo, P. Atkinson, O. G. Schmidt, R. Trotta, A. Rastelli, A. Wixforth, and H. J. Krenner, Nat. Nanotechnol. **10**, 512 (2015).
[2] D. A. Fuhrmann, S. M. Thon, H. Kim, D. Bouwmeester, P. M. Petroff, A. Wixforth, H. J. Krenner, Nat. Photon. **5**, 605-609 (2011).
[3] M. Weiß, S. Kapfinger, T. Reichert, J. J. Finley, A. Wixforth, M. Kaniber, and H. J. Krenner, Appl. Phys. Lett. **109**, 33105 (2016).
[4] R. Blattmann, H. J. Krenner, S. Kohler, and P. Hänggi, Phys. Rev. A **89**, 012327 (2014).

Edge conduction in monolayer WTe_2

Tauno Palomaki, Wenjin Zhao, Zaiyao Fei, Xiaodong Xu and David H. Cobden

Department of Physics, University of Washington

Monolayer WTe_2 was recently predicted to be a two-dimensional topological semimetal, with band inversion giving rise to helical edge states degenerate with the bulk bands [1]. Experimentally, however, we have found that below approximately 100 K it shows insulating behavior in the bulk, while edge conduction remains [2]. The edge conduction is strongly suppressed by an in-plane magnetic field and shows no gap as a function of gate voltage. Bilayer WTe_2 also becomes insulating at low temperatures, but does not show edge conduction. These observations are consistent with monolayer WTe_2 being a two-dimensional topological insulator, except for the fact that the conductance is below the quantized value and shows mesoscopic fluctuations. There are several other interesting aspects of this material. For example, the insulating state in the monolayer turns superconducting on electrostatic doping at temperatures below about 1 K. In addition, while monolayer WTe_2 is centrosymmetric, bilayer and thicker WTe_2 are polar, and we find that the polarization is switchable (it is ferroelectric) by gate voltage, with a clear signature in the in-plane conductance and a magnitude that can be determined using an adjacent graphene layer as a probe. We will present our ongoing efforts to understand the rich electronic behavior of monolayer and bilayer WTe_2 in the context of recent ARPES, STM, [3] and other measurements.

[1] X. Qian *et al.*, Science **346**, 1344-1347 (2014).
[2] Z. Fei. *et al*., Nat. Phys. **13**, 677-682 (2017).
[3] S.Tang, *et al*., Nat. Phys. **13**, 683-687 (2017).

Electric-field driven topological phase transition in InAs/In$_x$Ga$_{1-x}$Sb composite quantum wells

H. Irie [1], T. Akiho [1], K. Suzuki [1], F. Couëdo [1], K. Onomitsu [1] and K. Muraki [1]

[1] *NTT Basic Research Laboratories, NTT Corporation*

Two-dimensional topological insulators (2D TIs) have drawn increasing attention due to their spin-momentum locked edge states which are useful for spintronics applications. Among various 2D TI candidates, InAs/In$_x$Ga$_{1-x}$Sb composite quantum wells (CQWs) have a unique feature that the band alignment is tunable via electric field because of their double-layer structure which spatially separates electron and hole gases [1, 2]. This not only allows for electrical switching between TI and normal insulator (NI) phases in a single device, but also opens the possibility of creating (or erasing) edge states in the interior of the sample by defining topologically distinct regions by electrical means.

Here, we report on the experimental demonstration of an electric-field-driven topological phase transition (TI–NI transition) in InAs/In$_x$Ga$_{1-x}$Sb CQWs. It has recently been shown that the compressive strain in the In$_x$Ga$_{1-x}$Sb layer enhances the heavy-hole light-hole splitting, which leads to a large hybridization gap in the band inverted regime [3]. The CQW samples studied here comprise 5.5-nm InAs and 6.0-nm In$_{0.4}$Ga$_{0.6}$Sb layers sandwiched between AlSb barriers, processed into Hall bars with front and back gates. Figure 1(a) shows longitudinal resistivity ρ_{xx} vs. front gate voltage (V_{FG}), taken at different back gate voltages (V_{BG}). The high ρ_{xx} peak reaching ~$8h/e^2$ for V_{BG} = 8 V reflects the large hybridization gap in this CQW. With decreasing V_{BG}, the height of the ρ_{xx} peak first decreases and then turns to increase for V_{BG} < 1 V. This reentrant behavior can be understood as a manifestation of gap closing and reopening that is generally expected to accompany a topological phase transition. This is further corroborated by the observation that under a strong in-plane magnetic field ($B_{||}$) the ρ_{xx} peak exhibits markedly different behavior in the two regimes [Fig. 1(b)]. These results pave the way for realizing novel devices based on field-effect control of topological properties. At the presentation, we will also discuss the transport properties at the phase transition point where the system is expected to behave like a zero-gap semiconductor. This work was supported by JSPS KAKENHI Grant No. JP15H05854.

[1] K. Suzuki *et al.*, Phys. Rev. B **91**, 245309 (2015).
[2] F. Qu *et al.*, Phys. Rev. Lett. **115**, 036803 (2015).
[3] T. Akiho *et al.*, Appl. Phys. Lett. **109**, 192105 (2016).

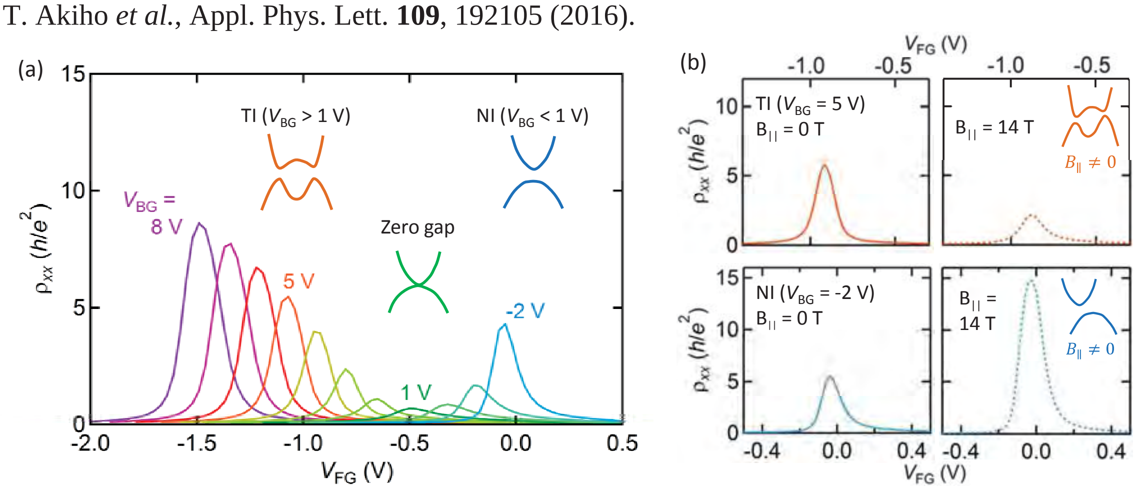

Fig. 1 (a) ρ_{xx} vs. V_{FG} at T = 2 K, taken at different V_{BG}'s from -2 to 8 V. The insets are schematic band dispersion of corresponding phases. (b) Effects of $B_{||}$ on the ρ_{xx} peak for TI and NI phases.

First-order phase transition of quantum Hall skyrmions observed by photoluminescence microscopy

J. N. Moore[1], J. Hayakawa[1], H. Iwata[1], T. Mano[2], T. Noda[2], G. Yusa[1]

[1]*Department of Physics, Tohoku University, Sendai 980-8578, Japan*
[2]*National Institute for Materials Science, Tsukuba, Ibaraki 305-0047, Japan*

Topologically nontrivial spin textures called skyrmions are believed to exist in the quantum Hall regime of 2D electrons when the number of fully occupied Landau levels ν is slightly greater than or slightly less than unity [1]. Evidence for skyrmions has come from the sharp decrease in electron spin polarization above and below $\nu = 1$ [2, 3] as well as a dramatically reduced nuclear spin depolarization time T_1 [4, 5] in agreement with predictions based on the Nambu-Goldstone spin wave mode [6]. Analogous to a classical 2D crystal, a skyrmion crystal state is predicted by KTNHY theory to transition into a liquid state [6], as some NMR relaxation and heat capacity experiments have supported [7, 8].

In GaAs quantum wells we have observed a discontinuity in the photoluminescence spectrum indicating the discontinuous drop in electron polarization slightly above $\nu = 1$. This is accompanied by an abrupt change in T_1, long-range ordering in the spatial pattern of electron polarization, and hysteresis as the filling factor is swept across the transition. These characteristics point to a first-order phase transition, the origin of which we try to identify by varying magnetic field strength and orientation, and temperature. We discuss the possibility that this phase transition is caused by a phenomenon other than the solid-to-liquid transition.

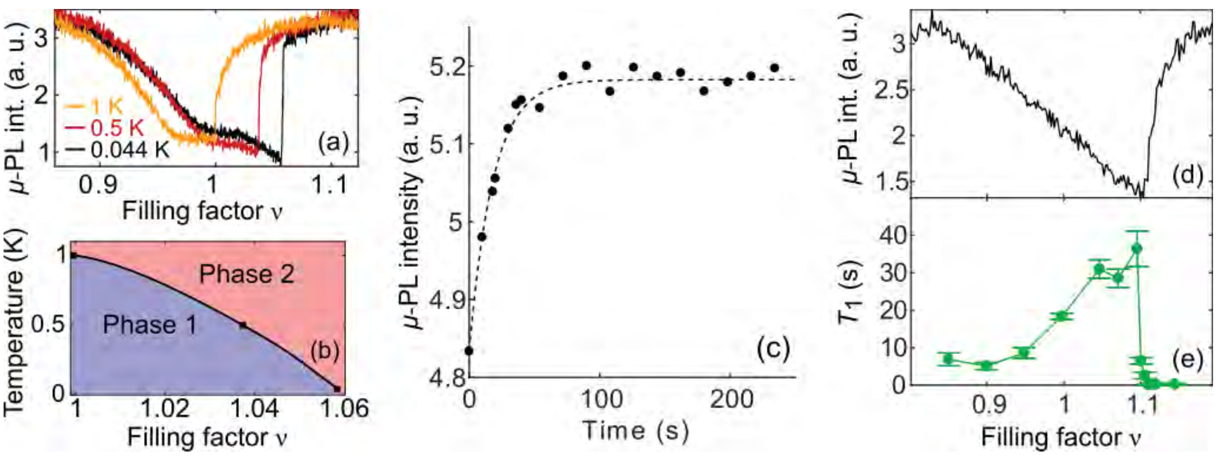

(a) Microscopic photoluminescence (μ-PL) intensity of the singlet trion peak as a function of ν swept by a back gate at three temperatures. B = 8 T. (b) Phase diagram plotting the ν values of the sharp features in (a). (c) μ-PL intensity measured after dynamically polarizing nuclear spins plotted as a function of relaxation time at $\nu = 0.9974$, B = 6 T. (d) μ-PL intensity vs. ν (e) T_1 measured at the same microscopic point as in (d) by fitting plots as in (c) to exponential decay curves.

[1] S. L. Sondhi, A. Karlhede, and S. A. Kivelson, Phys. Rev. B **47**, 16419 (1993).
[2] E. H. Aifer, B. B. Goldberg, and D. A. Broido, Phys. Rev. Lett. **76**, 680 (1996).
[3] P. Plochocka et al., Phys. Rev. Lett. **102**, 126806 (2009).
[4] K. Hashimoto et al., Phys. Rev. Lett. **88**, 176601 (2002).
[5] T. Guan et alTK., Chin. Phys. B **24**, 067302 (2015).
[6] R. Côté et al., Phys. Rev. Lett. **78**, 4825 (1997).
[7] V. Bayot et al., Phys. Rev. Lett. **79**, 1718 (1997).
[8] G. Gervais et al., Phys. Rev. Lett. **94**, 196803 (2005).

Qubit-assisted transduction for a detection of surface acoustic waves near the quantum limit

A. Noguchi[1,2], R. Yamazaki[1,2], Y. Tabuchi[1], and Y. Nakamura[1,3]

[1]*Research Center for Advanced Science and Technology (RCAST), The University of Tokyo, Meguro-ku, Tokyo, 153-8904, Japan,*
[2]*PRESTO, Japan Science and Technology Agency, Kawaguchi-shi, Saitama 332-0012, Japan,*
[3]*Center for Emergent Matter Science (CEMS), RIKEN, Wako-shi, Saitama 351-0198, Japan*

Hybrid quantum systems have been widely studied in quantum information science [1]. Among the several quantum systems, surface acoustic waves (SAW) have recently attracted much interest as an alternative quantum mode localized on a surface of a material [2]. In piezoelectric materials, SAW can be strongly coupled to electric fields between surface electrodes and are widely applied in compact microwave components because of their short wavelength and small losses. SAW can also couple to other physical systems [3] such as superconducting qubit, quantum dots and NV centers through various form of elastic effects. Opto-elastic interaction of SAW opens the possibility to achieve a quantum transducer from microwave photons to optical photons in the telecommunication band.

Here, we report experiments on a hybrid quantum system consisting of a SAW resonator, a superconducting qubit, and a MW resonator. We demonstrate microwave-driven parametric couplings induced by the nonlinearity of the qubit, which serves as a transducer or an interface between the phonons in the SAW resonator and the photons in the MW resonator. The thermal phonons in the sub-GHz SAW resonator are up-converted to the MW frequency range where near-quantum-limited measurement of photons is available. We observe thermal fluctuations in the SAW resonator below the mean phonon number of unity with an unprecedented sensitivity.

[1] G. Kurizki, P. Bertet, Y. Kubo, K. Mølmer, D. Petrosyan, P. Rabl, and J. Schmiedmayer, *Proc. Natl. Acad. Sci. U.S.A.* **112**, 3866 (2015).
[2] M. V. Gustafsson, P. V. Santos, G. Johansson, and P. Delsing, *Nat. Phys.* **8**, 338 (2012).
[3] M. J. A. Schuetz, E. M. Kessler, G. Giedke, L. M. K. Vandersypen, M. D. Lukin, and J. I. Cirac, *Phys. Rev. X* **5**, 031031 (2015).

Efficient unidirectional transduction between electrical microwaves and surface acoustic waves and routing of propagating microwave phonons at the quantum level

Maria K. Ekström [1], Thomas Aref [1], Johan Runeson [1], Johan Björck [1], Isac Boström [1], Haruki Sanada [1,2], Gustav Andersson [1], Baladitya Suri [1] and Per Delsing [1]

[1] *Chalmers University of Technology, Kemivägen 9, 412 96 Göteborg, Sweden*
[2] *NTT Basic Research Laboratories, 3-1, Morinosato-Wakamiya, Atsugi, Kanagawa, 243-0198 Japan*

It has recently been shown that surface acoustic waves (SAWs) can interact with artificial atoms at the quantum level [1]. This has opened up for new possibilities utilizing SAWs (phonons) instead of electromagnetic waves (photons) in quantum optics experiments. Here we explore two of these experiments; 1) developments towards detecting single phonons and 2) routing of propagating phonons.

In order to detect single phonons, there is a great need for efficient conversion between photons and phonons. Conventional inter-digital transducers (IDTs) have a theoretical minimum insertion loss of 3 dB, due to their symmetric bidirectional nature. Unidirectional transducers (UDTs) [2] release most of their SAW energy in one preferred direction and have previously been studied at room temperature for classical low loss SAW filters. Here we study UDTs at microwave frequencies and at low temperature, in order to use them as photon-to-phonon converters at the quantum level. We found that the UDT delay lines had 4.7 dB less insertion loss than the IDT delay lines and a directivity of 22 dB per UDT, which indicates that 99.4 % of the power goes in the desired direction. The power lost in the undesired direction accounts for more than 90 % of the total loss in IDT delay lines, but only 3 % of the total loss in the UDT delay lines [3]. The improved photon-to-phonon conversion is useful for studying quantum optics with SAW. However, a balance between directionality and impedance matching must be achieved for maximum conversion efficiency.

Routing of propagating phonons relies on scattering of propagating waves from a single artificial atom. Similar experiments were performed with propagating electromagnetic waves scattered by a superconducting artificial atom [4,5] and using this type of scattering, catch and release of propagating photons was demonstrated [6-8]. To route propagating phonons, one can benefit from their five orders of magnitude slower speed than the speed of photons in vacuum. It takes the phonons about 140 ns to traverse from the artificial atom (superconducting transmon qubit) to the pick-up IDT in our device. Using an external magnetic field or an on-chip flux line, the artificial atom could be tuned on or off resonance with the SAWs and in this way the field was either reflected or transmitted. On resonance in continuous mode and at low powers we found 96 % extinction in the transmitted field. The artificial atom could also route 100 ns SAW pulses, which enables one to conduct experiments where the SAW pulse can be captured between two artificial atoms for a substantial time and be released in a controlled way.

[1] M.V. Gustafsson, T. Aref, A. Frisk Kockum, M.K. Ekström, G. Johansson and P. Delsing, Science **346**, 207-211 (2014).
[2] K. Yamanouchi and H. Furuyashiki, Electron. Lett. **20**, 989 (1984).
[3] M.K. Ekström *et al*, Appl. Phys. Lett. **110**, 073105 (2017).
[4] O. Astafiev *et al*, Science **327**, 840-843 (2010).
[5] I.-C. Hoi *et al*, Phys. Rev. Lett. **107**, 073601 (2011)
[6] Y. Yin *et al*, Phys. Rev. Lett. **110**, 107001 (2013).
[7] M. Pierrea *et al*, Appl. Phys. Lett. **104**, 232604 (2014).
[8] E. Flurin *et al*, Phys. Rev. Lett. **114**, 090503 (2015).

Reducing 1/f noise in quantum devices by surface spin desorption

S. E. de Graaf[1], L. Faoro[2], J. Burnett[3], A. Adamyan[3], A. Ya. Tzalenchuk[1,4], S. E. Kubatkin[3], T. Lindstrom[1] and A. V. Danilov[3]

[1] *National physical laboratory, Hampton Road, Teddington, TW11 0LW, UK*

[2] *Laboratoire de Physique Theorique et Hautes Energies, Universites Paris 6 et 7, place Jussieu 75252 Paris, Cedex 05 France*

[3] *Department of Microtechnology and Nanoscience, Chalmers University of Technology, SE-412 96 Goteborg, Sweden*

[4] *Royal Holloway, University of London, Egham, TW20 0EX, UK*

Reducing noise and decoherence in solid state quantum devices will enable enhanced performance of a wide range of sensors and circuits, however, such efforts have been largely inhibited by the lack of knowledge about the origin of this noise and decoherence. We correlate measurements of frequency (dielectric) noise and loss in superconducting resonators made from NbN on Al2O3 with ultrasensitive in-situ electron spin resonance (ESR) measurements on the same devices [1]. We find that after removing a large fraction of surface spins by a simple heat treatment, the magnitude of the dielectric noise is reduced by almost 10 times [2]. Our data is in excellent agreement with a model for strongly interacting two-level systems [3,4], allowing us to attribute the origin of the dielectric noise to ESR-active slow two-level charge fluctuators on the surface of our devices. Here we show that surface spins directly affect the performance of high-Q superconducting resonators, but the chemical fingerprint of the ESR spectrum together with noise and loss data enables a whole new route to identifying the origin of noise in quantum circuits.

[1] S.E. de Graaf et al., Phys. Rev. Lett. **118**, 057703 (2017).
[2] S. E. de Graaf et al., arXiv: 1705.09158
[3] L. Faoro et al., Phys. Rev. B **91**, 014201 (2015).
[4] J. Burnett et al., Nature Communications **5**, 4119 (2014).

Effects of Phonon-Bottleneck in Spin Relaxation of Er:YSO

Rangga P. Budoyo[1]**, Kosuke Kakuyanagi**[1]**, Hiraku Toida**[1]**, Yuichiro Matsuzaki**[1]**, Imran Mahboob**[1]**, William J. Munro**[1]**, Hiroshi Yamaguchi**[1]**, and Shiro Saito**[1]

[1] *NTT Basic Research Laboratories, NTT Corporation, Atsugi, Kanagawa, Japan*

We measured the microwave and magnetic relaxation of electron spins of even Er^{3+} dopants in a Y_2SiO_5 crystal as a function of temperature (20 to 200 mK) and magnetic field (3.25 to 6.50 mT) using an electron paramagnetic resonance spectrometer based on a tunable Josephson bifurcation amplifier. The longest measured relaxation times approached 40,000 s at 20 mK. Applying a strong microwave excitation pulse resulted in a non-exponential relaxation. The (weak microwave) relaxation rate showed a quadratic temperature dependence. The temperature dependence and the non-exponential decay suggest a phonon-bottlenecked spin relaxation. In addition, magnetic field dependence of relaxation rate showed structures corresponding to energy level crossing with ^{167}Er hyperfine transitions, suggesting cross-relaxation effects. We discuss the phonon-bottleneck model, the source of bottleneck in Er:YSO, as well as the effects of other possible relaxation processes, including cross-relaxation, spin diffusion and quantum tunneling.

Progress on superconducting multi-qubits system

Xiaobo Zhu

University of Science and Technology of China, Shanghai, China

In this talk, I will show our recent progress on multi-qubits system. We designed and fabricated several versions of quantum processor, on which integrated up to ten quibts. The typical T_1 and T_2 time are both longer than 20 micro-seconds. The fidelity of single-bit gate and two-bit CZ gate are calibrated by randomized benchmarking. For the single-bit, the fidelity is measured higher than 99.9% and for the CZ gate it reaches 99.4% in the best case. We use a four-qubit superconducting quantum processor to solve a two-dimensional system of linear equations based on a quantum algorithm proposed by Harrow, Hassidim, and Lloyd (Phys. Rev. Lett. 103, 150502, 2009), yield a process fidelity of 0.837 ± 0.006.[1] I will also show the results on the production and tomography of genuinely entangled Greenberger-Horne-Zeilinger states with up to 10 qubits connecting to a bus resonator in a superconducting circuit. The resulting 10-qubit density matrix is probed by quantum state tomography, with a fidelity of 0.668 ± 0.025.Our results demonstrate the largest entanglement created so far in solid-state architectures, and pave the way to large-scale quantum computation.[2]

[1] Y. Zheng, *et al*. Phys. Rev. Lett. 118, 210504 (2017).
[2] C. Song, *et al.*, Phys. Rev. Lett. (Accepted)

Acknowledgements

The experiment was carried out in University of Science and Technology of China (Shanghai), Prof. Haohua's group in Zhejiang University, and Prof. Dongning's group in Institute of Physics Chinese Academy of Sciences. The theory was done by Prof. Yuxi's group in Tsinghua University, Prof. Changpu's group in China Beijing Computational Science Research Center, Prof. William J. Munro in NTT Basic Research Laboratories and Prof. Kae Nemoto in National Institute of Informatics. The sample fabrication is supported by the micro-fabrication lab on IOP-China, National Center for Nanoscience and Technology and USTC.

MEMO

Poster Session Ⅰ
Abstract

Energy detuning control of a superconducting flux qubit using microwave irradiation

H. Toida[1], T. Ohrai[1,2], Y. Matsuzaki[1], K. Kakuyanagi[1], H. Yamaguchi[1], and S. Saito[1,2]

[1] *NTT Basic Research Laboratories*
[2] *Tokyo University of Science*

To realize practical quantum devices, both coherent property and controllability of a qubit is crucial. Superconducting qubits are one of the solid state candidate and their coherence time reach ~0.1 ms with 3D architectures [1]. However, qubits in 3D cavities have smaller controllability due to intrinsic difficulty of wiring.

We demonstrate one possible solution for the controllability of the superconducting flux qubit in a 3D cavity by coupling the qubit with a superconducting quantum interference device (SQUID). In our device, the SQUID works as a magnetic flux tunable inductor in a resonance circuit, which mediates microwave control tone and magnetic flux penetrating through the qubit.

In the experiment, we irradiate two microwave tones to the device: one is a spectroscopy tone of the qubit and the other is a energy detuning control tone. We control the energy detuning of the qubit at several operating points of the qubit (Fig. 1). We observe that we can control the energy of the qubit depending on the sign of the energy detuning when the excitation frequency matches to the SQUID based tunable resonator ($\sim$ 3.45 GHz). We confirm linear relationship between the energy tuning and microwave power at least up to $\sim$ 1.5 GHz.

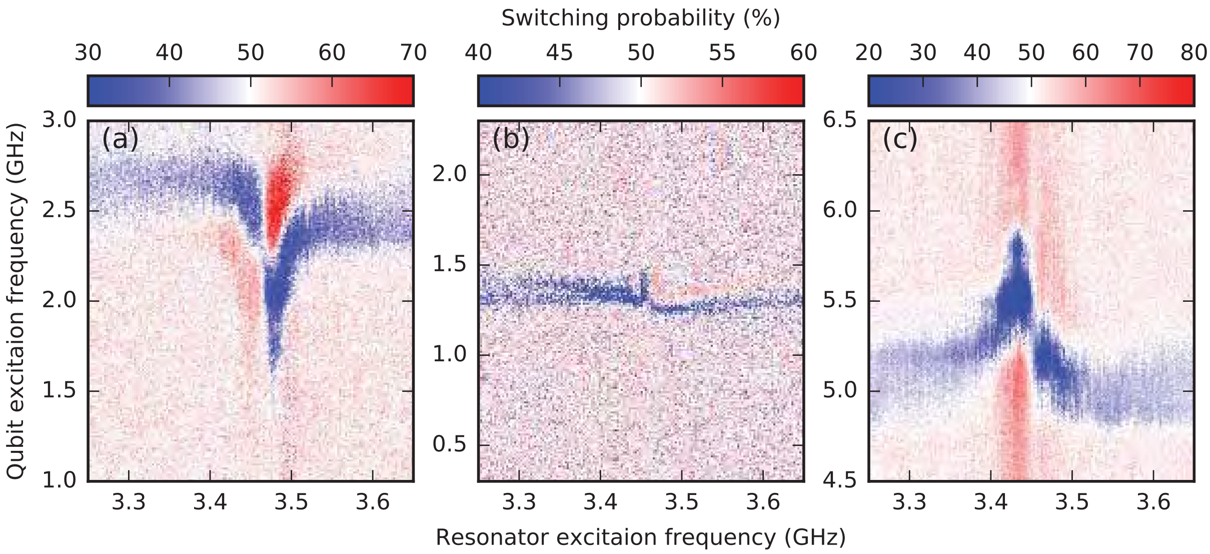

Figure 1: Energy detuning control of a superconducting flux qubit. Operating point is fixed at (a) negative, (b) near zero, and (c) positive detuning.

[1] C. Rigetti, J. M. Gambetta, S. Poletto, B. L. T. Plourde, J. M. Chow, A. D. Córcoles, J. A. Smolin, S. T. Merkel, J. R. Rozen, G. A. Keefe *et al.*, Phys. Rev. B **86**, 100506 (2012).

Superconducting flux qubits embedded in a 3D cavity

S. Saito[1], I. Mahboob[1], H. Toida[1], Y. Matsuzaki[1], K. Kakuyanagi[1], W. J. Munro[1], Y. Nakamura[2,3], and H. Yamaguchi[1]

[1] *NTT Basic Research Laboratories, NTT, Kanagawa, 243-0198, Japan*
[2] *Research Center for Advanced Science and Technology, the University of Tokyo, Tokyo 153-8904, Japan*
[3] *Center for Emergent Matter Science, RIKEN, Saitama, 351-0198, Japan*

Signigicant worldwide effort have been undertaken to improve the coherence time of superconducting qubits. Recently a 3D cavity architecture has been developed to drastically elongate the coherence time of transmon qubits to 92 μs [1,2]. On the other hand, flux qubits were also improved using high quality shunt capacitors [3]. A coherence time of 85 μs has been oberved. In this case the C-shunt flux qubit was coupled to a 2D coplanar waveguide resonator to perform a dispersive qubit readout. A 3D cavity is expected to provide a cleaner electromagnetic environment for qubits compared to the typical coplanar resonator. Therefore we put a C-shunt flux qubit into a 3D cavity to improve its coherence.

We fabricated a C-shunt flux qubit on a sapphire substrate. The structure of the qubit is similar to a 3D transmon. Here we replaced the Josephson junction of the transmon by a 3 Josephson junction type flux qubit (see Figure 1). The two pads of the anntena works as a shunt capacitor for the qubit. The measured coupling strength between the qubit and the cavity was 79 MHz, enough for dispersive qubit readout. From qubit spectroscopy, we estimate a Josephson energy E_J and a charging energy E_c of typical junctions as 190 GHz and 2.35 GHz, respectively. The 3rd junction is α = 0.45 times smaller than the typical junctions and the shunt capacitor is 50 fF. The qubit transition frequency at the optimal point (Φ_{qb} = 0.5 Φ_0) is 5.0714 GHz and the relaxation time is about 30 μs. Figure 2 shows the Ramsey decay time T_{2R} and echo decay time T_{2E} around the optimal point. Although the coherence times are much shorter than 3D transmons or C-shunt flux qubits, we have a room to improve electromagnetic shielding and filtering of measurement lines

When a long coherence flux qubit is realized, it will be useful not only for quantum computation but also as a sensitive magnetic field sensor. Recently we demonstrated electron spin resonance (ESR) of nitrogen vacancy (NV) center in diamond using a superconducting quantum interference device [4]. By using the flux qubit as the spin detector, we should realize ESR with single spin sensitivity.

[1] C. Rigetti, et al., Phys. Rev. B 86, 100506R (2012).
[2] H. Paik, et al., Phys. Rev. Lett. 107, 240501 (2011).
[3] F. Yan, et al., Nature Commun. 7, 12964 (2017).
[4] H. Toida, et al., Appl. Phys. Lett. **108**, 052601 (2016).

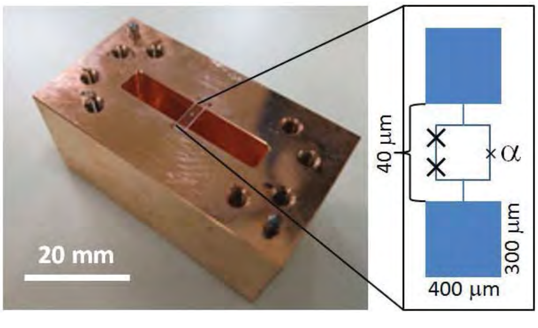

Fig.1. 3D cavity and a C-shunt flux qubit

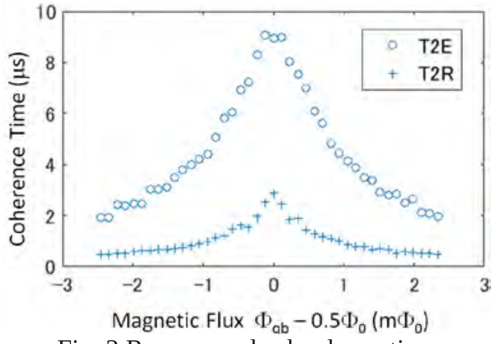

Fig. 2 Ramsey and echo decay time

Excitons in capacitively coupled chains of small Josephson junctions

H. Shimada, K. Matsudo, C. Ishida, H. Murai and Y. Mizugaki

Department of Engineering Science, The University of Electro-Communications, Chofu, Tokyo 182-8585, Japan

In capacitively coupled two chains of mesoscopic Josephson junctions, a variety of current induction phenomena can be observed depending on the parameters such as the biases on the chains, the applied magnetic field, the strength of coupling, temperature, etc [1,2]. In this study, we demonstrate the transport of Cooper-pair excitons and quasiparticle excitons in such a system with large coupling capacitance C_c. The system is two chains of 20 mesoscopic Al/AlO_x/Al junctions with each facing electrodes being coupled via C_c (1-6 fF) that is greater than the capacitance C (~ 1 fF) of the junction. Here, "exciton" means the bound state of each entity (a Cooper pair or a quasiparticle) and its positive hole due to the Coulomb interaction via the coupling capacitance. The transport of these excitons manifested itself as current induction in the opposite direction when one of the chains was biased to pass a current in one direction and the other unbiased. This should be due to the correlated tunnelings of the constituent entities of the exciton in the same direction.

The Cooper-pair excitons appeared when the bias voltage V was small (< 1 mV), while the quasiparticle excitons appeared when V was above the superconducting-gap voltage (~ 40 Δ/e = 8 mV, Δ being the superconducting gap of Al and e the elementary charge). In the latter case, we claim that the recombination phonons with energy 2Δ associated with the quasiparticle tunnelings in the biased chain mediate the generation of non-equilibrium quasiparticles in the unbiased chain and formation of the bound state of a quasiparticle and a positive hole, i.e. anti-quasiparticle, in the two chains [3,4].

In both cases, the current induction characteristics were more prominent when the coupling strength C_c/C was larger and the temperature T was lower, indicating the larger probability of forming the excitons. From the temperature dependence of the current-induction coefficient in the rage 80 mK < T < 1 K, we obtained the binding energies of these excitons E_b of the order of 100 μeV [5]. The magnitude of the obtained E_b's is consistent with that deduced from the equivalent capacitance model, indicating the relevance of the exciton-transport picture.

[1] H. Shimada and P. Delsing, Phys. Rev. Lett. **85**, 3253 (2000).
[2] H. Shimada, C. Ishida, and Y. Mizugaki, Phys. Rev. Lett. **109**, 196801 (2012).
[3] W. Eisenmenger and A. H. Dayem, Phys. Rev. Lett. **18**, 125 (1967).
[4] O. O. Otelaja, et al., New J. Phys. **15**, 043018 (2013).
[5] F. E. Williams and H. Eyring, J. Chem. Phys. **15**, 289 (1947).

A 3D JPA

Imran Mahboob[1†], Hiraku Toida[1], Kosuke Kakuyanagi[1], Yasunobu Nakamura[2] and Shiro Saito[1]
[1] *NTT Basic Research Laboratories, NTT Corporation, Atsugi-shi, Kanagawa, Japan*
[2] *The Research Center for Advanced Science and Technology, The University of Tokyo, Japan*
[†]imran.mahboob@lab.ntt.co.jp

Josephson parametric amplifiers (JPAs) pioneered decades ago [1] have re-emerged as essential components for quantum non-demolition readout of superconducting qubits. The Josephson junction at the heart of the JPA is invariably embedded in a waveguide resonator in the guise of superconducting quantum interference device (SQUID). The JPA can then be activated in a four-wave/three-wave mixing configuration by pumping current/flux at the natural/twice the natural frequency of the resonator to non-linearly modulate the Josephson inductance [2, 3].

Meanwhile 3D cavities have emerged as clean electromagnetic environments thus leading to ultra-high quality factor resonators which offer a superior circuit QED architecture and it has resulted in qubits with unprecedented lifetimes and coherence [4, 5]. Here we extend this platform to build a 3D JPA namely a high quality factor 3D resonator embedded with a flux pumped SQUID. Specifically this architecture offers a reduced participation ratio from the inherent non-linearity of the SQUID inductance to the total circuit inductance thus leading to a dilution in the Josephson non-linearity which should result in an enhanced dynamic range for the JPA. In addition to offering amplification with unprecedented fidelity this architecture also lays the foundations to study side-band quantum optics with microwave photons [6].

[1] B. Yurke et al. Phys. Rev. A **39**, 2519 (1989)
[2] M. A. Castellanos-Beltran and K. W. Lehnert, Appl. Phys. Lett. **91**, 083509 (2007)
[3] T. Yamamoto et al., Appl. Phys. Lett. **93**, 042510 (2007)
[4] H. Paik et al. Phys. Rev. Lett. **107**, 240501 (2011)
[5] M. Reagor et al. Phys. Rev. B **94**, 014506 (2016)
[6] A. J. Sirois et al. Appl. Phys. Lett. **106**, 172603 (2015)

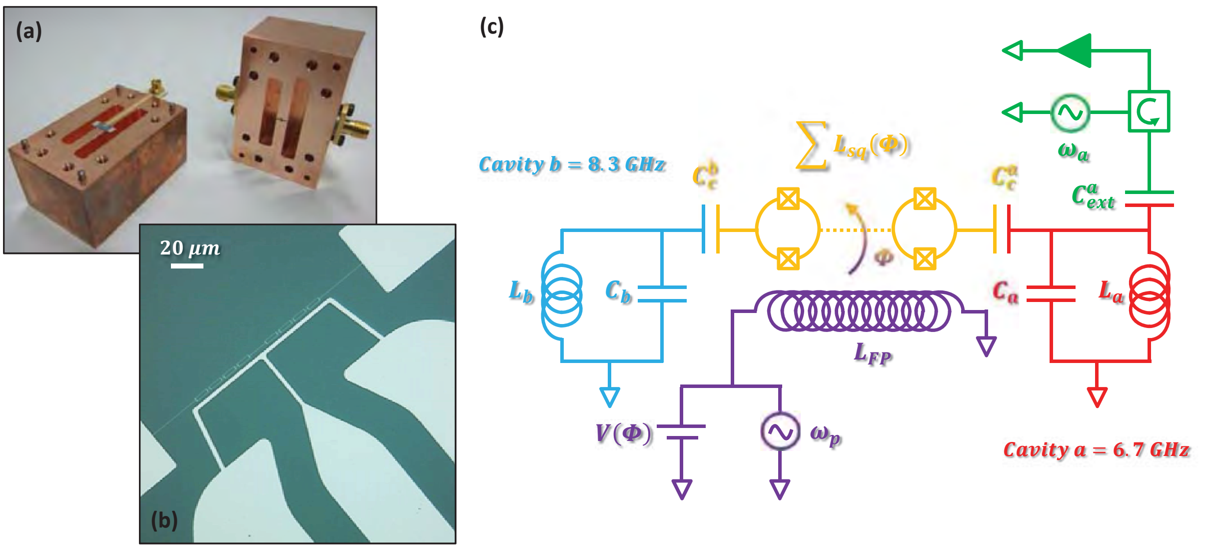

Figure 1: (a) A photograph showing two 3D cavities embedded with SQUIDs that are capacitively coupled to the cavities via large rectangular antennae and flux pumped via a coplanar waveguide on a ceramic substrate. (b) An optical image showing an array of 8 Al/AlO_2 SQUIDs, patterned via e-beam on a highly resistive silicon substrate, which are galvanically connected to the antennae and inductively coupled to the flux pump line. (c) A simplified circuit schematic depicting the 3D cavities capacitively coupled to the array of flux pumped SQUIDs where one of the cavities is probed.

Quantum Dynamics of a Josephson Junction-Driven Cavity Mode System in the Presence of Voltage Bias Noise

Hui Wang[1], M. P. Blencowe[1], A. D. Armour[2] and A. J. Rimberg[1]

[1] *Department of Physics and Astronomy, Dartmouth College, Hanover, New Hampshire 03755, USA*
[2] *School of Physics and Astronomy and Centre for the Mathematics and Theoretical Physics of Quantum Non-Equilibrium Systems, University of Nottingham, NottinghamNG7 2RD, UK*

When a Josephson junction (JJ) device is embedded within a superconducting microwave cavity, the energy supplied by a dc voltage bias can be converted into microwave photons [1, 2, 3]. The resulting radiation is predicted to display non-classical properties over a wide range of conditions, some of which have now been demonstrated in experiment [3].
In Ref. [4] we showed using a simple theoretical model of a single JJ embedded in a high-Q cavity that amplitude squeezing might occur even at very large cavity occupation numbers. However, in that analysis the presence of voltage bias noise was neglected. Since it is not possible to entirely eliminate bias noise in real devices, it is important to determine its effect on the quantum dynamics and in particular on the predicted amplitude squeezing of the microwave steady states which are expected to be sensitive to various sources of noise.

In our present work [5], we therefore extend the analysis of Ref. [4] to account for bias noise. We give a semiclassical analysis of the average photon number as well as photon number variance (Fano factor F) for a JJ embedded microwave cavity system, where the JJ is subject to a fluctuating (i.e. noisy) bias voltage with finite dc average. Through the ac Josephson effect, the dc voltage bias drives the effectively nonlinear microwave cavity mode into an amplitude squeezed state ($F < 1$), as has been established previously [4], but bias noise acts to degrade this squeezing. We find that the sensitivity of the Fano factor to bias voltage noise depends qualitatively on which stable fixed point regime the system is in for the corresponding classical nonlinear steady state dynamics. Furthermore, we show that the impact of voltage bias noise is most significant when the cavity is excited to states with large average photon number.

[1] O. Astafiev, K. Inomata, A. O. Niskanen, T. Yamamoto, Yu. A. Pashkin, Y. Nakamura and J. S. Tsai, Nature (London) **449** 588 (2007).
[2] F. Chen, J. Li, A. D. Armour, E. Brahimi, J. Stettenheim, A. J. Sirois, R. W. Simmonds, M. P. Blencowe, and A. J. Rimberg, Phys. Rev. B 90, 020506 (2014).
[3] M. Westig, B. Kubala, O. Parlavecchio, Y. Mukharsky, C. Altimiras, P Joyez, D. Vion, P. Roche, M. Hofheinz, D Esteve, M Trif, P. Simon, J. Ankerhold and F. Portier, arXiv:1703.05009 (2017).
[4] A. D. Armour, M. P. Blencowe, E. Brahimi, and A. J. Rimberg, Phys. Rev. Lett. **111**, 247001 (2013).
[5] H. Wang, M. P. Blencowe, A. D. Armour, and A. J. Rimberg, ar Xiv:1704.07476 (to appear in Phys. Rev B).

Realization of a Nanowire Superinductance

David Niepce, Jonathan Burnett and Jonas Bylander

Chalmers University of Technology, Microtechnology and Nanoscience
SE-41296 Göteborg, Sweden

Recent years have seen tremendous progress in the preservation of quantum coherent states in superconducting circuits, a development driven by both device and materials engineering. A still outstanding problem in many device architectures, with applications in quantum information processing and quantum metrology, is caused by decoherence due to charge fluctuations. The sensitivity to charge fluctuations can be suppressed by embedding the circuit in a high-impedance microwave environment—a superinductance [1]—i.e. a non-dissipative, inductive circuit element with impedance greater than the quantum resistance ($R_Q = h/4e^2 \simeq 6.5\,\mathrm{k}\Omega$) and low losses at the frequency of the circuit (several GHz). This requirement cannot be met using the ordinary, geometric inductance of a wire due to its unavoidable shunt capacitance, but superinductance was realized using a Josephson junction array [2].

An attractive alternative to arrays is offered by the high kinetic inductance of strongly disordered superconducting thin films. We have fabricated niobium-nitride nanowires with widths down to 40 nm and thickness typically 20 nm, implementing a superinductance with impedance $Z = 6.8\,\mathrm{k}\Omega$ [3]. We demonstrate internal quality factors $Q_i = 25,000$ at single photon excitation, significantly higher than values reported in devices with similar materials and geometries [4]. Moreover, we show that the dominant dissipation in our nanowires is not an intrinsic property of the disordered films, but can instead be understood within the well-studied framework of two-level systems [5].

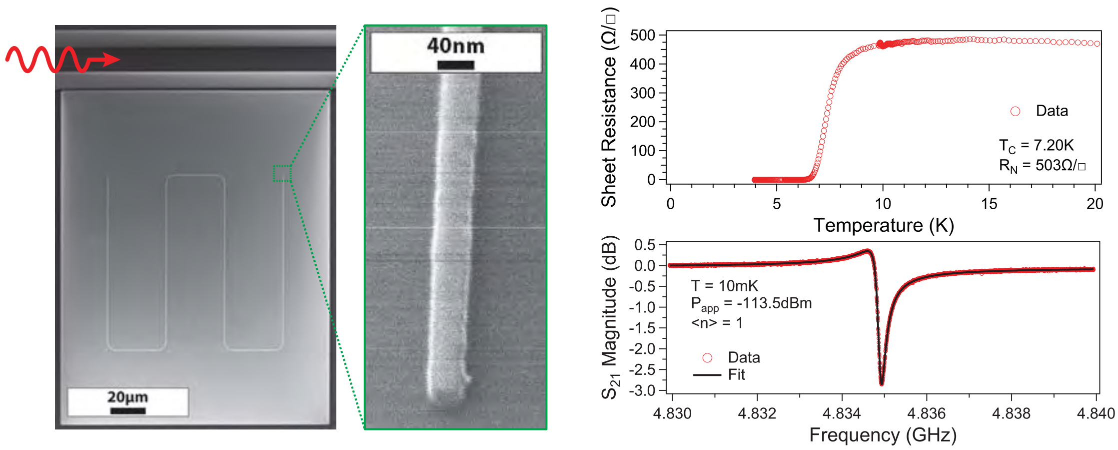

Figure 1: **Left:** SEM micrograph of a nanowire resonator coupled to its feed line; the NbN feed line and ground plane are shown in black, the Si substrate is in gray, and the 40 nm × 680 µm nanowire is light gray. The closeup shows a helium FIB image of the nanowire (courtesy of O.W. Kennedy, University College London). **Top right:** $R(T)$ characteristic of a nanowire. **Bottom right:** S_{21} magnitude response of the device on the left, in the single-photon regime, with fit.

[1] V. E. Manucharyan *et al.*, Science **326**, 113-116 (2009).
[2] N. A. Masluk *et al.*, Phys. Rev. Lett. **109**, 137002 (2012).
[3] D. Niepce *et al.*, submitted.
[4] O. V. Astafiev *et al.*, Nature **484**, 355-358 (2012).
[5] J. Burnett *et al.*, Phys. Rev. Applied **8**, 014039 (2017).

Coherent emission of a continuously driven three-level artificial atom

I. Antonov[1], R. Shaikhaidarov[1], T. Hönigl-Decrinis[1,2], V.N. Antonov[1,2], O.V. Astafiev[1,2,3]

[1] *Royal Holloway, University of London, Egham, Surrey TW20 0EX, United Kingdom*
[2] *National Physical Laboratory, Teddington, TW11 0LW, United Kingdom*
[3] *Moscow Institute of Physics and Technology, 141700 Dolgoprudny, Russia*

Operating with three levels in artificial atoms enables the observation of intricate quantum interference phenomena such as electromagnetically induced transparency [1] and Autlers-Townes splitting [2]. In this work we demonstrate the additional capability of quantum frequency mixing in this system, by converting two incident microwave fields of different frequencies to an output field at exactly a single frequency.

We illuminate the artificial atom with two external microwave fields, thus changing its energy-level populations. The strict requirement that relaxation can only occur between the available three levels results in coherent emission at a *single* mixed frequency. This enables a higher degree of emission control compared to the classical mixing case, where emissions would be observed at the sums and differences of the incident frequencies [3].

The three-level artificial atom is an aluminium superconducting loop interrupted by four Josephson junctions - a general flux qubit geometry [4]. We observe emission at a single mixed frequency and model the evolution of its strength with different driving regimes by numerical simulations. For example, detuning the driving fields from the inter-level transition frequencies results in the suppression of interaction of radiation with the atom and, correspondingly, a weaker emission strength.

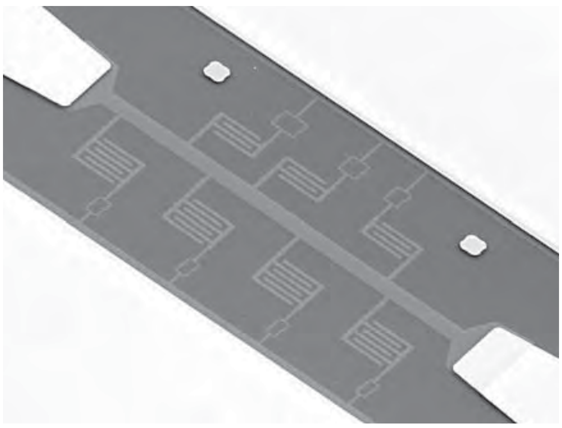

(a) SEM image of the superconducting flux qubits, capacitively coupled to the transmission line.

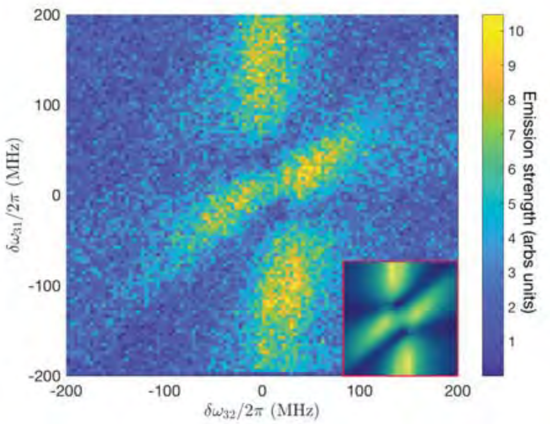

(b) Measured artificial atom emission as a function of the driving field detunings, $\delta\omega$, compared to the simulation (inset).

[1] A.A Abdumalikov, O. Astafiev, A.M. Zagoskin, et. al, Phys. Rev. Lett. **104**, 193601 (2010).
[2] M. Baur, S. Filipp, R. Bianchetti, et. al, Phys. Rev. Lett. **102**, 243602, (2009).
[3] M. Scully, M. Zubairy, "Quantum Optics", Cambridge University Press (1997).
[4] J. E. Mooij, T.P. Orlando, L. Levitov, et.al, Science, **285**, 1036, (1999).

Coupling a superconducting qubit to light using hybrid qubit-quantum dot nanostructures

V.E. Elfving [1], S. Das [1] and A.S. Sørensen [1]

[1] *Niels Bohr Institute, University of Copenhagen*

Several advances in quantum computation have been achieved with superconducting qubits in recent years. In parallel to this, methods of quantum communication and quantum key distribution have been developed using optical photons as flying qubits. In order for quantum computers to effectively communicate with each other, and for quantum networks to extend their range by quantum repeaters, an interface between these two physical systems is highly desirable.

Strenuous efforts have been made to coherently couple superconductors and light. However, such an interface is complicated by the large energy mismatch between superconducting qubits (micro eV's) and optical photons (eV's). As a consequence of this mismatch even the absorption of a single or few optical photons can significantly disturb a superconducting qubit, making it necessary to screen them from light.

To tackle this issue, we theoretically propose a hybrid system incorporating a semiconductor quantum dot (QD) embedded in a photonic nanostructure as an interface between a superconducting qubit and an optical photon.

The oscillation of a Cooper pair between superconducting islands introduces an electric field in its immediate surroundings depending on the state of the superconducting qubit. Due to the strong dipole moment and the associated Stark shift in quantum dots, combined with the recently achieved narrow linewidth, a significant shift in the QD transition energy can be achieved by the oscillation of a single cooper pair.

We theoretically describe a Raman scheme mediated by the QD, which flips the state of the superconducting qubit state by emitting a red detuned optical photon. For further enhancement of the efficiency, we employ a scheme where two QD's embedded in a photonic nanostructure waveguide optically couple to each other and form a 'dark state'. At certain spacing of the QD's, the photonic excitation lifetime can be greatly extended; as a consequence the effective coupling to the qubit and therefore the Raman process can be made highly efficient. The Raman scheme can be extended to generate entanglement between distant superconducting qubits through entanglement swapping with an interferometry setup, and can thus connect different superconducting quantum computers through teleportation.

Strong light-matter coupling can be achieved for quantum dots, with efficient coupling to single photons. As a consequence, the envisioned light matter interface can be achieved at very low light levels, possibly involving incident photons fields containing merely a few or a single photon(s). This alleviates the challenge of the large energy mismatch between superconductors and optical fields since it will lead to minimal absorption in the superconducting qubits. The resulting hybrid system can then form the basis of a large scale "quantum internet" based on super conducting systems.

Giant Lamb shift observed in deep-strongly-coupled superconducting qubit-oscillator circuit

Z. Ao [1,2], F. Yoshihara [2], T. Fuse [2], S. Ashhab [3], K. Kakuyanagi [4], S. Saito [4], T. Aoki [1], and K. Semba [2]

[1]*Depertment of Applied Physics, Waseda University, Tokyo, Japan*
[2]*National Institute of Information and Communications Technology, Koganei, Japan*
[3]*Qatar Environment & Energy Research Institute, Doha, Qatar*
[4]*NTT Basic Research Laboratories, Atsugi, Japan*

A cavity can enhance the interaction between an electromagnetic field and an atom, and make the effect of the vacuum easier to observe. One observable effect of the vacuum is the Lamb shift, which was found as a radiative energy level shift of about 0.4 ppm of the optical transition frequency in a hydrogen atom [1]. A large Lamb shift, corresponding to 1.4% of the bare-qubit frequency, was observed in a circuit quantum electrodynamics system [2].

Here, we report a giant Lamb shift observed in a superconducting flux qubit deep-strongly coupled to an LC resonator, where the coupling strength exceeds both the resonant frequency of the cavity and the transition frequency of the qubit [3]. The deep-strongly coupled qubit-LC resonator circuit can be described by the Rabi-model Hamiltonian H_{Rabi}:

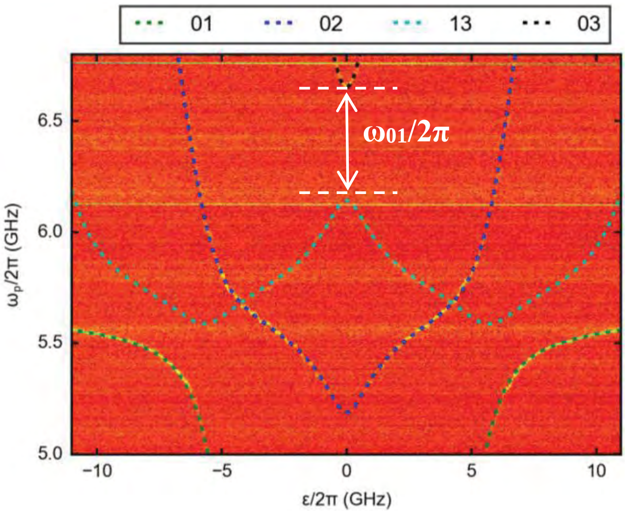

Measured and calculated transition energy spectra. 0, ⋯, 3 represent the ground, ⋯, 3rd excited state. Green, blue, cyan, and black dotted line represents the ε dependence of transition frequency ω_{01}, ω_{02}, ω_{13}, and ω_{03}, respectively.

$$H_{Rabi} = -\frac{\hbar}{2}(\Delta\sigma_x + \varepsilon\sigma_z) + \hbar\omega_0\left(a^\dagger a + \frac{1}{2}\right) + \hbar g\sigma_z(a + a^\dagger).$$

Here, $\hbar\Delta$ and $\hbar\varepsilon$ are respectively the tunneling energy and the energy bias between the clockwise and anti-clockwise circulating current states of the flux qubit, σ_x and σ_z are Pauli operators, $\omega_0/2\pi$ is the resonant frequency of the LC resonator, $a^\dagger$ (a) is the creation (annihilation) operator, and g is the coupling strength. The measured transition energy spectra of the coupled system were fit by H_{rabi} to obtain $\omega_0/2\pi$ = 5.59 GHz, $g/2\pi$ = 5.63 GHz, and the bare-qubit transition frequency $\Delta/2\pi$ = 3.84 GHz. The qubit transition frequency is predicted to be suppressed as $\omega_{01} = \Delta\exp(-2g^2/\omega_0^2)$ in the limit of $\Delta \ll \omega_0$ [4]. From the measured transition energy spectra, $\omega_{01}/2\pi$ = 510 MHz, was obtained from the difference between the observed $\omega_{03}/2\pi$ and $\omega_{13}/2\pi$ at $\varepsilon = 0$. This result shows that the deep-strong coupling between the qubit and the vacuum caused a giant Lamb shift of 3.33 GHz, corresponding to 86.7% of $\Delta/2\pi$. Although $\Delta/2\pi$ is comparable to $\omega_0/2\pi$, this result agrees with the analytical expression which gives a Lamb shift of 3.34 GHz, corresponding to 87.0% of $\Delta/2\pi$.

[1] W. E. Lamb and R. Retherford, Phys. Rev. **72**, 241 (1947).
[2] A. Fragner et al., Science **322**, 1357 (2008).
[3] F. Yoshihara, T. Fuse et al., Nature Phys. **13**, 44 (2017).
[4] S. Ashhab and Franco Nori, Phys. Rev. A **81**, 042311 (2010).

Parity symmetry and selection rules in a qubit-harmonic oscillator coupled system

Tomoko Fuse [1], Fumiki Yoshihara [1], Sahel Ashhab [2], Kosuke Kakuyanagi [3], Shiro Saito [3], and Kouichi Semba [1]

[1]*National Institute of Information and Communication Technology, Koganei, Tokyo, Japan*
[2]*Qatar Environment and Energy Research Institute, Doha, Qatar*
[3]*NTT Basic Research Laboratories, Atsugi, Kanagawa, Japan*

The Rabi Hamiltonian, $H = \hbar\omega_o(a^\dagger a + 1/2) + \hbar\Delta\sigma_z/2 + \hbar g(a + a^\dagger)\sigma_x$ [$a^\dagger$ (a): photon creation (annihilation) operator, σ_z (σ_x): qubit Pauli matrix, $\hbar\omega_o$: photon energy, $\hbar\Delta$: qubit energy gap, $\hbar g$: coupling energy], describes a qubit – harmonic oscillator coupled system where the interaction term is orthogonal to the qubit term. In a system described by the Rabi model, the energy eigenstates are also eigenstates of the parity operator $\sigma_z(-1)^{a^\dagger a}$. This is understood by considering the symmetry in the states and operators at g = 0, as shown in Table 1. Although the transition energies change a lot with increasing g, as shown in Figure 1, this parity symmetry still holds in the energy eigenstates even in the deep strong coupling regime, where the coupling energy exceeds the bare photon energy and the qubit energy.

In the presentation, experimentally measured transition energy spectra of the flux qubit – LC oscillator coupled circuit will be shown in the deep strong coupling regime, and the selection rule observed in the transitions will be discussed, associated with the parity symmetry of the coupled circuit.

parity	+	-
qubit state	$\lvert g\rangle = (\lvert\uparrow\rangle + \lvert\downarrow\rangle)/\sqrt{2}$	$\lvert e\rangle = (\lvert\uparrow\rangle - \lvert\downarrow\rangle)/\sqrt{2}$
photon state	$\lvert$even number$\rangle$	$\lvert$odd number$\rangle$
qubit operator	σ_z	$\sigma_x = \sigma_+ + \sigma_-$
photon operator	$\hat{a}^\dagger\hat{a}$	$\hat{a} + \hat{a}^\dagger$

Table 1: Parity symmetry in the states and operators at g = 0.

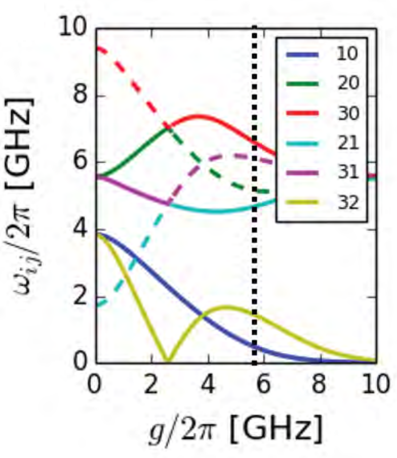

Figure 1: Calculated transition energy spectra of the qubit –harmonic oscillator coupled circuit. The circuit parameters obtained in the measurements are used. "ij" transition is the transition from the energy eigenstate |j> to |i>. The lower energy eigenstates are labeled with the smaller number (|0> is the ground state). Solid (dashed) curves indicate the allowed (forbidden) transitions.

[1] F. Yoshihara, T. Fuse, S. Ashhab, K. Kakuyanagi, S. Saito and K. Semba: Nature Physics **13**, 44 (2017).

Parity-preserving light-matter system mediates effective two-body interactions

Thi Ha Kyaw [1], Sebastian Allende [2], Leong-Chuan Kwek [1,3,4,5], and Guillermo Romero [2]

[1] *Centre for Quantum Technologies, National University of Singapore, 3 Science Drive 2 Singapore 117543*
[2] *Departamento de Física, Universidad de Santiago de Chile (USACH), Avenida Ecuador 3493, 9170124, Santiago, Chile*
[3] *MajuLab, CNRS-UNS-NUS-NTU International Joint Research Unit, UMI 3654, Singapore*
[4] *Institute of Advanced Studies, Nanyang Technological University, 60 Nanyang View, Singapore 639673*
[5] *National Institute of Education, Nanyang Technological University, 1 Nanyang Walk, Singapore 637616*

The ultrastrong coupled (USC) qubit-cavity system or quantum Rabi system (QRS) is extensively studied for its potential impetus to speed up quantum information processing at subnanosecond timescales [1,2], particularly within the framework of circuit quantum electrodynamics [3]. For instance, Ref. [1] proposed the use of a tunable qubit–cavity coupling strength [4] to attain ultrafast two-qubit gates. Nevertheless, the major caveat of the above mentioned proposal is the need of various magnetic fluxes acting upon a flux qubit, during quantum gate operations. A typical flux qubit is micrometre in size, thus it is very hard to implement micrometre resolution magnetic field lines threading the qubit without making any interference among them. With our proposed framework [5], the magnetic crosstalk problem could be overcome, while it might preserve the similar quantum computing performance as [1].

Here, we present a parity-preserving USC system that mediates effective two-body interactions, with four compelling characteristics that might have important implications in superconducting circuit-based quantum computing (i–iii) and solid-state physics (iv) communities. (i) Strong two-qubit interaction with an increase in the qubit–cavity coupling strength of the QRS (g_p/w_{cav}) is demonstrated. (ii) A tunable qubit–qubit interaction could be performed by sweeping only the qubits energy gap for fixed QRS parameters, without requiring complex flux qubit architectures of [1]. (iii) Manipulation of the qubits energy gap does not change the underlying Z_2 symmetry, with which generalisation to a system, with N qubits and a QRS, can easily be extended; thereby we provide an intuitive physical insight. (iv) Enhanced excitation transfer between the two non-identical qubits with increase in g_p/w_{cav} is shown, while one qubit experiences an incoherent pumping and the other one experiences a loss mechanism. From extensive numerical studies, we will provide an interesting physical insight that might shed some light on the cavity-enhanced exciton transport in disordered medium [6], especially within the context of polyatomic molecules in the USC regime [7].

[1] G. Romero, D. Ballester, Y. Wang, V. Scarani, and E. Solano, Phys. Rev. Lett. **108**, 120501 (2012).
[2] Y.-D. Wang, A. Kemp, and K. Semba, Phys. Rev. B **79**, 024502 (2009).
[3] A. Blais, R. S. Huang, A. Wallraff, S. M. Girvin, and R. J. Schoelkopf, Phys. Rev. A **69**, 062320 (2004).
[4] B. Peropadre, P. Forn-Díaz, E. Solano, and J. J. García-Ripoll, Phys. Rev. Lett. **105**, 023601(2010).
[5] T. H. Kyaw, S. Allende, L.-C. Kwek, and G. Romero, Quantum Sci. Technol. **2**, 025007 (2017).
[6] J. Schachenmayer, C. Genes, E. Tignone, and G. Pupillo, Phys. Rev. Lett. **114**, 196403 (2015).
[7] M. Mazzeo et. al., Appl. Phys. Lett. **104**, 233303 (2014).

Superradiance with local phase-breaking effects

Nathan Shammah[1], Neill Lambert[1], Franco Nori[1,2], and Simone De Liberato[3]

[1] *CEMS, RIKEN, Wako-shi, Saitama 351-0198, Japan*
[2] *Department of Physics, University of Michigan, Ann Arbor, Michigan 48109-1040, USA*
[3] *School of Physics and Astronomy, University of Southampton, Southampton, SO17 1BJ, United Kingdom*

We study the superradiant evolution of a set of N two-level systems spontaneously radiating under the effect of phase-breaking mechanisms [1]. We investigate the dynamics generated by nonradiative losses and pure dephasing, and their interplay with spontaneous emission. Our results show that in the parameter region relevant to many solid-state cavity quantum electrodynamics experiments [2], even with a dephasing rate much faster than the radiative lifetime of a single two-level system, a sub-optimal collective superfluorescent burst is still observable. Using an algorithm based on a permutational invariant technique, we simulate exactly the dissipative dynamics of several two-level systems ($N > 10^3$) [2]. We also apply our theory to the dilute excitation regime, often used to describe optical excitations in solid-state systems. In this regime, excitations can be described in terms of bright and dark bosonic quasiparticles. We show how the effect of dephasing and losses in this regime translates into intermode scattering rates and quasiparticle lifetimes [1].

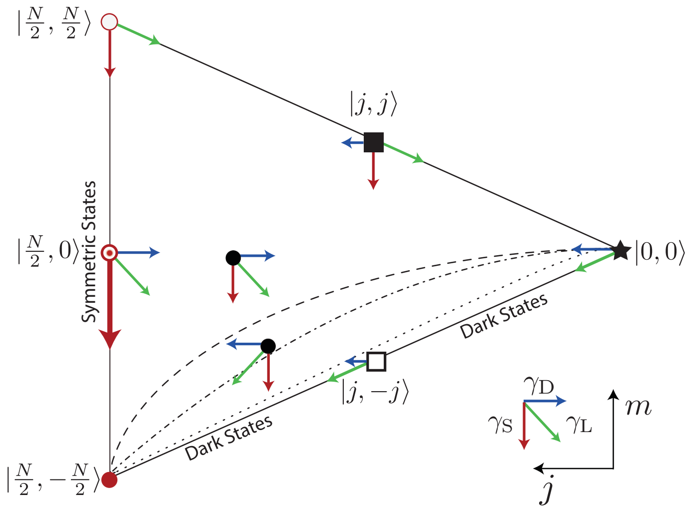

[1] N. Shammah, N. Lambert, F. Nori, and S. De Liberato, Phys. Rev. A **96**, 023863 (2017).
[2] N. Shammah and S. De Liberato, Phys. Rev. B **92**, 201402(R) (2015).
[3] N. Shammah, S. Ahmed, N. Lambert, F. Nori, and S. De Liberato, *in preparation.*

Non-Markovian effect on energy flow

Ryuta Tezuka [1] **and Chikako Uchiyama** [1,2]

[1] *Graduate School of Interdisciplinary Research, University of Yamanashi, 4-3-11, Takeda, Kofu, Yamanashi 400-8511, Japan*
[2] *National Institute of Informatics, 2-1-2 Hitotsubashi, Chiyoda-ku, Tokyo 101-8430, Japan*

Control of energy flow between multiple environments has been investigated from the viewpoint of science as well as engineering [1]. For example, quantum pumping is one of the challenging issue, which aims to find a directed flow of quantum particles through a joint system between two environments under time-dependent modulations such that the bias is averaged out during a period. Ren, Li, and Hanggi [2] succeed to describe the transferred heat under the out-of-phase and sufficiently slow (adiabatic) temperature modulations with the geometrical phase. But, when we rely on such adiabatic modulations, it requires infinitely long time to finish the pumping in principle. Since the experimental techniques in nanoscale has been developing quickly, it might be necessary to provide a basic information on the control of energy flow which finishes in a finite time. While the study is extended to include the non-adiabatic effect [3], as the time scale to be considered to be shorter, we need to take into account the correlation time of the interaction between the relevant system and its environment, which is called as a non-Markovian effect. Such treatment is done for a system where a two-level system interacts with an environment[4]. But, it is necessary to extend the system to include multiple environments.

In this work, we present about a non-Markovian effect on energy flow with a model where a two-level system interacts with two kinds of environments as shown in Fig.1.

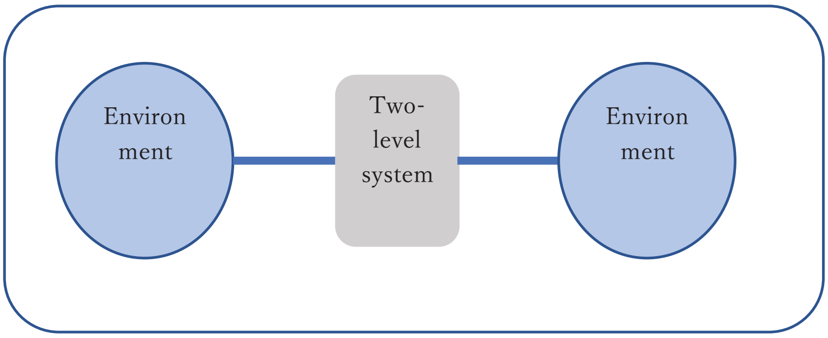

Fig.1. Schematic picture of model treated in this work.

Using a formula obtained by the full counting statistics, we show the dynamics of quantity of energy exchanged between the two-level system and the environments. Especially, even the temperature of the both of the environments are the same, we find the energy backflow can occur in the shorter time region. In this presentation, we show the detailed condition to find the energy backflow. We hope that such information would provide a basic information for design of quantum energy control as quantum pumping in a finite period.

[1] L. Wang and B. Li, Phys. World. **Mar. 21**, 27 (2008); N. Li, J. Ren, L. Wang, G. Zhang, P. Hanggi, and B. Li, Rev. Mod. Phys. **84**, 1045 (2012).
[2] J. Ren, P. Hanggi, and B. Li, Phys. Rev. Lett. **104**, 170601 (2010).
[3] C. Uchiyama, Phys. Rev. E **89**, 052108 (2014).
[4] G. Guarnieri, C. Uchiyama, and B. Vacchini, Phys. Rev. A. **93**, 012118 (2016).

Upper bound on the two-way assisted private capacity of various quantum channels

Kyohei Tsuji and Yasuhiro Tokura

Graduate School of Pure and Applied Sciences, University of Tsukuba

In the last three decades, various quantum key distribution (QKD) protocols have been proposed. Moreover, they have been studied not only theoretically but also experimentally (for example, [1]). In 2014, Takeoka et al.[2, 3] have shown that, regardless of the QKD protocol used, a secret key agreement capacity of lossy optical channel is upper bounded by squashed entanglement of that channel. However, there is room for improvement on this estimation of upper bound. As the aforementioned work, understanding the limit of QKD protocols is useful to improve themselves and to assess the performance of quantum repeater for quantum communications[4].

Original squashed entanglement E_{sq} was defined by Christandl and Winter[5], and it is given by

$$E_{\mathrm{sq}}\left(\rho^{AB}\right) \equiv \inf\left\{\frac{1}{2}I(A;B|E) : \rho^{AB} = \mathrm{Tr}_E\left(\rho^{ABE}\right)\right\}.$$

where $I(A;B|E) = S(AE)+S(BE)-S(ABE)-S(E)$ is the quantum conditional mutual information of ρ^{ABE} and the infimum is taken over all extensions of ρ^{AB}, i.e., $\mathrm{Tr}_E\,\rho^{ABE} = \rho^{AB}$. ρ^A stands for the state on subsystem A and $S(A) = S(\rho^A)$ is the von Neumann entropy. By using the squashed entanglement, Takeoka et al.[2] established capacities for not only lossy optical channel but also some fundamental channels such as Pauli channels, dephasing channel, and so on. Here, we study squashed entanglement of two-way assisted private capacity of various quantum channels and compare our result with the previous work[2].

This work was supported by CREST JST (JPMJCR15N2).

[1] M. Sasaki, et al., Opt. Exp. **19**, 10387 (2011).
[2] M. Takeoka, S. Guha, and M. M. Wilde, IEEE Trans. Inf. Theory **60**, 4987 (2014).
[3] M. Takeoka, S. Guha, and M. M. Wilde, Nat. Commun. **5**, 5235 (2014).
[4] K. Goodenough, D. Elkouss, and S. Wehner, New J. Phys. **18**, 063005 (2016).
[5] M. Christandl and A. Winter, J. Math. Phys. **45**, 829 (2004).

Two-way quantum computer

Akihito Takemura and Yasuhiro Tokura

Graduate School of Pure and Applied Sciences, University of Tsukuba

The research field for the quantum computers is very active since if it is realized, it enables some of the hard problems, which need an expotential time by conventional computers, to be solved in a polynomial time. Historically, the quantum circuit models had been widely used to discuss various quantum algorithms and are now actaully implimented in " IBM Q - Quantum Experience " [1]. In this research, we forcus one-way quantum computer which is one of the quantum computer models[2]. There are two reasons to focus this model. For the first reason, it is a new approach completely different from a quantum computer in a circuit model. For the second reason, experimental demonstration is still unexplored.

In this model, there are two components. The entire resource is provided as a specific entangled state, which is called a cluster state, of a large number of qubits. The other is measurement with arbitrary basis. If there is no limit on the number of qubits that can be used, arbitrary calculations (CNOT gate and 1 qubit unitary transformation) can be realized. Unfortuntely, generating cluster states and measuring arbitrary qubits are still experimentally hard task, except for, possibly, the cold-atom systems. In the qubit system realized in condensed-matter, experimentally feasible geometry in near future of the qubit ensemble is $2{\times}n$ system as shown in Fig.1. If we proceed the measurement from the left to right, which makes the flow of information only in one direction, we can handle at most two effective qubits. We studied the possibility to extend the operation by adding the measurement process from the right to left. We had investigated the possible quantum operations with four qubits realized in this $2{\times}n$ system.

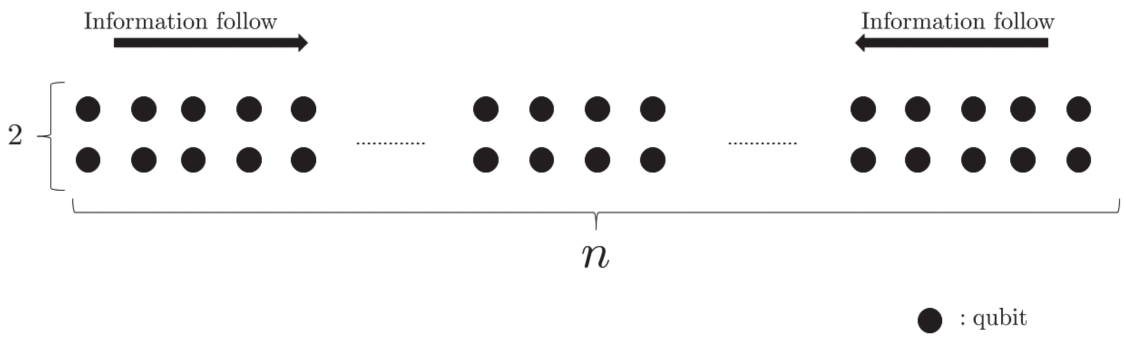

Figure 1: $2{\times}n$ system

[1] "IBM Q - Quantum Experience", https://quantumexperience.ng.bluemix.net/qx/editor
[2] R. Raussendorf and H. J. Briegel, Phys. Rev. Lett. 86, 5188-5191 (2001).

Effects of strong atom-cavity coupling on the entanglement dynamics of two atoms

Sumiya Kato, Ryosuke Suzuki, Kyo Yoshida, and Yasuhiro Tokura

Graduate School of Pure and Applied Sciences, University of Tsukuba

The cavity quantum electrodynamics (cavity QED) is the study of the interaction between light and atoms or other particles in a cavity, under conditions where the quantum nature is significant[1]. Cavity QED is an important hybrid quantum system, which allows the studies on coherent dynamics between different physical systems, and is now extended in other fields, for example, circuit QED[2].

The Jaynes-Cummings model is a basis in the theory of coherent interaction between a two-level atom and a cavity mode[3]. This model is exactly solvable, under the rotating wave approximation (RWA). However, there are strong coupling regimes that RWA can not be applied. They are so-called ultrastrong coupling and deep strong coupling regimes (USC/DSC). These regimes are characterized by ratios between the atom-cavity coupling strength (g) and the cavity mode frequency (ω) of $g/\omega \sim 1$ for the USC regime, and $g/\omega \gtrsim 1$ for the DSC regime[4][5]. Recently, such physics beyond RWA has attracted attention[6].

In the USC/DSC regimes, we can expect to be able to observe phenomena that could not have occurred in the regime that the RWA can be applied. For example, it is known that loss of entanglement, so-called entanglement sudden death (ESD), is prevented by the strength of coupling between the cavities and the atoms[7]. So, in order to investigate the effect of the USC/DSC, we consider two entangled atoms strongly coupled with the cavity mode[8] and examine the dynamics of entanglement.

[1] S. Deleglise et al., Nature 455, 510 (2008).
[2] A. Blais et al., Phys. Rev. A 69, 062320 (2004).
[3] E.T. Jaynes and F.W. Cummings, Proc. IEEE 51, 89 (1963).
[4] P. Forn-Diaz et al., Phys. Rev. Lett. 105, 237001 (2010).
[5] J. Casanova et al., Phys. Rev. Lett. 105, 263603 (2010).
[6] F. Yoshihara et al., Nature Phy. 13, 44-47 (2017).
[7] M. Pandit et al., arXiv, 1612.01165 (2016)
[8] Y. Tabuchi et al., Sci. Res. 349, 6246, 405-408 (2010)

Multi-mode Quantum Rabi Model and Superluminal Signalling

Carlos Sánchez Muñoz[1], Franco Nori[1,2], and Simone De Liberato[3]

[1] *CEMS, RIKEN, Saitama, 351-0198, Japan*
[2] *Department of Physics, University of Michigan, Ann Arbor, MI 48109-1040, USA*
[3] *School of Physics and Astronomy, University of Southampton, Southampton, SO17 1BJ, United Kingdom*

Technological development in the implementation of systems where an optical resonator and an effective two-level system interact strongly has made it increasingly easy to access non-perturbative regimes known as ultra or deep strong coupling, where the coupling rate is of the order of the frequency of the bare modes and counter rotating terms in the Hamiltonian play a relevant role [1,2]. In this work, we address the adequacy of the single-mode Rabi model to describe such systems, and discuss how in those regimes the single-mode approximation yields unphysical result leading to superluminal signalling. We show that the multi-mode description of the field, necessary to account for light propagation at finite speed, yields physical observables, such as transition energies or population dynamics, that differ radically from their single-mode counterpart. Our analysis evidences the fundamental inadequacy of the single-mode Rabi model to describe such systems in the ultrastrong coupling regime and reveals phenomena of fundamental interest on the dynamics of the electric field inside the cavity, where a free photonic wavefront and a bound state of virtual photons are shown to coexists.

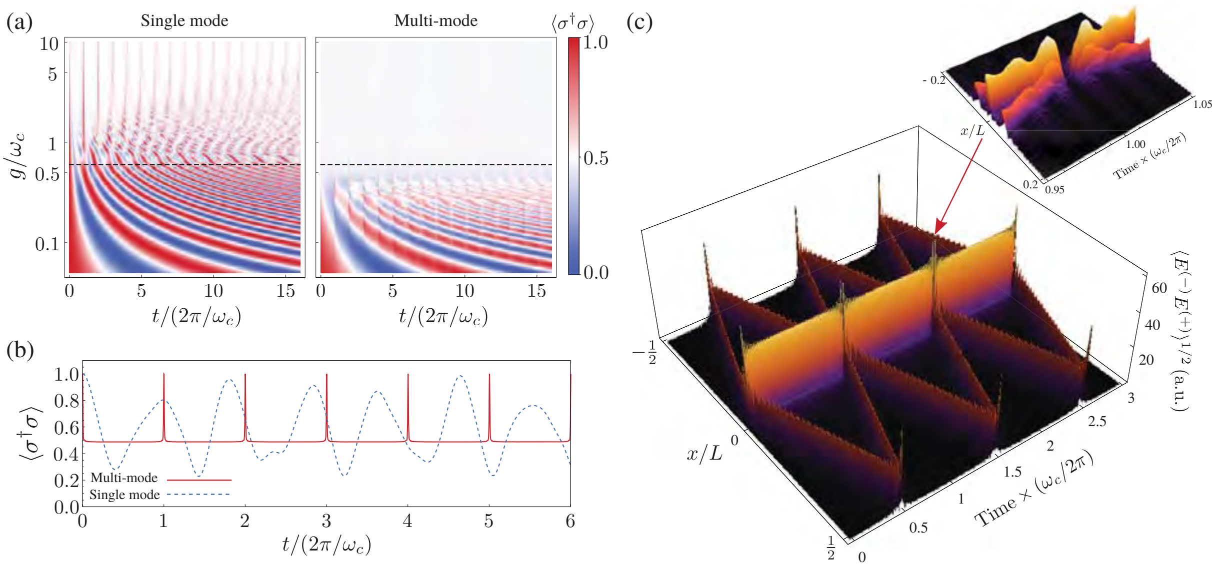

Figure 1: Breakdown of the Rabi model observed trough the dynamics of the 2LS population. (a) Contour plot of the 2LS population as a function of time and coupling rate. (b) Evolution of the population of an initially excited 2LS for the single-mode (blue, dashed) and multi mode (red, solid) cases, for a coupling rate of $g/\omega_c = 0.6$ (c) Amplitude of the electric field inside the cavity as a function of space and time, for $g/\omega_a = 0.6$.

[1] C. Ciuti, G. Bastard, and I. Carusotto, Phys. Rev. B **72**, 115303 (2005).
[2] J. Casanova, G. Romero, I. Lizuain, J. J. García-Ripoll, and E. Solano, Phys. Rev. Lett. **105**, 263603 (2010).

State Preparation and Lifetime Measurements through Spectral Hole Burning in $^{167}Er^{3+}:Y_2SiO_5$

M. IJspeert [1], M. Hiraishi [1,2], T. Tawara [1,2,3,†], K. Shimizu [1], H. Omi [1,3], S. Adachi [4] and H. Gotoh [1]

[1] *NTT Basic Research Laboratories, NTT Corporation, Atsugi, Kanagawa, Japan*
[2] *Department of Physics, Tokyo University of Science, Tokyo, Japan*
[3] *NTT Nanophotonics Center, NTT Corporation, Atsugi, Kanagawa, Japan*
[4] *Graduate School of Engineering, Hokkaido University, Sapporo, Japan*
†tawara.takehiko@lab.ntt.co.jp

Rare-earth doped crystals are promising candidates for solid-state quantum storage devices that allow for optical coherent manipulation. Rare-earth ions exhibit narrow optical homogeneous linewidths that approach the radiative lifetime limit ($T_2 = 2T_1$), highlighting their potential as quantum memories [1]. Erbium-doped systems in particular, with an optical transition (~1.5 μm) coinciding with the telecom wavelength, offer a platform for quantum information networks [2]. Protocols for storing photons in ensembles of atoms often require state preparation within a so-called Λ-system, i.e. a three-level structure with two long lived ground states that can effectively be coupled to an excited state through optical transitions. The corresponding relaxation times impose an upper limit on such manipulations. In this work, we demonstrate state preparation through spectral hole burning (SHB) and estimate the relaxation times of the optically exited and ground state in $^{167}Er^{3+}:Y_2SiO_5$. This opens up possibilities for telecom-band storage protocols in $^{167}Er^{3+}$-doped solids.

For SHB, an isotopically purified $^{167}Er^{3+}$-doped Y_2SiO_5 crystal (0.001% $^{167}Er^{3+}$ concentration) is kept at a temperature of 2.4 K. A 195 THz CW ECLD light source (1 kHz linewidth) is split into modulated pump and probe beams, with fixed (10.3 GHz) and swept (10-13 GHz) modulation frequencies respectively. Fig 1(a) shows the probe transmission that reveals the inhomogeneous broadening of the optical transition. At the pump modulation frequency of 10.3 GHz, we observe a narrow hole (increased transmission), associated with the depleted hyperfine ground state of the Λ-system (see inset Fig. 1(a)). Likewise, the antihole (decreased transmission) appearing at a detuning of 11.18 GHz heralds the presence of an overpopulated hyperfine ground state. The separation of 880 MHz between the hole and antihole positions equals the hyperfine splitting between the two ground states in this Λ-system [3]. The lifetime measurement scheme consists of a 45 ms pump pulse, followed by a 250 ms probe pulse, which is now tuned at the antihole frequency. The obtained antihole amplitude is shown in Fig 1(b). The fitted double-exponential curve reveals time constants of T_1 = 9.3 ms and t_1 = 134 ms, which correspond to the relaxation times of the optically excited and ground state respectively.

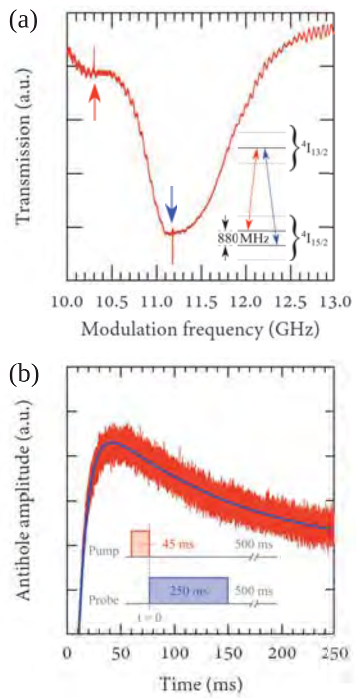

Fig. 1 (a) SHB transmission spectrum and Λ-system structure (inset). Arrows indicate the locations of the hole (red) and antihole (blue) and their corresponding energy transitions.
(b) Antihole amplitude decay with double-exponential fit and pulse sequence (inset).

Through spectral hole burning, we have achieved state preparation of a Λ-system in $^{167}Er^{3+}:Y_2SiO_5$. The existence of an antihole indicates that the electron population is transferred to one of the hyperfine ground states. The relaxation times of the optically excited (9.3 ms) and ground state (134 ms) leave room for future research of quantum state manipulation in $^{167}Er^{3+}$-doped materials at telecom wavelength.

This work was supported by JSPS KAKENHI Grant Numbers JP15H04130, JP16H01057 and JP16H03821. Ref.:

[1] Ph. Goldner et al., (Amsterdam, 2015) Vol. 46, p. 1.
[2] H. J. Kimble, Nature **453**, 1023 (2008).
[3] E. Baldit et al., Phys. Rev. B **81**, 144303 (2010).

Cooperatively Coupled Motion with Superradiant and Subradiant Atoms

Kuan-Ting Lin [1], **Guin-Dar Lin** [1,2]

[1] *Department of Physics, National Taiwan University, Taipei 10617, Taiwan*
[2] *Center for Quantum Science and Engineering, National Taiwan University, Taipei 10617, Taiwan*

To perform quantum computation, the quantum devices/systems must be cooled down to gain high fidelity. In this study, we investigate the cooling mechanism via coupled motion of two cooperative atoms in Doppler cooling process. The dipole-dipole interaction introduces the mutual decay channel and split super-radiant and sub-radiant states. The Doppler force is thus modified due to the collective emission and coupled recoil. Such a cooperative effect is more evident when the inter-atom separation is less than or comparable to a wavelength. In the optical molasses setup, we find that, along the axis of two atoms, there present mechanically sable and unstable regions alternatively as separation increases. To observe the effect, we propose a trapped-ion system where the ion distance can be varied, and find that the temperature can go down beyond the regular Doppler limit due to subradiance.

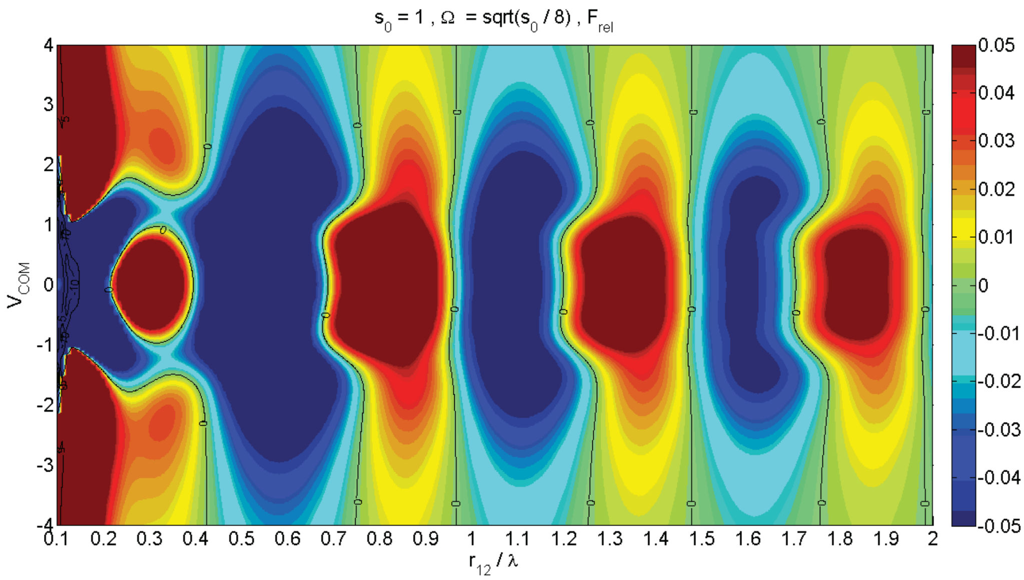

Fig 1. The classical fixed point. The stable and unstable regions alternatively changes as separation increases.

Scalable Quantum Computing with an Ion Crystal Stabilized by Tweezers and Sympathetic Cooling

Yu-Ching Shen[1] **and Guin-Dar Lin**[1,2]

[1] *Department of Physics, National Taiwan University, Taipei 10617, Taiwan*
[2] *Center for Quantum Science and Engineering, National Taiwan University, Taipei 10617, Taiwan*

Scalability of quantum computing based on ions in a linear RF trap has been a challenge due to instability of crystallization and heating. We propose a scalable scheme combining with local optical tweezers and sympathetic cooling. We analyze the temperature of ions measured by their position fluctuation. We calculate the steady state profile of the ions' position fluctuation for both the longitudinal and the transverse mode. For the longitudinal mode, the optical tweezers introduce a dominant energy scale, which enhances the efficiency of removal of local phonons. For the transverse mode, the optical tweezers block the heat propagation, and hence worsen the efficiency of cooling. We show that we can suppress the heating by arranging optical tweezers and laser cooling. We also discuss the relaxation dynamics and show that the relaxation time scale can be reached in experiment.

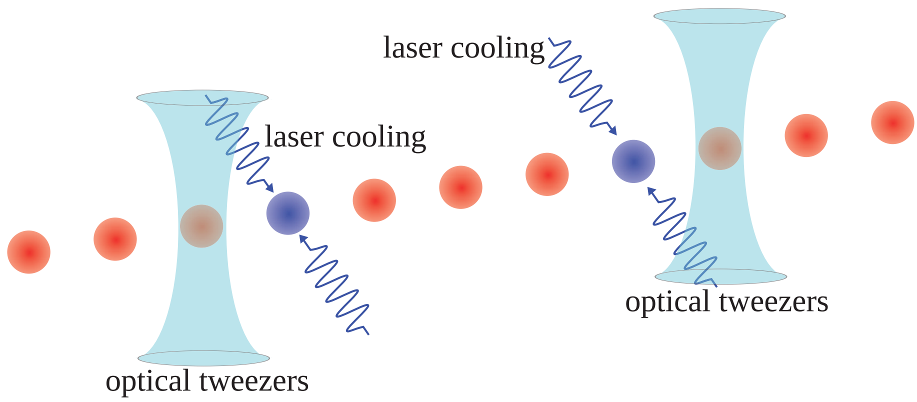

Figure 1: The architecture for the trapped ion computation. We arrange the optical tweezers and cooling ions to stabilize the ion chain and suppress the heating.

Atom interferometry with the Sr optical clock transition inside an optical guide

Tadahiro Takahashi[1,2], **Tomoya Akatsuka**[1], **and Hidetoshi Katori**[1,2]

[1] *Department of Applied Physics, Graduate School of Engineering, The University of Tokyo, Bunkyo-ku, Tokyo 113-8656, Japan*
[2] *Quantum Metrology Laboratory, RIKEN, Wako, Saitama 351-0198, Japan*

Matter wave interferometry with ultracold atoms has developed into a powerful tool for the precision measurement [1]. In particular, inertial sensing is one of the main applications of the atom interferometry due to its high sensitivity to the acceleration [2]. We demonstrate an optically guided atom interferometry based on the $^1S_0 - {}^3P_0$ clock transition of ^{87}Sr atoms. The optical guide is realized by the“magic” wavelength trapping laser [3] where the clock transition frequency is not changed by the electromagnetic field of the optical guide. As a proof-of-principle demonstration, we operate an atom interferometry in a focused Gaussian beam as shown in Fig. 1(a), which measures the axial acceleration of the atoms induced by the intensity gradient of the beam [4].

Moreover, we are developing an optically guided atom interferometry inside a hollow-core photonic crystal fiber (HC-PCF). The HC-PCF suppresses the attenuation of the guiding laser to less than 1 dB/m and realizes spatially uniform guiding potential to minimize the axial accelation [5] (Fig. 1(b)). We observe the $^1S_0 - {}^3P_0$ clock transition of ^{87}Sr atoms inside the HC-PCF with a linewidth of 110 Hz (Fig. 1(c)). This result demonstrates a 9-ms-coherence time of the clock transition which is sufficient for the investigation of the axial acceleration of atoms in the optical guide tuned to the “magic” wavelngth [4].

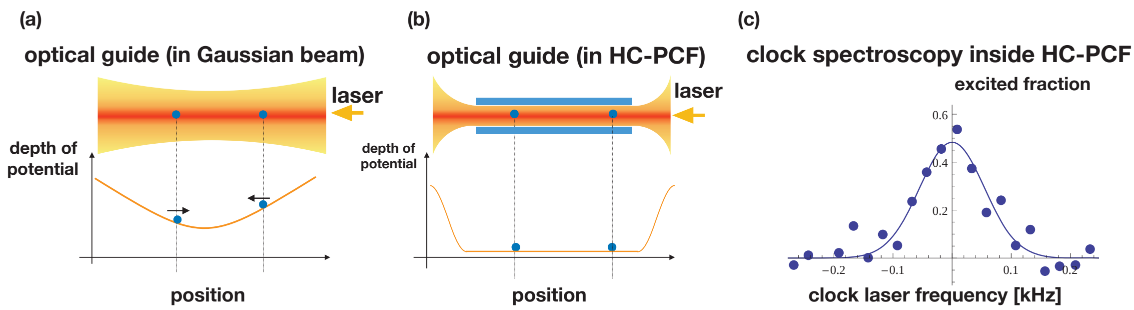

Figure 1: The scheme of the trapping potential of (a) an optical guide in a Gaussian beam and (b) in a HC-PCF. (c) Clock spectrum of ^{87}Sr atoms inside a HC-PCF.

[1] C. J. Bordé, Phys. Lett. **140**, 10 (1989).
[2] T. Mazzoni *et al.*, Phys. Rev. A **92**, 053619 (2015).
[3] H. Katori *et al.*, Phys. Rev. Lett. **91**, 173005 (2003).
[4] T. Akatsuka *et al.*, to be submitted.
[5] Y. Wang *et. al.*, Opt. Lett. **36**, 669 (2011).

Efficient Single-Photon Coupling between an Optical Nanofiber and a Diamond Nanowire

Y. Yonezu[1,2], K. Wakui[2], K. Furusawa[2], M. Takeoka[2], K. Semba[2], and T. Aoki[1]

[1] *Waseda University, Shinjuku, Tokyo, Japan*
[2] *NICT, Koganei, Tokyo, Japan*

Nitrogen-Vacancy (NV) centers in diamond are promising solid-state quantum emitters that can be utilized for various quantum applications [1]. For such applications, efficient coupling of single photons from NV centers to a single-mode fiber (SMF) is indispensable. Recently, various diamond nanophotonic devices have been demonstrated for efficient coupling of single photons to a single cavity or waveguide mode [2]. However, efficient coupling of the devices to a SMF is a difficult challenge.

A promising approach for solving the challenge is to utilize an optical nanofiber [3–6]. The nanofiber is the sub-wavelength-diameter waist region of a tapered optical fiber. The evanescent field of the guided mode of the nanofiber enables us to efficiently collect single photons from quantum emitters near the surface of the nanofiber. Furthermore, the single photons can be coupled to a SMF with low loss via the adiabatically tapered regions [4]. Recently, coupling systems between the nanofiber and NV centers embedded in a spherical diamond nanocrystal have been reported both theoretically [5] and experimentally [6]. However, in the 100-nm-sized spherical nanocrystal case, the theoretical maximum coupling efficiency for the sum of both fiber ends is limited to less than 25% [5].

Here, we propose a novel efficient coupling system between the nanofiber and a diamond nanowire (Fig.1). The diamond nanowire is a cylindrical-structured diamond nanocrystal whose diameter is a few hundred nm and length is a few µm. By numerically simulating the coupling efficiency and investigating the optimal system geometry, the maximum coupling efficiency as high as 75% for the sum of both fiber ends is obtained (Fig.2). In this presentation, we will describe (1) the details of the numerical simulation [7] and (2) a simple fabrication method of the diamond nanowire [8].

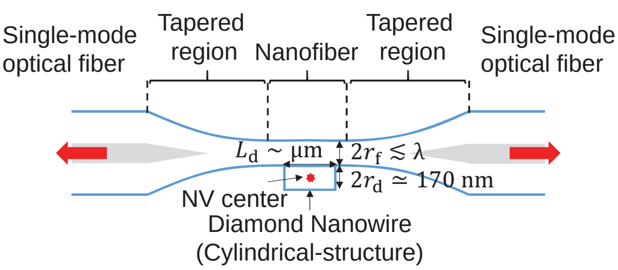

Fig. 1. Schematic of the coupling system.

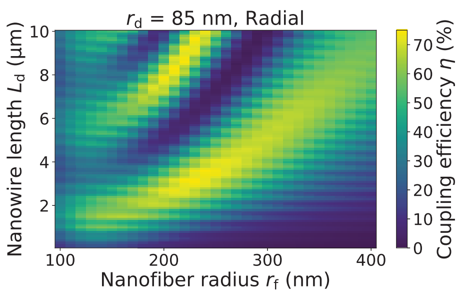

Fig. 2. Coupling efficiency as a function of the system geometry.

[1] M. W. Doherty *et al.*, Phys. Rep. **528**, 1 (2013).
[2] M. Loncar and A. Faraon, MRS bulletin **38**, 144 (2013).
[3] R. Yalla *et al.*, Phys. Rev. Lett. **109**, 063602 (2012).
[4] R. Nagai, and T. Aoki, Opt. Exp. **22**, 28427 (2014).
[5] M. Almokhtar *et al.*, Opt. Exp. **22**, 20045 (2014).
[6] T. Schröder *et al.*, Opt. Exp. **20**, 10490 (2012).
[7] Y. Yonezu *et al.*, submitted.
[8] K. Wakui *et al.*, Jpn. J. Appl. Phys. **56**, 058005 (2017).

Field and temperature dependent cavity coupling for highly sensitive on-chip spin detection

G. Franco,[1,*] M. Martens,[1] L. Chen,[2] A. Zabalo,[1] N. Dalal,[3] and I. Chiorescu[1,†]

[1] *Department of Physics and The National High Magnetic Field Laboratory, Florida State University, Tallahassee, Florida 32310, USA*
[2] *SIMIT, Chinese Academy of Sciences, Shanghai, China 200050*
[3] *Department of Chemistry and Biochemistry, Florida State University, FL 32306*

The ability of probing the spin-photon interaction of different single molecule magnets using Electron Spin Resonance (ESR) is of great interest due to possible application as a molecular quantum memory[a]. From the point of view of both qubit operation and fabrication, a quantum computer will require its components to have an on-chip design. The use of on-chip superconducting microwave cavities[b] have the advantage of a sharply defined resonance frequency that can be tuned to match that of the qubit, allowing us to effectively manipulate the state of the spin. Here we will present a method to tune the coupling of a superconducting cavity operating at ~20GHz using losses induced by temperature and field. The cavities are made from silicon/niobium (Si/Nb) films and the effect of variable parameters such as temperature and magnetic field are studied for both an empty cavity and a cavity loaded with the molecular magnet $K_6\left[V_{15}^{IV}As_6^{III}O_{42}\left(D_2O\right)\right]\cdot 8D_2O$. This system, known as V_{15}, has shown Rabi oscillations[c] as well as spin-orbit dependence of the coherence time[d,e]. From the zero-field temperature dependence of the resonance frequency of the empty cavity we have observed that thermally induced losses have the effect of decreasing the resonance frequency, while reaching critical coupling at a well-defined temperature. Loading the cavity with a sample of shifts the critical coupling parameters. Their values can be tuned by applying a magnetic field to the superconducting cavity, in plane and/or perpendicular. A small shift in the resonance frequency when an in plane field is applied is described by the nonlinear Meissner effect[b], whereas in the presence of a perpendicular field a much larger shift was observed, attributed by the formation of vortices in the waveguide. Finally, results of placing the sample on the cavity at critical coupling will be presented.

[a] M. Blencowe, Nature **468**, 2010
[b] N. Groll *et. al.*, PRB **81**, 2010
[c] S. Bertaina *et. al.*, Nature **453**, 2008
[d] M. Martens *et. al.*, PRB **89**, 2014
[e] M. Martens *et. al*., arxiv:1505.03177

Non-unitary evolution of the square root of density matirces

Kaito Asai and Yasuhiro Tokura

Graduate School of Pure and Applied Sciences, University of Tsukuba

In quantum mechanics we often handle two kinds of values; expectation value and eigenvalue. In 1988, Aharonov, Albert, and Vaidman have proposed a new kind of value; weak value[1]. The weak value of an observable $\hat{A}$ is defined as following;

$$A_w := \frac{\langle\psi_f|\hat{A}|\psi_i\rangle}{\langle\psi_f|\psi_i\rangle}, \tag{1}$$

where $|\psi_i\rangle$, $|\psi_f\rangle$ are called initial state and final state, respectively. The final state is specified by a measurement called post-selection which is one of the most important features in the concept of weak measurement. Obviously this quantity is defined only in pure systems. Recently some generalizations of the weak value into mixed systems have proposed by Wiseman[2] and Lundeen and Bamber[3]. The linear response, one of the most successful tactics to handle non-equilibrium systems, of the post-selected systems is first considered by Ban[4]. We have studied a new definition of the weal value in mixed systems from different perspective and its linear response[5][6]. The definition of the weak value is as following;

$$A_w^{\text{mixed}} := \frac{\mathrm{Tr}[(\rho_f^{\frac{1}{2}})^\dagger \hat{A}\rho_i^{\frac{1}{2}}]}{\mathrm{Tr}[(\rho_f^{\frac{1}{2}})^\dagger \rho_i^{\frac{1}{2}}]}, \tag{2}$$

where $\rho_f^{\frac{1}{2}}$ and $\rho_i^{\frac{1}{2}}$ are the square root of the density matrices representing the initial state and the final state, respectively. We have also studied that the square root of density matrices behave like state vectors when the system evolves with unitary operators. Thus we are going to report how the square root of density matrices behave when the system is attached to heat bath and evolves with non-unitary operators.

Acknowledgement
This work is supported by CREST JST (JPMJCR15N2).

[1] Y. Aharonov, D. Z. Albert, L. Vaidman, Phys. Rev. Lett. **60**, 1351 (1988).
[2] H. M. Wiseman, Phys. Rev. A,**65**, 032111(2002).
[3] J. S. Lundeen, C. Bamber, Phys. Rev. Lett.**108**, 070402 (2012).
[4] M. Ban, Phys. Lett. A, **379**, 284 (2015).
[5] K. Asai, Y. Tokura, 2016 JPS Spring meeting .
[6] K. Asai, Y. Tokura, VI QUANTUM INFORMATION SCHOOL AND WORKSHOP, Paraty 2017.

Spin resonance beyond the rotating wave approximations

Kazuki Yokohama and Yasuhiro Tokura

Graduate School of Pure and Applied Sciences, University of Tsukuba

We consider two level systems driven by an external classical oscillating field. Larmor frequency characterizes the dynamics of the magnetic moment of a spin under an external static magnetic field. If we applied the pulsed oscillating transversal magnetic field whose frequency is equal to the Larmor frequency, the magnetic moment, which was in the ground state, absorbs an energy quantum from the field, and is raised to an excited state. We install a detector, which measures the energy of the pulse after exchanging the energy with the magnetic moment. The measured energy deprived by the magnetic moment depends on the frequency of the pulse. The bigger the difference between the frequency of the applied pulse and Larmor frequency, the smaller the energy deprived becomes. By plotting the energy deprived as a function of the applied frequency, there exists a peak with certain full width at half maximum (FWHM). In general, the FWHM depends on the pulse width and the relaxation time of the two level systems.

In this presentation, we focus on the relations between the interaction Hamiltonian and the observed FWHM of the resonance signal. Here, we disregard the effect of the relaxation time. We compare two types of the interaction Hamiltonian. The first case is under the rotating wave approximation (RWA) to the interaction Hamiltonian, and the second case is without RWA. It is known that the resonant frequency of the latter case is larger than the formal one (Bloch-Siegert shift [2]). In this presentation, we focus on the FWHM of the resonant peak depending on the approximations. We discuss the relation between the FWHM for a given pulse width and the amplitudes of the applied pulse [3].

[1] C. P. Slichter, Principles of Magnetic Resonance (Springer Series in Solid-State Sciences 1), 1996.
[2] F. Bloch and A. Siegert, Phys. Rev. **57,** 522 (1940).
[3] I. Pietikainen, et al., Phys. Rev. B **96**, 020501 (R) (2017).

Toward coherent feedback control in quantum transport in magnetic field

Ryosuke Suzuki, Sumiya Kato, Kyo Yoshida and Yasuhiro Tokura

Graduate School of Pure and Applied Sciences, University of Tsukuba

In the classical control theory, feedback is a fundamental concept. A theoretical study to extend the target of such feedback control to the quantum state was made in the 1990 ' s [1]. In addition, due to technological progress in recent years, feedback control of the quantum states, which is called quantum feedback control, has been experimentally realized [2]. Conventional quantum feedback control in these studies is performed as follows. A macroscopic detector performs measurements on the system, a classical controller receives the results of the measurements, which is classical information, and apply a potential to the system depending on the results to alter the behavior of the quantum system. In this picture, the detector tends to destroy coherence in the process of making measrements. On the other hand, another method called coherent feedback control has been proposed [3], in which the detector, and the controllers are quantum systems that interact coherently with the system to be controlled. And the controller gets and feeds back quantum information.

Recently, the application of coherent feedback control to quantum transport has been studied [4]. Prior research has analyzed general systems by the scattering approach and analysis of concrete systems has not been done. Then, we focused on quantum transport in the magnetic field, in particular, the electric conduction in the ring-shaped conductor connected to the leads in the magnetic field. The Aharonov-Bohm effect appears remarkably in such a system. By the Aharonov-Bohm effect, the conductance of the ring oscillates according to the magnetic flux penetrating the ring. Therefore, the conductance can be controlled by performing coherent feedback control that changes the magnetic field depending on the state of the system. In order to discuss such feedback control, we conducted theoretical analysis of the above system and clarified the properties of the system.

[1] H. M. Wiseman, G. J. Milburn, Phys. Rev. Lett. **70**, 548 (1993).
[2] R. Inoue, S. Tanaka, R. Namiki, T. Sagawa, Y. Takahashi, Phys. Rev. Lett. **110**, 163602 (2013).
[3] S. Lloyd, Phys. Rev. A **62**, 022108 (2000).
[4] C. Emary, J. Gough, Phys. Rev. B **90**, 205436 (2014).

Role of density on microwave photoresistance in 2D electron gas

Xiaojun Fu[1], Mikhail D. Borisov[1], Qianhui Shi[1], Quentin A. Ebner[1], Michael A. Zudov[1], Qi Qian[2], John D. Watson[2], and Michael J. Manfra[2,3]

[1] *School of Physics and Astronomy, Univ. of Minnesota, Minneapolis, MN 55455, USA*
[2] *Department of Physics and Astronomy and Birck Nanotechnology Center, Purdue Univ., West Lafayette, Indiana 47907, USA*
[3] *School of Materials Engineering, School of Electrical and Computer Engineering, and Station Q Purdue, Purdue Univ., West Lafayette, Indiana 47907, USA*

Microwave-induced resistance oscillations (MIRO) [1] emerge when a two-dimensional electron gas (2DEG) is exposed to microwave radiation of frequency ω and a perpendicular magnetic field B, owing to the effect of Landau quantization on the radiation-assisted electron-impurity scattering [2]. At low microwave power, MIRO can be described by [2]

$$\delta R/R_0 = -(2\pi\omega/\omega_c)\mathcal{P}\lambda^2\eta\sin(2\pi\omega/\omega_c)\,, \qquad (1)$$

where R_0 is the resistance at $B=0$, $\omega_c = eB/m^\star$ is the cyclotron frequency, $m^\star$ is the effective mass, $\mathcal{P}$ is the effective microwave power, $\lambda = \exp(-\pi/\omega_c\tau_q)$ is the Dingle factor, τ_q is the quantum lifetime, and η is the factor depending on disorder and electron-electron scattering rates.

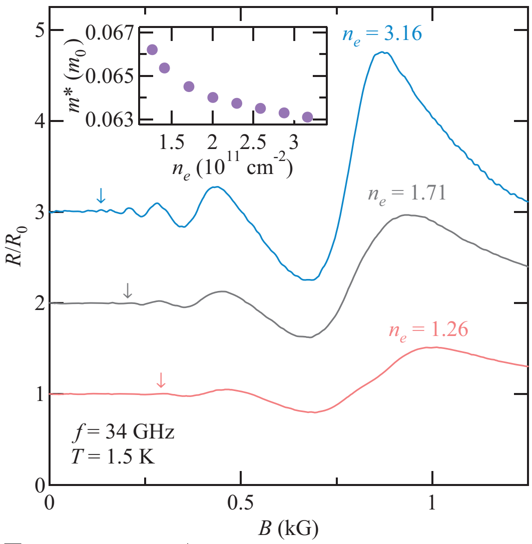

Figure 1: R/R_0 vs B at $n_e \approx 1.26, 1.71,$ and 3.16×10^{11} cm^{-2} (as marked) at $T =$ 1.5 K and $f = 34$ GHz. Inset: $m^\star$ vs n_e.

Here, we investigate how MIRO evolve with the carrier density n_e in a GaAs/AlGaAs quantum well equipped with an *in situ* grown back gate, an aspect which has not been previously explored. First, we show that the MIRO frequency monotonically decreases with n_e [3]. This finding can be linked to the renormalization of the effective mass by electron-electron interactions (cf. inset in Fig. 1), which are sensitive both to n_e and to quantum confinement of our 2DEG [3]. Second, we find that the MIRO amplitude substantially *increases* with n_e (cf. Fig. 1). While higher n_e leads to a larger radiation absorption (larger $\mathcal{P}$) and a longer τ_q, both of which favor such an increase, these effects should be completely overwhelmed by the anticipated concomitant decrease in η [2]. Remarkably, however, our analysis of the MIRO amplitude is incompatible with such a decrease, showing just the opposite trend, i.e., that η steadily increases with n_e. Finally, we observe that the fundamental oscillation maximum moves towards the cyclotron resonance with increasing n_e. Taken together, these unexpected findings indicate that our understanding of microwave photoresistance remains incomplete, calling for futher theoretical and experimental studies.

[1] M. A. Zudov, R. R. Du, J. A. Simmons, and J. L. Reno, Phys. Rev. B **64**, 201311(R) (2001).
[2] I. A. Dmitriev, A. D. Mirlin, D. G.Polyakov, and M. A. Zudov, Rev. Mod. Phys. **84**, 1709 (2012).
[3] X. Fu, Q. A. Ebner, Q. Shi, M. A. Zudov, Q. Qian, J. D. Watson, and M. J. Manfra, Phys. Rev. B **95**, 235415 (2017).

Fine structure of microwave-induced resistance oscillations

Qianhui Shi[1], Michael A. Zudov[1], Ivan A. Dmitriev[2], Kirk W. Baldwin[3], Loren N. Pfeiffer[3], and Kenneth W. West[3]

[1] *School of Physics and Astronomy, Univ. of Minnesota, Minneapolis, MN 55455, USA*
[2] *Department of Physics, University of Regensburg, 93040 Regensburg, Germany*
[3] *Department of Electrical Engineering, Princeton Univ., Princeton, NJ 08544, USA*

When a two-dimensional electron gas (2DEG) is exposed to microwave radiation and a perpendicular magnetic field B, the magnetoresistance acquires prominent $1/B$-periodic oscillations [1]. These microwave-induced resistance oscillations (MIRO) are commonly attributed to the effect of Landau quantization on the radiation-assisted scattering off impurities [2]. In the regime of low power, MIRO, as a function of $1/B$, are well described by a damped sine function with maxima and minima symmetrically offset by a quarter-cycle from the nodes at cyclotron resonance harmonics. It has been shown that with increasing radiation intensity, the MIRO amplitude undergoes a crossover from a linear to a square-root power dependence and, concomitantly, the MIRO extrema move closer to the nodes [3].

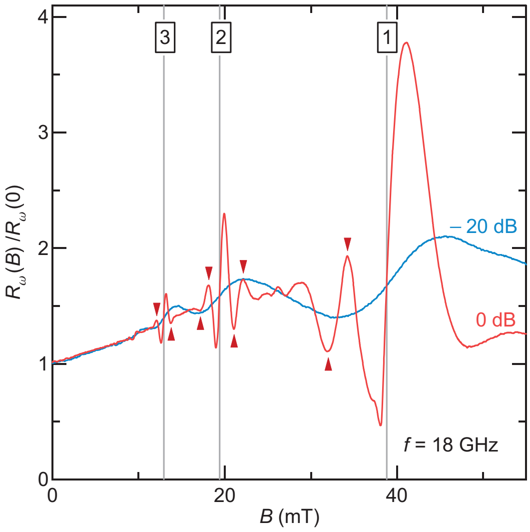

Figure 1: Longitudinal magnetoresistance normalized to its zero-field value $R_\omega(B)/R_\omega(0)$, measured at $f = 18$ GHz for two different power levels corresponding to an attenuation of 0 and 20 dB.

Here, we report on a new photoresistance effect in an ultraclean (mobility $\mu \approx 3 \times 10^7$ cm^2/Vs) 2DEG – a fine structure of MIRO [4]. This fine structure is manifested by multiple secondary sharp extrema, residing beside the primary ones, which emerge at high radiation power (see Fig. 1). Theoretical considerations reveal that this fine structure originates from *multiphoton*-assisted scattering off short-range impurities. Unique properties of the fine structure allow us to access all experimental parameters, including microwave power, to separate displacement and inelastic contributions to photoresistance, and to evaluate the role of electron heating by microwave radiation, all in a single experiment. Furthermore, the fine structure offers a convenient means to quantitatively assess the correlation properties of the disorder potential, allowing direct separation of short- and long-range disorder contributions to the electron mobility. The analysis shows that the mobility in our 2DEG is limited by short-range disorder.

[1] M. A. Zudov, R. R. Du, J. A. Simmons, and J. L. Reno, Phys. Rev. B **64**, 201311(R) (2001).
[2] I. A. Dmitriev, A. D. Mirlin, D. G. Polyakov, and M. A. Zudov, Rev. Mod. Phys. **84**, 1709 (2012).
[3] A. T. Hatke, M. Khodas, M. A. Zudov, L. N. Pfeiffer, and K. W. West, Phys. Rev. B **84**, 241302(R) (2011).
[4] Q. Shi, M. A. Zudov, I. A. Dmitriev, K. W. Baldwin, L. N. Pfeiffer, and K. W. West, Phys. Rev. B **95**, 041403(R) (2017).

Dispersion engineering of a PPLN waveguide for the generation of spectrally-pure photon pairs

Antoine Bergeot[1], Takahiro Kashiwazaki[2], and Nobuyuki Matsuda[1]

[1] *NTT Basic Research Laboratories, NTT Corporation*
[2] *NTT Device Technology Laboratories, NTT Corporation*

Spontaneous parametric down-conversion (SPDC) in a nonlinear crystal is a versatile nonlinear process for the generation of correlated photons for quantum information technologies including quantum communication, computation, and metrology. Especially photon pairs with high spectral purity (separability) are essential for an efficient generation of pure heralded single photons, the generation of which requires the extended phase matching, *i.e.*, group velocity matching (GVM) in SPDC process [1]. Periodically poled $LiNbO_3$ (PPLN) crystals are widely used for the photon pair generation. However, the GVM condition of PPLN was not investigated until very recent work by Laudenbach *et al.* [2], where the generation of photon pairs with high spectral purity was shown available using bulk PPLN crystal. Here we further tailor the GVM condition by employing a waveguide structure. We found a GVM condition that realizes the generation of pure heralded single photons in the telecommunication wavelength range under the type-II phase matching condition.

We consider a PPLN ridge waveguide (Fig. 1) that can be fabricated using a direct bonding and dry etching technique [3]. We performed the numerical simulation of the joint spectral amplitude of SPDC photons using Sellmeier equations shown in Refs. [4,5]. We obtained the GVM wavelengths shift up to approximately 200 nm toward shorter wavelength side due to the significant dispersion modification introduced by the large core-cladding refractive index contrast realized by air cladding. With the poling period of 9.0 μm, the waveguide length of 30 mm, the pump wavelength of 990 nm and the cross-sectional dimension shown in Fig. 1(a), we obtained the joint spectral amplitude shown in Fig. 1(b) under the type-II phase matching and the GVM between the pump and the idler modes. The joint spectrum exhibits the signal wavelength in L-band along with the spectral purity as high as 97.9%, indicating the generation of heralded single photons in the telecommunication wavelength using a PPLN waveguide.

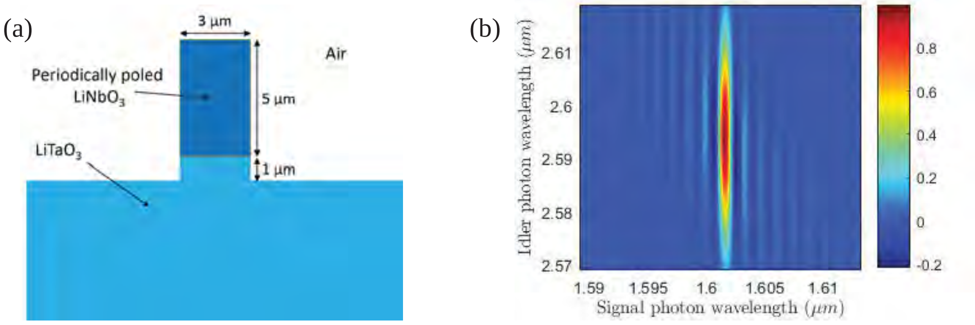

Fig. 1. (a) Cross section of the PPLN waveguide. (b) Calculated joint spectral amplitude enabling the generation of spectrally-pure heralded single photons in the telecommunications wavelength.

[1] P. J. Mosley *et al.*, Phys. Rev. Lett. **100**, 133601 (2008).
[2] F. Laudenbach *et al.*, Opt. Express **24**, 2712 (2016).
[3] T. Umeki *et al.*, Opt. Express **19**, 6326 (2011).
[4] O. Gayer *et al.*, Appl. Phys. B **91,** 343 (2008).
[5] I. Dolev *et al.*, Appl. Phys. B **96,** 423 (2009).

Shaped microwave pulses for measuring hybrid quantum devices

Ailsa Keyser[1,2], Sebastian de Graaf[1], Mark Oxborrow[2], Tobias Lindström[1]

[1] *National Physical Laboratory, Hampton Road, Teddington, TW11 0LW, UK*
[2] *Imperial College London, Prince Consort Road, SW7 2AZ, UK*

Research into hybrid quantum devices is motivated by the potential to combine the long coherence times of natural spin systems with the scalability of circuit quantum electrodynamics for applications in solid state quantum information processing [1]. Electron Spin Resonance (ESR) is a standard technique for the measurement of a spin system, using an inductively-coupled microwave resonator to excite the spins with pulsed radiation, and detect their characteristic magnetic field response [2]. It has further been used to probe the spins present on the surface of quantum devices, from which it is possible to attribute chemical fingerprints to sources of decoherence [3].

All else being equal, resonators with high-Q factors yield better ESR sensitivity (which scales with $\sqrt{Q}$). However, the 'ringdown' time taken for the energy to dissipate from the resonator might then exceed the characteristic decay time of the spins, concealing their signal [2]. The high Q also distorts the excitation signal applied to the spins. To try to overcome these issues, and develop practical ESR which benefits from high-Q resonators, we combine ringdown suppression and control theory to apply shaped microwave pulses, to enable efficient manipulation and detection of spin ensembles on short timescales.

Ringdown suppression uses a phase-inverted pulse of sufficient energy to drive the resonator oscillations to zero [4]. Preliminary results from a high-Q dielectric resonator of resonant frequency 8.7 GHz (figure 1), show the ringdown suppressed by 65% through the use of a square-shaped compensation pulse. To alter the pulse distribution in the frequency domain, frequency-swept pulses and pulse shaping around the point of phase modulation are also considered. We further discuss the application of shaped pulses and optimal control theory to high-Q superconducting planar micro-resonators, which are natural candidates for extending practical ESR to small numbers of spins.

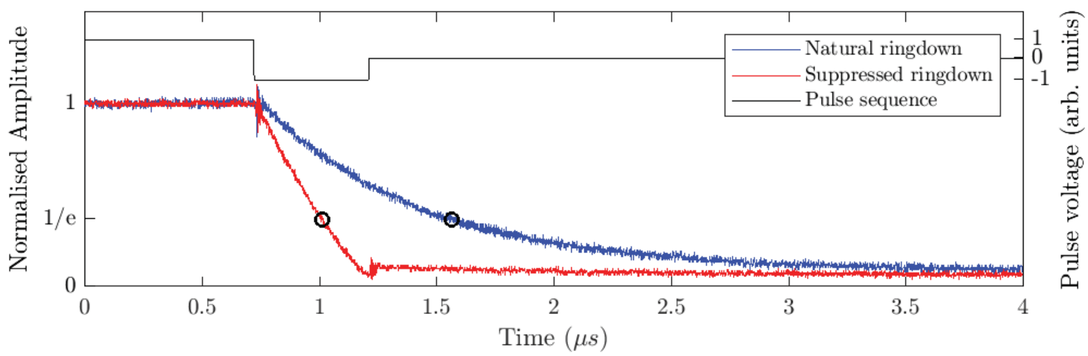

Figure 1: A control sequence with a 490 ns compensation pulse of relative amplitude 1.2 (right axis), causes a 65% suppression of the natural ringdown (left axis).

[1] I. Wisby *et al.*, Appl. Phys. Lett. 105, 102601 (2014).
[2] T. W. Borneman, D. G. Cory, J. Magn. Reson. 225, 120–129 (2012).
[3] S. E. de Graaf *et al.*, Phys. Rev. Lett. 118, 57703 (2016).
[4] D. I. Hoult, Rev. Sci. Instrum. 50, 193–200 (1979).

Characterization of low loss microstrip resonators as a building block for circuit QED in a 3D waveguide

D. Zoepfl[1,2], P. R. Muppalla[1,2], C. M. F. Schneider[1,2], S. Kasemann[3], S. Partel[3], and G. Kirchmair[1,2]

[1] *Institute for Quantum Optics and Quantum Information of the Austrian Academy of Sciences, A-6020 Innsbruck, Austria*
[2] *Institute for Experimental Physics, University of Innsbruck, A-6020 Innsbruck, Austria*
[3] *Research Centre for Microtechnology, Vorarlberg University of Applied Sciences, A-6850 Dornbirn, Austria*

We fabricated aluminum and niobium microstrip resonators and characterized them in a rectangular waveguide (see illustration). Our novel approach combines the low loss advantages of three dimensional structures with a compact planar design [1]. The setup allows flexible coupling to the resonator, which depends on its position within the waveguide. The waveguide represents a well defined microwave environment, free of wirebonds, which minimizes losses [2]. This makes this setup also appealing for testing materials.

In the low temperature, low power regime, we measure a single photon internal quality factor of up to one million. The demonstrated quality factor is comparable to state of the art coplanar waveguide resonators [3, 4], but does not require complex fabrication procedures. We measured the internal quality factor with increasing temperature. The data shows good agreement with models predicting decreasing losses to two level systems [5] and increasing conductive losses with temperature [6].

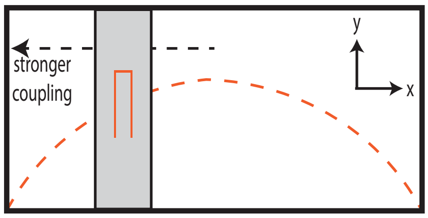

Waveguide cross section with microstrip resonator. The dashed line indicates the electric field strength. The field propagates in z direction. In case of a mcirostrip resonator with equal leg length, the coupling, which takes place to the electric field, is weakest in the center and increases towards the walls.

In a next step, we want to use microstrip resonators for qubit readout in a novel waveguide Quantum-Electro-Dynamics architecture [7]. This represents an ideal platform for analogue quantum simulation of spin models. In another experiment we plan to put a SQUID in the center of the microstrip resonator. This will allow us to use the here presented resonator as a magnetometer or even as a parametric amplifier [8].

[1] D. Zoepfl et al., AIP Advances **7**, 085118 (2017)
[2] J. Wenner et al., Superconductor Science and Technology **17**, 065001 (2011).
[3] A. Brunoet al., Applied Physics Letters **106**, 182601 (2015).
[4] A. Megrant et al., Applied Physics Letters **100**, 113510 (2012).
[5] D. P. Pappas et al., IEEE Transactions on Applied Superconductivity **21**, 871 (2011).
[6] Saito K., Kneisel P. Proceedings of the 1999 Workshop on RF Superconductivity (1999).
[7] M. Dalmonte et al., Physical Review B **92**, 174507 (2015).
[8] M. Hatridge et al., Phys. Rev. B **83**, 134501 (2011).

Probing the spectral density of the surface electromagnetic fields through scattering of waveguide photons

Guang-Yin Chen [1]

[1] *Dep. of Physics, National Chung Hsing University, Taichung, Taiwan*

The spectral density of the metal-surface electromagnetic fields will be strongly modified in the presence of a closely-spaced quantum emitter [1]. In this work [2], we propose a feasible way to probe the changes of the spectral density through the scattering of the waveguide photon incident on the quantum emitter. The variances of the lineshape in the transmission spectra indicate the coherent interaction between the emitter and the pseudomode resulting from all the surface electromagnetic modes. We further investigate the quantum coherence between the emitter and the pseudomode of the metal-dielectric interface.

[1] A. Gonz´alez-Tudela, P. A. Huidobro, L. Mart´ın-Moreno, C. Tejedor, and F. J. Garc´ıa-Vidal, Phys. Rev. B 89, 041402 (2014)..
[2]G. Y. Chen, Sci. Rep. **6**, 21673 (2016).

Slow microwave propagation guided by one-dimensional left-handed metamaterials

Yu-Han Chang[1], Vanna C. Silalahi[1] and Watson Kuo[1,2]

[1]*Department of Physics, National Chung Hsing University, Taichung 402, Taiwan*

[2]*Institute of Nanoscience, National Chung Hsing University, Taichung 402, Taiwan*

Abstract

We study microwave transmission by one dimensional (1D) array of coupled double split ring resonators (DSRR) and complementary split ring resonators (CSRR) as shown in Fig. 1(a). The transmission property strongly depends on the inter-resonator coupling between a DSRR and the adjacent CSRR. Because of the negative permeability of DSRR and permittivity of the CSRR, the structure is a left-handed metamaterial and shows negative phase velocity. By changing the ring orientations, the microwave passband splits due to breakdown of inversion symmetry, as shown in Fig. 1(c). Because of the formation of photonic bandgap, the microwave propagation also show slow group velocity, down to ~0.01 of the light speed in vacuum.

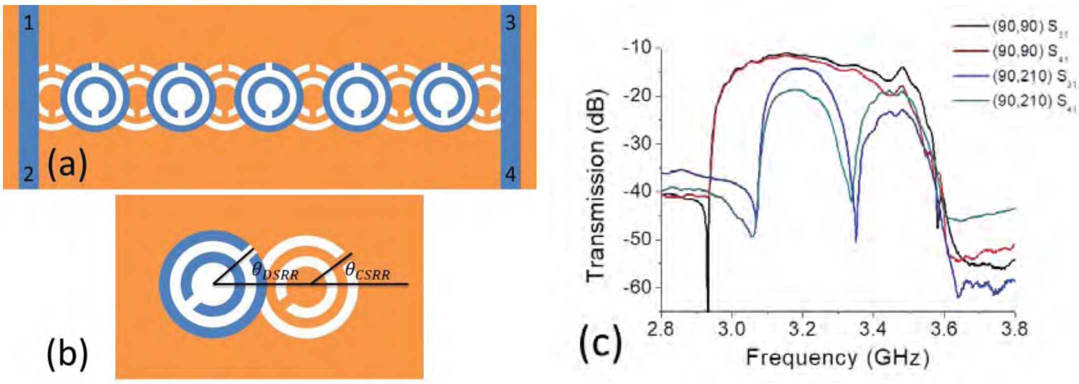

Fig 1. (a) The schematic of the 1D array and the measurement ports. Blue color is on top side and orange color is on bottom side. (b) The orientation configuration is labelled by two angles $(\theta_{DSRR}, \theta_{CSRR})$. (c) Transmission amplitude for single passband case $(90°, 90°)$ and split-passband case $(90°, 210°)$.

Optical characterization of VLSI graphene NEMS

Samer Houri [1*], Santiago Cartamil-Bueno [1], Peter G. Steeneken [1], and Herre S. J. van der Zant [1]

[1] *Kavli Institute of Nanoscience, Delft University of Technology, 2628 CJ, Delft, The Netherlands*

Graphene, the one atom thick two-dimensional allotrope of carbon, offers exceptional mechanical properties such as its high Young's modulus ~ 1TPa, its high fracture strain ~130 GPa, and its low density. This makes graphene the material of choice for the ultimate scaling of nanoelectromechanical systems (NEMS).

Using a colorimetry technique it is possible to characterize a large number of suspended graphene membranes (SGM), whereby the light reflected from the SGMs under an optical microscope is passed through a narrow line-width filter before entering the microscope camera, as shown schematically in Figure 1(a). Combining color filtered optical images, with image processing tools allows the characterization of large arrays of SGMs thus yielding statistically significant information about key physical properties, such as yield and its dependence on geometrical factors, adhesion energy to the silicon substrate [1], as well as the gas permeability of graphene membranes [2].

By choosing the correct color filter the suspended graphene membrane can be rendered easily recognizable under an optical microscope. This is shown in Figure 1(b), where the choice of the correct wavelength filter (660 nm) makes the suspended drum highly visible compared to an adjacent wavelength (600 nm). If the membrane is deflected, under the effect of say pressure difference across it, the light reflected from the SGM will change due to interference in a manner that is dependent on its deflection. By applying a step pressure difference across the membrane and observing the change in the intensity of reflected light over time, it is possible to extract the gas permeation of the membrane by fitting the time dependent reflectivity of the SGM, this is shown in Figure 1(c). Finally by applying an electrostatic force to the SGM, the membrane deflects and changes its spectral response, thus enabling applications as nanoelectro-optic modulators as shown in figure 1(d).

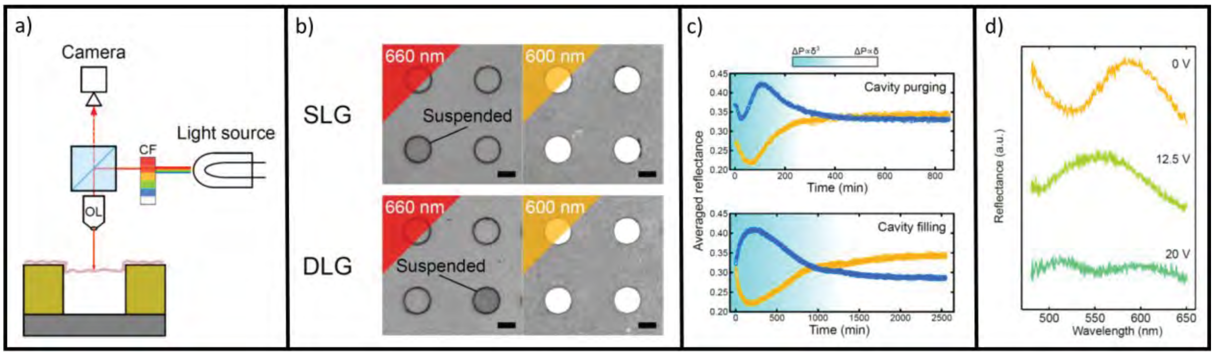

Figure 1. Colorimetry setup consisting of an optical microscope and color filters (a), taken from [1]. Making SGMs visible by the correct choice of color filter (b) for single (top) and double (bottom) layer graphene, from [1]. Time-dependent reflectivity of an SGM after undergoing a pressure step (c), taken from [2]. Spectral response of an electrostatically actuated SGM (d).

[1] S. J. Cartamil-Bueno, A. Centeno, A. Zurutuza, P. G. Steeneken, H. S. J. van der Zant and S. Houri, Nanoscale (2017).
[2] S. J. Cartamil-Bueno, P. G. Steeneken, A. Centeno, A. Zurutuza, H. S. J. van der Zant and S. Houri, Nano Letters, 2016, **16**, 6792–6796.

* Current affiliation: *NTT-BRL, NTT Corporation, Atsugi-shi, Kangawa243-0198, Japan.*

Acoustically modulated single-photon sources

Paul L. J. Helgers (helgers@pdi-berlin.de)[1,2], Klaus Biermann[1], Haruki Sanada[2], Yoji Kunihashi[2] and Paulo V. Santos[1]

[1] *Paul-Drude-Institut für Festkörperelektronik Berlin, Germany*
[2] *NTT Basic Research Laboratories, NTT Corporation, Atsugi, Japan*

Photons are promising candidates for long-range transmission of quantum information [1], making single-photon sources (SPS) crucial elements for this technology. We investigate a concept of acoustically driven SPSs based on GaAs quantum-well-wires (QWWR) on GaAs substrates [2]. For their fabrication, mesas (~30 nm deep) are patterned on the substrates, using photolithography and wet chemical etching. The mesas are then overgrown with a quantum well by molecular beam epitaxy, leading to the growth of QWWRs at the mesa sidewall [3].

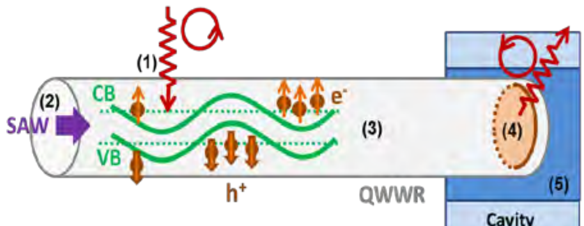

Figure 1: QWWR based single-photon source

The operation of the SPS is illustrated in Fig. 1. A circularly polarized laser excites spin-polarized electron-hole pairs at one end of the QWWR (1). A surface acoustic wave (SAW) is then applied (2). The propagating SAW carries a piezoelectric potential, which spatially separates electrons (e^-) and holes (h^+), and transports (3) them to a quantum-dot-like (QD) recombination center (4) at the opposite QWWR end [4]. The recombination center first traps a single charge carrier during one half of the SAW cycle. Charge carriers of opposite polarity arrive half a SAW period later, causing recombination and emission of single photons. The one-dimensionality of the QWWR reduces Dyakonov-Perel spin dephasing [5], correlating emission and excitation polarizations. The QWWR is embedded into a microcavity, improving the SPS properties.

Photoluminescence from such QWWRs indicates unwanted trapping of carriers and spin-flip scattering along the transport path [6], partly caused by local variations of the QWWR width due to line-edge-roughness (LER) of the mesas. Using atomic force microscopy (AFM), we show that our mesas are subject to a LER amplitude comparable to the QWWR width and that LER is mainly caused by optical lithography. In order to improve the edge smoothness, we are presently investigating QWWRs defined by e-beam lithography. Furthermore, we observe PL emission and charge carrier transport in GaAs(113)A QWWRs, as well as in GaAs(001) QWWRs embedded in a cavity. When subjected to a SAW, these cavity-embedded QWWRs show a clear indication of charge transport. We thus show the feasibility of charge transport of QWWRs embedded in a cavity and will evaluate the potential of these structures to be used as efficient acoustically driven sources of polarized single photons.

[1] P. Kok et. al., Rev. Mod. Phys. V79 (2007)
[2] O. D. D. Couto et al., Nature Photonics 3 (2009)
[3] R. Nötzel et al., APL68, 1132, 1996 ; J. Lee et al. IEEE Trans. Nanotechnology V6 N1 (2007)
[4] C. Rocke et al., Phys. Rev. Lett. 78 N21 (1997)
[5] A. W. Holleitner et al., New J. Phys. 9 342 (2007) ; S. Pramanik et al., IEEE-Nano 2003 V2 (2003)
[6] F. Alsina et al., Phys. Stat. Sol. 5 no 9 (2008)

This project has received funding from the European Union's Horizon program under grant agreement No 642688.

Efficiency bounds on quantum thermoelectric heat engine with broken time-reversal symmetry: the role of inelastic processes

Kaoru Yamamoto[1], Ora Entin-Wohlman[2,3], Amnon Aharony[2,3] and Naomichi Hatano[4]

[1]*Department of Physics, The University of Tokyo, Kashiwanoha 5-1-5, Kashiwa, Chiba 277-8574, Japan*
[2]*Raymond and Beverly Sackler School of Physics and Astronomy, Tel Aviv University, Tel Aviv 69978, Israel*
[3] *Physics Department, Ben Gurion University, Beer Sheva 84105, Israel*
[4]*Institute of Industrial Science, The University of Tokyo, Kashiwanoha 5-1-5, Kashiwa, Chiba 277-8574, Japan*

It has been argued that breaking time-reversal symmetry can enhance thermoelectric efficiency. Benenti *et al.* recently claimed [1] that in this case one can achieve the Carnot efficiency with a finite power, which appears to contradict the second law of thermodynamics. This idea has attracted much interest recently; see refs. [2, 3] for example.

In order to investigate this claim and to seek high efficiency, we consider a mesoscopic thermoelectric device made of an Aharonov-Bohm ring threaded by a magnetic flux, incorporating electron-phonon scattering [4]. The model has a quantum dot and three reservoirs: two electronic reservoirs and a bosonic one. Electrons are inelastically scattered by bosons at the quantum dot (Fig. 1). This three-terminal model can be reduced to an effective two-terminal one, that complies with the requirements of Benenti *et al.*

With this model, we find the following two results [5]: First, we find that, contrary to Benenti's claim [1], such a device cannot reach the Carnot efficiency under a magnetic field because of the non-negativity condition on the entropy production of the original model with three reservoirs. Second, we find that breaking time-reversal symmetry and including the electron-phonon interaction can enhance the thermoelectric efficiency significantly beyond the one without the interaction (Fig. 2).

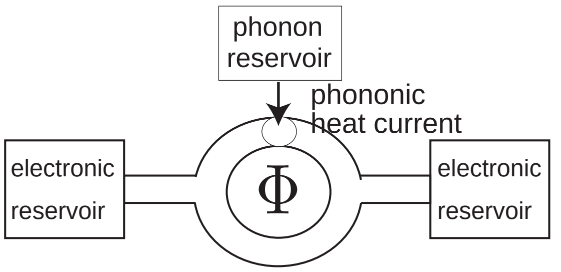

Figure 1: Three-terminal model with phonon reservoir and AB ring threaded by a magnetic flux Φ.

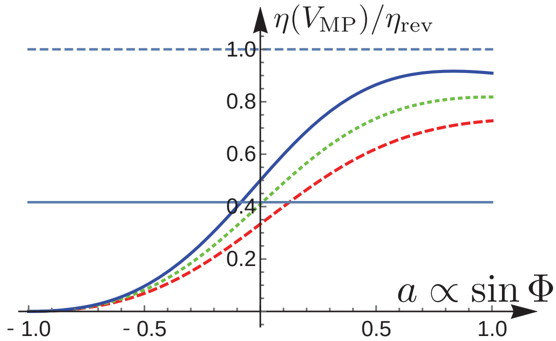

Figure 2: The efficiency at maximal power under a magnetic field $a \propto \sin\Phi$.

[1] G. Benenti, K. Saito, and G. Casati, Phys. Rev. Lett. **106**, 230602 (2011).
[2] N. Shiraishi, K. Saito, and H. Tasaki, Phys. Rev. Lett. **117**, 190601 (2016).
[3] N. Shiraishi and H. Tajima, Phys. Rev. E **96**, 022138 (2017).
[4] O. Entin-Wohlman and A. Aharony, Phys. Rev. B **85**, 085401 (2012).
[5] K. Yamamoto, O. Entin-Wohlman, A. Aharony, and N. Hatano, Phys. Rev. B **94**, 121402(R) (2016).

Evanescently-coupled optomechanical device with a GaAs optical disk - mechanical beam structure

M. Asano*, R. Ohta, H. Okamoto, T. Tawara, H. Gotoh, H. Yamaguchi

NTT Basic Research Laboratories, NTT Corporation
3-1 Morinosato Wakamiya, Atsugi-shi, Kanagawa 243-0198, Japan
*asano.motoki@lab.ntt.co.jp

Optomechancial devices such as photonic crystals (PhC) and whispering-gallery-mode (WGM) resonators have been actively studied towards quantum-limited displacement measurement and quantum information processing [1]. Whereas the single PhCs and the WGM resonators indicate high optical and mechanical Q factors, it is hard to independently control the optical and mechanical properties (e.g. resonant frequencies) because the material properties and the device structure affect on both properties. On the other hands, an optical disk and a mechanical beam distantly separated with a gap much smaller than the optical wavelength enable to realize high controllability of the optical and mechanical properties while inducing optomechanical coupling via radiation pressure of the evanescent field [2]. Moreover, the mechanical beam separated from the optical disk has a possibility to install the electromechanical system [3] by fabricating them from piezoelectric materials instead of the conventional Si materials (e.g. Si, SiO_2 and SiN).

In this presentation, we report the observation of optomechanical coupling in an optical disk and a mechanical beam fabricated from a piezoelectric GaAs layer (thickness: 200 nm). An optical disk (diameter: 10 μm) and a mechanical beam (length: 20 μm, width: 600 nm) were fabricated with a gap distance about 150 nm by reactive ion etching and electron beam lithography. A silica tapered fiber was used to couple the probe light into the optical disk. Figure 1 shows an illustration of the schematic image of our system. In order to detect the mechanical motion with high sensitivity, we constructed the balanced homodyne detection system to measure the phase modulation of the probe light. The mechanical motion was driven by the white noise injection from an extra piezoelectric actuator installed on the back of our sample. The optical phase modulation spectrum from the mechanical fundamental mode was obtained over the detection noise when the mean noise amplitude of 10 mV was injected (see Fig.2). We would optimize the device structure (e.g. the gap distance) towards the detection of minimal displacement, and would install the electromechanical system without degradation of the optical properties thanks to the separated disk-beam structure. This work is partly supported by MEXT KAKENHI (No. JP15H05869, JP16H01057)

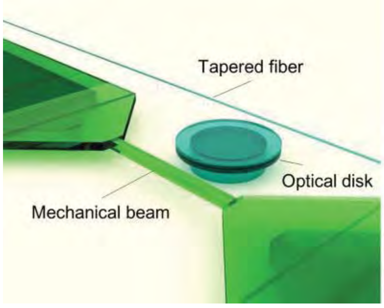

Fig. 1 Illustration of schematic image of our system.

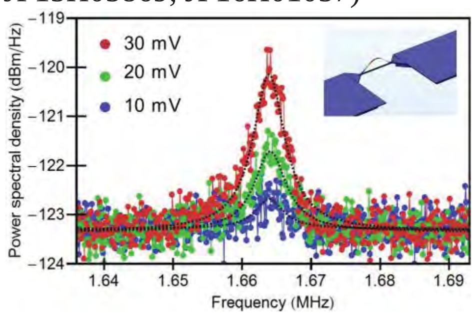

Fig. 2 Phase modulation spectra for the three mean noise amplitudes. The inset shows the displacement profile of the mechanical fundamental mode estimated from FEM.

[1] M. Aspelmeyer et al., *Rev. Mod. Phys.* **86**, 1391 (2014).
[2] R. Schilling et al., *Phys. Rev. Appl.* **5**, 054019 (2016).
[3] H. Okamoto et al., *Nat. Phys.* **9**, 480 (2013).

Coarse-grain molecular dynamics simulation of vertical lamellar phase of diblock copolymer in a thin film

Toru Yamaguchi, Hirotaka Tanaka, Nicolas Clement, and Akira Fujiwara

NTT Basic Research Laboratories, NTT Corporation, 3-1 Morinosato Wakamiya, Atsugi, Kanagawa 243-0198, Japan
Phone: +81-46-240-2633, Fax: +81-46-240-4317, E-mail: yamaguchi.toru@lab.ntt.co.jp

Directed self-assembly of block copolymers has been recently attracting considerable attention as a powerful technique for sub-10-nm lithography. We have already experimentally investigated the ordering properties of randomly aligned domains in a thin film. For the purpose of understanding of these ordering properties, we investigated the applicability of coarse-grain molecular dynamics simulation to a block copolymer film.

All the simulations were carried out with the HOOMD-blue software packages [1, 2]. In a first step, we systematically investigated the bulk phase behavior of a symmetric diblock copolymer A_nB_n composed of an A block with n beads and B block with n beads (n = 1, 2, 3, 4, 6, 12). The block copolymer is simulated by the bead-spring model where the finitely extensible nonlinear elastic (FENE) potential is used for bond interaction and the Lennard-Jones (LJ) (12-6) potential for non-bonded interaction. The immiscibility between two blocks is introduced just by decreasing the depth of the LJ potential between bead A and bead B. In spite of the simple model, it reveals that: (1) the lamellar phase is formed at $n \geq 2$; (2) an order-disorder transition occurs as the temperature increases, which qualitatively matches with the block copolymer phase diagram. In a second step, we simulated the lamellar phase in a thin block copolymer film by using the A_2B_2 model that is the smallest block copolymer capable of forming the lamellar phase. It is found that: (1) the vertical lamellar phase is formed on a neutral surface; (2) finger print pattern appears; (3) the domain increases as the time proceeds, which indicates the similar behavior as that observed in a real block copolymer film. From the above results, it is highly like that the dynamics of orientational ordering in a block copolymer film can be explained even by using the coarse-grained model.

[1] J. A. Anderson, C. D. Lorenz, and A. Travesset, Journal of Computational Physics 227(10): 5342-5359, May 2008. [2] J. Glaser, T. D. Nguyen, J. A. Anderson, P. Liu, F. Spiga, J. A. Millan, D. C. Morse, S. C. Glotzer. Computer Physics Communications 192: 97-107, July 2015.

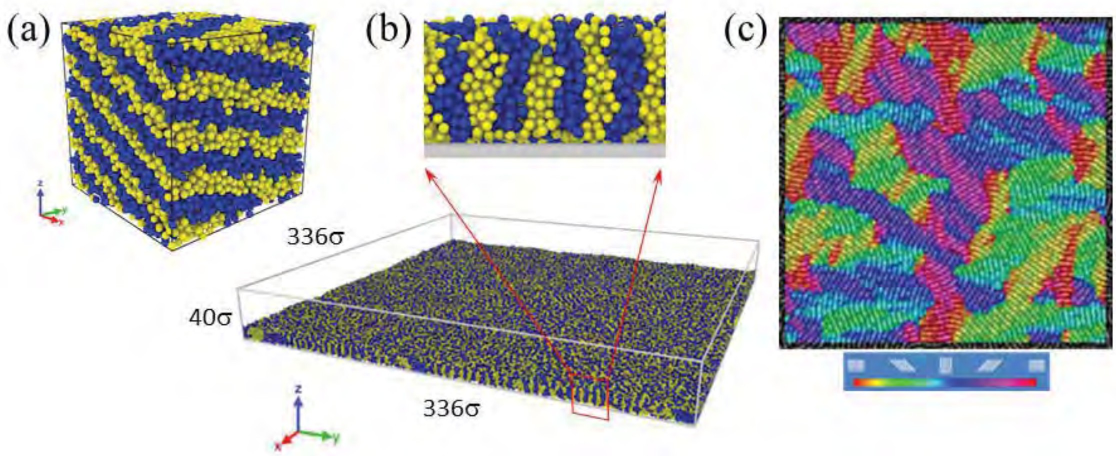

Figure 1 (a) Typical configuration of A_2B_2 bulk phase of 13,824 beads. (b) Typical configuration of A_2B_2 film of 903,168 beads on a neutral surface. σ is the unit of length that corresponds to the separation distance between beads when the LJ potential is zero. (c) False color orientation map of lamellar domains corresponding to the configuration in (b).

Theory of a carbon-nanotube polarization switch

Ken-ichi Sasaki

NTT Basic Research Laboratories, NTT Corporation, 3-1 Morinosato Wakamiya, Atsugi, Kanagawa 243-0198, Japan

A carbon nanotube (CNT) absorbs light whose linear polarization is parallel to the tube's axis, while transmits light whose polarization is perpendicular to it (see Fig.1). The optical anisotropy of a CNT enables aligned CNTs to function as an optical polarizer[1]. Recently, we theoretically predicted that the polarization dependence is reversed by charge doping[2]. Namely, a doped CNT transmits light with parallel polarization and absorbs perpendicularly polarized light (see Fig.1). The absorption of perpendicularly polarized light originates from the resonant excitation of collective oscillations of electrons (plasmon), which differs entirely from the excitation of individual electrons by a parallel polarized light in an undoped CNT. This theory of plasmon resonance accounts qualitatively for the anomalous absorption peaks observed experimentally in doped CNTs. Here we show the doping dependence of the absorption spectrum calculated using the Kubo formula (see Fig. 2). We discuss that the correction to the absorption spectrum due to the Coulomb interaction is negligible for a doped CNT because of a screening effect caused by intraband electron-hole pairs.

Fig. 1

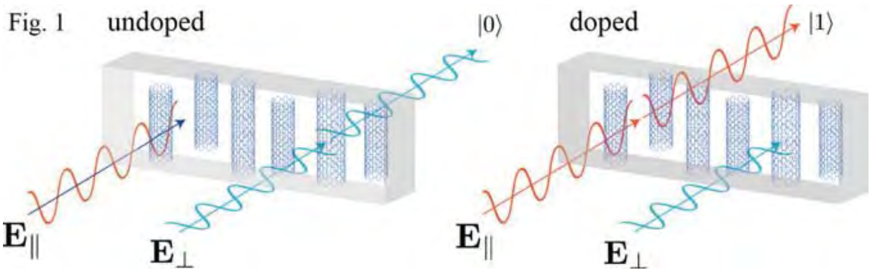

To change the polarization direction of light transmitted through a typical Polaroid lens, it is necessary to rotate the lens itself. However, according to the theory of doping dependence, a CNT polarizer can invert the polarization of the transmitted light by 90 degrees without having to spatially rotate the polarizer; in other words, it is expected to function as an electronic polarization switch. In regard to cutting-edge optical transmission technology, the two degrees of freedom of polarized light are utilized to double the amount of information being transmitted. Different information like images and sound is transcribed to orthogonal polarization and transmitted. A polarization switch based on CNTs can be used to manipulate information within highly miniaturized structure for optical transmission.

Fig. 2

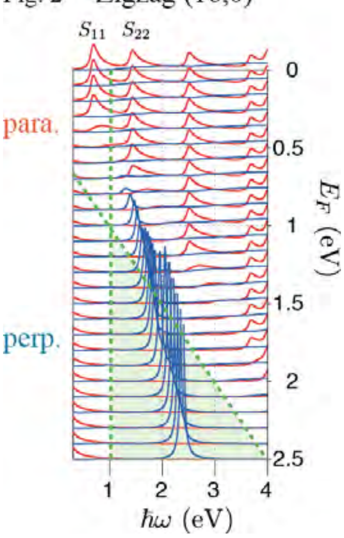

[1] S. Shoji et al., Phys. Rev. B **77**, 153407 (2008); B. G. Kang et al., Nanotechnology **21**, 405202 (2010). [2] K. Sasaki, S. Murakami, and H. Yamamoto, Appl. Phys. Lett. **93**, 125402 (2016).

Fig. 1(left); Undoped CNTs transmit only perpendicular polarized light. (right) Doped CNTs transmit only parallel polarization. Since the polarization of the transmitted light rotates 90 degrees by doping, the aligned CNTs function as a polarization switch. Fig. 2; Red (blue) spectra show the absorption of parallel (perpendicular) polarization.

Structure-dependent optical and electrical transport properties of Ni-doped ZnO nanorods by spray pyrolysis

Ganesh E. Patil and G. H. Jain

Department of Physics, KKHA Arts, SMGL Commerce & SPHJ Science College, Chandwad Maharashtra 423101 INDIA

Hexagonal pillar shaped Ni-doped ZnO nanorods with different sizes have been successfully synthesized by spray pyrolysis technique (SPT). The equal amount of methanol and water is used as a solvent to dissolve the AR grade Zinc acetate and Nickel Chloride with different concentrations for precursor solution. This solution is sprayed on to the glass substrate heated at 350 oC. The films were characterized by ultra-violet spectroscopy (UV), photoluminescence spectroscopy (PL), X-ray diffraction (XRD), field emission scanning electron microscopy (FESEM) and transmission electron microscopy (TEM). The deposition of thin films results in a layer comprising well-shaped hexagonal nanorods with diameter of 90–120 nm and length of up to 200 nm. The results are explained using FESEM, XRD and room temperature photoluminescence spectroscopy.

We investigate the dependence of functional properties on structure and morphology and show how the correlation between electrical and optical properties can be studied to evaluate energy gap, conduction band effective mass and transport mechanisms. These characterizations show that the Ni doping increases the deep level defect and also the structural strain that is caused by the annealing treatment. The hexagonal pillar shaped Ni-doped ZnO nanorods can tune the optical and electrical transport properties.

Parity-dependent shot noise in a superconductor-nanowire quantum dot

K. Takase [1], Y. Ashikawa [1,2], G. Zhang[1], K. Tateno[1], Y. Okazaki[1], and S. Sasaki[1,2]

[1] *NTT Basic Research Laboratories, NTT Corporation, Japan*
[2] *Department of Physics, Tohoku University, Japan*

Hybrid devices consisting of semiconducting nanowire and superconducting electrode is a fascinating playground to explore exotic physics such as a quantum supercurrent transistor [1], the Andreev bound states including its interplay with the Kondo effect [2], and recently discovered Majorana bound states [3–5]. Here, we report on shot noise measurements performed on an InAs quantum dot suspended between two superconducting electrodes. We find a clear alternation for the shot noise value, indicating that super-Poissonian/Poissonian tunneling occurs with respect to a parity of the electron occupation in the quantum dot. We attribute the mechanism to the interplay with charging energy, level spacing, and superconducting gap.

The sample is fabricated from an InAs nanowire grown by vapor-liquid-solid method [6]. InAs was placed on a pre-patterned substrate and then Ti/Al was deposited to InAs upper surface [Fig. 1(a)], which was prepared to be clean by Ar etching to make good contacts between superconductor and nanowire. Figure 1 (b) shows gate voltage (V_g) and source-drain voltage (V_{sd}) dependence of a differential conductance (dI/dV_{sd}) and shot noise being represented in the form of Fano factor F ($F = S/2eI$ with S of the shot noise value, e of electron charge and I of current). We can find a Coulomb diamond pattern, in which the size of the Coulomb diamond depends on the electron parity, i.e., larger (smaller) diamond is observed for even (odd) parity. More importantly, we find that Fano factor is significantly different between even and odd occupation, being ~2 (1) for even (odd) parity, directly indicating that electron is dominated by super-Poissonian (Poissonian) cotunneling transport. With increasing magnetic fields, we observe that super-Poissonian shot noise is suppressed and such a parity dependence disappears above the critical field of the superconducting electrodes. By examining the size of the charging energy and level spacing and taking the superconducting gap into consideration, we demonstrate that parity-dependent shot noise is reasonably explained by the interplay with charging energy, level spacing, and superconducting gap.

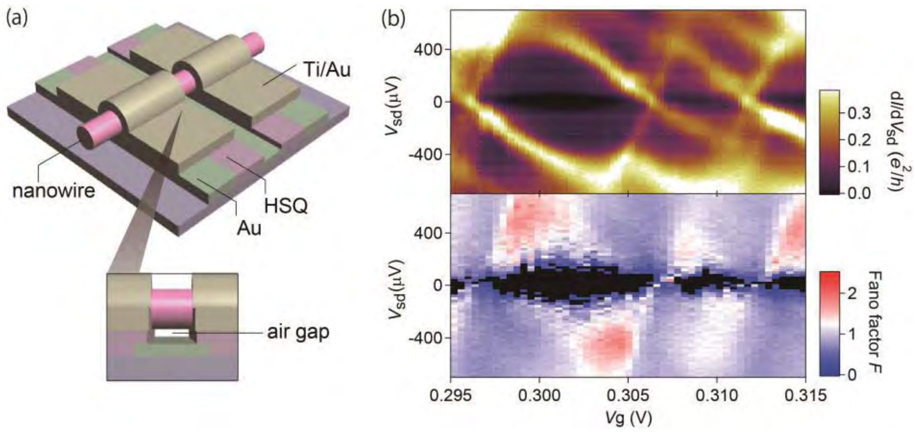

Fig. 1(a) Schematic illustration of our device. (b) Differential conductance (top) and Fano factor (bottom) plotted as a function of V_{sd} and V_g.

[1] P. Jarillo-Herrero et al., Nature **439**, 953 (2006).
[2] T. Sand-Jespersen et al., Phys. Rev. Lett. **99**, 126603 (2007).
[3] V. Mourik et al. , Science **336**, 1003 (2012).
[4] S. M. Albrecht et al., Nature **531**, 206 (2016).
[5] M. T. Deng et al., Science **354**, 1557 (2016).
[6] K. Tateno et al, Nano Lett. **12**, 2888 (2012).

Giant gate control of Rashba spin-orbit interaction in a gate-all-around InAs/InP core-shell nanowire

K. Takase [1], D. Ibrahimagic [1], K. Tateno[1] and S. Sasaki[1]

[1] *NTT Basic Research Laboratories, NTT Corporation, Japan*

III-V semiconductor nanowire (NW) has been attracting material for a nanoscale spin-FET taking advantage of large Rashba spin-orbit interaction (SOI) as well as for a next-generation high-mobility integrated circuits replacing Si technology. Here, we report on a newly-developed gate-all-around (GAA) InAs/InP core-shell nanowire FET, which realizes the highest gate-controllability of Rashba SOI among those obtained for two-dimensional electron gas formed in III-V quantum wells [1,2] and various types of III-V nanowire FETs [3–5].

Our device is fabricated from an InAs/InP core-shell nanowire grown by vapor-liquid-solid method [6]. We first coat the core-shell NW with Al_2O_3 (~ 6 nm) with ALD, and then fabricate gate electrode almost uniformly around the coated NW [Fig. 1(a)], by combining the pre-patterned substrate and electron-beam deposition. Magnetotransport measurements reveal that magneto-conductance (ΔG) with respect to B shows a transition from a dip to a peak with increasing gate voltage (V_g) [Fig. 1(b)]. This indicates a crossover from weak localization to a weak antilocalization, which is known to occur in the presence of strong Rashba SOI. By fitting B dependence of ΔG, we extract spin-orbit length and then converted to Rashba coupling parameter α_R. Figure 1(c) compares α_R obtained for our device and that previously reported for two-dimensional electron gas formed in a quantum well and for a variety of NW FETs. This demonstrate that V_g controllability of ours are higher than best value ever obtained for ion-gated InAs NW using electric double layer [4] and the best value obtained for MOS-type NW FET [5]. This high tunability indicates that our device will open up a way for a prototype of highly effective nanoscale spin FET.

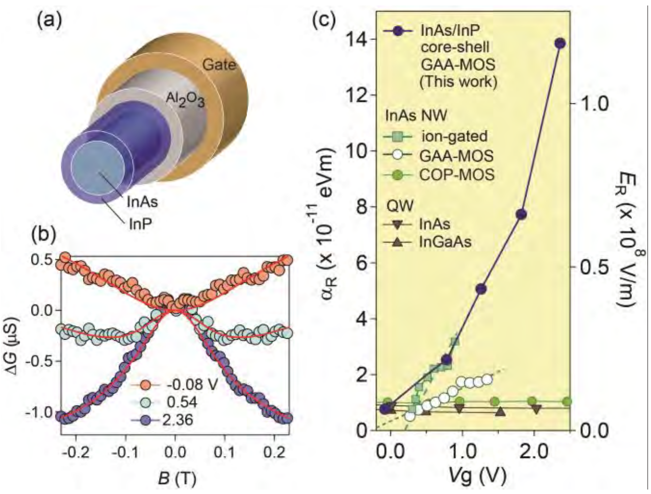

Fig. 1(a) Schematic illustration of the InAs/InP core-shell nanowire. (b) B dependence of ΔG obtained for different V_g. (c) Rashba coupling parameter α_R vs V_g for a variety of III-V FETs [1-5].

[1] H. C. Koo, J. H. Kwon, J. Eom, J. Chang, S. H. Han, and M. Johnson, Science **325**, 1515 (2009).
[2] J. Nitta, T. Akazaki, H. Takayanagi, and T. Enoki, Phys. Rev. Lett. **78**, 1335 (1997).
[3] A. E. Hansen, M. T. Björk, C. Fasth, C. Thelander, and L. Samuelson, Phys. Rev. B **71**, 205328 (2005).
[4] D. Liang and X. P. A. Gao, Nano Lett. **12**, 3263 (2012).
[5] K. Takase, Y. Ashikawa, G. Zhang, K. Tateno, and S. Sasaki, Sci. Rep. **7**, 930 (2017).
[6] K. Tateno, G. Zhang, H. Gotoh, and T. Sogawa, Nano Lett. **12**, 2888 (2012).

Telecom-band light emitting diodes based on bottom-up InAs/InP heterostructure nanowires

Guoqiang Zhang[1,2], Masato Takiguchi [1,2], Kouta Tateno[1,2], Takehiko Tawara[1,2], Masaya Notomi[1,2], and Hideki Gotoh[1]

[1] *NTT Basic Research Laboratories,* [2] *NTT Nanophotonics Center*

NTT Corporation, 3-1 Morinosato-Wakamiya, Atsugi, Kanagawa, 243-0198, Japan

Telecom-band light sources are extremely important for optical data communication. Bottom-up semiconductor nanowires (NWs) offer the possibility of enhancing the degree of freedom for 3D integration and enduring large lattice mismatch for breaking the limitation of material combination. Hence they are being extensively studied in optoelectronic devices. Although ultraviolet, visible, and near-infrared NW light emitting diodes (LEDs) have been demonstrated, room-temperature telecom-band NW LEDs have not been reported a lot. Here we demonstrate telecom-band NW LEDs operating at room temperature by using multi-stacked InP/InAs heterostructure NWs.

We synthesized the InP/InAs NWs in a metalorganic vapor phase epitaxy (MOVPE) system in the self-catalyzed vapor-liquid-solid (VLS) [1, 2]. Diethylzinc (DEZn) and ditertiarybutylsulfide (DTBS) are used as the source materials for the doping control of p- and n-type InP segments. The active region contains 5-10 periods of InP/InAs superlattice-like units (Fig. 1). The NWs were then embedded in transparent benzocyclobutene (BCB) material. The ITO and Au-Ni-Zn was deposited for the contact of n-type InP NW and p-type InP substrate (Fig. 2). The electrical characteristics show typical I-V curve of a p-n diode (Fig. 3). We studied the electroluminescence (EL) property by using a Micro-PL system. The device exhibits luminescence when biased (Fig. 4a). We confirmed the EL spectrum from a single NW with a peak λ of 1.25 μm (Fig. 4b). The well-established growth technique of InP/InAs hetero-NW [1] enables to tune the luminescence peak by the thickness of InAs active layer in a wide range.

This work was supported by JSPS KAKENHI (Grant NO.: 15H05735 and 16H03821.)

[1] G. Zhang, et al. Nanotechnology **26**, 115704 (2015). [2] G. Zhang, et al. ACS Nano **9**, 10580 (2015).

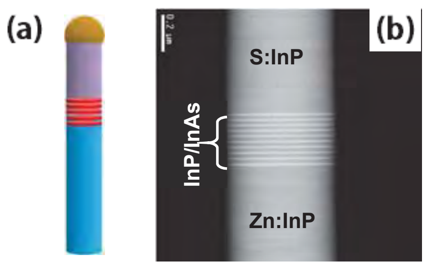

Fig. 1. (a) Schematic diagram of the p-i-n NW with multiple InP/InAs units. (b) HAADF-STEM image of a NW with the 10-layer InAs active layers.

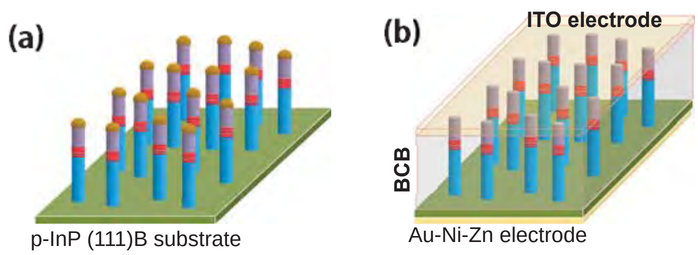

Fig. 2. Schematic diagrams of (a) as-grown NWs on p-InP (111)B substrate and (b) fabricated device for LED. The NWs were embedded in transparent BCB polymer material.

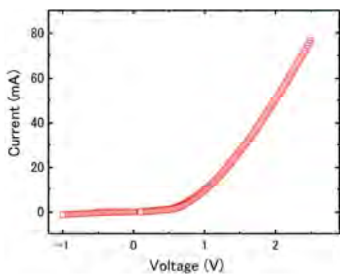

Fig. 3. Typical I-V curve exhibiting diode-like characteristics.

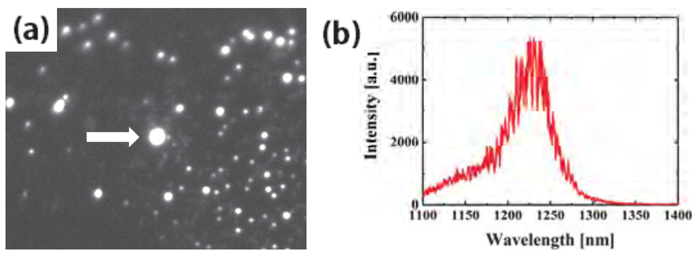

Fig. 4. (a) Spatially-resolved EL image (156μm×195 μm) of NW LED when biased at 2.3 V (current: 66 mA). (b) EL spectrum collected from a single NW shown in (a) by a white arrow.

Probing Photonic States in 1D space using Quantum Wave Mixing

T. Hönigl-Decrinis [1,2], A. Yu. Dmitriev [3], R. Shaikhaidarov [1,3], V. N. Antonov [1,3] and O. Astafiev [1,2,3]

[1] *Physics Department, Royal Holloway, University of London, Egham, TW20 0EX, UK*
[2] *National Physical Laboratory (NPL), Teddington, TW11 0LW, UK*
[3] *Moscow Institute of Physics and Technology, 141700 Dolgoprudny, Russia*

Superconducting artificial atoms are remarkably attractive to study quantum optics phenomena on chip. Here, we demonstrate that when a non-linear medium is scaled down to a single quantum scatterer, a series of effects beyond classical physics are revealed. In particular, Quantum Wave Mixing (QWM) [1] is a result of elastic scattering of electromagnetic waves on a single artificial atom.

We investigate two regimes of QWM: Coherent wave mixing and quantum wave mixing with non-classical superposed states. In the former, two pulsed waves with frequencies slightly detuned to each other are scattered on the single artificial atom resulting in a symmetric spectrum with an infinite number of side peaks (Fig.1(a)). The amplitude of each of these peaks oscillates in time according to Bessel functions with the orders determined by the number of interacting photons (Fig.1(b)). In the latter regime, a time delay between the two pulses is introduced causing a striking difference in the spectrum, which now exhibits a finite number of narrow coherent emission peaks (Fig.2). Furthermore, the spectrum in the latter regime is asymmetric with the number of positive frequency peaks (due to stimulated emission) always exceeding by one compared to the negative frequency peaks (due to absorption).

Thus in QWM, the spectrum of elastically scattered radiation is a fingerprint of the interacting photonic states. Moreover, the artificial atom visualizes photon-state statistics, for example distinguishing coherent, one- and two-photon superposed states in the quantum regime. Our results give new insight into nonlinear quantum effects in microwave optics with artificial atoms.

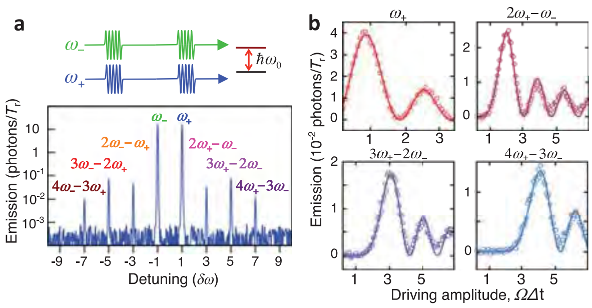

Fig. 1. Dynamics of coherent wave mixing

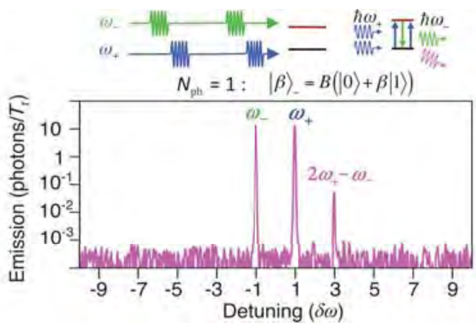

Fig. 2. Quantum wave mixing with non-classical states

[1] A. Yu. Dmitriev et al (2017). Quantum wave mixing and visualisation of coherent and superposed photonic states in a waveguide. Manuscript submitted for publication

Electrical control of a quantum non-linearity in a nano-photonic waveguide

D. Hallett [1], A. P. Foster [1], B. Royall [1], D. Hurst [1], P. Kok [1], E. Clarke [2], M. S. Skolnick [1] and L. R. Wilson [1]

[1] *Department of Physics and Astronomy, University of Sheffield, Sheffield S3 7RH, UK*
[2] *Department of Electronic and Electrical Engineering, University of Sheffield, Sheffield S3 7RH, UK*

This work demonstrates on-chip electrical control of the quantum optical nonlinearity arising from the interaction of a weak resonant laser with a single semiconductor quantum dot (QD) embedded in a nano-photonic waveguide (Fig. 1a). The electrically tuneable and switchable non-linearity is found to reduce the transmission of a weak resonant laser through the waveguide by up to 40% (Fig. 1b-c). Observation of a clear, voltage-controlled bunching signal in the photon statistics of the transmitted light demonstrates the single-photon character of the nonlinear response (Fig. 1d). Control of the QD charge state with applied bias enables the study of the neutral and charged exciton complexes. The electrical control of this quantum optical nonlinearity opens up promising avenues for future research. In particular, this work demonstrates local control of the nonlinearity and allows for individual control of separate quantum emitters enabling devices using two or more indistinguishable emitters.

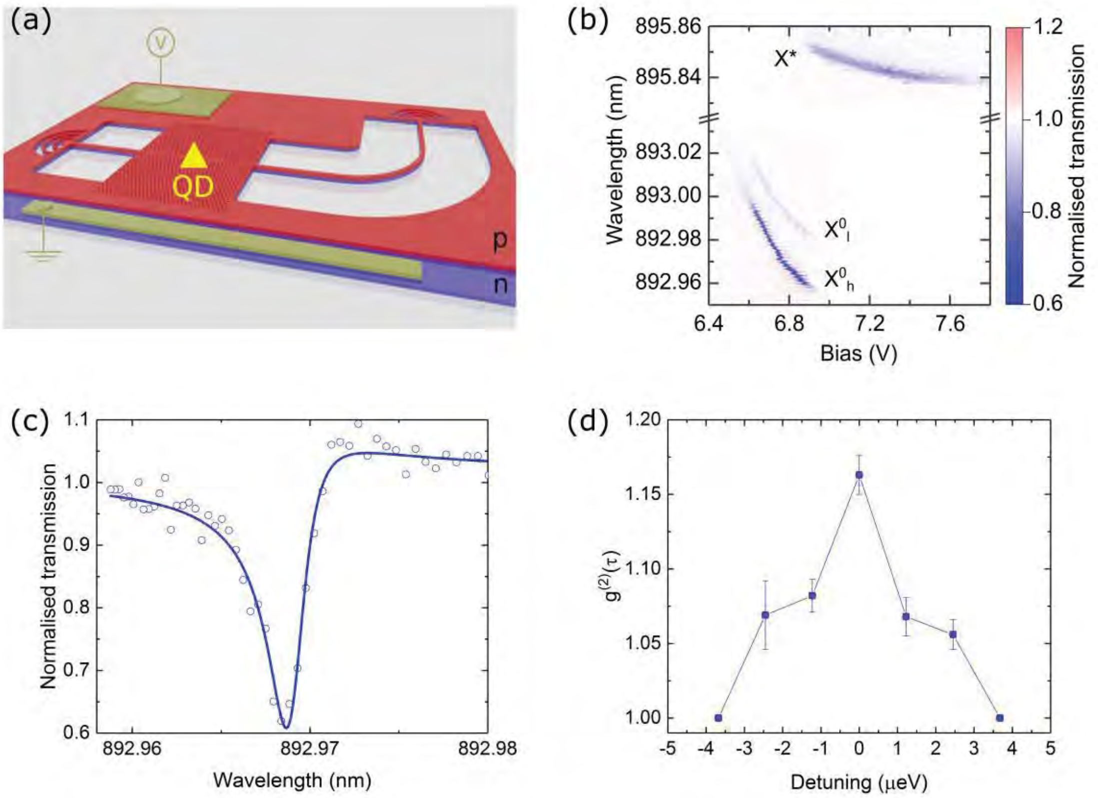

Figure 1. (a) Device Schematic. The QD is embedded in a GaAs *p-i-n* photonic crystal waveguide, which is coupled to two nanobeam waveguides terminated by Bragg outcouplers.
(b) Transmission through the waveguide as a function of laser and voltage across the diode. Interaction is seen with two charge states of a single QD (X^0 and X^-).
(c) Waveguide transmission spectrum at fixed bias. Extinction of the laser by 40±2% is observed for zero detuning between the laser and the X^0 spectral line.
(d) Bunching of the transmitted light as a function of detuning between X^0 and the laser. Bunching of 1.16±0.01 is observed at zero detuning.

Evaluation of 2*f*-to-3*f* self-referencing interferometer using dual-pitch PPLN ridge waveguides

K. Hara[1,2], K. Hitachi[1], A. Ishizawa[1], T. Nishikawa[2], and H. Gotoh[1]

[1] *NTT Basic Research Laboratories, 3-1 Morinosato, Atsugi-shi, Kanagawa 243-0198, Japan*
[2] *Tokyo Denki University,5 Senju-Asahi-cho, Adachi-ku, Tokyo 120-8551, Japan*

Techniques for stabilizing the carrier-envelope offset (CEO) frequency of an optical frequency comb are prerequisites for precision spectroscopy. Recently, ways to widen the spacing of optical frequency combs have been intensively studied. In stabilizing such optical frequency combs, it would be difficult to generate a one-octave supercontinuum (SC) spectrum, because the pulse energy per pulse is inversely proportional to the repetition rate of an optical frequency comb. An alternative way to stabilize the CEO frequency is to use a 2*f*-to-3*f* self-referencing interferometer (SRI), in which only a 2/3-octave bandwidth of SC light is required. Here we report a reduction in pulse energy with a dual-pitch (DP-) periodically poled lithium niobate (PPLN) ridge waveguide [Fig. 1(a)]. The DP-PPLN ridge waveguide only requires 2/3-octave bandwidth of SC light (1230-1800 nm) for generating a CEO beat. The threshold value for frequency stabilization with the DP-PPLN waveguide was less than half compared with that obtained with a conventional single-pitch (SP-) PPLN waveguide [1].

In the experiment, we used a passively mode-locked Er-doped fiber laser system, which delivered 100-fs, 1.5-nJ laser pulses at a repetition rate of 250 MHz with a center wavelength of 1560 nm [Fig. 1(b)]. To estimate the required pulse energy for stabilizing the CEO frequency, we adjusted the input pulse energy by inserting an X-dB attenuator (X = 1–5). This light was then launched into a short highly nonlinear fiber to generate SC light. Then, the SC light was injected into a DP- (SP-) PPLN ridge waveguide to generate a CEO beat. CEO signals of more than 35 dB were observed for 0.51-nJ SC light with the DP-PPLN waveguide, whereas they were observed for 1.11-nJ SC light with the SP-PPLN waveguide [Fig. 1(c)]. In addition, we evaluated the instability of the CEO frequency when it was stabilized with the DP-PPLN ridge waveguide. By reducing the pulse energy, the phase noise of a CEO frequency stabilized with the DP-PPLN ridge waveguide was lower than that with the SP-PPLN ridge waveguide. These results suggest that a DP-PPLN ridge waveguide is more advantageous than an SP-PPLN ridge waveguide for stabilizing the CEO frequency.

This work was supported by JSPS KAKENHI Grant Numbers JP17H02803, JP16H04379.

[1] K. Hitachi *et al*., Appl. Phys. Lett. **110**, 241107 (2017)

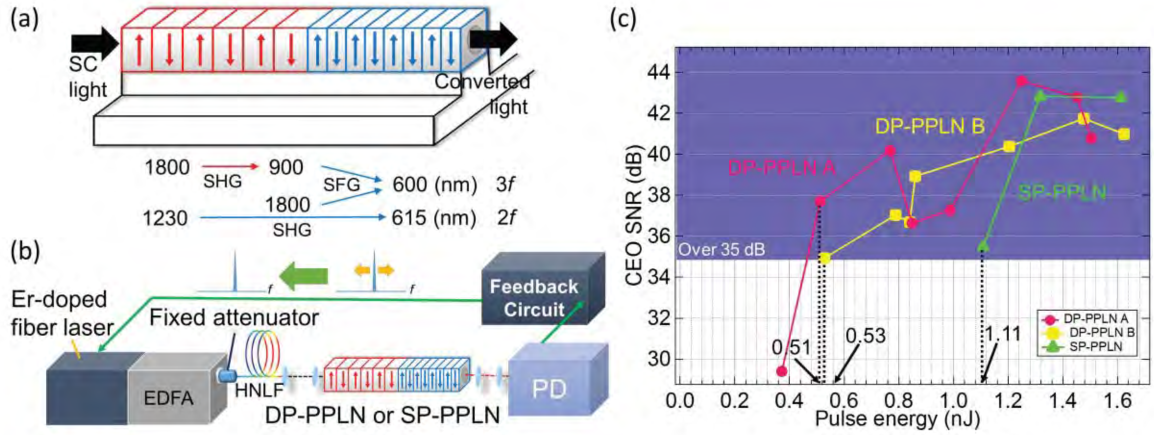

Fig. 1 (a) Dual-pitch PPLN ridge waveguide. (b) Experimental setup. (c) Laser pulse energy dependence of SNR of a CEO signal.

Valley-contrasting eigenmodes in photonic crystals with triangular lattice

Taiki Yoda [1,2] **and Masaya Notomi** [1,2,3]

[1] *Department of Physics, Tokyo Institute of Technology*
[2] *NTT Basic Research Laboratories, NTT Corporation*
[3] *Nanophotonics center, NTT Corporation*

The valley degree of freedom, which labels the degenerate energy extrema in momentum space, is one of the internal degree of freedom in periodic systems. In contrast to the electron spin, the valley degree of freedom appears ubiquitously in photonic crystals (PhC). In particular, PhCs with triangular and honeycomb lattices possess K and K' valleys. Thus, PhCs with these lattices are applicable to valley photonics. However, valley modes proposed in Ref. [1] are not confined to PhCs. Slab-type PhCs with guided valley modes have been proposed in Refs. [2,3]. These slabs consist of complicated honeycomb-based air-hole structure, which may not be suitable for fabrication.

In this talk, we investigate air-hole-type valley PhC slabs with simple triangular lattice. The TM photonic bands for the triangular lattice with *circular* air holes form Dirac cones at the K and K' point, and has no photonic band gap (Fig. 1a). We design a valley PhC with *triangular* air holes as shown in Fig. 1b. The band structure of the valley PhC with the effective refractive index $n_{\mathrm{eff}} = 2.6$ is plotted in Fig. 1b. The triangular shape of air hole breaks the original six-fold rotational symmetry and inversion symmetry. Consequently, a finite gap opens at the Dirac cone of the K and K' points. Next, we investigate angular momentum of eigenmodes at the K and K' points. At the K point, phase vortices are located at the center of the air hole and the corner of the unit cell. The Poynting vector rotates around the phase vortices, and the direction of the rotation depends on chirality of the phase vortices. The orbital angular momentum (OAM) density at the K point is shown in Fig. 2a. In valley PhCs without inversion symmetry, the OAM in the unit cell is finite. The OAM at the K' point is opposite to that at the K point due to time-reversal symmetry (Fig. 2b). Furthermore, the in-plane magnetic field has local right- and left-handed circular polarizations, and these circular polarizations produce local spin angular momentum. We also calculate edge modes which occur at interfaces between two PhCs with different valleys. Finally, the 3D band structure of the valley PhC with the refractive index n=3.46 and finite thicknesses is calculated (Fig. 3). The calculation shows that our valley PhC has confined valley modes with OAM. Our PhC slab consists of larger air-holes than valley PhCs proposed previously, and thus it is advantageous to fabrication.

[1] T. Ma and G. Shvets, New J. Phys. **18**, 025012 (2016)
[2] M. J. Collins, et al., Phys. Rev. A 94 063827 (2016)
[3] S. Iwamoto and Y. Arakawa, ICO-24, F1E-03 (2017)

Figure 1

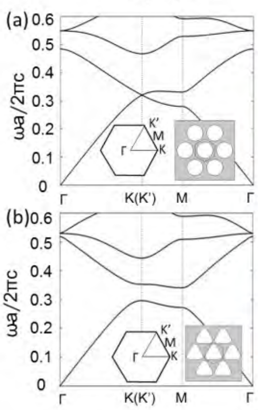

Figure 2

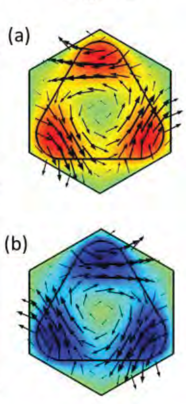

Figure 3

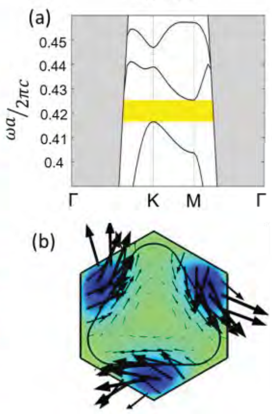

Figure 1
Band structure of 2D PhC with (a) circular and (b) triangular hole

Figure 2
Orbital angular momentum density and Poynting vector at (a) K and (b) K' point

Figure 3
Band structure of PhC slab with thickness h=0.5a

Integrated Optics in 3C Silicon Carbide

F. Martini [1]**, A. Politi** [1]

[1] *Department of Physics and Astronomy, University of Southampton, Southampton, SO17 1BJ*

Silicon Carbide is an extremely attractive material since it combines desirable optical properties, due to its non-centrosymmetric crystal structure, and the presence of quantum emitters, both essential for the realization of a scalable monolithic quantum photonic platform[1]. The presence of a Si substrate, needed for the heteroepitaxial growth of high-quality 3C SiC layer, hampered the development of photonics components. Here we report the demonstration of efficient grating couplers, sub-µm waveguides and ring resonators thanks to a novel fabrication approach that suspends all the photonic components. By taking advantage of the high field enhancement achieved in the rings together with small modal area of the waveguide, we report the demonstration of frequency conversion by means of four wave mixing (FWM), measuring for the first time the Kerr nonlinear index.

The components were realized following the fabrication procedure reported in Fig.1. (a-f). A first electron beam lithoghraphy step is used to pattern the waveguides and a second one defines holes along the photonic structures, required as access points for a following vapor etch that suspends all the optical components by removing the Si substrate [2]. Fig. 1.(g) reports a SEM picture of a suspended multi-mode (MM) ring. The devices were characterized using a CW tunable laser and polarization maintaining fiber arrays. The maximum coupling efficiency of the grating coupler were -6dB for the uniform single-mode (SM) grating coupler and -6.6dB for the apodized MM case, meanwhile the half width half maximum was 38nm and 18nm, respectively. Finally, we measured the intrinsic quality factors for the SM and MM ring resonators with a radius of 20µm to be 8,700 and 25,000, respectively, corresponding at the linear propagation losses of 50dB/cm and 21dB/cm [2].

The small modal volume achieved in the ring resonators was exploited to demonstrate frequency conversion by four wave mixing. In order to enhance the nonlinear process, we employed a 10µm MM ring with a quality factor of 7,400. As shown from the normalized transmission in the inset of Fig.1.h, the ring is close to be critically coupled, thus providing the highest field enhancement. In Fig.1.h is reported the FWM gain in function of the pump power, showing the expected nonlinear behavior. By fitting the data with the nonlinear gain equation, we retrieved the nonlinearity of the structure $\gamma=3.86\pm0.03\,W^{-1}m^{-1}$ and the Kerr nonlinearity to be $n_2=5.31\pm0.04\times10^{-19}m^2/W$[3].

These results are of a fundamental interest for exploiting nonlinear effects in this material and a decisive step toward the development of 3C SiC quantum photonics.

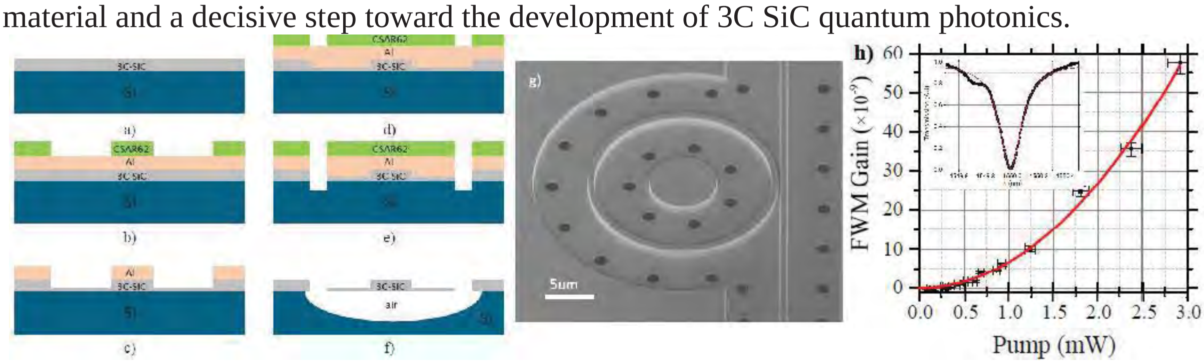

Fig. 1.Fabrication process (a-g). h) FWM gain in SiC ring resonator and resonance of the ring (inset).

[1] J. L. O'Brien, A. Furusawa, and J. Vučković, Nat. Photonics **3**, 687–695 (2009).
[2] F. Martini and A. Politi, Opt. Express **25**, 10735–10742 (2017).
[3] F. Martini and A. Politi, arXiv preprint arXiv:1707.03645 (2017).

$CsPbBr_3$-perovskite nanowire-induced nanocavities in SiN photonic crystals

S. Sergent[1,2], M. Takiguchi[1,2], T. Tsuchizawa[1,3], J. Chen[4], Y. Fu[4], H. Taniyama[1,2], E. Kuramochi[1,2], S. Jin[4], and M. Notomi[1,2]

[1] *NTT Nanophotonics Center*
[2] *NTT Basic Research Laboratories*
[3] *NTT Device Technology Laboratories*
[4] *University of Wisconsin - Madison*

Subwavelength nanowires (NWs) positioned in grooved photonic crystals (PhC) have recently emerged as a versatile nanophotonic platform to achieve high quality factor nanocavities from the infra-red range [1] down to the ultra-violet range [2] and nanolasers operating at telecommunication wavelengths [3]. This hybrid approach allows for the coupling of nanocavities to virtually any NW material and has already been implemented with InAsP NWs in silicon PhCs [1] and ZnO NWs in silicon nitride PhCs [2]. We show here that the latter PhC platform can be extended to subwavelength $CsPbBr_3$-perovskite NWs [4] and demonstrate the realization of NW-induced nanocavities in the green range (Fig 1). In such cavities, we achieve experimental quality factors as high as $Q_{exp} = 1.1 \times 10^3$ (Fig 1 (c)) for a mode volume $V_m = 1.3(\lambda/n_r^{SiN})^3$, as deduced from three-dimensional finite-difference time-domain (3D-FDTD) calculations (Fig. 1 (a)) [5]. This result confirms the versatility of our hybrid approach to couple any type of nanowire material to a PhC nanocavity and this first integration of a perovskite NW in a nanophotonic platform opens the path toward the realization of efficient nanolasers and the study of quantum electrodynamics effects.

This work was supported by JSPS KAKENHI Grant Number 15H05735.

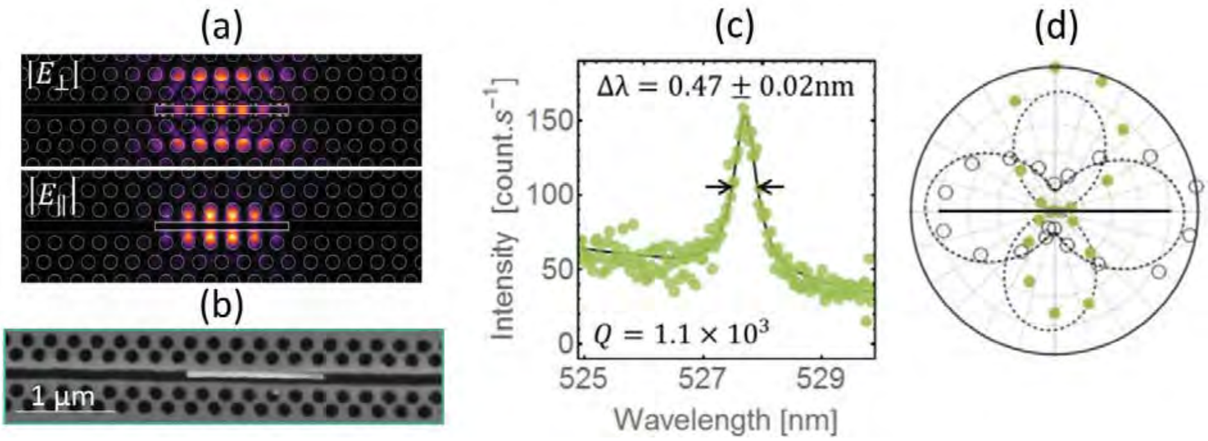

Figure 1. (a) 3D-FDTD calculations of a NW-induced nanocavity. (b) Scanning electron microscope image of a fabricated $CsPbBr_3$-perovskite NW nanocavity. (c) Microphotoluminescence spectrum of the nanocavity resonance. (d) Polarization properties of the nanocavity resonance (closed circles) and NW emission (open circles) in good agreement with 3D-FDTD calculations (see (a)).

[1] M. D. Birowosuto *et al.*, Nature Materials **13**, 279 (2014).
[2] Sergent et al., ACS Photonics **4**, 1040 (2017).
[3] M. Takiguchi et al., APL Photonics **2**, 046106 (2017).
[4] Fu et al., ACS Nano **10**, 7963 (2016).
[5] Sergent et al., Opt. Express **13**, 279 (2016).

Poster Session Ⅱ
Abstract

Spin diffusion dynamics under spin-orbit magnetic field in undoped GaAs quantum wells

H. Sanada[1], Y. Kunihashi[1], Y. Tanaka[1], H. Gotoh[1], K. Onomitsu[1], M. Kohda[2], J. Nitta[2], and T. Sogawa[1]

[1] *NTT Basic Research Laboratories, NTT Corporation, Atsugi, Japan*
[2] *Department of Materials Science, Tohoku University, Sendai, Japan*

Preserving spin states in semiconductor nanostructures is essential for future spintronic devises. Exciton spins have been extensively studied because the polarization-dependent selection rule of the inter-band optical transition provides rich information about their spins [1]. However, the time scale on which we can observe their spin dynamics is limited by the recombination lifetime, which is often less than 1 ns. In this report, we discuss unexpected spin dynamics with long relaxation times (>10 ns) and small diffusion coefficient (~2 cm^2/s) observed in an undoped GaAs quantum well (QW).

The sample was an undoped 20-nm-thick GaAs/AlGaAs (001) QW grown by MBE. We measured time and spatially resolved photoluminescence (PL) and Kerr rotation (KR) at 8 K. The PL and PL excitation (PLE) peaks of the excitons had linewidths narrower than 0.7 meV, indicating that the crystal quality is sufficiently high for us to discuss the exciton behavior. The time-resolved KR in the absence of an external magnetic field shows that the photo-injected spins survived for 16 ns in a small area (FWHM ~6 μm) irradiated by circularly polarized pump laser. This decay time was one order of magnitude longer than the radiation lifetime and it decreased as we increased the temperature or the pump spot size.

To gain further insight into this unexpected spin dynamics, we studied spin diffusion by measuring the probe-position dependence of the spin precession [Fig. 1(a)]. Figure 1(b) shows the time-resolved KR for different probe positions on the X (|| [100]) and Y (|| [010]) axes under an external magnetic field B_{ext} = 49 mT applied in the X direction. The oscillations at the centers (X = 0 and Y = 0) correspond to the spin precession determined by $\mathbf{B}_{ext}$. For both scanning directions, the Gaussian envelopes of the spatial profiles do not expand clearly over time. However, the precession frequency Ω increases linearly in the X direction whereas it is constant in the Y direction. This behavior cannot be explained without spin diffusion, and its direction dependence is consistent with the symmetry of the *k*-linear Dresselhaus spin-orbit interaction. A linear fit to Ω(X) [Fig. 1(c)] provided dΩ/dX = 7.7 MHz/μm, from which we obtained D_s ~ 2 cm^2/s according to the theory [2]. These results suggest that the electron spins diffuse very slowly under the Dresselhaus spin-orbit field. The ability to access such long-lived spin dynamics with slow diffusion might offer the possibility of memorizing quantum information in solid-state systems.

This work was supported by JSPS KAKENHI Grant Numbers JP15H05699 and JP16H03821.

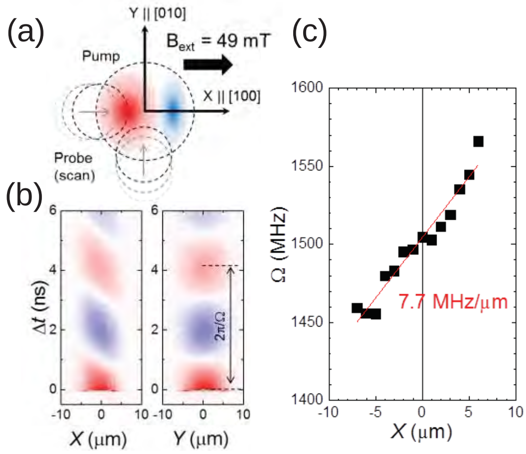

Fig.1 (a) Schematic configuration of the spin diffusion measurement. (b) KR signals plotted as a function of delay Δ*t* and probe positions (*X* and *Y*). (c) X dependence of the precession frequency.

[1] A. Vinattieri *et al*., APL **63**, 3164 (1993), H. Gotoh *et al*., APL **73** (1998), T. Amand *et al*., PRL **107**, 172402 (2015).
[2] M. Kohda *et al*, APL **107**, 172402 (2015).

Spin chain applications for quantum information processing

Marta P. Estarellas, Irene D'Amico, and Timothy P. Spiller

York Center for Quantum Technologies University of York
YO10 5DD York, United Kingdom

One of the most essential processes involved in classical computation is that related to the information manipulation. Each component or register of a computer needs to communicate to others by exchanging information encoded in bits and transforming it through logical operations. Hence the theoretical study of methods for information transfer and processing in classical information theory is of fundamental importance for telecommunications and computer science, along with study of errors and robustness of such methods. In quantum information scenarios, there arises a whole new set of paradigms and devices, based on manipulations of qubits – the quantum analogues of conventional data bits. Such systems can offer completely new capabilities, or show enormous advantage against their classical analogues, but at the same time present a whole new set of technical and conceptual challenges to overcome. The full and detailed understanding of quantum processes and studies of theoretical models and devices therefore provide the first logical steps to the future technological exploitation of these new machines. In this line, our work focuses on spin chains, series of coupled qubits. Spin chains form a generic and flexible class of theoretical models that can be applied to model a wide range of different physical systems, and a variety of quantum device applications.

In particular, we examine different coupling pattern configurations of spin chains as well as their use as quantum devices for quantum information tasks. Both dynamical studies and the eigenstate spectrum analysis have been considered, demonstrating the presence of spatial localisation and topological protection of quantum states. We have also investigated the effects of different sources of static noise (which could arise from fabrication errors), showing that localisation is very resilient against disorder [1]. This makes these generic devices good candidates for robust quantum information processing applications. Subsequently, we have also considered the use of these topological defects as tool to manipulate the properties and behaviour of spin chain states for quantum devices. For example, we demonstrate that one type of chain is suitable as hardware for a quantum entangling gate protocol, which exploits the natural dynamics of the chain [2,3]. We show that, after extraction at a given known time, this protocol produces two maximally entangled qubits with very high fidelity. The protocol is very robust to certain types of static disorder, offering the potential for a practical entanglement generation resource across a range of physical systems. A second stage of the protocol is proposed, where the two entangled qubits are localised, and thus stored, in a protected state.

In summary, we present a variety of flexible spin chain configurations with practical characteristics for a range of quantum device applications. Our work further expands the applicability and use of the already well-known spin chain models in quantum information and demonstrates the potential of these systems for future quantum technologies.

[1] Marta P. Estarellas, Irene D'Amico, Timothy P. Spiller, Scientific Reports, **7**, 42904 (2017).
[2] Marta P. Estarellas, Irene D'Amico, Timothy P. Spiller, Phys. Rev. A. **95**, 042335 (2017).
[3] Kieran N. Wilkinson, Marta P. Estarellas, Irene D'Amico, Timothy P. Spiller, (submitted) arXiv:1708.05650 (2017).

Geometric Phase Switching in Circular and Polygonal Mesoscopic Rings

Henri Saarikoski,[1] Andres Reynoso,[2] Diego Frustaglia,[3] Jose-Pablo Baltanás,[3]
Makoto Kohda,[4] and Junsaku Nitta[4]

[1]RIKEN Center for Emergent Matter Science (CEMS), Wako, Saitama 351-0198, Japan
[2] Instituto Balseiro and Centro Atómico Bariloche, 8400 Bariloche, Argentina
[3] Departamento de Física Aplicada II, Universidad de Sevilla, E-41012 Sevilla, Spain
[4] Department of Materials Science, Tohoku University, Sendai 980-8579, Japan
E-mail: henri.saarikoski@riken.jp

The geometric (Berry) phase acquired by an electron in a cyclic evolution depends strongly on the topology of the driving fields. An oscillating field in the adiabatic limit does not result in a Berry phase in contrast to a rotating field that gives a Berry phase of $\boldsymbol{\pi}$. Therefore a topological transition of the geometric phase can be achieved with a relatively small change in the driving field resulting in a huge change in the geometric phase. This idea of a Berry phase switch was recently demonstrated in graphene resonators [1].

We consider here theoretically topological geometric phase switching in quasi-two-dimensional mesoscopic ring systems where the geometric phase is of nonadiabatic (Aharonov-Anandan) type of geometric phase. The ring system is either circular or polygonal (Fig. 1a). The driving field results from interplay between complex spin-orbit (SO) and in-plane magnetic fields. The effective field acting on electron spin includes both Bychov-Rashba and Dresselhaus [001] SO interaction as well as an in-plane magnetic field. A prominent feature in resistance emerging in such a complex effective field is anisotropic resistance with respect to in-plane field direction. Phase of anisotropy oscillates both with SO as well as in-plane fields due to spin rotation dynamics on the Bloch sphere.

We find that the topological transition of the effective geometric phase [2] is imprinted both in the resistance as well as in anisotropy oscillations, even at vanishing Dresselhaus fields in squares (Fig. 1b). In circular rings the characteristic jumps in the anisotropy pattern emerge at low Dresselhaus fields (Fig. 1c). These features are captured by a 1D model and emerge also in 2D transport simulations of multi-mode disordered quantum rings using the Kwant code [3].

[1] F. Ghahari *et al.*, Science **356**, 845–849 (2017).
[2] H. Saarikoski, J. E. Vázquez-Lozano, J. P. Baltanás, F. Nagasawa, J. Nitta, and D. Frustaglia, Phys. Rev. B **91**, 241406(R) (2015).
[3] C. W. Groth *et al.*, New J. Phys **16**, 063065 (2014).

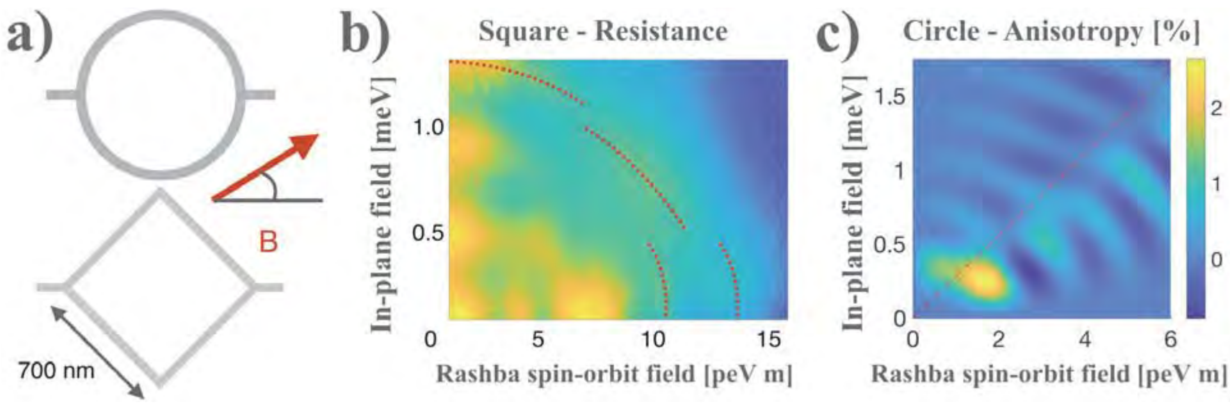

Fig. 1. a) Circular and square mesoscopic rings. The geometric phase switching manifests as jumps in the interference pattern of both resistance (b) and anisotropy (c). The Dresselhaus interaction strength is 0.3 peV m in (c).

Diffusion-suppressed drift-spin dynamics in GaAs quantum wells

Y. Tanaka [1], Y. Kunihashi[1], H. Sanada [1], H. Gotoh[1], K. Onomitsu[1], M. Kohda[2], J. Nitta[2], and T. Sogawa[1]

[1]*NTT Basic Research Laboratories, NTT Corporation, Atsugi, Japan*
[2]*Department of Materials Science, Tohoku University, Sendai, Japan*

Control of electron spin dynamics during drift transport without magnetic field is a key to developing spintronic devices. When two-dimensional electrons are exposed to an in-plane electric field, they precess around the effective magnetic field caused by spin-orbit interaction (SOI). The resultant spin distributions change dynamically owing to the drift-diffusion equation [1]. Because the diffusion reduces the spin densities over time, a small diffusion coefficient (D_s) is ideal for the efficient transfer of spins. Here, we report our experimental and simulated results of spatial-temporal precession of the drifting electron spins with suppressed D_s. We observed an unexpected feature of precession phase in Kerr rotation data, which agreed well with the results of our Monte Carlo simulation based on random walk model for drifting electron spins with different D_s .

The sample was an *n*-doped GaAs quantum well and cooled to 8 K. As illustrated in Fig. 1(a), the spins excited by pump pulses (ϕ 8 μm) were transported by an in-plane electric field, and the out-of-plane component of spin (M_z) after a time delay (t) were measured by the Kerr effect of probe pulses (ϕ 2.5 μm). Figure 1(b) shows M_z data plotted as a function of pump-probe distance (y) and t. In general, the *k*-linear SOI induces velocity-independent spatial spin precessions, resulting in the constant-phase lines that are parallel to the t axis in $M_z(y,t)$ map. It has been reported that the slope of the constant-phase lines become positive because of the cubic term of the Dresselhaus SOI [2]. In our experiment, however, we found negative slopes, which cannot be understood with the previous interpretation. We discuss this unexpected phenomenon with a Monte Carlo simulation using different D_s values. We found positive slopes for D_s = 30 μm^2/ns, whereas those for 5 μm^2/ns have negative slopes, which are same as we observed in the experiment. This negative slope appears only in the systems with sufficiently small D_s, thus we consider this originates from the transient phenomenon of spin diffusion.

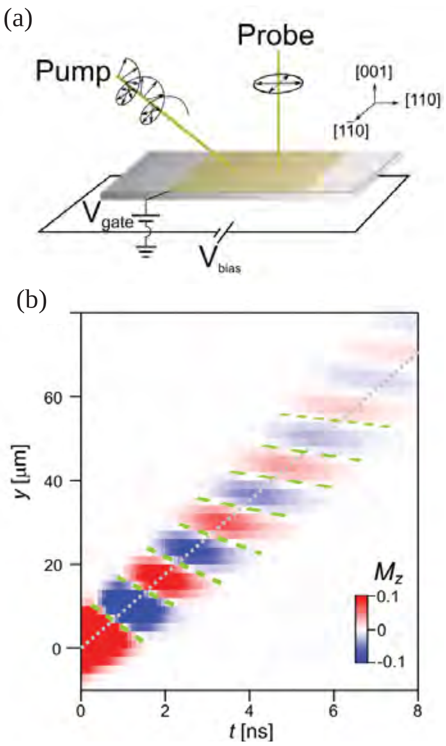

Fig.1(a): Experimental setup. (b): M_z color map obtained by the experiment. Dashed lines show constant phase lines of M_z .

This work was supported by JSPS KAKENHI Grant Numbers JP15H05699 and JP16H03821.

References

[1] M.P. Walser *et al*., Nat. Phys. **8**, 757 (2012).
[2] P. Altmann *et al*., PRL **116**, 196802 (2016).

In-plane spin-filtering with Rashba-Dresselhaus interaction

Y. Hashimoto, X. Yao[1], Y. Iwasaki, T. Nakamura and S. Katsumoto

Institute for Solid State Physics, University of Tokyo
5-1-5 Kashiwanoha, Kashiwa, Chiba 277-8581, Japan

One of the main obstacles in semiconductor quantum spintronics is the sensitivity to temperature. Though it was shown that the electron spin can maintain quantum coherence over 10 μm at room temperature in a vertical-type device[1], many of the experiments in quantum spintronics have been carried out in lateral devices, in which the quantum effects ordinary disappear far below liquid Nitrogen temperature. A possible quantum device robust against temperature is the resonant tunneling diodes. Here we report magnetoresistance originated from Rashba-Dresselhaus spin-orbit interaction (SOI) in the combination of a double barrier diode [2] and an epitaxially grown iron film.

The InGaAs double quantum well resonant diode structure is the one proposed in ref.[2], *i.e.*, the direction of perpendicular electric field is reverted by p-type doping in the center barrier. The film was grown by MBE on an InP substrate. A body centered cubic β-iron film of 20 nm was deposited onto the top of as grown surface in the MBE chamber at room temperature. In the proposal, only Rashba SOI is considered but in the real device, Dresselhaus-type SOI coexists and gives in-plane anisotropy. Hence, magnetoresistance caused by Rashba SOIs with inverse direction in the two quantum well at finite bias should have anisotropy for in-plane magnetic field. The film was cut into a square prism of $200{\times}200$ (μm)^2 area. The two-wire device shows well defined resonant peaks in the I-V characteristics as well as the characteristic magnetoresistance even at room temperature though the data presented below were taken at 5 K.

Figure 1(a) shows the anisotropy of hysteretic in-plane magnetoresistance at the source-drain bias of -0.5 V. Though the line-shape is reminiscent of so called anisotropic magnetoresistance in ferromagnetic film, the large change in the resistance and strong supression for perpendicular magnetic field tell that this is a completely different effect and we believe this comes from the combination of Rashba and Dresselhaus SOI. As shown in Fig.1(b) however, the amplitude of the magnetoresistance grows rapidly with the bias voltage above the resonant value. This is not expected for a single resonant energy level and probably we need to consider the second level at a higher bias.

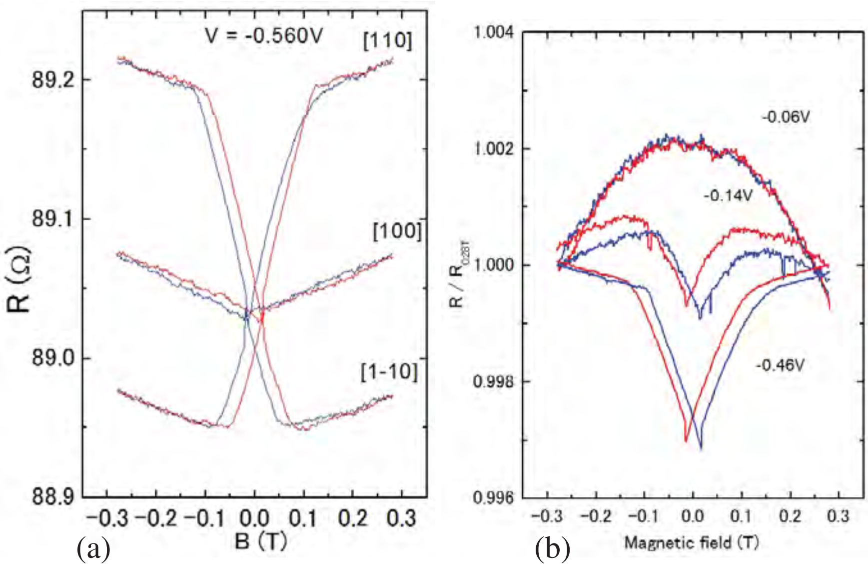

(a) (b)

Fig.1 (a) Magnetoresistance at 5 K. The growth axis is [001]. The blue lines are for down sweep of magnetic field while the red ones for up sweep. (b) Same as (a) for magnetic field along [110] for three representative bias voltages. A resonance exists around -0.12 V.

[1] I. Appelbaum, B. Huang and D. J. Monsma, Nature **447**, 295 (2007).
[2] T. Koga *et al.*, Phys. Rev. Lett. **88**, 126601 (2002).

[1]Also in Department of Physics, Beijing University, Beijing, China.

Evaluation of spin orbit interaction by weak anti-localization measurement in copper nitride system

Ryoto Enoki[1], Hiromu Gamo[1], Shutaro Karube[1,2], Makoto Kohda[1,2], Yoji Kunihashi[3], Haruki Sanada[3] and Junsaku Nitta [1,2]

[1] *Material Science and engineering, Tohoku, University, Sendai 980-8579, Japan*
[2] *Center for Spintronics Research Network, Tohoku University, 980-8577, Japan*
[3] *NTT Basic Research Laboratory, Atsugi 243-0198, Japan*

It is well known that Cu is material with very weak spin orbit interaction (SOI). However, it has been recently reported that SOI in Cu is enhanced by oxidation or impurity doping [1, 2]. In this research, we doped nitrogen impurities to Cu thin films and demonstrated the enhancement of SOI in N doped Cu by comparison to the non-doped Cu. This approach can provide further comprehension of enhancement of SOI by impurities doping in weak SOI materials. In addition, this is industrially more profitable method as enhancement of SOI due to the cheapness of Cu and N.

Both pure Cu (9 nm) and CuN (9.5 nm) thin films were deposited on SiO_2 substrate by RF sputtering machine. Substrate temperature during sputtering in Cu and CuN was RT and 100°C[3] respectively. CuN films were sputtered by varying N_2 gas pressure between 0.03 and 0.1 Pa during the sputtering.

To evaluate spin relaxation lengthL_{so}, we focused on quantum correction of the magneto conductance (MC). The results of MCs were fitted by Hikami-Larkin-Nagaoka formula [4].

Experimental MC results for pure Cu and CuN are shown in Fig. 1 (a) and (b), respectively. In Fig. 1(a), positive MC observed for pure Cu 9 nm film represents weak SOI. On the other hand, negative MC signals (*i.e.* weak-anti localization (WAL)) are observed in all CuN thin films. The magnetic field region showing WAL is enlarged by increasing the N_2 partial pressure. This transition from positive to negative MCs shown in Fig. 1 directly indicates the enhancement of SOI by doping N impurities to Cu thin films.

In order to realize the more quantitative analysis, the relationship between L_{so} and N_2 pressure during sputtering is shown in Fig. 2. From this figure, L_{so} becomes 20 times shorter than minimum value of that in pure Cu films. We have demonstrated that the strength of SOI in CuN can be tuned by controlling partial N_2 pressure during sputtering.

[1] Hongyu An *et al.*, Nat. Commun. **7,** 13069 (2016).
[2] Y. Niimi *et al.*, Phys. Rev. Lett. **109**, 156602 (2012).
[3] T. Nosaka *et al.*, Thin. Solid. Films. **348**, 8 (1999).
[4] S. Hikami *et al.*, Prog. Theor. Phys. **63**, 707 (1980).

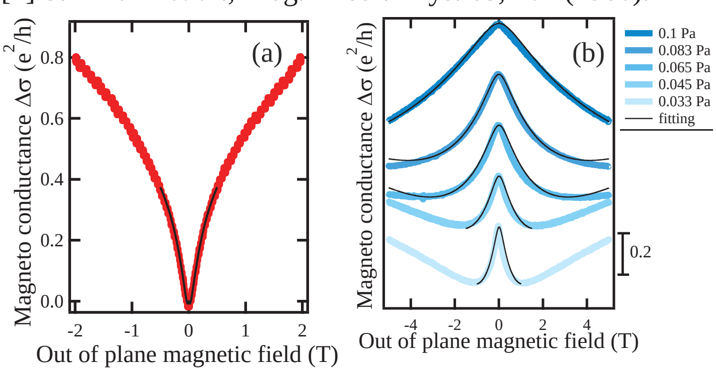

Fig. 1. MC of (a) pure Cu (9 nm) and (b) CuN (9.5 nm) respectively at 2K.

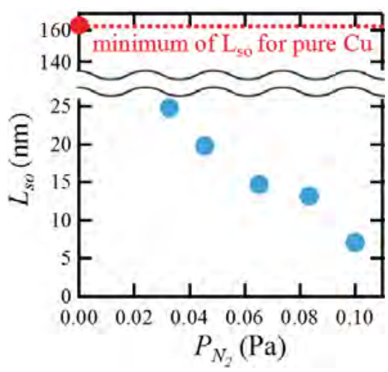

Fig. 2. The relationship between spin relaxation length and N_2 partial pressure during sputtering.

Spin-current induced mechanical torque in a chiral molecular junction

Naoki Sasao , Hiroki Okada, and Yasuhiro Utsumi

Department of Physics Engineering, Mie University, Tsu, Mie, 514-8507, Japan

Recently, the chiral induced spin selectivity effect (CISS) in molecular junctions has attracted much attention [1,2,3]. Unpolarized electron spins injected from a source electrode to a chiral molecule get spin-polarized during the propagation and emitted to a drain electrode [3]. The CISS effect is considered to be the consequence of the spin–orbit interaction (SOI) and the spin-filter effect has been observed in the double-strand DNA (dsDNA) [2,3]. On the other hand, it is known that the mechanical angular momentum and the spin angular momentum are mutually converted. For magnetic materials, such a conversion effect, the gyromagnetic effect, has been theoretically studied recently [4]. In the chiral molecular junction, we expect that the spin current can be converted into the mechanical torque, which induces the quantized mechanical motion [5]. However, such effects have not investigated yet even theoretically for molecular junctions.

We consider the single-stranded DNA (ssDNA) connected to the source drain lead [Inset of Fig. 1(b)]. We adopt a modified tight binding model [Fig. 1 (a)], in which the SOI is accounted for by the Aharonov-Casher phase [6]. We derive the spin continuity equation in the presence of the SOI, which connects the spin current and the mechanical torque acting on the ssDNA. When a spin-polarized electron is injected from the source lead, the spin current is transformed into the mechanical torque via the SOI. Figure 1(b) is the energy dependence of the mechanical torque T for various length n, the number of sites of the ssDNA. The magnitude of the mechanical torque periodically varies depending on the number of sites n [Fig. 1(c)]. We found that the period of the oscillations is shorter than the size of the unit cell, which is N=10 in our calculations. It is due to a finite pitch h, which causes a special dependence of the direction of the effective magnetic field; It induces an additional rotation when the spin passes through the unit cell.

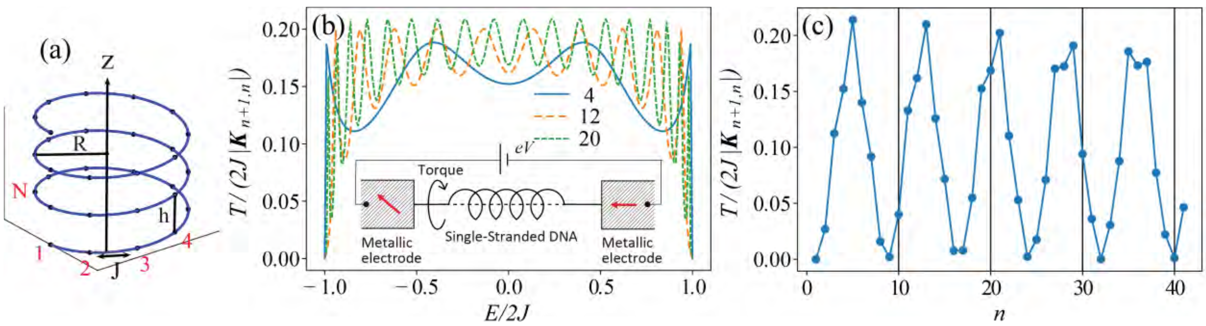

Fig.1 : Schematic picture of the ssDNA (a) and the chiral molecurlar junction [Inset of Fig. 1 (b)]. The ssDNA can rotate aroud the helical axis due to the mechanical torque. The hopping amplitude between the nearest neghabour sites is J. The number of sites per unit cell is N=10. The radius R=10 [Å] and pitch h=0.34 [nm]. (b) The energy dependence of the mechanical torque for n=4 (solid line), 12 (dashed line), and 20 (dotted line). The strength of the SOI is $|K_{n+1,n}|$=0.1. (c) The size dependence of the mechanical torque for an electron with the energy E=0.

[1] K. Michaeli, N. Kantor-Uriel, R. Naaman and D. H. Waldeck, Chem. Soc. Rev., **45**, 6478-6487 (2016)
[2] B.Göhler, V. Hamelbeck, T. Z.Markus,M. Kettner, G. F. Hanne, Z.Vager, R. Naaman, and H. Zacharias, Science **331**, 894 (2011)
[3] Z. Xie, T. Z. Markus, S. R. Cohen, Z. Vager, R. Gutierrez, R. Naaman,Nano Lett. 2011**, 11,** 4652-4655
[4] M. Matsuo, E. Saitoh, and S. Maekawa, Journal of the Physical Society of Japan **86**, 011011 (2017)
[5] A. A. Kovalev, L. X. Hayden, G. E.W. Bauer, and Y. Tserkovnyak, PRL **106**, 147203 (2011)
[6] S. Matityahu, Y. Utsumi, A. Aharony, O. Entin-Wohlman, C. A. Balseiro, Phys. Rev. B **93**, 075407 (2016)

Spin-orbit semimetal $SrIrO_3$ in the two-dimensional limit

D. J. Groenendijk[1], C. Autieri[2], J. Girovsky[1], M. Carmen Martinez-Velarte[1], N. Manca[1], G. Mattoni[1], A. M. R. V. L. Monteiro[1], N. Gauquelin[3], J. Verbeeck[3], A. F. Otte[1], M. Gabay[4], S. Picozzi[2], and A. D. Caviglia[1]

[1]*Kavli Institute of Nanoscience, Delft University of Technology, Delft, Netherlands*
[2]*Consiglio Nazionale delle Ricerche CNR-SPIN, UOS L'Aquila, Chieti, Italy*
[3]*Electron Microscopy for Materials Science (EMAT), University of Antwerp, Belgium*
[4]*Laboratoire de Physique des Solides, Université Paris-Sud, France*

By tuning the thickness of complex oxide films on a single unit cell level, it is possible to tailor the delicate balance between competing energy scales and trigger phase transitions. In this work [1], we investigate the 5d oxide $SrIrO_3$ which, in the three-dimensional limit, is a narrow-band semimetal at the borderline of a Mott transition due to a combination of strong spin-orbit coupling and electron correlations [2]. We find that a semimetal-insulator transition occurs at a film thickness between 3 and 4 unit cells and study the evolution of the electronic structure across the transition by (magneto)transport and scanning tunneling spectroscopy (STS). The paramagnetic susceptibility is found to be strongly enhanced while approaching the transition point, which is indicative of the opening of a Mott gap and the concomitant enhancement of magnetic order. Our results are corroborated by first-principles density functional theory (DFT) calculations, which reproduce the critical thickness of the transition and show that the insulating state in the two-dimensional limit is antiferromagnetically ordered. Our study provides crucial insights into the electronic and magnetic properties of ultrathin $SrIrO_3$ and shows its potential as a novel platform for engineering the interplay of magnetism and spin-orbit coupling at oxide interfaces.

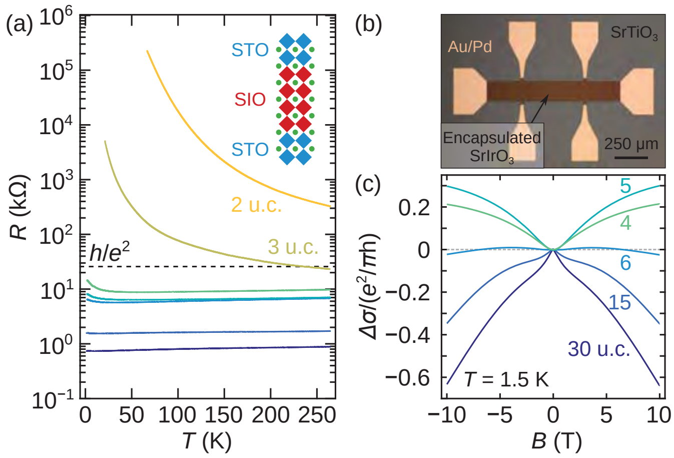

Figure 1: (a) Resistance (R) versus temperature (T) measurements of $SrIrO_3$ films of different thicknesses (b) Optical image of a Hall bar used for (magneto)transport measurements. (c) Out-of-plane magnetoconductance ($\Delta\sigma$) measured at 1.5 K.

[1] D. J. Groenendijk, C. Autieri, J. Girovsky, M. Carmen Martinez-Velarte, N. Manca, G. Mattoni, A. M. R. V. L. Monteiro, N. Gauquelin, A. F. Otte, M. Gabay, S. Picozzi, and A. D. Caviglia, arXiv preprint arXiv:1706.08901 (2017).

[2] Y. F. Nie, P. D. C. King, C. H. Kim, M. Uchida, H. I. Wei, B. D. Faeth, J. P. Ruf, J. P. C. Ruff, L. Xie, X. Pan, C. J. Fennie, D. G. Schlom, and K. M. Shen, *Phys. Rev. Lett.* **114**, (2015).

Strain-induced Dirac state shift in topological insulator Bi_2Se_3 nanowires

C. Schindler[1], C. Wiegand[2], J. Sichau[1], L. Tiemann[1], K. Nielsch[2], R. Zierold[1], R. Blick[1]

[1] *Center for Hybrid Nanostructures, University of Hamburg, 22607 Hamburg, Germany*
[2] *Insitute for Metallic Materials, IFW Dresden, 01069 Dresden, Germany*

Topological insulators (TIs) have been subject of extensive research in recent years due to the possibility to study relativistic particles in solid-state matter as well as potential application in a broad range of future electronic and spintronic devices. In this study, we performed magneto-transport experiments on single-crystalline bismuth selenide (Bi_2Se_3) nanowires, one of the earliest TI materials that has shown to exhibit a well-defined Dirac cone on the surface [1]. Our Bi_2Se_3 nanowires are mechanically modulated in order to investigate the possibility to tune Dirac states by strain. The concept of strain-engineering was predicted theoretically [2] and has been demonstrated on internally strained grain boundaries in MBE-grown films, either by tunneling experiments [3] or optical methods [4]. However, to our best knowledge it has never been confirmed by magneto-transport measurements on externally strained TI devices.

Our Bi_2Se_3-nanowires have been grown by Vapor-Liquid-Solid (VLS) growth and were placed over 200 nm-deep trenches that were etched into a SiO_2 substrate. As the devices are less than 80 nm in height, their elasticity leads to a significant bending, which results in tensile strain at the bottom surface of the wire and compressive strain at its top surface. We have confirmed the bending of our wires by a standard AFM technique. For a magnetic field perpendicular to the electric current direction along the wire, we observe Shubnikov-de-Haas (SdH) oscillations that are superimposed to a parabolic magneto-resistance as well as a weak antilocalization peak. By applying a multi-frequency Lifshitz-Kosevich model, we can identify bulk and surface bands. Surfaces under compressive or tensile strain ($\varepsilon = \pm 0.1\%$) experience a significant Dirac shift of $\Delta E = \pm 30$ meV as compared to relaxed surface states. For surface states under tensile strain we also observe an increased carrier mobility. The opportunity to externally tune the Dirac states therefore could lead to further improvement in future TI devices.

References

[1] J. G. Analytis *et al.* Two-dimensional surface state in the quantum limit of a topological insulator. *Nature Phys.* **6**(12), 960 (2010).
[2] S. M Young *et al.* Theoretical investigation of the evolution of the topological phase of Bi_2Se_3 under mechanical strain. *Phys. Rev. B - Condensed Matter and Materials Physics* **84**(8), 2–5 (2011).
[3] Y. Liu *et al.* Tuning Dirac states by strain in the topological insulator Bi_2Se_3. *Nature Physics* **10**, 1–6 (2014).
[4] T.-H Kim *et al.* Tuning the Fermi level with topological phase transition by internal strain in a topological insulator Bi2Se3 thin film. *Nanoscale* **8**(2), 741–51 (2016).

Disorder-induced dephasing in backscattering-free quantum transport

Clemens Gneiting[1], **Franco Nori**[1,2]

[1] *Quantum Condensed Matter Research Group, RIKEN, Saitama 351-0198, Japan*
[2] *Department of Physics, University of Michigan, Ann Arbor, Michigan 48109-1040, USA*

The possibility of backscattering-free transport in topological insulators renders them promising candidates for applications in quantum information processing, where reliable transmittance of quantum states is a prerequsite for successful implementations. However, even though edge states are robust against backscattering, they are not immune to disorder effects when it comes to dephasing, as described by a disorder-induced deformation of states. This poses a potential obstacle to their successful deployment as carriers of quantum information. Here, we present our analysis of such disorder-induced dephasing. Employing a quantum master equation description, we are able to quantify the time evolution of disorder-perturbed edge mode states. Based on this, we can show that the disorder-induced dephasing remains bound. Moreover, we identify a gap condition to remain in the backscattering-free regime between the bulk bands.

[1] C. Gneiting, F. Nori, Phys. Rev. A **96**, 022135 (2017).
[2] C. Gneiting, F. Nori, arXiv:1705.08177.

Probing helicity and the topological origins of helicity via non-local Hanbury-Brown and Twiss correlations

A. Mani [1], **C. Benjamin** [1]

[1] *School of Physical Sciences, National Institute of Science Education & Research, HBNI, Jatni-752050, India.*

Quantum Hall edge modes are chiral while quantum spin Hall edge modes are helical. However, unlike chiral edge modes which always occur in topological systems, Helical edge modes may arise in a trivial insulator too. These trivial Helical edge modes are not topologically protected and therefore need to be distinguished from Helical edge modes arising due to topological reasons. Earlier conductance measurements were used to identify these helical states, in this work we report on the advantage of using the non local shot noise as a probe for the helical nature of these states as well as to reveal their topological or otherwise origin and compare them with the chiral quantum Hall states. We see that in similar set-ups affected by same degree of disorder and inelastic scattering, non local shot noise "HBT“ correlations can be positive for helical edge modes but are always negative for the chiral quantum Hall edge modes. Further, while trivial Helical edge modes exhibit negative non-local ”HBT” charge correlations, topological Helical edge modes can show positive non-local "HBT“ charge correlation. We also study the non-local spin correlations and Fano factor for clues as regards both the distinction between chirality/helicity as well as the topological/trivial dichotomy for Helical edge modes.

[1] Arjun Mani & Colin Benjamin, Probing helicity and the topological origins of helicity via non-local Hanbury-Brown and Twiss correlations, SCIENTIFIC REPORTS, 7: 6954 (2017).

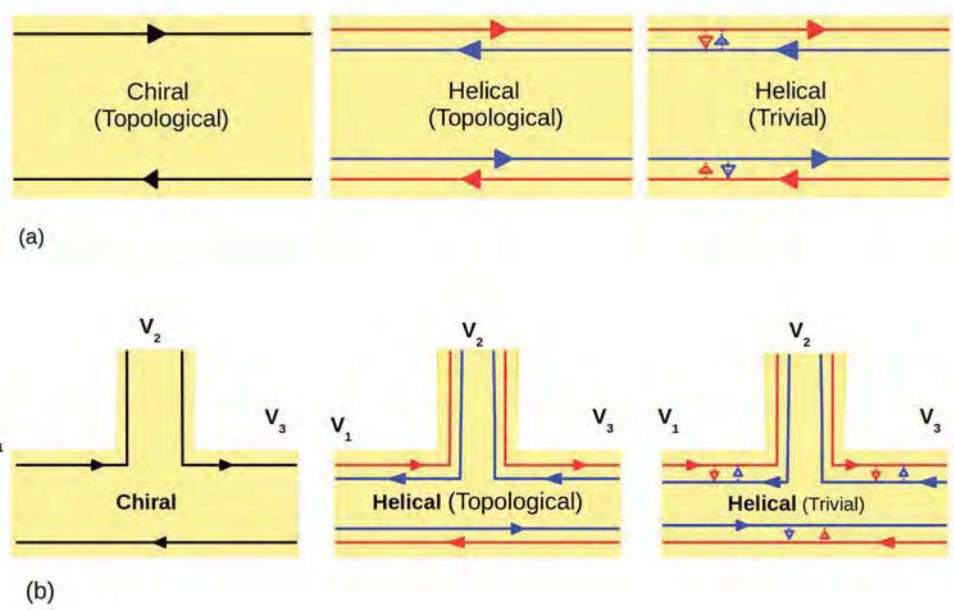

Figure 1. (a) Chiral vs Helical (Topological) vs quasi-Helical (Trivial), (b) 3-terminal QH, QSH(topological) and QSH(trivial) bar.

Topological classification of single-wall carbon nanotubes

R. Okuyama[1], W. Izumida[2], and M. Eto[1]

[1] *Faculty of Science and Technology, Keio University, Yokohama 223-8522, Japan*
[2] *Department of Physics, Tohoku University, Sendai 980-8578, Japan*

The single-wall carbon nanotube (SWNT) is a unique one-dimensional (1D) system made by rolling up graphene sheet. It can be either metallic or semiconducting depending on its chirality. Even for a metallic SWNT, a narrow energy gap opens between the conduction and valence bands due to the mixing of σ and π orbitals by the finite curvature of tube surface and spin-orbit interaction. The narrow energy gap is tunable by a magnetic field in the axial direction; it is closed at a feasible field strength of $B \sim 1 - 10$ T.

Both metallic and semiconducting SWNTs can be regarded as 1D topological insulators owing to the sublattice symmetry for A and B lattice sites [1]. The electronic states are characterized by a $\mathbb{Z}$ topological invariant, winding number, in both the absence (class BDI) and presence (AIII) of magnetic field. The winding number is related to the number of edge states localized in the tube ends via the bulk-edge correspondence. We have shown that some chiralities of semiconducting [1] and metallic [2] SWNTs are topologically non-trivial. For the metallic SWNT, the winding number is abruptly changed when the narrow energy gap is closed by applying a magnetic field. This topological phase transition can be observed as a change in the number of edge states.

In the present study, we classify all possible chiralities of SWNTs by means of topology. The winding number is analytically evaluated by using a 1D lattice model [2], which effectively describes curvature effects and spin-orbit interaction [3]. The results are summarized in the figure, where a hexagon from the leftmost hexagon indicates the chiral vector (circumference of tube), $\boldsymbol{C}_\mathrm{h} = n\boldsymbol{a}_1 + m\boldsymbol{a}_2$. d_t is the diameter. We find that the majority of SWNTs, denoted by pink and white hexagons, are topologically non-trivial as explained below.

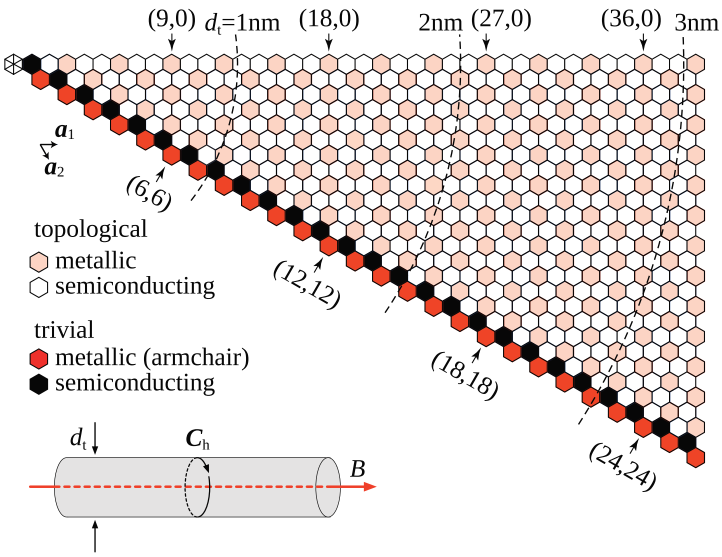

A SWNT is metallic when $n \equiv m \pmod 3$. We show that all metallic SWNTs except for $n = m$ (armchair type) are topologically non-trivial. Furthermore, the topological phase transition always occurs when the energy gap is closed by applying the magnetic field. On the other hand, armchair SWNTs are topologically trivial regardless of the magnetic field.

SWNTs are semiconducting when $n \not\equiv m \pmod 3$. They are topologically non-trivial except for $|n - m| = 1$.

[1] W. Izumida, R. Okuyama, A. Yamakage, and R. Saito, Phys. Rev. B **93**, 195442 (2016).
[2] R. Okuyama, W. Izumida, and M. Eto, J. Phys. Soc. Jpn **86**, 013702 (2017).
[3] W. Izumida, K. Sato, and R. Saito, J. Phys. Soc. Jpn **78**, 074707 (2009).

Conduction impedance effects in atomically thin materials

N.J. Townsend[1], I. Amit[1], T.J. Octon[1], J.D. Mehew[1], F. Reale[2], C. Mattevi[2], C.D. Wright[1], M.F. Craciun[1] & S. Russo[1]

[1] *College of Engineering, Mathematics and Physical Sciences, University of Exeter, Exeter, EX4 4QL, UK*
[2] *Department of Materials, Imperial College London, London, SW7 2AZ, UK*

The rise of 2D based technology has paved the way to numerous exciting applications in electronics, photovoltaics and sensing. Atomically thin $MoTe_2$ is one of the best candidates to replace bulk semiconductors in transistor-based devices, where added functionality (e.g., mechanical flexibility) is required. For optimal functionality, the complete picture of the charge transport mechanisms through the device needs to be fully understood.
In this work, we present experimental evidence for the formation of Schottky barriers as low as 10meV between $MoTe_2$ and metal electrodes at cryogenic temperatures. By varying the electrode work functions, we demonstrate that Fermi level pinning due to metal induced gap states at the interfaces occurs at 0.14eV above the valence band maximum. This is the first experimental observation of thermionic emission at temperatures as low as 40K, which is unexpected due to tunnelling usually being the dominant effect at these temperatures. However, as the thermal width of the Fermi-Dirac distribution is comparable with our measured barrier heights, thermionic emission is likely to be the dominant mechanism.[1]
A further investigation reveals a novel transport effect, dubbed threshold voltage transient effect, which is manifested in the hysteresis in the transfer curves. By probing the transient currents measured during cycles of pulses through the gate electrode, we are able to distinguish between our novel model for charge trapping dynamics and other transport phenomena, showing that the time-dependent change in threshold voltage is the dominant effect on observed hysteretic behaviour.[2]

[1] N.J. Townsend, I. Amit, M.F. Craciun & S.Russo “Ultra-low Schottky barriers in MoTe2” ***submitted***.
[2] I. Amit, T.J. Octon, N.J. Townsend, F. Reale, C.D. Wright, C. Mattevi, M.F. Craciun & S. Russo Adv. Mater. **29,** 1605598 (2017).

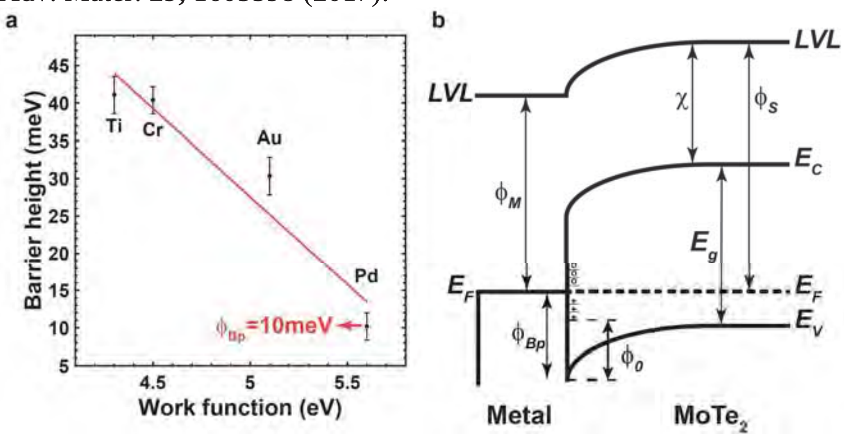

Figure 1: **a** The measured Schottky barrier heights comparing all the measured devices. The linear fit indicates strong pinning of the Fermi level due to the presence of mid-gap states. **b** Schematic energy band diagram of the metal/*p*-type semiconductor interface showing band bending of the conduction band edge, E_C, the valence band edge E_V and the local vacuum level *LVL* when the Fermi levels E_F are aligned and the system is in thermal equilibrium.

Electronic Properties of Laser-Patterned 2H/1T′ Interface in Exfoliated Multilayer $MoTe_2$

Kohei Sakanashi[1], Kota Kamiya[1], Hidemasu Ouchi[1], Tomoki Yamanaka[1], Peter Krueger[1], Katsuhiko Miyamoto[1], Takashige Omatsu[1], Jonathan P. Bird[2], and Nobuyuki Aoki[1]

[1] *Department of Materials Science,Chiba University,Chiba 263-8522,Japan*
[2] *Department of Electrical Engineering, University at Buffalo, SUNY, Bufflo, New York 14260-1920, USA*

These days, the transition metal dichalcogenides (TMDs) is receiving the large attention because of its rich physical properties such as polymorphism, valley degeneracy and more. Among them, the polymorphism has been expected to apply for realizing the future monolithic electronic devices. In recent report [1], it was shown that the few-layerd $MoTe_2$ crystal exhibits the structural phase transition from semiconducting 2H phase to metallic 1T′ phase by applying the strain especially laser irradiation. And then the interface of 2H/1T′ shows Ohmic homojunction. However, $MoTe_2$ shows not only n- or p-type but also ambipolar property. It is unclear whether the interface of two phases always becomes Ohmic contact, or not.

In this study, we used a green color laser light of 58 mW/μm^2 and wrote lines on an exfoliated multilayer $MoTe_2$ crystal as shown in Fig.1. And then we confirmed the phase transition form 2H to 1T′ phase by Raman spectroscopy as shown in Fig.2. We also evaluate the contact property at the interface of 2H/1T′ phases via trasnport measurement and Scanning Gate Microscopy which uses the Atomic Force Microscope tip as a local gate electrode. This technique is used to visualize an existence of local barrier formation in Field Effect Transistor cannel[2].

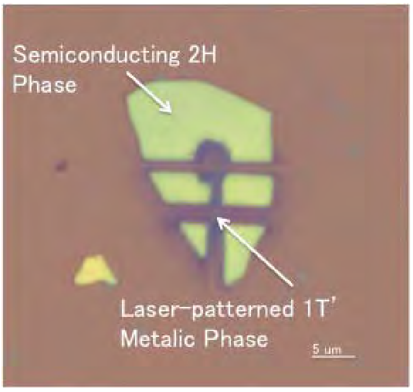

Figure 1: Laser-patterned $MoTe_2$ crystal

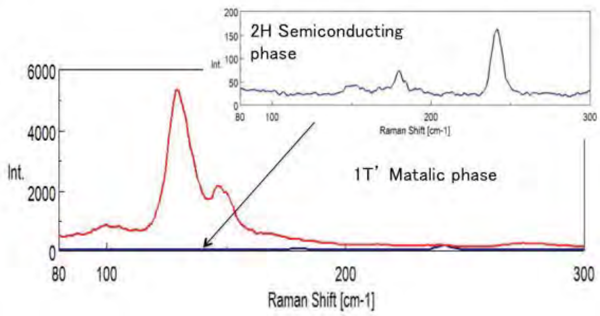

Figure 2: Raman spectrum of 2H and 1T′ phase

[1] S. Cho *et al*, Scinece, **349**, 6248,625 (2015).
[2] M. Matsunaga *et al*, ACS Nano, **10**, 9730-1-8 (2016).

Influence of metal contacts on metal-insulator transition in molybdenum disulfide field effect transistors

Tatsuya Iwabuchi, Kensuke Arai and Yoshihiro Shimazu

Department of Physics, Yokohama National University, Yokohama 240-8501, Japan

Transition metal dichalcogenides are promising layered materials for realizing novel nanoelectronic and nano-optoelectronic devices. Molybdenum disulfide (MoS_2), a typical transition metal dichalcogenide, has been extensively investigated partly due to the presence of a sizable band gap, which enables the use of MoS_2 as a channel material in field-effect transistors (FET). The gate-voltage-tunable metal–insulator transition and superconductivity using MoS_2 have been demonstrated in previous studies. These interesting phenomena can be considered as quantum phase transitions in two-dimensional systems. The dependence of the transport properties on the contact metal has rarely been investigated. We studied the transport properties of multilayer MoS_2 flakes with Ti/Au and Al contacts in a FET geometry from room temperature to 13 K. We found that the temperature dependences of the sheet resistance, relevant to the MIT, are different for the devices with the two types of contacts. While the back-gated FETs with Ti/Au contacts were insulating at low temperatures [1] for all the values of the gate voltage used in this study, the MIT at low temperatures was observed in the FETs with Al contacts. It was also found that the threshold voltage for FET switching was considerably lower for the devices with Al contacts. These results indicate the significant influence of the Al contacts on the properties of MoS_2 devices, and are explained by the assumption that the Al contacts induce higher carrier density in MoS_2 flakes. The higher carrier density in the Al-contacted device may possibly be caused by electron transfer from Al to MoS_2, which is expected on the basis of the work functions of Al (4.54 eV) and Au (5.40 eV). We will also report Raman spectra measured for the devices with Ti/Au and Al contacts.

[1] B. Radisavljevic and A. Kis, Nat. Mater. **12**, 815 (2013).

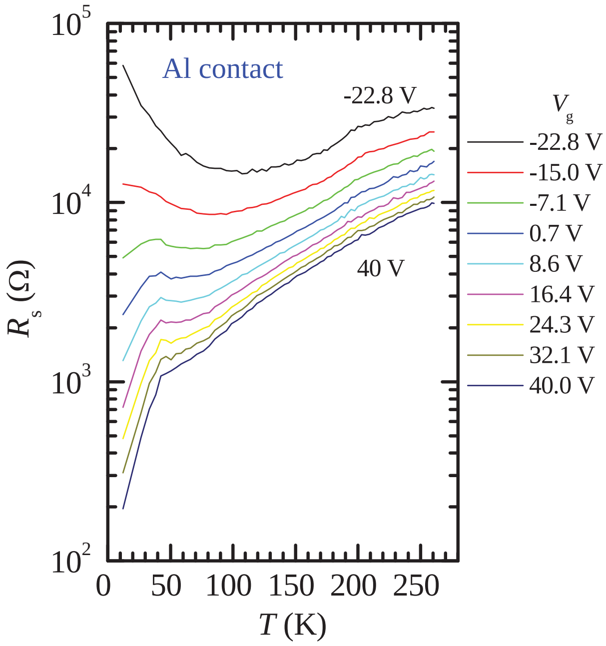

Fig. 1. Sheet resistance R_s of a FET using a multilayer MoS_2 flake (thickness ~16 nm) with Al contacts as a function of temperature for various values of back-gate voltage V_g. The resistance decreases with increasing V_g at all the temperatures. MIT is observed at low temperatures with the critical resistance of ~10 kΩ. For the Ti/Au-contacted device, the insulating behavior was observed at low temperatures for all the values of V_g, while MIT-like behavior was observed near room temperature.

A Simulation of Two-Dimensional Crystal Heterostructure Solar Cells Quantum Efficiency

Parham Pashaei[1,2], Graham Allegretto[1], Peyman Servati[1]

[1] *Department of Electrical and Computer Engineering, University of British Columbia, Vancouver, V6T 1Z4 Canada*
[2] *Quantum Matter Institute, University of British Columbia, Vancouver, British Columbia V6T 1Z4, Canada*

Two-dimensional atomically thin crystals have recently raised significant interest for optoelectronic and photovoltaic studies [1,2]. In this report, we have studied the potentials of two-dimensional (2D) materials for solar cell applications with a theoretical simulation. A background review of 2D materials and current 2D-based solar cells is given and promising structures of this new category of solar cells are summarized and investigated. The structures are simulated using experimental absorption data of individual monolayers found in literature and their external quantum efficiency (EQE) is estimated. As an example, our simulations matching with experiments within a reasonable approximation is shown. For a multilayer solar cell, the simulations suggest up to 36.68% EQE for 10 p-n stacks. The results presented in this study show the promising potential of 2D material-based solar cells as well as providing a platform for future experiments.

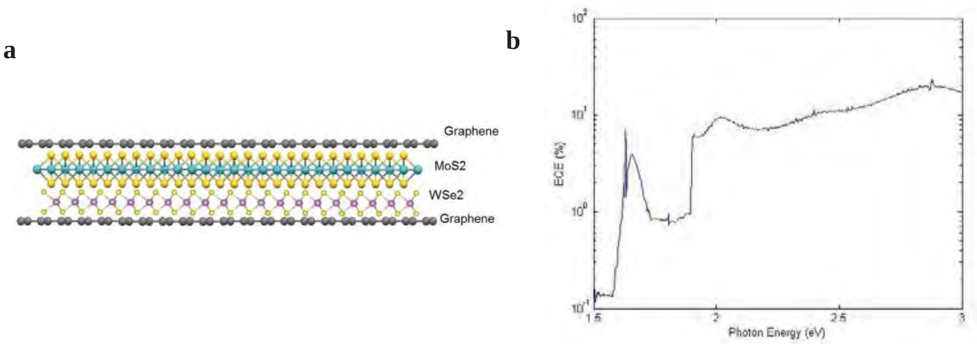

Fig.1. External quantum efficiency simulation results for a 2layer-2layer graphene-WSe2-MoS2-graphene heterostructure. (a) Cross-section image of the structure (b) simulation results.

[1] Bernardi, M.; Palummo, M.; Grossman, J. C. Extraordinary Sunlight Absorption and One Nanometer Thick Photovoltaics Using Two-Dimensional Monolayer Materials. Nano Lett. 2013, 13, 3664− 3670.
[2] Furchi MM, Pospischil A, Libisch F, Burgdörfer J, Mueller T. Photovoltaic effect in an electrically tunable van der Waals heterojunction. Nano letters. 2014, 14(8): 4785-91.

Enhanced optical activity of atomically thin $MoSe_2$ proximal to nanoscale plasmonic slot-waveguides

M. Blauth, G. Mélen, M. Prechtl, O. Hartwig, J. Harms, M. Kaniber, and J. J. Finley

Walter Schottky Institut and Physik Department, Technische Universität München, Am Coulombwall 4, 85748 Garching, Germany

Atomically thin, two-dimensional semiconductors have recently attracted strong interest, both in the fields of nano-optics and nano-electronics [1]. Combining these materials with nano-plasmonic waveguides opens the way to build integrable plasmonic light sources [2] and detectors with subwavelength footprints.

In this contribution we present numerical simulations and experimental studies of the coupling of monolayer $MoSe_2$ crystals to proximal plasmonic waveguides. Detailed numerical studies on plasmonic waveguides demonstrate the presence of guided plasmonic modes confined within nanometer regions at the surface of the waveguides, yielding a transverse mode volume of down to 0.02 λ^2. Low temperature confocal spectroscopy reveals the appearance of emission between 1.55eV and 1.61eV, redshifted from the $MoSe_2$ exciton and trion emission [3]. We find degrees of polarization of up to 40%, which are in good agreement with spontaneous emission calculations that indicate radiation from the $MoSe_2$ into the supported plasmonic modes. As evidence for coupling of the emission into these modes, we present optical propagation length measurements revealing L_{SPP} = (380±60)nm, thereby, proving the plasmonic character of the observed luminescence [4]. By electrically contacting the plasmonic waveguides we perform photocurrent measurements on the $MoSe_2$ - plasmonic hybrid system. Excitation energy dependence of the photocurrent shows peaks at 1.67eV and 1.85eV corresponding to the A and B exciton resonance, respectively. We further show that excitation power density dependent photocurrent exhibits pronounced non-linearities for extraction fields exceeding 100kV/cm. This could be exploited in future ultra-fast pump-probe spectroscopy, yielding new insight into the photocurrent dynamics of this hybrid system.

[1] K. Mak et al. Phys. Rev. Lett. 105, 136805 (2010).
[2] K. Huang et al. Nat. Photon 8, 244 (2014).
[3] A. Branny et al. Appl. Phys. Lett. 108, 142101 (2016).
[4] M. Blauth et al. 2D Mater. 4, 21011 (2017).

Engineering coherent color centers in two dimensional materials

Hou Songyan[1,2], Muhammad Danang Birowosuto[1], Umar Saleem[1,2], Teo Hang Tong Edwin[1,2], Wang Hong[1,2]

[1] *CINTRA UMI CNRS/NTU/THALES 3288, Research Techno Plaza, 50 Nanyang Drive, Border X Block, Level 6, Singapore 637553, Singapore*

[2] *School of Electrical and Electronic Engineering, Nanyang Technological University, 50 Nanyang Avenue, 639798, Singapore*

Email: hous0002@e.ntu.edu.sg

Unique optical properties of two-dimensional (2D) semiconductors such as graphene, transition metal dichalcogenides (TMDCs), and boron nitride have attracted considerable attention. Among all potential electronics device, photoelectrical properties of 2D hexagonal boron nitride (hBN) are of great importance due to its wide bandgap, in which optically localized active defects can act as SPEs. Despite that SPEs have been found recently in hBN after annealing and electron irradiation[1][2], there is an urgent need but it is still a significant challenge to engineer SPEs in hBN.

For the purpose of commercial applications, it is significant to generate color centers at desired locations to be matched with other electronical components. Laser writing is now widely used owing to its flexibility to control the energy and position. Laser irradiation is also used to create color centers in cBN crystal and diamond, although the emission is very weak with broad peaks.

Here, we find bright color centers in hBN can be engineered with laser writing technology and abbreviation of surface during laser writing processing provides precise locations of color centers in hBN[3]. The color centers are confined around laser writing void and sharp emission with a full width at half-maximum (FWHM) around 1 nm is also found from irradiated area. The emission is well polarized with dipole characteristics and SPEs are also found from color centers. Our findings suggest the potential applications of laser writing as an efficient tool to engineer color centers in quantum communications.

[1] T. T. Tran, K. Bray, M.l J. Ford, M. Toth, I. Aharonovich, Nat. nano. **11**, 37 (2016).

[2] T. T. Tran, C. Elbadawi, D. Totonjian, C. J. Lobo, G. Grosso, H. Moon, D. R. Englund, M. J. Ford, I. Aharonovich, M. Toth, ACS Nano **10**, 7331 (2016).

[3] S.Y. Hou, M.D. Birowosuto et al. submitted (2017)

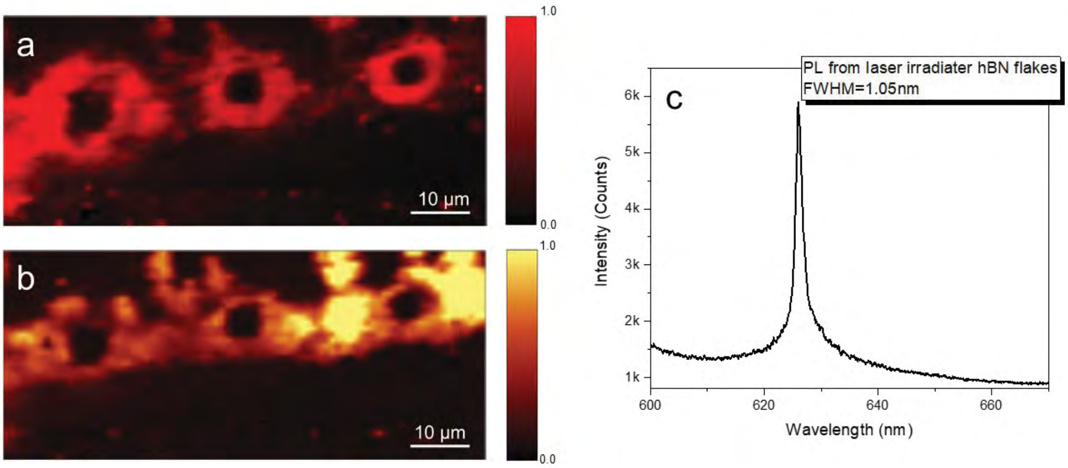

Generation of color centers from hBN flakes after laser writing process. a, PL mapping (628 nm) of hBN flakes, indicating the generation of bright color centers after laser writing process. b, hBN Raman peak (1370 rel/cm) mapping, indicating the residual of hBN flakes after laser writing process. c, PL spectra with narrow width from laser irradiated region.

Ultrafast all optical modulation in graphene-loaded plasmonic waveguides

Masanori Hata [1,2], **Masaaki Ono** [2,3], **Hisashi Sumikura** [2,3], **Kengo Nozaki** [2,3], **Eiichi Kuramochi** [2,3], **Masaya Notomi** [1,2,3]

[1] *Department of Physics, Tokyo Institute of Technology*
[2] *NTT Basic Research Labs*
[3] *NTT Nanophotonics Center*

Graphene has great potential in photonics and optoelectronics applications owing to its unique optical and electronic properties. Recently, graphene-based optical modulators have been actively investigated [1,2]. However, light-matter interactions in conventional graphene-based photonic devices are relatively small due to single-atom thickness of graphene, and it sets limit on modulation depth or device size.

Here we report compact, ultrafast graphene-plasmonic all-optical modulator based on saturable absorption of graphene. In order to enhance light-matter interactions, we employed Metal-Insulator-Metal (MIM) plasmonic waveguides with subwavelength field confinement.

Fig.1a shows a schematic illustration of our device. The MIM consists of Au with an air slot, whose cross-section is 40 nm×50 nm. The tapered structure enables efficient mode conversion from a Si waveguide to a MIM waveguide [3]. MIM structures were fabricated on an SOI substrate by EB lithography technique and Au evaporation/liftoff process. We then transfer commercial CVD-grown graphene onto samples by wet transfer technique.

We measured optical transmission of 10μm long samples with a fiber pulse laser (1.7 ps, 1.55μm), and clearly observed saturable absorption of graphene at higher input power (Fig. 1b). We fitted this transmission curve using saturable absorption formula to estimate saturation power, and obtained 120 mW (corresponding pulse energy is 205 fJ). Next we conducted pump-probe experiment to measure the relaxation time of saturation. The pump and probe pulses were generated from the same laser source (1.7 ps, 1.55μm). The probe pulses were modulated by an acousto-optic modulator, and detected by a lock-in amplifier. Fig.1 c shows the pump-probe signal. The contrast between the signal peak and the tail reached 2.6 dB, and full-width at half maximum (FWHM) of 2.2 ps was obtained.

In summary, we have demonstrated graphene-plasmonic all optical modulator which has ultra-compact footprint, ultrasmall operation energy, and ultrafast response time. In the talk, we will also discuss cavity structure for further enhancement of light-matter interactions.

[1] M. Liu et al., Nature **474**, 64 (2011).
[2] W. Li et al., Nano. Lett. **14**, 955 (2014).
[3] M. Ono et al., Optica. **3**, 999 (2016).

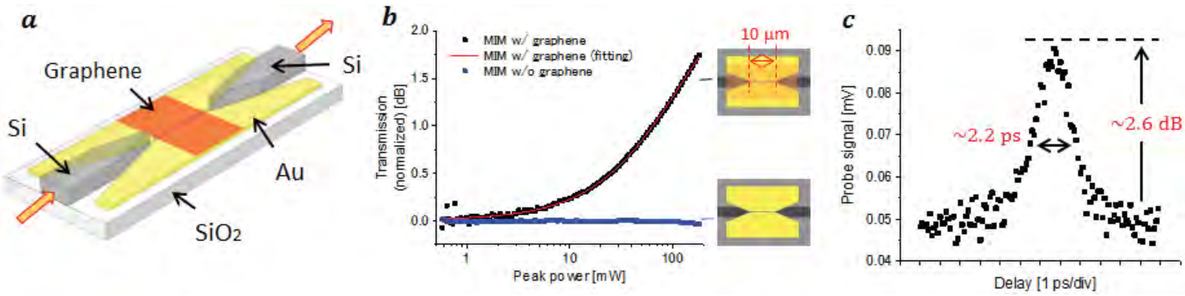

Figure (a) Schematic image of graphene-plasmonic optical modulator. (b) Transmission of a 10 μm long sample as a function of the peak power of input pulses. (c) Probe light signal as a function of pump-probe time delay with a pump energy of 155 fJ, probe energy of 0.56 fJ.

Excitation power dependence of nonequilibrium carrier relaxation dynamics in graphene

Y. Hasegawa[1,2], K. Oguri[1], K. Kato[1], T. Nishikawa[2] and H. Gotoh[1]

[1] *NTT Basic Research Laboratories, NTT Corporation*
[2] *Graduate School of Engineering, Tokyo Denki University*

Graphene is expected as material of the ultrafast optoelectronic devise. Recently, time-resolved spectroscopy in graphene has been carried out in order to investigate carrier relaxation process [1-3]. When graphene is irradiated with ultrafast pulse laser, photoexcited carrier relaxes by carrier-carrier scattering and carrier-phonon scattering. Although the relaxation process in picosecond range has been well studied, there are few reports on the relaxation process faster than tens of femtosecond order. Here, we measured excitation power dependence of transient reflectivity in graphene in order to further understand carrier relaxation process in 10s of femtosecond order.

Time-resolved differential reflectivity measurements were carried out with 10-fs Ti:sapphire oscillator at center wavelength of 780 nm [4]. The graphene sample was grown on SiO_2 substrate by chemical vaper deposition. This measurement is equivalent to observation of optical conductivity change of graphene [1].

The transient reflectivity of graphene at a pump power density of 20 μJ/cm^2 is shown in Fig. 1. A large negative reflectance change was observed at time zero. After, zero crossing occurred and positive reflectance change slowly relaxed. The initial negative reflectance suggests that the Pauli blocking effect suppresses the inter-band transition. On the other hand, the subsequent positive reflectance can be interpreted as absorption of additional free carriers induced by the intra-band transition. We identify that the data consists of negative single-exponential and positive bi-exponential decay. The origin of the relaxation most probably corresponds to carrier-carrier scattering (τ_1), carrier-phonon scattering (τ_2), and the slowdown of carrier cooling (τ_3) which is known as hot phonon effect [2]. Also, we measured the excitation power dependence of transient reflectivity at 20-100μJ/cm^2. When excitation power is increased, τ_3 increased from 851 fs to 1.51 ps and τ_2 decreased from 49 fs to 11 fs. The fact that τ_3 becomes longer can be explained by the enhancement of the hot phonon effect [2]. In addition, the excitation power dependence of τ_2 can be explained by intra-band phonon scattering efficiently occurs due to the increase of the photoexcited carrier. On the other hand, contrary to intuition, τ_1 becomes longer from 27 fs to 58 fs with the increase pump intensity. One possible reason for this result is the decrease in the energy difference between the initial nonequilibrium carrier distribution (t=0) to an equilibrium hot Fermi distribution with the increase in the excitation power [5]. We measured transient reflectivity in graphene. The experimental result clarifies the ultrafast relaxation process on the time tens of femtosecond in graphene.

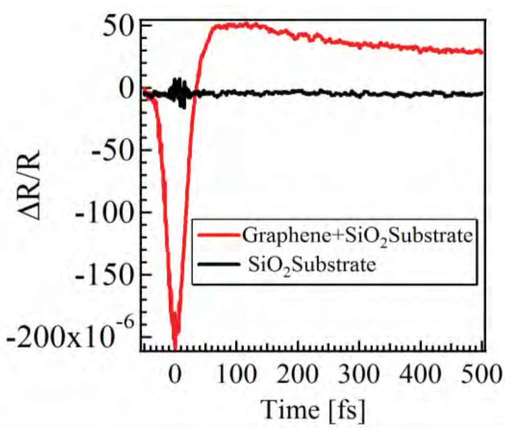

Fig. 1 Transient reflectivity of graphene at 20 μJ/cm^2.

This work was partially supported by JSPS KAKENHI Grant No. 16H02120.

[1] T. Li et al., Phys. Rev. Lett. **108**, 167401 (2012)
[2] B. Gao et al., Nano Lett. **11**, 3184 (2011)
[3] M. Breusing et al,. Phys. Rev. B **83**, 153410 (2011)
[4] K. Kato et al., J. Appl. Phys. 111, 113520 (2002)
[5] T. Winzer and E. Malic, J. Phys.: Condens. Matter **25**, 054201 (2013)

Modulating plasmons in graphene by substrate modification

Makoto Takamura, Norio Kumada, Shengnan Wang and Kazuhide Kumakura

NTT Basic Research Laboratories

Graphene plasmons offer unique possibilities for controlling light in nano-devices and for optoelectronics. One of the advantages of graphene plasmonics beyond noble metals is the capability to control plasmonic properties, which has been achieved by using electric doping to vary the carrier density in graphene [1]. Chemical doping is another promising approach, which will be applicable to plasmon waveguides [2]; however, only a few experiments have been reported so far.

In this study, we investigated plasmonic behavior in graphene chemically doped by substrate modification with a self-assembled monolayer (SAM) of organic compounds. We used 3-amino-propyltriethoxysilane to form an SAM at the interface between graphene and a SiO_2 substrate, which modifies the carrier density of graphene. Graphene grown by a chemical vapor deposition method was transferred onto the substrate partly covered with the SAM. The van der Pauw (vdP) measurements showed carrier densities were ~1×10^{12} cm^{-2} with the SAM and ~1×10^{13} cm^{-2} without it, respectively. Propagating plasmons were imaged with a scattering-type scanning near-field optical microscope (s-SNOM) [1].

Figure 1 shows topography and near-field amplitude images obtained with the s-SNOM at an incident wavelength of 10.7 μm. The boundary between the graphene on the substrate with and without the SAM is clearly seen from a height difference (Fig. 1a). Interference fringe patterns are observed at edges and wrinkles in the near-field image (Fig. 1b), which are signatures of plasmonic reflections [1]. The separations between the interference patterns correspond to half of the plasmon wavelengths ($\lambda_p/2$). The wavelengths of the plasmons launched in graphene are estimated to be λ_p ~160 nm with the SAM and λ_p ~260 nm without it. The carrier densities estimated from the λ_p are consistent with the vdP measurements. These results indicate that plasmon properties have been spatially modulated by the chemical doping. Furthermore, an interference pattern is observed at the boundary between graphene with and without the SAM. This indicates that the boundaries between graphene regions with different carrier densities act as plasmonic reflectors. The substrate modification method may enable us to realize nanoscale graphene plasmonic devices.

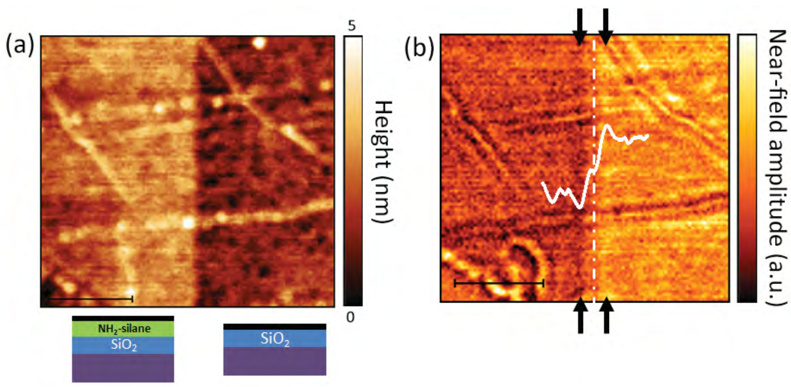

Fig. 1 (a) Topography and (b) near-field amplitude images of graphene at infrared wavelengths of 10.7 μm. The white line indicates a near-field amplitude profile across the boundary between the graphene on the substrate with and without the SAM. Scale bars are 500 nm.

[1] Z. Fei et al., Nature, **487**, 82 (2012) and J. Chen et al., Nature, **487**, 77 (2012).
[2] A. Vakil and N. Engheta, Science, **332**, 1291 (2011).

Effects of Interaction on Charge Fractionalization in Tomonaga-Luttinger Liquids

P. Brasseur[1], N. H. Tu[1], Y. Sekine[1], K. Muraki[1], M. Hashisaka[2], T. Fujisawa[2], and N. Kumada[1]

[1] *NTT Basic Research Laboratories, NTT Corporation*
[2] *Department of Physics, Tokyo Institute of Technology*

Interacting fermions in a one-dimensional system can be described by Tomonaga-Luttinger liquid (TLL) theory. An electron injected in a TLL breaks up into left- and right-moving collective waves carrying charge fractions. This charge fractionalization has been experimentally observed. However, investigation of interactions on TLL properties, such as charge fractions and the velocity of the collective waves, is still lacking.

In this work, we investigate the charge fractionalization under controlled interaction strength [1]. Such experiments became possible using TLLs composed by two quantum Hall edge channels (ECs) with controlled distance. We used graphene separated into two parts by etching with width W and length L [Fig. 1(a)]. Capacitively coupled ECs around the etched line form an artificial TLL. Charged wavepacket is injected to one of the ECs and the current on each EC is detected as a function of time by two detectors Det1 and Det2. When the wavepacket with charge Q reaches the TLL region, it breaks up into wavepackets with charge rQ and $(1-r)Q$, where r is the fractionalization ratio. From the amplitude and time position of the current peaks on Det1 and Det2, r and the TLL mode velocity v are obtained, respectively. We demonstrate that r increases while v decreases with decreasing W [Fig. 1(b)]. The experimentally obtained relation between r and v follows an analytical function without any adjustable parameters [Inset of Fig. 1(b)]. These results verify the TLL theory over a wide parameter range. This work was supported by JSPS KAKENHI Grant Number JP15H05854.

[1] P. Brasseur *et al.*, Phys. Rev. B **96**, 081101(R) (2017).

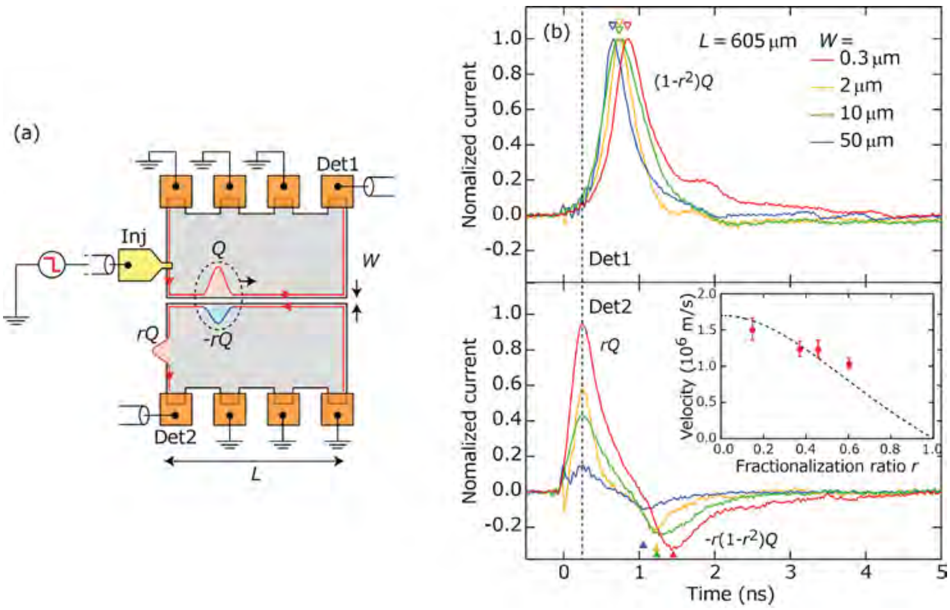

Fig. 1(a) Schematic of a sample. An injection gate (yellow) and ohmic contacts (orange) are patterned on graphene (grey). (b) Current on (top) Det1 and (bottom) Det2 as a function of time. The current is normalized by the peak amplitude at Det1. Inset shows v as a function of r.

Evolution of graphene alignment on recrystallizing polycrystalline Cu-foil for chemical vapor deposition growth

Yui Ogawa[1], Satoru Suzuki[1], Hiroki Hibino[1,2], Kazuhide Kumakura[1]
1. NTT Basic Research Labs., 2. Kwansei Gakuin Univ.

Chemical vapor deposition (CVD) of graphene onto copper (Cu) surfaces is promising method for inexpensive and large-scale graphene growth [1]. The orientation of graphene domains can be controlled by changing the Cu's crystalline surface before and after CVD graphene growth [2-4]. However, it is not yet understood how the orientation of graphene will be affected if Cu's crystallographic orientation changes during CVD. In this work, we investigated graphene alignment against the time evolution of a Cu foil recrystallization during CVD graphene growth.

First, to efficiently provide large Cu grains, we optimized the recrystallization pre-annealing process for commercial Cu foils (thickness of 20 μm, purity of 99.9%, Nilaco). Cu foils can be recrystallized because of large strain and dislocation created during the foil production with multiple rolling processes and following relaxation processes in the high-temperature annealing treatment [4]. Annealed Cu foils were characterized with an optical microscope, x-ray diffraction, and electron back scattering diffraction. It was found that H_2 gas played an important role in the recrystallization of Cu foils, and centimeter-scale Cu grains with a (111) crystal plane were obtained. Controlling the temperature and pressure was also effective for optimizing pre-annealing conditions. Cu foils were fully recrystallized to the single crystalline (111) plane with 5% H_2 in Ar above 1000 °C at 20 Torr, while 80% H_2 needed for full recrystallization at 950 °C.

Next, to investigate the alignment of the CVD graphene, we compared two areas on the Cu foil [Fig. (a) and (b)]. Before CVD growth [Fig.(a)], the area bordered by blue (area A) was already recrystallized into Cu(111), but the area bordered by red (area B) was still in the polycrystalline state. After CVD growth [Fig.(b)], however, the whole area has a (111) surface because the CVD temperature was as high as the pre-annealing temperature. On the both areas, CVD graphene was partially formed with a hexagonal shape. The orientation relationship between the graphene and Cu foil was evaluated by low-energy electron diffraction and microscopy (LEED and LEEM). In the dark-field LEEM image of graphene domains grown on area B in Fig. (c), red domains are aligned along Cu (111), while others are misaligned. Estimated areas of the aligned graphene domain were 79% and 46% on area A and B, respectively. In the case of area B, the recrystallization of the Cu foil and CVD graphene growth were managed at the same time, and the degree of graphene domains' alignment was lower even though the Cu surface had (111) plane. Therefore, an optimal Cu surface should be prepared before CVD graphene growth.

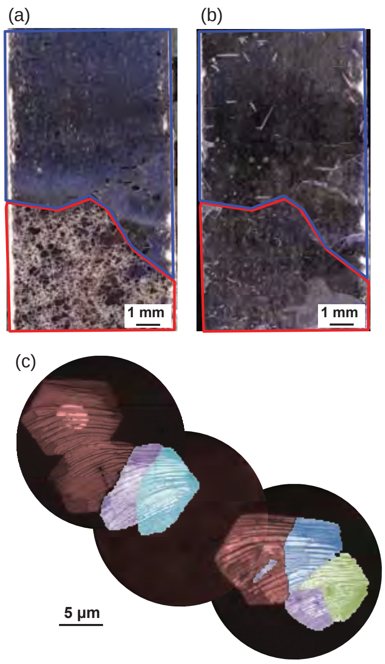

Optical micrographs Cu foil (a) before and (b) after CVD graphene growth. (c) Dark field LEEM images colored to reflect the crystal orientation of graphene domains grown on the B foil.

Reference:
[1] S. Bae *et al.*, *Nat. Nanotechnol.* **5** (2010) 574.
[2] L. Gao *et al.*, *Nano Lett.* **10** (2010) 3512.
[3] Y. Ogawa *et al.*, *J. Phys. Chem. Lett.* **3** (2012) 219.
[4] Y. Wu *et al.*, *Nanoscale* **8** (2016) 930.
[5] L. Brown *et al.*, *Nano Lett.* **14** (2014) 5706.
[6] S. Schmidt *et al.*, *Science* **305** (2004) 229.

SIMPLE – Single Ion Multispecies Positioning at Low Energy – A Single Ion Implanter for Quantum Technologies

Nathan Cassidy[1,2], Roger Webb[1], Richard Curry[3], Paul Blenkinsopp[2], Ian Brown[2], Tony Adams[2], Ben Murdin[4], Luke Antwis[1] and David Cox[4]

[1]*Surrey Ion Beam Centre, University of Surrey, Guildford, GU27XH, UK*
[2]*Ionoptika Ltd., B6 Millbrook Close, Chandler's Ford, Hampshire, SO534BZ, UK*
[3] *The Photon Science Institute, University of Manchester, Oxford Road, Manchester M139PL, UK*
[4]*Advanced Technology Institute, University of Surrey, Guildford, GU2 7XH, UK*

Quantum technologies and solid state quantum computation based on the intrinsic two level dynamics of electron spin in semiconductors has attracted widespread attention because of the strong microelectronic integration. Within the subsector of single dopant based qubits there are two main sets of dopant and substrate which look to be most promising; a single phosphorus impurity in a silicon substrate [1] and the nitrogen vacancy center in diamond [2]. Single dopants have exhibited extremely long spin-coherence and spin-relaxation time [3] which contribute to the critical 'closed box' requirement of a quantum system, and coherent control of impurity wave functions of these single dopants has also been demonstrated [4].
A number of techniques have been utilised to construct solid state quantum devices including the use of scanning tunneling microscopy and hydrogen resist lithography for single atom manipulation [5]. These have demonstrated the potential of such devices but are very limited in their flexibility and ability to scale-up.

Current ion beam technology can produce sub 10nm spot sizes with nm precision of beam placement, but subsequent ion implantation creates damage that must be annealed. There are however, significant advantages in terms of flexibility, and vastly greater speed with the ability to implant a range of ion species into substrates enabling levels scale-up far beyond current laboratory developed devices.

SIMPLE- Single Ion Multispecies Positioning at Low Energy, is an ion beam system with the capability to deterministically place ions into a substrate with sub-20nm precision. The tool is being developed at Ionoptika, and will use current state of the art focused ion beam technology to act as an implantation tool, along with ultrahigh vacuum systems to create a clean environment for the construction of qubit systems. In the regime of controlled single ion implantation the process is essentially statistical in nature, and the key to deterministic implantation will be the >98% detection rate for the event of a single ion implantation through multiplied secondary electron detection. A series of liquid-metal ion sources capable of delivering a range of ions including C, P, Si, S, Se, Bi and Er will be used along with a separate gas source for N ions. When detector efficiency is 100% with a dark count of 100/s and using a 10fA beam current with a pulse length of 400ns, Monte Carlo simulations of a 10x10 array demonstrate there is a 29% probability of implanting a perfect array of single dopants.

[1] B. E. Kane, Nature. **393**, 6681 (1998).
[2] M. V. G. Dutt et al., Science. **316**, 5829 (2007).
[3] A. M. Tyryshkin et al., Nat. Materials. **11** 2 (2011).
[4] P. T. Greenland et al., Nature. **465**, 7301 (2010).
[5] M. Fuechsle et al., Nat. Nanotechnology. **7** 4, (2012).

Effects of strain and electric filed on single Erbium ions in silicon nano-transistors

Guangchong Hu[1], Qi Zhang[1, 2], Gabriele G. de Boo[1], Milos Rancic[3], Brett C. Johnson[4], Jeff C. McCallum[4], Jiangfeng Du[2], Matthew J. Sellars[3], Chunming Yin[1*], Sven Rogge[1]

[1]*Centre of Excellence for Quantum Computation and Communication Technology, School of Physics, University of New South Wales, Sydney, New South Wales 2052, Australia.*
[2]*CAS Key Laboratory of Microscale Magnetic Resonance, Department of Modern Physics, and Synergetic Innovation Center of Quantum Information and Quantum Physics, University of Science and Technology of China, Hefei 230026, China*
[3]*Centre of Excellence for Quantum Computation and Communication Technology, RSPE, Australian National University, Canberra, Australian Capital Territory 0200, Australia.*
[4]*Centre of Excellence for Quantum Computation and Communication Technology, School of Physics, University of Melbourne, Melbourne, Victoria 3010, Australia*
**E-mail: c.yin@unsw.edu.au*

Electric field and strain affect the performance of nanoscale microelectronic devices significantly. Here we present a study of electrical field and strain shift on the optical transition of single Erbium ions in a silicon transistor. We also propose to utilize these effects to build atomic sensors for non-destructive 3D imaging of local strain and electric field in nano-transistors.

Semiconductor device fabrication techniques approch the sub-10-nm node, where the heating and variability effects limit the further develop of nano-electronics[1]. Thus, an atomistic understanding of nano-devces turns into a crucial requirement for continuing to improve transistor performance. The local environment inside the channel, such as strain, has a significant influence on the carrier mobility. Ten years ago, the tool revolution forced a departure from the traditionally planar device geometry[2]. This has made it possible to further optimize the carrier mobility by utilizing strain[3]. Carrier mobility also has a quite sensitive response to the local electric field. A major problem is that the strain in the channel cannot be directly measured. It can only be deduced from the electrical performance of the transistor based on a model for the charge carrier mobility and under the assumption that no other parameters affect the mobility than the strain[4]. Therefore, a non-destructively attained 3D map of strain and electric field in nano-transistor channel would represent be a leap forward in understanding and optimizing these devices.

Here we present both the Stark effect and the effect of strain on single Erbium ions in silicon transistors based on single ion spectroscopy[5]. The sub 50 neV linewidth of the absorption spectra enables the study the electric field and strain in the channel of the transistor. The Stark shift is controlled by the gate-tuned macroscopic electric field and the strain effect is induced by a piezoelectric substrate on which the transistor is mounted. The optical response of single erbium ions allows us to determine the local electric field and strain inside nano-transistors and this could be potentially mapped in three dimensions with high spatial resolution.

[1] Waldrop, M. M., Nature 530, 144–147 (2016).
[2] Ferain, I., Colinge, C. A. & Colinge, J.-P. Nature 479, 310–316 (2011).
[3] Chu, M., Sun, Y., Aghoram, U. & Thompson, S. E., Annu. Rev. Mater. Res. 39, 203–229 (2009).
[4] R Lander, CMOS Nanoelectronics: Innovative Devices, Architectures, and Applications., 2012.
[5] C. Yin, M. Rancic, G. G. de Boo, S.Rogge, Nature 497, 91 (2013).

Mechanism of single-electron pumping via a single-trap level in silicon

G. Yamahata[1], S. P. Giblin[2], M. Kataoka[2], T. Karasawa[1], and A. Fujiwara[1]
[1] *NTT Basic Research Laboratories, 3-1 Morinosato Wakamiya, Atsugi, Kanagawa 243-0198, Japan.*
[2] *National Physical Laboratory, Hampton Road, Teddington, Middlesex, TW11 0LW, United Kingdom.*

A clock-controlled single-electron (SE) pump can generate an accurate current of *ef*, where *e* is the elementary charge and *f* is frequency of the input signal. It can be used for the metrological current standard, which could contribute to the redefinition of the SI ampere [1]. An important point for realizing a practical current standard is high-accuracy operation with a high current level (high *f*). Recently, we have demonstrated high-frequency SE pumping via a single-trap level in silicon [2]. To achieve the desirable operation, we must understand the transfer mechanism in detail. Here, using a high-accuracy measurement system [3, 4], we explore the mechanism of SE pumping via the single-trap level [5].

The SE pump comprises a silicon nanowire with a double-layer gate structure [Fig. 1(a)]. We select a device that has a single trap in the nanowire under G1. The two fine lower gates (G1, G2) are used to form potential barriers in the nanowire and the large upper gate is used to induce charge carriers in the nanowire. Additionally, by applying a high-frequency signal with frequency *f* to G1, we can transfer a single electron from the source to drain leads via the single trap level [2], resulting in an output current I_P of *ef*. We measure I_P using not only a normal ammeter but also a high-accuracy measurement system calibrated by primary standards with a measurement uncertainty of about 10^{-6} [3, 4].

Figure 1(b) shows I_P measured by the normal ammeter as a function of voltage applied to G2 at $f = 7.4$ GHz, at which $ef \sim 1.19$ nA. We focus on the yellow-highlighted range of V_{G2} and perform measurements using the high-accuracy measurement system [Fig. 1(c)]. The deviation of I_P from *ef* is only about 2×10^{-5} at the flattest point, which is a new benchmark in the nanoampere regime [5]. Then, we fit I_P using models assuming equilibrium (thermal limit) electron capture by the trap level during gate modulation, which are widely used for fitting of characteristics in tunable-barrier SE pumps [6]. The fit agrees well with the low-resolution result but disagrees with the high-accuracy one. Then, we add a constant offset term of about -2×10^{-5} to the fit model and obtain a fitting curve that has a good agreement with our result. This indicates that there is a small gate-independent error source, which could be related to an error in the electron loading process due to the shallow trapping energy or a small gate leakage in the first test device. These results are important to optimize the operation of SE pumping toward realization of a practical current standard based on SE pumping.

[1] J. P. Pekola *et al.*, Rev. Mod. Phys. **85**, 1421 (2013). [2] G. Yamahata *et al.*, Nat. Commun. **5**, 5038 (2014). [3] S. P. Giblin *et al.*, Nat. Commun. **3**, 930 (2012). [4] G. Yamahata *et al.*, Appl. Phys. Lett. **109**, 013101 (2016). [5] G. Yamahata *et al.*, Sci. Rep. **7**, 45137 (2017). [6] B. Kaestner *et al.*, Rep. Prog. Phys. **78**, 103901 (2015).

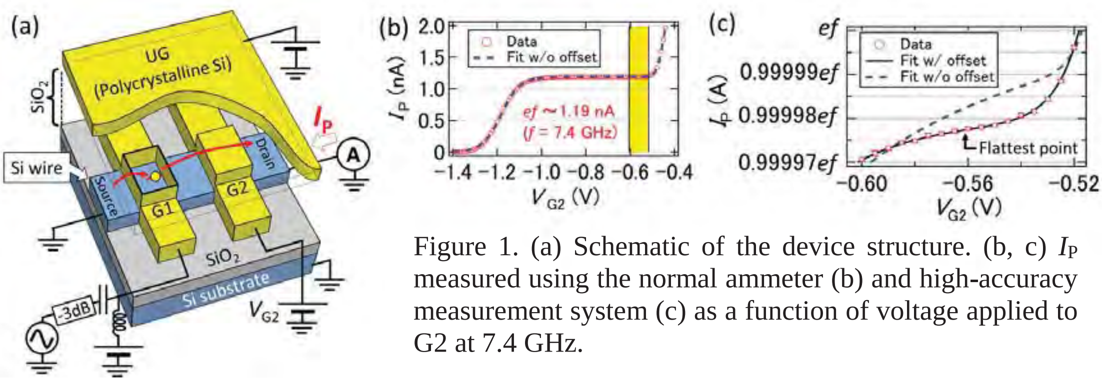

Figure 1. (a) Schematic of the device structure. (b, c) I_P measured using the normal ammeter (b) and high-accuracy measurement system (c) as a function of voltage applied to G2 at 7.4 GHz.

Dependence of threshold voltages on temperature observed in random arrays of Au nanoparticles

M. Moriya[1], M. Moribayashi[1], K. Matsumoto[1], H. T. T. Tran[1], H. Shimada[1], Y. Kimura[2], A. Hirano-Iwata[3], and Y. Mizugaki[1]

[1] *The University of Electro-Communications, Chofu, Tokyo, 182-8585, Japan*
[2] *Tokyo University of Technology, Hachioji, Tokyo 192-0982, Japan*
[3] *Tohoku University, Sendai, Miyagi 980-8579, Japan*

Single-electron (SE) devices have been investigated because of advantages of nanometer-order scale and low power consumption. Gold nanoparticles (Au NPs) have been used as island electrodes. However, the NP should be set in a gap in the order of nanometer between the source (S) and drain (D) electrodes, so the high accuracy is required to set the NP [1].

We have fabricated random arrays of Au NPs by dropping a solution containing Au NPs on the sub-micrometer gap between electrodes. In this article, several random arrays were fabricated and the dependence of threshold voltages on temperature was discussed.

A solution containing 30-nm-diameter NPs, that containing 5-nm-diameter NPs, and a mixed solution containing 5-nm-diameter NPs and 30-nm-diameter NPs were dropped to fabricate NP array I, NP array II, and NP array III, respectively. Fig. 1 is a SEM image of an Au NP array with a configuration of the measurement system. Au NPs were dispersed around the electrodes.

In Fig. 2, current – voltage curves for (a) NP array I, (b) NP array II, and (c) NP array III are shown. For (b), the curve has no current suppressed region. But for (a) and (c), each curve has current suppressed region. The threshold voltages, V_{TH} are defined as the edges of the region.

Fig. 3 is a dependence of absolute value of V_{TH}, $|V_{TH}|$ on temperature for NP array I and III. The value of each $|V_{TH}|$ decreases with increasing temperature. This means Coulomb blockade effect has been observed for these arrays. The minimum temperature at which $|V_{TH}|$ reaches to be zero for NP array III is higher than that for NP array I.

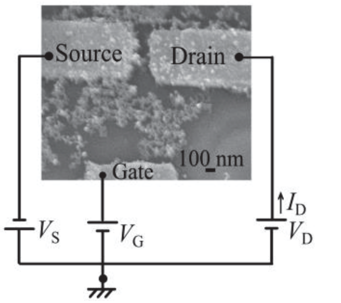

Fig. 1 SEM image of an Au NP array with a configuration of the measurement system.

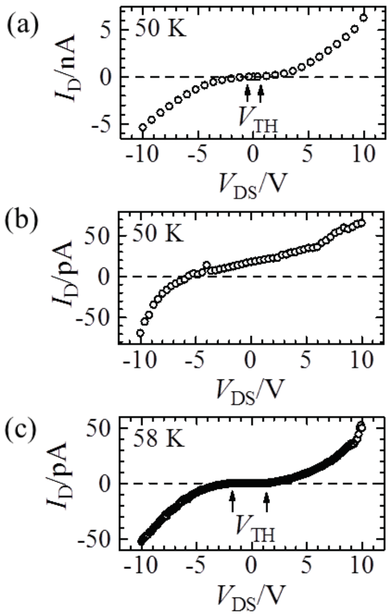

Fig. 2 *I-V* curves. (a) NP array I, (b) NP array II, (c) NP array III.

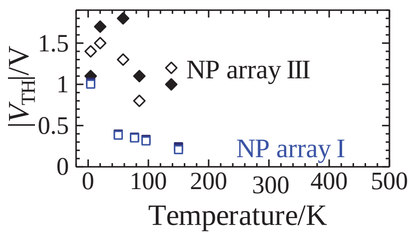

Fig. 3 Dependence of $|V_{TH}|$ on temperature for NP array I and III.

Acknowledgements

This work was partly supported by JSPS KAKENHI Grant Number 15K13999 and by JST CREST Grant Number JPMJCR14F3, Japan.

[1] Y. Azuma et. al, Jpn. J. Appl. Phys. 49, 090206 (2010).

Fluctuation of information content and the local particle number super-selection in a quantum conductor

Yasuhiro Utsumi

Department of Physics Engineering, Mie University, Tsu, Mie, 514-8507, Japan

Entanglement, the nonlocal correlation existing only between quantum systems, is the resource of the quantum information processing. In a mesoscopic conductor, e.g. a quantum dot coupled to the left and right leads [Fig. (a)], entangled fermions can be created by applying a source-drain bias voltage [1]: An electron-hole pair spreading between the two leads can be regarded as an EPR pair. The entanglement entropy is a convenient measure of such entanglement. In a many particle system, one has to account for the local particle number super-selection in order to estimate the accessible entanglement [1,2]. Moreover, the entropy in the information theory is an average of the self-information, which is a random variable. Therefore, we expect that fluctuation of the entanglement entropy would contain valuable information on the entanglement.

We theoretically investigate the probability distribution of the self-information associated with the reduced density matrix of a subsystem A, which is the left lead and the quantum dot [Fig. (a)], obtained after the measurement of the particle number [3]. For this purpose, we calculate the Rényi entanglement entropy under the particle number constraint by exploiting the multi-contour Keldysh Green function [4]. Figure (b) is the time dependence of the accessible entanglement entropy for a small transmission probability $T=0.1$. When two particles are injected $N_{\rm att}=2$, the accessible entropy is $2T(1-T)\ln 2$, which is associated with one electron-hole EPR pair. It grows as the time increases and approaches to the binary entropy $-N_{\rm att}[T\ln T+(1-T)\ln(1-T)]$. Figure (c) shows probability distributions of the fluctuations of accessible entanglement entropy for various transmission probabilities. The peak position coincides with the accessible entanglement entropy. The minimum value is 0, which is realized when all electrons are transmitted or reflected. The maximum value $N_{\rm att}\ln 2$ is achieved when half of injected particles are transmitted. In this case, each injected electron carries one bit $\ln 2$.

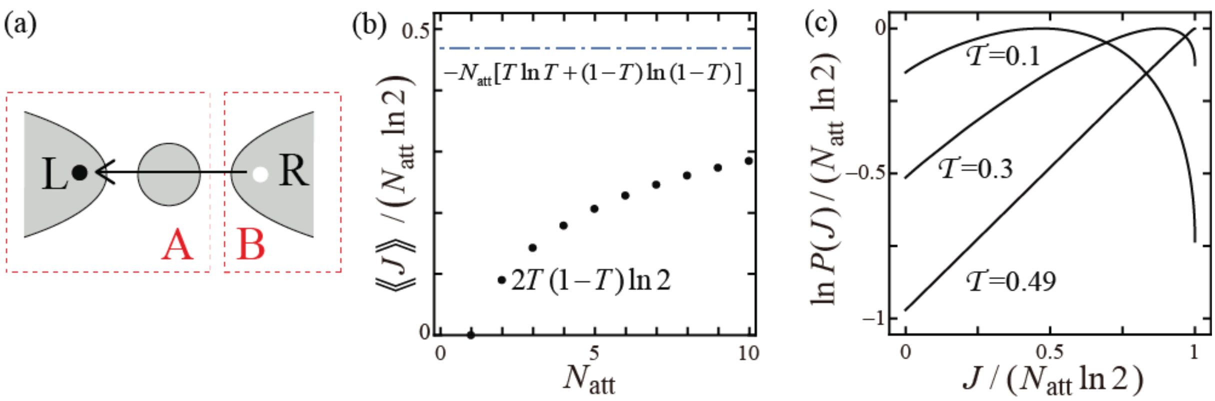

[1] C. W. J. Beenakker, *Proceedings of the International School of Physics Enrico Fermi*, **162** (IOS Press, Amsterdam, 2006).
[2] H. M. Wiseman and J. A. Vaccaro, Phys. Rev. Lett. **91**, 097902 (2003).
[3] Y. Utsumi, Phys. Rev. B **92**, 165312 (2015); **96**, 085304 (2017)
[4] Yu. V. Nazarov, Phys. Rev. B **84**, 205437 (2011); M. H. Ansari and Yu. V. Nazarov, Phys. Rev. B **91**, 104303 (2015); Phys. Rev. B **91**, 174307 (2015).

Enhancement of the impact ionization rate in direct gap semiconductors driving the fast I-MOS nanotransistors

Alexander N. Afanasiev, Andrew A. Greshnov, and Georgy G. Zegrya

Ioffe Institute, 194021 St. Petersburg, Russia

The progress in development of high speed CPU has saturated during the last decade with changing to multi-core trend, meaning that calculating power of a standard ALU is not sufficient for modern applications. Such extensive way of evolution implying wasting of materials (including HfO_2) is hardly satisfactory, however, state-of-the-art MOSFET technology is unstable above 5 GHz clock frequency, due to forced increase of voltage and overheating. Since 2000's, a few novel types of FET have been proposed to replace MOSFET and to overcome the operation limitations by using non-trivial transport mechanisms instead of drift-diffusion, such as tunneling and impact ionization(II). About a decade ago the concept of transistor with field effect control of impact ionization (I-MOS) [1] was proposed, and very sharp slopes of the switching characteristic up to 1 meV/dec were demonstrated experimentally using vertical design of I-MOS (at $V_{DS} \approx 2\,\mathrm{V}$ [2]).

Further optimization of I-MOS and decreasing voltages below $1\,\mathrm{V}$ is possible using A_3B_5 direct gap semiconductors, while enhancement of the II rate with decreasing E_g is perspective for development of the ultra fast I-MOS nanotransistors, with the clock frequencies above 10 GHz, and moderate heating output. Nowadays, most of the simulation software for transistor modelling is based on the semi-phenomenological theory dealing with electric field dependent II coefficient [3] rather than quantum mechanical rate. This approach is inapplicable to the nanoscales, which are under the interest here, because of the sharp potential profiles, and consistent study of the II rate is required for this area of application. Our results shows that proper dependence of the II rate $\mathcal{W}$ on the excess energy $\Delta = E - E_{th}$ is $\mathcal{W} = A \cdot \Delta^2 + B \cdot \Delta^3$ (Ref. [4]), with the coefficients given by

$$A = \frac{4\omega_B^*}{3E_G^2}\frac{Q^4}{P^4}\mathcal{I}(\mathbf{k}/k)\frac{E_g + \Delta_{so}/2}{E_g + \Delta_{so}/3},\ B = \frac{\omega_B^*}{18E_g^3}\frac{E_g + \Delta_{so}}{E_g + 2\Delta_{so}/3}, \tag{1}$$

where $\omega_B^* = m_c e^4/2\hbar^3\epsilon^2$ is the Bohr frequency of the conduction band electrons, P and Q are the momentum matrix elements for c-v and c'-v transitions at $k = 0$, and $E_G = E_{c'} - E_v$ [5]. This expression is derived in a consistent way, it unifies the quadratic and cubic answers due to Keldysh [6] and Gelmont [7], it is free of the strange powers like 2.5, 4.3 [8], and predicts strong anisotropy of the quadratic term [4] ($\mathcal{I}(\mathbf{k}/k)$ in Eq. (1)). Our estimation shows that the cubic term dominates over the quadratic one at the effective temperature $T^* = 300\,\mathrm{K}$ for semiconductors with $E_g < 1.5\,\mathrm{eV}$, and for the particular case of InAs ($E_g = 0.4\,\mathrm{eV}$) the ratio between them is as small as 2%. Thus, the quadratic term can be neglected in Eq. (1) and $\mathcal{W}$ increases as a power of E_g with decreasing band gap, giving rise to intensification of the II in the narrow gap semiconductors and I-MOS transistors with these materials.

[1] K. Gopalakrishan, P. B. Griffin, J. D. Plummer, IEEE Trans. Electron. Dev. **52**, 69 (2005).
[2] U. Abelein *et al.*, Solid State Electronics **51**, 1405 (2007).
[3] Silvaco International, Atlas Users Manual: Device Simulation Software (2016).
[4] A. N. Afanasiev, A. A. Greshnov, G. G. Zegrya, JETP Lett. **105** 586 (2017).
[5] c' denotes the second conduction band in the 14 band kp model.
[6] L. V. Keldysh, Sov. Phys. JETP **10**, 509 (1960).
[7] B. Gelmont, K. Kim, M. Shur, Phys. Rev. Lett. **69**, 1280 (1992).
[8] K. Y. Choo, D. S. Ong, J. Appl. Phys. **96**, 5649 (2004).

High fidelity readout and error correction of single electron pump

Hirotaka Tanaka, Gento Yamahata and Akira Fujiwara

NTT Basic Research Laboratories, Kanagawa, Japan
E-mail: tanaka.hirotaka@lab.ntt.co.jp

Single electron pump has great capability to transfer electrons one by one. This capability is considered useful for accurate electric current standard in addition to single electron logic devices and memories, which consumes lower energy and require smaller space.

Single electron pumps are able to operate in the GHz range [1]. However their uncertainties in the pump current are still between around 10^{-4}-10^{-6} and must to be improved because pump performance degradation is often seen with increasing frequency [2]. A self-referenced single electron pump based on error accounting [3] has recently been proposed to count the number of transferred electrons by using series of single electron pumps and detectors. But this method cannot generate a current equal to ef (e: elementary charge f : frequency) as a controlled way. Here we propose an error correction scheme in the single electron transfer to realize an accurate current source. Error detection and correction are used in various conventional digital information processing and communication systems. These approaches have achieved a fair improvement in the error rate in various type of memory devices such as NAND flash, HDD, wireless communication line, etc., to a reasonably good error rate. As regards error correction in the single electron transfer, one possible way is to detect errors with a charge sensor and correct them by transferring more or fewer electrons as compensation.

We propose several type of error correction schemes. For highly accurate current, it is desirable to utilize error correction in the time domain, where we transfer a bundle of electrons at a low frequency and detect errors. Number of electron is compensated by shifting the timing of the next charge transfer to adjust the net current so that it is equal to $ef_{\text{base-ck}}$, where $f_{\text{base-ck}}$ is the frequency of the base clock. In the presentation, We will describe our error correction scheme in more detail.

1. M. D. Blumenthal et al., Nat. Phys. **3**, 343 (2007), A. Fujiwara et al., APL **92**, 042102 (2008).
2. M. Kataoka et al., PRL **106**, 126801 (2011), G. Yamahata et al., APL **106**, 023112 (2015).
3. L. Fricke et al., PRL **112**, 226803, (2014).

Quantum Interference and Single Electron Transport in CVD Graphene Nanoribbon

Jyun-Hong Chen[1], Yuan-Liang Zhong[1*], Lain-Jong Li[2] and Chii-Dong Chen[3]

[1] *Department of Physics and Center for Nanotechnology, Chung Yuan Christian University, Chung Li, Taiwan*
[2] *Materials Science and Engineering, King Abdullah University of Science and Technology (KAUST), Saudi Arabia*
[3] *Institute of Physics, Academia Sinica, Taipei 115, Taiwan*

We have studied the quantum interference and electron transport in suspended graphene nanoribbon. Graphene was grown on copper foil by chemical vapor deposition (CVD) and then transfered to SiO_2/Si substrate. The wires width of graphene nanoribbon (Figure 1a) are from 50, 75 and 245 nm to 705 nm for studying quantum interference [1] and electron transport. The temperature dependence of resistivity was observed an enhance resistivity at low temperature, due to electron-electron interaction effect, with decreasing temperature (Figure 1b). Furthermore, a single electron transport was observed in the smallest wire width 50 nm. Our results indicated electron transport in weak-disorder CVD graphene nanoribbon from diffusion transport, or ballistic transport to single electron transport when wire width was decreased.

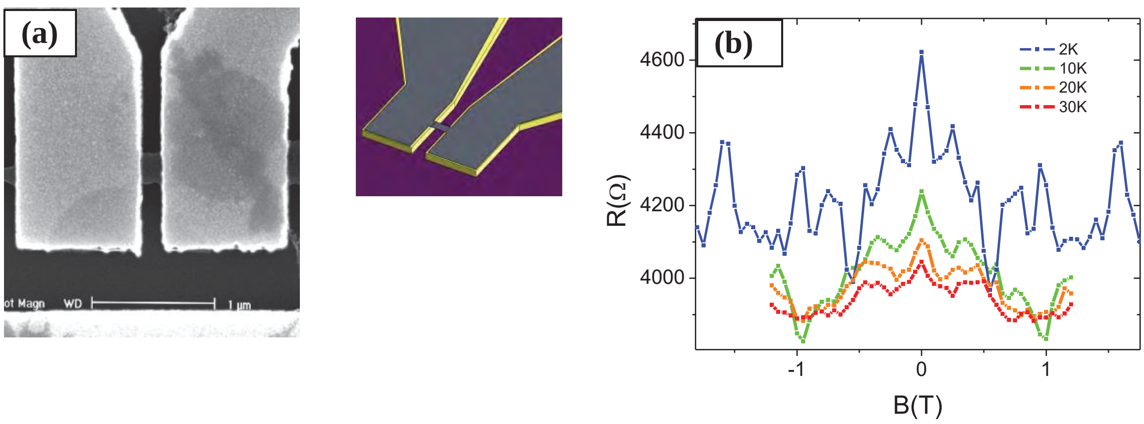

Figure 1. (a) Graphene device SEM image and device diagram. (b) Magnetoresistance of graphene nanoribbon at different temperatures.

[1] Yuan-Liang Zhong, Andrei Sergeev, Chii-Dong Chen, and Juhn-Jong Lin, Phys. Rev. Lett. **104**, 206803 (2010).

* ylzhong@cycu.edu.tw

Gate-based dispersive readout of a classical-quantum CMOS single-electron memory cell

Simon Schaal[1], Sylvain Barraud[2], John J. L. Morton[1,3], and M. Fernando Gonzalez-Zalba[4]

[1] *London Centre for Nanotechnology, University College London, London, United Kingdom*
[2] *CEA/LETI-MINATEC, CEA-Grenoble, Grenoble, France*
[3] *Dept. of Electronic & Electrical Engineering, University College London, United Kingdom*
[4] *Hitachi Cambridge Laboratory, J. J. Thomson Avenue, Cambridge, United Kingdom*

Quantum computers require interfaces with classical electronics for efficient qubit control, measurement and fast data processing. Fabricating the qubit and the classical control layer using the same technology is appealing because it will facilitate the integration process, improving feedback speeds and offer potential solutions to wiring and layout challenges. Integrating classical and quantum devices monolithically, using complementary metal-oxide-transistor (CMOS) processes, enables the processor to profit from the most mature industrial technology for the fabrication of large scale circuits. In this talk, I will present the integration of a single-electron charge storage CMOS quantum dot with a CMOS transistor for control of the readout via gate-based dispersive sensing using a lumped element LC resonator [1]. The control field-effect transistor (FET) and quantum dot are fabricated on the same chip using fully-depleted silicon-on-insulator technology. A charge sensitivity of δq=165 μe/√Hz is obtained when the quantum dot readout is enabled by the control FET. Additionally, a single-electron retention time of the order of a second is observed when storing a single-electron charge on the quantum dot at milli-Kelvin temperatures. These results demonstrate first steps towards time-based multiplexing of gate-based dispersive qubit readout in CMOS technology and the development of an all-silicon quantum-classical processor [2].

[1] M. F. Gonzalez-Zalba et al., Probing the limits of gate-based charge sensing, Nat. Commun. **6**, 6084 (2015).
[2] S. Schaal et al., Conditional dispersive readout of a CMOS quantum dot via an integrated transistor circuit, arXiv:1708.04159 , (2017).

Landau-Zener-Stückelberg interference in a charge qubit of a one-electron double quantum dot

Takeshi Ota, Kenichi Hitachi, and Koji Muraki

NTT Basic Research Laboratories, NTT Corporation, 3-1, Morinosato-Wakamiya, Atsugi, 243-0198, Japan

Recently, Landau-Zener (LZ) transitions have received renewed interest as an alternative approach to control single-qubit states. LZ transitions occur when a system is passed through an avoided crossing that arises from quantum mechanical coupling of two levels, where the transition probability is determined by the velocity, or the rate at which the Hamiltonian is varied. A single passage can serve as a coherent beam splitter for the incoming state. Successive sweeps through the avoided crossing back and forth induce multiple LZ transitions and thus interference between the superposition states generated on the incoming and outgoing passages. In analogy to optics, the final state also reflects the phase evolution between the two beam splitters. The effect, known as the Landau-Zener-Stückelberg (LZS) interference, has been demonstrated for superconductor charge and flux qubits [1] and semiconductor charge [2] and spin qubits [3].

Here we report LZS interference in a charge qubit of a one-electron double quantum dot (DQD). By applying high-frequency non-adiabatic voltage pulses to the DQD [Fig. 1(a)], we observe coherent charge oscillations in a time domain. By comparing experimental results with density matrix simulations, we find that there is a significant enhancement in oscillation amplitude of a final-state probability due to LZS interference when gate operation involves the double passage through the avoided crossing. We also show that LZS interference pattern becomes to be more pronounced by employing largely distorted (adiabatic) pulses whose rise/fall time is comparable to the timescale determined by the avoided crossing gap [Fig. 1(b)]. Our results also suggest the significant importance of the pulse shaping for the precise quantum mechanical control of the charge states.

[1] For example, S.N. Shevchenko, *et al*., Physics Reports **492**, 1 (2010).
[2] G. Cao, *et al*., Nature Comm. **4**, 1401 (2013).
[3] J. R. Petta, *et al*., Science **327**, 669 (2010).

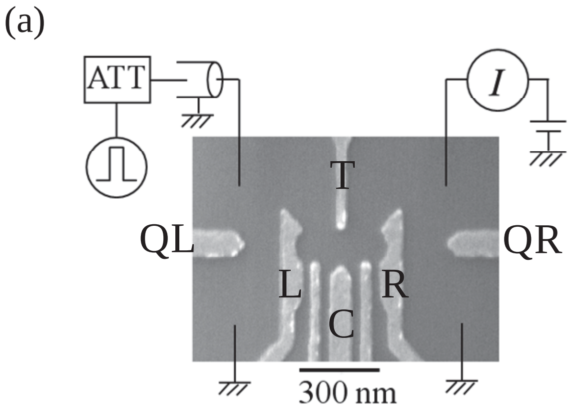

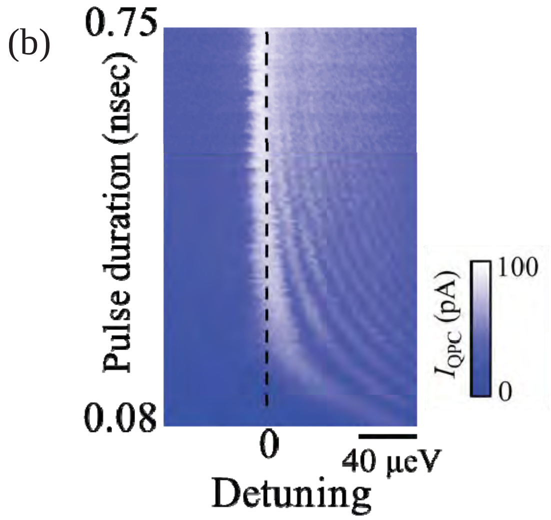

Fig. 1(a) Device structure and the experimental setup. The charge state of the DQD is measured by the QPC defined by the gates QR and R. (b) Pulse-induced QPC current I_{QPC} as a function of pulse duration and detuning.

Tuning hole spin physics in InAs quantum dot molecules*

Arthur Lin[1], **Mathew Doty**[2], **and Garnett Bryant**[1,3]

[1] *Joint Quantum Institute, University of Maryland-College Park and National Institute of Standards and Technology, College Park, Maryland 20742, USA*

[2] *Department of Materials Science and Engineering, University of Delaware, Newark, Deleware 19716, USA*

[3] *Quantum Measurement Division, National Institute of Standards and Technology, Gaithersburg, Maryland 20899, USA*

Long lifetimes and fast all-optical control qualify hole spin in InAs quantum dots (QDs) as an excellent candidate for qubits. By vertically stacking two QDs to create a quantum dot molecule (QDM), one can introduce an inter-dot tunneling barrier that mediates spin-mixing between the two dots [1]. This spin-mixing process enables coherent spin rotations and nondestructive spin readout [2], both essential to qubit design. In addition, QDMs grant us additional freedom to fine-tune hole state resonance frequencies and g-factors via external electric fields, further solidifying the argument to use such systems for qubits and qubit control.

Modifying the inter-dot barrier of GaAs to form a GaBiAs alloy can be used to specifically tune the hole coupling between the two dots. At low Bi concentrations, an inter-dot region of GaBiAs provides a lower barrier for hole states, increasing the tunneling rate and interaction strength between the two dots, while minimally affecting conduction electrons and split-off bands. This allows us to engineer QDMs with improved response to spin-mixing and enhanced opportunities for g-factor modification.

We use an atomistic tight-binding theory to model InAs QDMs grown on a GaAs substrate, with an inter-dot region of GaBiAs. We discuss how Bi concentration, alloy configuration, and layer thickness influence hole spin physics. We present results for the energies of hole states relavent for spin qubits, and the physics of tuning them to resonance via an electric field. We achieve a three-fold increase in hole *tunnel coupling* between the two dots for a well-designed GaBiAs barrier. We also discuss how strain and electronic effects introduced by the Bi independently alter hole state behavior. With strain strongly influencing energy separation, and electronic effects affecting tunneling pathways, both contributions are needed to achieve and understand the increased hole coupling.

Hole spin-mixing requires geometrical symmetry breaking, for example, from lateral offset of the dots in the QDM. We further assess the enhancement of *spin-mixing* possible in offset dots with a GaBiAs inter-dot barrier. Mechanisms for this enhancement is discussed. Ultimately, we demonstrate that by enhancing hole *coupling* through barrier control, we further improve the usefulness of hole *spin-mixing* in QDMs, increasing its utility for qubit architecture.

*This material is based upon work supported by the NSF under Grant No. DMR-1505628.

[1] E. Stinaff, M. Scheibner, A. Bracker, I. Ponomarev, V. Korenev, M. Ware, M. Doty, T. Reinecke, D. Gammon, Science **311**, 636 (2006).

[2] S. Economou, J. Climente, A. Badolato, A. Bracker, D. Gammon, and M. Doty, Phys. Rev. B **86**, 085319 (2012).

In-plane nuclear field formation in individual InAlAs quantum dots: role of nuclear quadrupole effects

S. Yamamoto[1], R. Matsusaki[1], R. Kaji[1], and S. Adachi[1]

[1]*Division of Applied Physics, Graduate School of Engineering, Hokkaido University, Sapporo 060-8628, Japan*

We investigate the formation mechanism of an in-plane nuclear field in single self-assembled $In_{0.75}Al_{0.25}As/Al_{0.3}Ga_{0.7}As$ quantum dots (QDs). In a current theoretical framework for the dynamics in a coupled electron-nuclear spin system of a QD, a *large* nuclear field up to ∼1 Testa orthogonal to a photo-injected electron spin is impossible to be generated. However, the drastically distorted Hanle curves from a standard Lorentzian shape are observed as shown below and in Ref. 1. The results suggest strongly that a QD electron experiences only a small total transverse field. Then, the formation mechanism of an in-plane field which can compensate the applied field is necessary to be fully revealed. The complete understanding of the mechanism leads directly to the possible applications with the optical manipulation of a nuclear field.

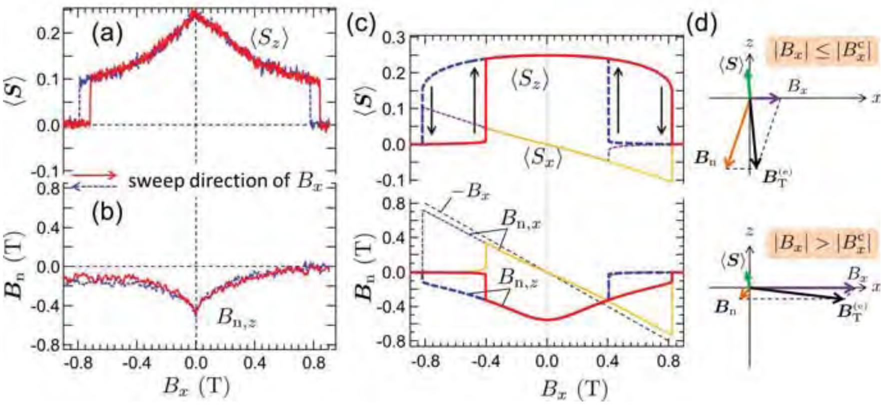

Figure 1: (a) The observed $\langle S_z \rangle$ and (b) the observed $B_{n,z}$ in Hanle effect measurements. (c) The calculated results by a proposed model, (d) Schematics of $\langle \boldsymbol{S} \rangle$ and $\boldsymbol{B}_n$.

We propose an improved model for dynamic nuclear spin polarization including the nuclear quadrupole interaction (QI). Figure 1(a) indicates the observed anomalous Hanle curve in a single InAlAs QD. Since the σ^+ and σ^- PL components from a positive trion were detected under the external transverse field B_x, also $B_{n,z}$ could be evaluated experimentally as shown in Fig. 1(b). Here, the QI plays a role to stabilize a part of nuclear spins along with z-axis. The calculated results in Fig. 1(c) reproduce well the experimental ones in Fig. 1(a) and (b) at the following characteristic points;

1. a large value of $\langle S_z \rangle$ is preserved even under a large $|B_x|$ until the critical field B_x^c,
2. $\langle S_z \rangle$ changes abruptly at B_x^c and shows the hysteretic (thus, bistable) behavior,
3. $\langle S_z \rangle$-curve is almost symmetric with respect to the sweep direction of B_x,
4. $|B_{n,z}|$ reduces gradually with increasing $|B_x|$.

In the calculations, the sign inversion of the nuclear g-factors is assumed (i.e. $g_x^n \cdot g_z^n < 0$). As shown in Fig. 1(c) and (d), the transverse component of $\boldsymbol{B}_n$ compensates the applied field B_x, and the total effective field $\boldsymbol{B}_T^{(e)}$ that is seen by an electron is determined dominantly by $B_{n,z}$. Therefore, a large value of $\langle S_z \rangle$ is kept under the condition $|B_x| \leq |B_x^c|$. On the other hand, in the region of $|B_x| > |B_x^c|$, the vector $\langle \boldsymbol{S} \rangle$ feels a large transverse field and $\langle S_z \rangle$ relaxes quickly since the induced $\boldsymbol{B}_n$ is quite small.

While the model calculations reproduced successfully the observed anomalies in the Hanle curves, further investigations are necessary to improve the quantitative agreement.

[1] O. Krebs et al., Phys. Rev. Lett. **104**, 056603 (2010).

Evaluations of the electron g-factor anisotropy and fluctuation of the Overhauser field in single quantum dots

R. Matsusaki[1], S. Yamamoto[1], R. Kaji[1], and S. Adachi[1]

[1]*Division of Applied Physics, Graduate School of Engineering, Hokkaido University, Sapporo 060-8628, Japan*

The carrier spin dynamics in semiconductor quantum dots (QDs) has attracted considerable interest for the potential applications in future semiconductor electro-optic devices and quantum information processing. Along this line, a complete understanding of the fundamental spin interactions in QDs is crucial as these interactions may limit the application performance. In this study, we evaluated some of key parameters to investigate the spin dynamics in single self-assembled $In_{0.75}Al_{0.25}As/Al_{0.3}Ga_{0.7}As$ QDs: the in-plane and out-of-plane g-factors of electron and hole ($g_k^{e(h)}, k{=}x, y, z$), the random fluctuation of the Overhauser field (ΔB_n), and the resultant electron spin dephasing time (T_Δ).

Figure 1(a) shows the Zeeman splitting (ΔE_Z) of the positive trion (X^+) PL spectra under a longitudinal magnetic field ($\boldsymbol{B}_z$). The abrupt change in ΔE_Z appears at the critical magnetic field B_z^{HC}, and it reflects the transition from the upper branch of nuclear spin polarization (NSP) to the lower branch of NSP. At the critical point, the effective magnetic field affecting on an electron spin $\boldsymbol{B}_{\mathrm{eff}}$ ($= \boldsymbol{B}_z + \boldsymbol{B}_n$, $\boldsymbol{B}_n$: the Overhauser field) vanishes, and thus, it allows us to evaluate the electron and hole g-factors separately. For our target QD, the electron and hole g-factors are deduced to be $g_z^e{=}-0.34 \pm 0.02$ and $g_z^h{=}2.57 \pm 0.01$. Further, the in-plane anisotropy of $g_\perp^{e(h)}$ was measured by rotating the sample around z-axis in Voigt geometry, and the result indicates that the anisotropy of $g_\perp^e$ is negligible for this QD.

In the absence of $\boldsymbol{B}_{\mathrm{eff}}$, the electron spin polarization $\langle S_z \rangle$, which is an ensemble average over a large number of measurements, decreases within T_Δ due to the random nature of $\Delta \boldsymbol{B}_n$, while each electron spin $\boldsymbol{S}$ precesses coherently around $\Delta \boldsymbol{B}_n$ during its lifetime (*frozen fluctuation model* [1]). However, if a large $\boldsymbol{B}_{\mathrm{eff}}$ ($\gg \Delta \boldsymbol{B}_n$) appears, the reduction of $\langle S_z(t) \rangle$ is suppressed strongly. Figure 1(b) shows the degree of circular polarization (DCP) of X^+ PL as a function of the electron Zeeman splitting (ΔE_Z^e). Here, the X^+-DCP works as a measure of $\langle S_z \rangle$. The most important feature is that the observed X^+-DCP has a dip centered at the point $\Delta E_Z^e{\sim}0$, and it agrees well with the expected one from the dynamics model. Comparing with the calculated result (solid line), we can deduce the dephasing time $T_\Delta{=}0.8$ ns. Further, the magnitude of $\Delta \boldsymbol{B}_n$ is estimated as 40 mT from the relation $\Delta B_n = \hbar/(g_z^e \mu_B T_\Delta)$. This value is comparable to those in InAs QDs (~30 mT), InGaAs QDs (~10.5 mT), and InP QDs (~15 mT).

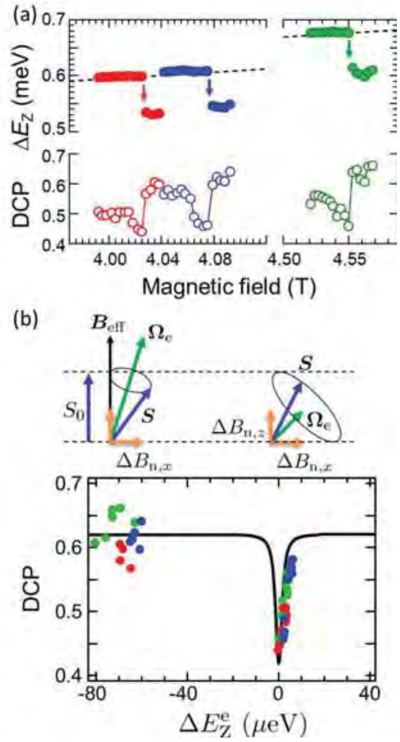

Figure 1: (a) The observed Zeeman splitting and DCP near three different B_z^{HC}. (b) X^+-DCP as a function of ΔE_Z^e. The solid curve is the calculated result. Schematics of electron spin precession around torque vector $\boldsymbol{\Omega}_e$ are depicted.

[1] I. A. Merkulov, Al. L. Efros, and M. Rosen, Phys. Rev. B **65**, 205309 (2002).
[2] R. Matsusaki, R. Kaji, S. Yamamoto, H. Sasakura, and S. Adachi, arXiv:1703.06046 (2017).

Electrical transport in low dimensional systems fabricated in a (110) GaAs quantum well

Tomohiro Nakagawa[1], Rio Fukai[1], Yuji Sakai[1], Haruki Kiyama[1], Julian Ritzmann[2], Arne Ludwig[2], Andreas D. Wieck[2], and Akira Oiwa[1]

[1] *The Institute of Scientific and Industrial Research, Osaka University*
[2] *Lehrstuhl für Angewandte Festkörperphysik Ruhr-Univ. Bochum*

Quantum communication has been expected to offer an absolute secure communication method. The communication distance is, however, limited about 100 km due to losses of photons in the optical fibers. A number of researchers are trying to develop the new technologies that enable us the long distance quantum communication. Quantum repeaters are one of the promising schemes for this goal. The technology of quantum state conversion between flying qubits, photons and quantum memories in solid state is necessary for the quantum repeater. We have been studied the trapping and detecting of single electron spins generated by the photons absorbed in gate-defined quantum dots using a quantum point contact charge sensor [1-3].

In the proposed scheme of the quantum state conversion, a superposition level of electron up- and down-spin has to be accessable from just one of the Zeeman split light hole levels under an in-plane magnetic field [4]. In GaAs quantum wells (QWs) grown on low-symmetry surface (110), one may excite selectively one of the Zeeman split heavy hole levels due to a finite in-plane hole g-factor [5], and realize the quantum state conversion in higher efficiency compared to the case of light holes. We aim to fabricate the gate defined quantum dots (QDs) on (110) QWs and to demonstrate the quantum state conversion between single photons and single electrons in the QD. However, the doping to the (110) GaAs QWs is, in general, difficult and quantum transport through the low dimensional structures formed by metal surface gate electrodes in (110) GaAs QWs have not been fully studied yet.

We grew modulation doped (110) GaAs QWs and evaluated the basic characteristics by the conventional Shubnikov-de Haas oscillation. Then, we fabricated gate defined one dimensional channels. In our early experiments using (110) QWs with low mobility, we could not clearly observe the quantized plateaus. We report the characterization of the improved QW and transport measurements on the quantum points contacts fabricated in the QW.

[1] K. Morimoto, *et al*., Phys. Rev. B. **90,** 085306 (2014).
[2] T. Fujita *et al*., Phys. Rev. Lett. **110**, 266803 (2013).
[3] T. Fujita *et al*., arXiv:1504.03696
[4] R. Vrijen and E. Yablonovitch, Physica E (Amsterdam) **10**, 569 (2001).
[5] R. Winkler, Phys. Rev. Lett. **85**, 4574 (2000).

Electrical Properties of Quinoidal Dipyranylidene Derivative and its Use as a Hole Transport Layer in Perovskite Solar Cells

Marc Courté,[1] Shen Chao,[1] Denis Fichou[1,2,3]

[1] Nanyang Technological University, School of Physical & Mathematical Sciences, 637371, Singapore.
[2] Sorbonne Universités, UPMC Univ Paris 06, UMR 8232, Institut Parisien de Chimie Moléculaire, F-75005, Paris, France.
[3] CNRS, UMR 8232, Institut Parisien de Chimie Moléculaire, F-75005, Paris, France.

Perovskite solar cells have attracted a great attention in the scientific field of photovoltaics due to their low cost, simple fabrication and promising power conversion efficiency (PCE). With excitons photogeneration processes, charge carrier extraction is an essential step to achieve high performance solar cells. At the moment, the hole transport materials (HTM) are currently the bottleneck for the realization of cost effective and stable devices, thus it is mandatory to develop alternative materials having good transport properties.

Here, the charge transport properties of dipyranylidene derivative, a large planar quinoïdal π-conjugated heterocycle, are investigated in field-effect transistor (FET) configuration and by conductive atomic force microscopy (c-AFM). The field-effect transistor properties show a clear p-type behavior with a high hole transport properties. The transfer characteristics Id/Vg present a clear hysteresis typical of a resistive memory effect. This memory effect is again observed by means of c-AFM in lateral mode using a nearby gold top-contact as the counter-electrode.

In addition, the dipyranylidene derivative is integrated into perovskite solar cells, as an hole transport layer in place of the standard Spiro-OMETAD. The $CH_3NH_3PbI_3$ perovskite solar cells using pristine dipyranylidene derivative showed a higher PCE than the standard non-doped Spiro-OMETAD. The presented results will demonstrate that dipyranylidene could be an excellent core for high mobility dopant-free HTMs for perovskite solar cells.

[1] M. Courté, S. G. Surya, R. Thamankar, C. Shen, V. R. Rao, S. G. Mhaisalkar, D. Fichou, *RSC Advances*, **7**, 3336-3342 (2017).
[2] C. Shen, M. Courté, A. Krishna, S.Tang, D. Fichou, *Energy Technol*. doi: 10.1002/ente.201700468 (2017).

Ferroelectricity and leakage current behavior investigation for $HfZrO_4$ film with Al_2O_3 interlayers

P. C. Han [1], C. H. Wu[1] and Edward Yi Chang [1]

[1] *National Chiao Tung University, Taiwan.*

Recently, HfO_2-based nanoscale ferroelectric has attracted great interests for negative capacitance FETs and ferroelectric FETs applications due to high scalability and process compatible with silicon technology [1, 2]. The ferroelectricity originates from the orthorhombic phase belonging to non-centrosymmetric space group. The existence of TiN capping layer is critical for the HfO_2-based ferroelectric crystallization, providing mechanical confinement during crystal nucleation and inhibiting the transformation to monoclinic phase [3]. However, annealing of oxide with TiN layer might result in oxygen migration and the formation of TiO_xN_y interlayers, contributing to fatigue of ferroelectric and reliability issues [4].

In this study, we found that by using Al_2O_3 interlayers instead of TiN capping layer, the $HfZrO_4$ oxide stack remained ferroelectric. This provides a more flexible fabrication process then the stack with TiN thin film. Four layers of 1nm Al_2O_3 adjacent to three layers of 8nm $HfZrO_4$ sandwich structure on Si were prepared by atomic layer deposition (ALD) at 250^{o}C. After the ALD process, post deposition annealing at 400^{o}C was performed. From the grazing incidence X-ray diffraction (GIXRD) patterns, the orthorhombic/tetragonal phase was clearly observed. The poly-crystalline structure was confirmed by transmission electron microscopy (TEM). In order to conduct the polarization-electric field (P-E) measurement, the sandwich oxide stack on TiN/Si was fabricated with the same oxide growth and annealing conditions. After annealing, a TiN layer was deposited as top electrode. From the P-E hysteresis curves, an obvious saturation corresponding to ferroelectric was observed. Positive-up negative-down (PUND) test was performed to minimize the influence of leakage current on measurement, preventing overestimation of the polarization. Twice the remanent polarization ($2P_r$) was 25 $\mu C \cdot cm^{-2}$, which is comparable with other reported results [5]. In addition, a smaller leakage current was observed due to the interruption of grain boundaries running through the entire film by the Al_2O_3 interlayers. In this work, replacing the TiN capping layer with the Al_2O_3 interlayers would greatly simplify the fabrication process of ferroelectric $HfZrO_4$. Detailed discussion on ferroelectricity and leakage behavior of different thickness oxide stacks will also be conducted.

[1]K.-S. Li, P.-G. Chen, T.-Y. Lai, C.-H. Lin, C.-C. Cheng, C.-C. Chen, Y.-J. Wei, Y.-F. Hou, M.-H. Liao and M.-H. Lee, IEEE Electron Devices Meeting (IEDM), 2015 IEEE International 22.6. 1 (2015).
[2]J. Müller, T. Böscke, D. Bräuhaus, U. Schröder, U. Böttger, J. Sundqvist, P. Kücher, T. Mikolajick and L. Frey, Applied Physics Letters **99**, 112901 (2011).
[3]T. Böscke, J. Müller, D. Bräuhaus, U. Schröder and U. Böttger, Applied Physics Letters **99**, 102903 (2011).
[4]K.-Y. Chen, P.-H. Chen and Y.-H. Wu, IEEE VLSI Technology, 2017 Symposium on T84 (2017).
[5]J. Müller, T. S. Böscke, U. Schröder, S. Mueller, D. Bräuhaus, U. Böttger, L. Frey and T. Mikolajick, Nano letters **12**, 4318 (2012).

Transport properties of Spray deposited Lead Telluride films

A.B. Gite[1] , V. B. Gaikwad[2], S. R. Jadkar[3], G. H. Jain[4], H. M. Pathan[5]

[1, 4] SNJB's Arts, Commerce Science College, Chandwad, Nashik, Maharashtra, India

[2] Principal, KTHM College Nashik, Maharashtra, India

[1, 3, 5] Advance Physics Laboratory, Department of Physics, Savitribai Phule Pune University, Pune 411 007 India.

Keywords: PbTe, Spray, SEM, EDX, XRD, FTIR

I Spray-deposited lead telluride films formed at different temperature and films were annealed. Annealed films were characterized for scanning electron microscopy (SEM), energy dispersive X-ray analysis (EDX), X-ray diffraction (XRD), Fourier Transform Infrared Spectroscopy (FTIR) and studied for resistivity, Hall constant, mobility, carrier density and thermoelectric power between 300 and 500 K. The films were smooth, dense and crystalline having cubic PbTe structure but they contained an excess of tellurium. The value of the effective mean free path obtained from the conductivity vs. 1/T graph was comparable with that for the bulk[1], [2]. Mobility variation with temperature suggested the predominance of ionized impurity scattering in the entire range of temperatures studied. The effective hole mass m_h^* was evaluated from the observed thermoelectric power and correlated with transport properties.

[1] S. H. Lee *et al.*, "Thermoelectric properties of individual single-crystalline PbTe nanowires grown by a vapor transport method," *Nanotechnology*, vol. 22, no. 29, p. 295707, 2011.

[2] J. J. Harris and B. K. Ridley, "High field transport in p type PbTe," *J. Phys. C Solid State Phys.*, vol. 5, no. 19, pp. 2746–2756, 1972.

Fluctuation of exergy efficiency in quantum transport

H. Okada, Y. Utsumi

Department of Physics Engineering, Mie-University, Mie 514-8507, Japan
E-mail: okada@q.phen.mie-u.ac.jp

The quantum transport in the view of the quantum thermodynamics of nanoscale circuits, has attracted much attention. In particular, an issue how to realize high efficiency of heat engine is actively studied [1, 2]. The efficiency has been extended into general system that multiple input-currents and output-currents are involved [3]. In the multi-process transport system, the efficiency is defined as a ratio between entropy production for output currents and that for input currents, which is called the *exergy efficiency*.

In this work, we focus on the effect of fluctuating currents flowing thorough a mesoscopic system on the efficiencies. In the nanoscale heat engine, the conversion efficiency between the heat and charge currents can fluctuate because each current fluctuates. Then, in order to evaluate the fluctuating efficiency of the heat engine, it is useful to consider the joint probability distribution of the currents and the probability distribution of the efficiency [4, 5]. By using this framework, we calculate the average of the exergy efficiency and find a measurement-time dependence. Within Gaussian approximation, which is associated with linear response regime, we obtained a no-go theorem that the exergy efficiency cannot exceed Carnot efficiency at all times [Figure 1].

We will apply our theory to the Aharonov-Bohm-Casher ring realized by double quantum dot [Figure 2]. In the system, the Aharonov-Bohm effect and the Aharonov-Casher effect are intermixed. By using two effects, we treat up-spin and down-spin currents as two independent components.

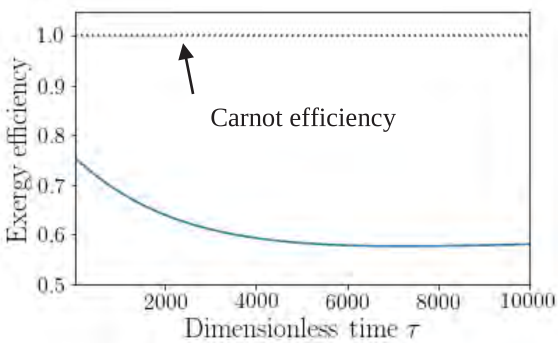

Figure 1 Measurement-time dependence of the exergy efficiency for three current components (one input-current and two output-currents). The maximum is determined by 3×3 transport matrix and three thermodynamic forces. Carnot efficiency of the exergy efficiency is one.

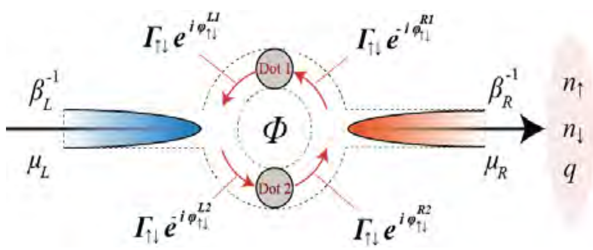

Figure 2 Schematic picture of the double-dot AB-AC ring. The system consists of two single-level quantum dots, left (cold) and right (hot) leads. Temperatures and chemical potentials in the left and right leads are denoted as $\beta_L^{-1}k_B$, $\beta_R^{-1}k_B$, μ_L, and μ_R, respectively. The charge and spin currents are defined as $n_\uparrow + n_\downarrow$ and $n_\uparrow - n_\downarrow$, respectively. Phases for up-spin and down-spin $\varphi_{\uparrow\downarrow}^{ld}$ (*l=L,R, d=1,2*) are independently regulated by using AB phase and AC phase.

[1] K. Yamamoto, O. Entin-Wohlman, A. Aharony, and N. Hatano, Phys. Rev. B **94**, 121402 (2016).
[2] N. Shiraishi, K. Saito, and H. Tasaki, Phys. Rev. Lett. **117**, 190601 (2016).
[3] J.-H. Jiang, Phys. Rev. E **90**, 042126 (2014).
[4] M. Polettini, G. Verley, and M. Esposito, Phys. Rev. Lett. **114**, 050601 (2015).
[5] Hiroki Okada and Yasuhiro Utsumi, J. Phys. Soc. Jpn. **86**, 024007 (2017).

Study of single electron wavepacket propagation in quantum hall edge states high above the Fermi energy

N. Johnson[1,2*], J. D. Fletcher[1], C. Emary[3], S. Ryu[4], H.-S. Sim[4], P. See[1], J. P. Griffiths[5], G. A. C. Jones[5], I. Farrer[6], D. A. Ritchie[5], M. Pepper[2], T. J. B. M. Janssen[1] and **M. Kataoka**[1]

[1] *National Physical Laboratory, Hampton Road, Teddington, Middlesex TW11 0LW, United Kingdom*
[2] *London Centre for Nanotechnology, and Department of Electronic and Electrical Engineering, University College London, Torrington Place, London WC1E 7JE, United Kingdom*
[3] *Joint Quantum Centre Durham-Newcastle, School of Mathematics and Statistics, Newcastle University, Newcastle upon Tyne NE1 7RU, United Kingdom*
[4] *Department of Physics, Korea Advanced Institute of Science and Technology, Daejeon 305-701, Republic of Korea*
[5] *Cavendish Laboratory, University of Cambridge, J. J. Thomson Avenue, Cambridge CB3 0HE, United Kingdom*
[6] *Department of Electronic and Electrical Engineering, University of Sheffield, Mappin Street, Sheffield S1 3JD, United Kingdom*

The NPL electron pump, an on-demand single electron source constructed in the GaAs/AlGaAs heterostructure, has been demonstrated to pump electrons individually with very high accuracy [1]. In this work, we study in detail the output of the electron pump, the hot individual electron wavepackets themselves. We make use of a detector barrier [2] to develop energy and temporal spectroscopy of the electron wavepackets, and further this technique, presenting a single electron based sampling oscilloscope, that demonstrates ultra-high bandwidth [3]. Using this detection technique, we can study the properties of the hot electrons, and present a direct measurement of the electron propagation velocity [4], and measurement of the LO-phonon scattering rate [5]. This includes understanding the electron propagation dependencies on energy, potential profile and magnetic field. Further, we demonstrate a method of suppressing the LO-phonon relaxation such that the coherence length of the hot electrons may be improved from ~μm to in excess of 1mm, creating the possibility of using hot single electrons for single-electron based electronics or quantum information schemes.

* Present Address: NTT Basic Research Laboratories, NTT Corporation, 3-1 Morinosato Wakamiya, Atsugi, Kanagawa 243-0198, Japan

[1] S.P. Giblin, M. Kataoka, J.D. Fletcher, P. See, T.J.B.M. Janssen, J.P. Griffiths, G.A.C. Jones, I. Farrer, and D.A. Ritchie, Nature Comms. **3** 930 (2012)
[2] J. D. Fletcher, P. See, H. Howe, M. Pepper, S.P. Giblin, J.P. Griffiths, G.A.C. Jones, I.Farrer, D.A. Ritchie, T.J.B.M. Janssen, and M. Kataoka, Phys. Rev. Lett. **111** 216807 (2013)
[3] N. Johnson, J.D. Fletcher, D.A. Humphreys, P. See, J.P. Griffiths, G.A.C. Jones, I. Farrer, D.A. Ritchie, M. Pepper, T.J.B.M Janssen, and M. Kataoka, Appl. Phys. Lett. **110** 102105 (2017)
[4] M. Kataoka, N. Johnson, C. Emary, P. See, J.P. Griffiths, G.A.C. Jones, I. Farrer, D.A. Ritchie, M. Pepper, T.J.B.M Janssen, Phys. Rev. Lett. **116** 126803 (2016)
[5] N. Johnson, C. Emary, S. Ryu, H.-S. Sim, P. See, J. D. Fletcher, J.P. Griffiths, G.A.C. Jones, I. Farrer, D.A. Ritchie, M. Pepper, T.J.B.M Janssen, and M. Kataoka, in preparation.

Effect of gate voltage sweep on integer quantum Hall transport properties of InAs quantum wells

T. Akiho, H. Irie, K. Onomitsu, and K. Muraki

NTT Basic Research Laboratories, NTT Corporation, Atsugi 243-0198, Japan

InAs is a promising material to explore exotic quasiparticles that emerge in superconductor/semiconductor heterojunctions [1] because it forms a good interface with superconductors. However, since InAs has an electron accumulation layer on its surface, InAs-based quantum wells are considered to have an edge potential profile significantly different from that of GaAs, the standard material that hosts high quality two-dimensional electron gases. Indeed, a recent study shows that trivial conducting states exist at the mesa edges of InAs/GaSb composite quantum wells even in the non-topological phase [2]. Thus, it is important to clarify and control the edge potential profile of InAs for exploring exotic quasiparticles in InAs-based quantum Hall/quantum spin Hall systems. In this study, we report the collapse of integer quantum Hall effects (IQHEs) that occurs above a certain magnetic field and their emergence after a gate voltage sweep, which we show to be related to the edge potential.

A structure consisting of a 20-nm-thick InAs layer and AlGaSb barriers was grown by MBE. The sample was fabricated into Hall bar devices (typically 50 μm width and 180 μm probe distance) with an Al_2O_3 gate insulator. The red dashed line in Fig. 1 shows longitudinal resistance (R_{xx}) as a function of magnetic field (B) at 1.5 K, taken without sweeping gate voltage after cooling at V_{FG} = 0 V. In contrast to the behavior at low fields, where IQHEs at Landau level filling factor ν = 4 and 5 are well developed, at high fields IQHEs collapse, as evidenced by the finite R_{xx} at ν = 2 and 3. van Wees *et al*. reported a similar breakdown of IQHEs and explained it using the Landauer-Büttiker model with counterflowing edge channels originating from the edge potential specific to InAs [3]. We find that, after sweeping V_{FG} to 3.5 V and then returning to 0 V, the IQHEs emerge, as shown by the vanishing of R_{xx} (Fig. 1, black solid line). The period of Shubnikov–de Haas oscillations in the low-field regime (inset) confirms that the density remains unchanged between the two measurements. We therefore ascribe the observed recovery of the IQHE characteristic to the change in the edge potential rather than the bulk property. In the presentation, we will also report on quantitative analysis using the Landauer-Büttiker model assuming counterflowing edge states.

This work was supported by JSPS KAKENHI Grant No. JP15H05854.

[1] R. S. K. Mong *et al*., Phys. Rev. X **4**, 011036 (2014).
[2] F. Nichele *et al*., New J. Phys. **18**, 083005 (2016).
[3] B. J. van Wees *et al*., Phys. Rev. B **51**, 7973 (1995).

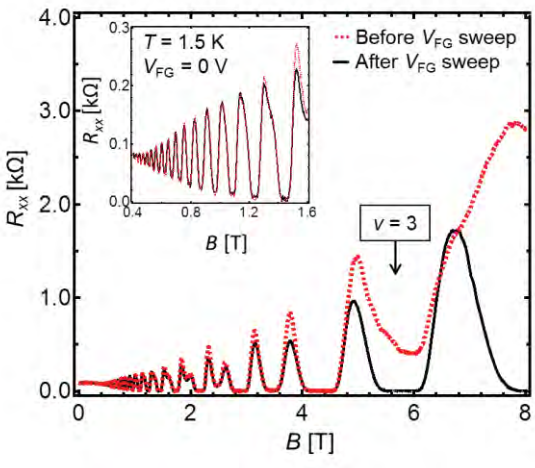

FIG. 1. R_{xx} vs B traces with V_{FG} = 0 V before sweeping V_{FG} (red dash line) and after sweeping V_{FG} (black solid line).

Excess conductance in quantum Hall edge transport driven by Andreev reflection

M. Onizaki, Y. Hashimoto, T. Nakamura and S. Katsumoto

Institute for Solid State Physics, University of Tokyo
5-1-5 Kashiwanoha, Kashiwa, Chiba 277-8581, Japan

Though a superconductor has an energy gap opening at the Fermi level, the Andreev reflection mechanism (ARM) connects metallic states and the condensate of Cooper pairs adiabatically[1] at the metal-superconductor interface. Here strong interest exists in the case we replace the metal with an insulator with non-trivial topology like a quantum Hall insulator (QHI). Some theories predict the conductive states at the quantum Hall edge are connected to the condensate adiabatically via the ARM. In such a situation a single edge state works both as an electron and a hole conduction channel, hence bares double of the quantum conductance $2G_\mathrm{q}$ ($G_\mathrm{q}\equiv 2e^2/h$). Let us call the conductance enhancement as excess conductance. When two superconductors are connected by a QHI, such adiabatic connection results in phase coherence of the two superconducting order parameters and cause supercurrent (or Cooper pair tunneling) between them [2]. In actual experiments, probably due to some imperfection in interfaces, the observation of clear zero-resistance supercurrent has not been reported yet and such an effect appears as excess current for finite voltage, *i.e.* additional excess conductance. Here we report transition of two-terminal transport through superconductor-QHI-superconductor junctions from a normal region to an Andreev-doubled region.

We fabricated NbTi/2-dimensional electron/NbTi (N2N) junction from an InAs 2-dimensional electrons (2DE) with inverted modulation doping (the mobility and the concentration are 1.03×10^{4} cm^2/Vs and 1.95×10^{12} cm^{-2}, respectively). In several trials, we prepared four (N2N) junctions with different normal resistances. One of them has a closed geometry island of 2DE while another has an open geometry one. These two have comparatively low junction resistances and showed small excess conductance above Andreev-doubled conductance as displayed in Fig.1 and multiple Andreev reflection. Though in the other two, four NbTi electrodes are connected to a single 2DE, a striking difference appears in the magneto-resistance as also shown in Fig.1. While one of which shows ordinary quantum Hall staircase, the resistance in the other is just a half of it revealing electron-hole transport by ARM. Surprisingly the excess conductance is observable even above the second critical magnetic field of the NbTi electrodes. We do not have concrete explanation for this but some localized superconductivity may exist even above the critical field while the global coherence is already lost.

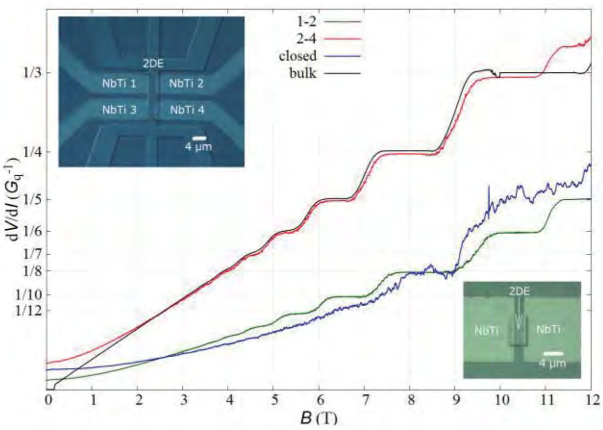

[1] P. W. Anderson, *Basic Notions of Condensed Matter Physics* (Benjamin, 1984).
[2] Y. Ishikawa and H. Fukuyama, J. Phys. Soc. Jpn. **68**, 2405 (1999).

Fig.1 Differential resistance as a function of magnetic field. The inset shows optical micrograph of the sample.

Detection limitation of resistively-detected NMR (RD-NMR) in Quantum Point Contact (QPC)

A. Noorhidayati[1], M. H. Fauzi[2], M. F. Sahdan[1], S. Maeda[1], K. Sato[1], K. Nagase[1], and Y. Hirayama[1,2]

[1]*Department of Physics, Tohoku University, Sendai 980-8579, Japan*
[2]*CSRN, Tohoku University, Sendai 980-8577, Japan*

QPC can be used to electrically generate the nuclear spin polarization [1] and allow us to measure electron magnetization in the QPC [2-3]. Even though the effect of nuclear spin polarization to the transport in QPC is well documented [1-3], there is no clear experimental demonstration on the limiting factor of RDNMR signal. Here we perform RD-NMR detection of ^{75}As in high-mobility (μ=147 m^{2}Vs at n$_s$=1.8x10^{15} m^{-2}) and low-mobility (μ=28 m^{2}Vs at n$_s$=1.8x10^{15} m^{-2}) QPC in the simplest possible case (i.e tuning the bulk filling factor ν_{bulk}=2 and ν_{qpc}=1). We vary the applied magnetic field B$_\perp$ and electron density to achieve ν_{bulk}=2 as shown in Fig. 1(c) and apply bias to the split gate (Vsg) so that only the up-spin channel is transmitted through. Fig 1(d) shows the amplitude of RD-NMR signal detected at $\nu_{qpc} < 1$ decreases with B$_\perp$. When we decrease the magnetic field, the up-spin and down-spin channel separation become obscure due to smaller Zeeman energy separation and density of states broadening (see Fig. 1(c)). The electron-nuclear spin-flip rate decreases and consequently reduces the number of polarized nuclei in the QPC. We managed to detect RD-NMR signal down to B$_\perp$=1.25T (3.5T) in high-mobility (low-mobility) QPC. We also observed the RD-NMR signal at different combination of even and odd filling factor (ν_{bulk}=4 and ν_{qpc}=3) as shown in figure 1(e,f). Pushing down the field limit would allow us to measure electron magnetization in the QPC in the low magnetic field regime, unexplored in the previous studies.

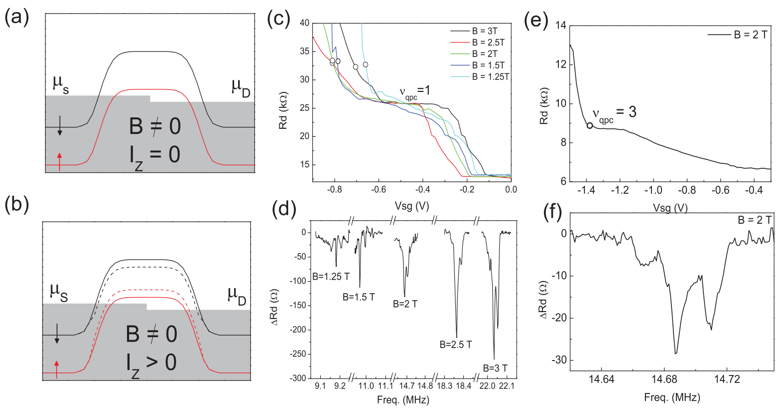

Figure 1: (a,b) Potential barrier feels by the up spin and down spin channel for $\langle I_Z \rangle$=0, $\langle I_Z \rangle > 0$. Overhausser field decrease the zeeman separation. (c) Transport measurement at B variation. The center of ν_{qpc}=1 keep at the same V_{SG} value. White circle indicates RD-NMR detection point. (d)RD-NMR signal of high-mobility wafer observed down to B =1.25T. (e) Transport measurement at ν_{qpc}=3. (f) RD-NMR signal observed at ν_{qpc}<3.

[1] Wald, et. al., Phys. Rev. Lett., 73:1011 (1994).
[2] Chida, et. al., Phys. Rev. B, 85:041309 (2012).
[3] Kawamura, et. al., Phys. Rev. Lett., 115:036601 (2015).

Nonlinear quantum transport in MgZnO/ZnO heterostructures

Qianhui Shi[1], Joseph Falson[2], Michael A. Zudov[1], Yusuke Kozuka[3], Atsushi Tsukazaki[4], Mashashi Kawasaki[3,5], Klaus von Klitzing[2], and Jurgen Smet[2]

[1] *School of Physics and Astronomy, Univ. of Minnesota, Minneapolis, MN 55455, USA*
[2] *Max Planck Institute for Solid State Research, D-70569 Stuttgart, Germany*
[3] *Department of Applied Physics and Quantum-Phase Electronics Center (QPEC), Univ. of Tokyo, Tokyo 113-8656, Japan*
[4] *Institute for Materials Research, Tohoku Univ., Sendai 980-8577, Japan*
[5] *RIKEN Center for Emergent Matter Science (CEMS), Wako 351-0198, Japan*

When a strong direct current I is passed through a two-dimensional electron or hole gas, its differential resistivity exhibits Hall field-induced resistance oscillations (HIRO). These oscillations stem from electron transitions between Hall field-tilted Landau levels mediated by backscattering off short-range impurities. Despite been known for more than a decade, HIRO have only been observed in GaAs/AlGaAs [1] and Ge/SiGe [2] heterostructures which are characterized by high mobility ($10^6 - 10^7$ cm^2/Vs), moderate carrier density ($\sim 10^{11}$ cm^{-2}), and low effective mass ($0.06 - 0.09\ m_0$).

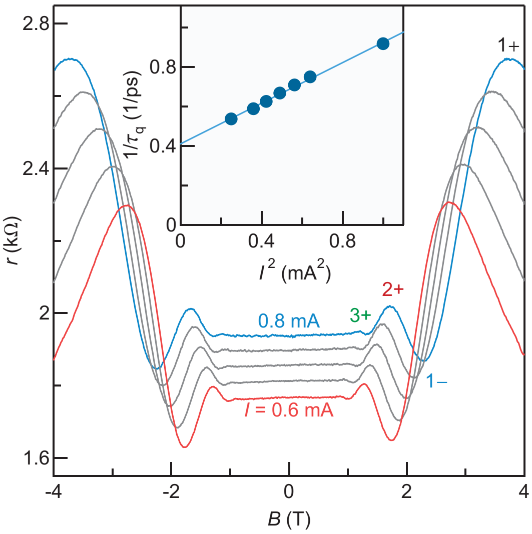

Figure 1: Differential magnetoresistance $r(B)$ at different I from 0.6 to 0.8 mA, in steps of 0.05 mA. The traces are *not* vertically offset. Inset: Quantum scattering rate τ_q^{-1} as a function of I^2.

Here, we report [3] on HIRO in a MgZnO/ZnO heterostructure, which has much lower mobility, much higher density, and much larger effective mass (see Fig. 1). The unique sensitivity of HIRO to the short-range component of the disorder potential allows us to unambiguously establish that the mobility of our MgZnO/ZnO heterostructure is limited by impurities residing near the 2D channel. In addition, we demonstrate [4] that at low direct currents and in the regime of overlapping Landau levels, the differential resistivity acquires a quantum correction proportional to both I^2 and the Dingle factor. The analysis shows that this correction is dominated by a I-induced modification of the electron distribution function and allows us to access both quantum and inelastic scattering rates. Taken together, these findings demonstrate remarkable universality of HIRO and that the nonlinear magnetotransport is a powerful technique to access various scattering times in 2D systems not necessarily having high mobility. As such, this approach has a potential to be applied to other emerging 2D materials.

[1] C. L. Yang, J. Zhang, R. R. Du, J. A. Simmons, and J. L. Reno, Phys. Rev. Lett. **89**, 076801 (2002).
[2] Q. Shi, Q. A. Ebner, and M. A. Zudov, Phys. Rev. B **90**, 161301(R) (2014).
[3] Q. Shi, J. Falson, M. A. Zudov, Y. Kozuka, A. Tsukazaki, M. Kawasaki, K. von Klitzing, and J. Smet, Phys. Rev. B **95**, 041411(R) (2017).
[4] Q. Shi, J. Falson, M. A. Zudov, Y. Kozuka, A. Tsukazaki, M. Kawasaki, and J. Smet, Phys. Rev. B **96**, 125401 (2017).

Hall field-induced resistance oscillations in a tunable-density wide GaAs/AlGaAs quantum well

Michael A. Zudov[1], Ivan A. Dmitriev[2], Benedikt Friess[3], Qianhui Shi[1], Vladimir Umansky[4], Klaus von Klitzing[3], and Jurgen Smet[3]

[1] *School of Physics and Astronomy, Univ. of Minnesota, Minneapolis, MN 55455, USA*
[2] *Department of Physics, Univ. of Regensburg, D-93040 Regensburg, Germany*
[3] *Max Planck Institute for Solid State Research, D-70569 Stuttgart, Germany*
[4] *Braun Centre for Semiconductor Research, Department of Condensed Matter Physics, Weizmann Institute of Science, Rehovot 76100, Israel*

Hall field-induced resistance oscillations (HIRO) emerge due to elastic electron transitions between Landau levels, tilted by the Hall field, as a result of backscattering off short-range disorder [1]. It is well known that in systems with several populated subbands, HIRO often mix with magnetointersubband oscillations [2]. However, it is also interesting to examine how HIRO are affected by subband populations in the absence of such mixing and to separate HIRO contributions from each occupied subband, which should give access to their individual scattering rates.

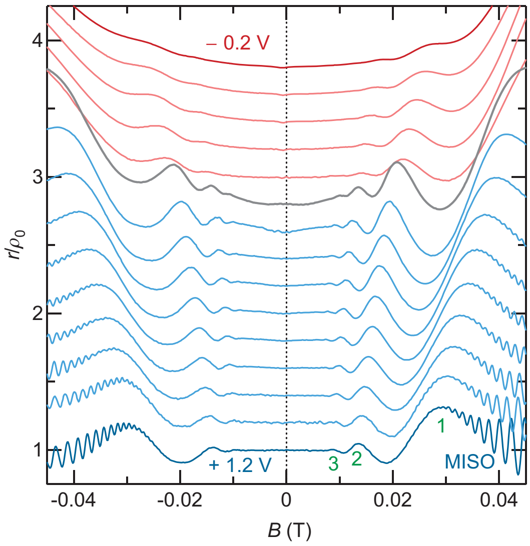

Figure 1: Differential resistivity r, normalized to ρ_0, vs B at $I = 50$ μA and at gate voltages from 0.2 V (top) to 1.2 V (bottom), in steps of 0.1 V. The traces are vertically offset for clarity by 0.2.

Here, we report [3] on HIRO in a 60 nm-wide GaAs quantum well with an *in situ* grown back gate, which allows tuning the electron density n (see Fig. 1). At low n, when all electrons are confined to the lowest subband (SB1), the HIRO frequency, proportional to the the cyclotron diameter and to the Hall field, scales with $n^{-1/2}$, as expected. Remarkably, population of the second subband (SB2) significantly enhances HIRO, while their frequency now scales with n^{-1}. We show that in this two-subband regime HIRO still originate solely from backscattering of SB1 electrons. The unusual n-dependence occurs because the population of SB2 steadily increases, while that of SB1 remains essentially unchanged. The enhancement of HIRO manifests an unexpected, step-like increase of the quantum lifetime of SB1 electrons, which reaches a record value of 52 ps in the two-subband regime. This enhancement likely stems from screening of the disorder by SB2 electrons, whose quantum lifetime, however, remains relatively short.

[1] C. L. Yang, J. Zhang, R. R. Du, J. A. Simmons, and J. L. Reno, Phys. Rev. Lett. **89**, 076801 (2002); M. G. Vavilov, I. L. Aleiner, and L. I. Glazman, Phys. Rev. B **76**, 115331 (2007).
[2] S. Wiedmann, G. M. Gusev, O. E. Raichev, A. K. Bakarov, and J. C. Portal, Phys. Rev. B **84**, 165303 (2011); G. M. Gusev, S. Wiedmann, O. E. Raichev, A. K. Bakarov, and J. C. Portal, Phys. Rev. B **83**, 041306 (2011).
[3] M. A. Zudov, I. A. Dmitriev, B. Friess, Q. Shi, V. Umansky, K. von Klitzing, and J. Smet, Phys. Rev. B **96**, 121301(R) (2017).

A double-gate delay line for edge magneto plasmons

C. J. Lin[1], M. Hashisaka[1,2], K. Muraki[2], T. Fujisawa[1]

[1] *Department of Physics, Tokyo Institute of Technology, Tokyo, Japan*
[2] *NTT Basic Research Laboratories, NTT Corporation, Atsugi, Kanagawa, Japan*
E-mail: lin.c.ad@m.titech.ac.jp.

A quantum Hall (QH) edge channel formed along a boundary of a two-dimensional electron gas (2DEG) provides chiral transport for edge magneto plasmons (EMPs) [1]. The almost linear dispersion is attractive for signal transmission hopefully up to the cyclotron frequency [2]. When the channel is formed by depleting 2DEG under a gate electrode on an AlGaAs/GaAs heterostructure, the EMP velocity can be controlled by changing the gate voltage. This provides a tunable delay line for plasmon transport. Here we propose and demonstrate a double-gate delay line that should allow wider velocity variation.

Figure 1(a) shows a cross section of the double gate structure. The location of the edge channel is mainly determined by voltage V_M on gate G_M, and the electron interaction in the channel is partially screened by gate G_S with zero or small voltage V_S. As the velocity increases with the interaction [3], we expect the lowest velocity when the channel is located under G_S for the potential profile (ii), the highest velocity for the channel farthest from G_S for (iii), and intermediate velocity for (i). The experiment was performed with the device shown in Fig. 1(b). The fundamental EMP mode is investigated in a perpendicular magnetic field of 1.79 T (the bulk filling factor ν at 2) at 1.5 K. The double-gate channel with a length of 110 μm is formed by G_M and G_S. We employed a pump-probe scheme to measure the time-of-flight from the time when a charge wave packet is generated by applying a short voltage pulse on gate G_E to the time when the packet is detected with a point contact defined by gate G_D and another synchronized voltage pulse. Figure 1(c) shows the detector current as a function of the time between the two pulses. Systematic measurements suggest that the expected signal associated with the excitation from the upper end (5 μm in width) of G_E appears as a shoulder labelled P_D. The large peak labelled P_I should originate from unexpected indirect excitation from the long side (180 μm in length) of G_E through a narrow depleted region labelled NDR (2×115 μm^2) to the double-gate channel. Their propagation times show non-monotonic variation with V_M, in agreement with the screening effect discussed with Fig. 1(a). The double-gate structure should be useful for wide tuning of delay time and tuning the interaction in the edge channels.

This work was supported by JSPS KAKENHI (JP15H05854 and JP26247051) and Nanotechnology Platform Program at Tokyo Tech.

[1] H. Kamata *et al.*, Phys. Rev. B **81**, 085329 (2010). [2] E. A. Shaner and S. A. Lyon, Phys. Rev. Lett. **93**, 037402 (2004). [3] D. Johnson and G. Vignale, Phys. Rev. B **67**, 205332 (2003).

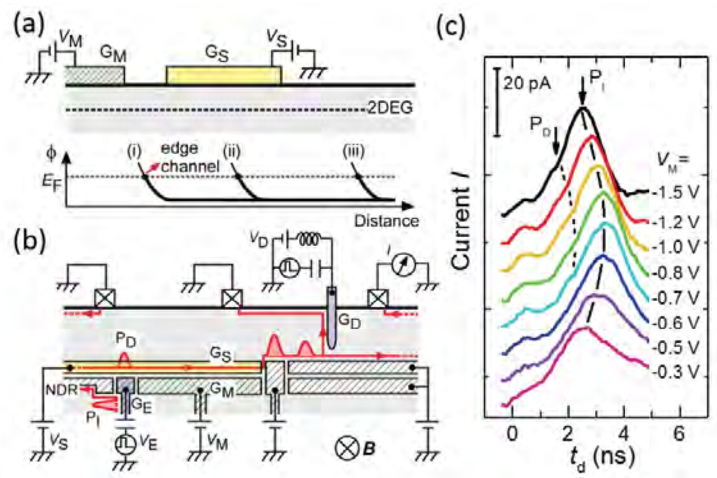

Fig. 1. (a) A cross section of the double-gate structure in the upper panel. The lower panel shows potential profiles for the lowest Landau level. (b) A schematic setup for the pump-probe measurement. The hatched gates other than G_M are biased at -1 V. (c) The detector current I as a function of the delay time t_d between the injector and detector pulses. The direct (P_D) and indirect (P_I) wave packets are marked by the arrows.

Effects of Two-Dimensional Electron System on the Coupling between Edge Channels on Opposite Sides of a Hall Bar

Ngoc Han Tu [1], Yoshiaki Sekine[1], Koji Muraki[1], Masayuki Hashisaka[1,2], Toshimasa Fujisawa[2], and Norio Kumada[1]

[1]*NTT Basic Research Laboratories, NTT Corporation, Japan*
[2]*Department of Physics, Tokyo Institute of Technology, Japan*

In integer quantum Hall (QH) effect regime, electrons propagate in edge channels (ECs) along the periphery of a two-dimensional electron system (2DES). The ECs are generally considered as ideal one-dimensional channels without interaction with opposite side of a device. However, a recent experiment using a system composed of two ECs separated by etching [1] has demonstrated that interaction between ECs is not negligible even when the separation is 50 μm. In this study, we investigate the coupling between ECs on opposite sides of a 50-μm-wide Hall bar by time-resolved transport measurement. We show how the way of coupling and the coupling strength change when the bulk of 2DES changes between the QH and non-QH states.

We used a graphene Hall bar device with the width W = 50 μm and the length L = 350 μm [Fig. 1(a)]. A charged wavepacket is injected into one of the ECs and the current on each EC is detected as a function of time by two detectors Det1 and Det2; Det1 is connected to the EC in which the charged wavepacket is injected, while Det2 is connected to the other. In the QH state at Landau level filling factor ν = 2 (B > 2 T), the measured current at Det2 shows a peak followed by a dip [Fig. 1(c)]. This behavior is expected for the capacitive coupling across the incompressible bulk 2DES. As the magnetic field is decreased to the boundary to the non-QH state (B ~ 2 T), the amplitude of the peak on Det1 decreases while those of the peak and dip on Det2 increase [Figs.1 (b) and (c)]. At the same time, the time delay, shown by solid triangles, increases. These results indicate that the capacitive coupling is stronger near the boundary to the non-QH state. We suggest that the stronger coupling is caused by the localized states inside the incompressible state. For lower magnetic field (B < 2 T), where R_{xx} is finite [inset of Fig. 1(c)], the current at Det2 shows a single peak as the result of conductive coupling through the compressible bulk 2DES. Our observation implies that interaction between ECs on opposite sides of a Hall bar should be included for better understanding of edge transport in QH states.

[1] P. Brasseur *et al*., Phys. Rev. B **96**, 081101(R) (2017).

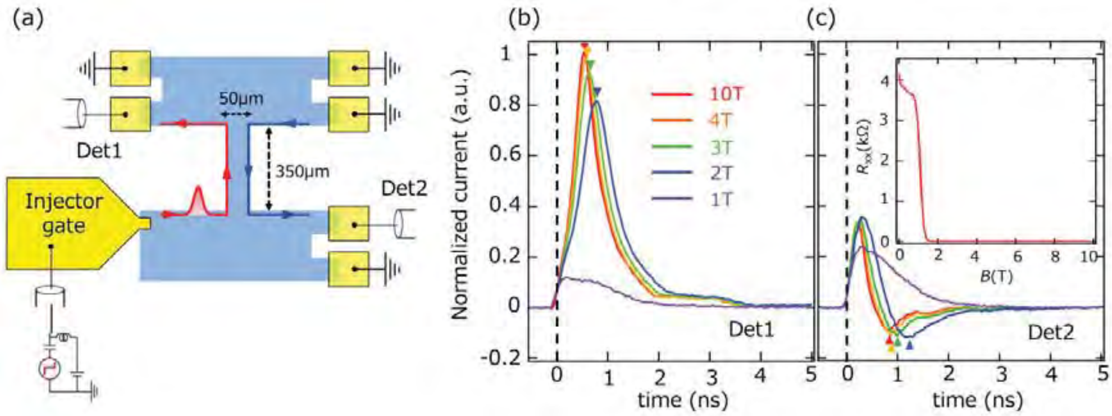

Figure 1. (a) Schematic of graphene device. (b) and (c) Current as a function of time at Det1 and Det2, respectively, for different magnetic fields B. Inset is the longitudinal resistance R_{xx} as a function of B.

Shot-noise signature of quantum many-body correlation in a non-equilibrium regime of a microscopic integer quantum Hall state

M. Hashisaka[1,2], K. Muraki[2], and T. Fujisawa[1]
[1]*Department of Physics, Tokyo Institute of Technology*
[2]*NTT Basic Research Laboratories*

Quantum Hall (QH) effects break down under a high bias. While this QH-effect breakdown presents as an intriguing example of nonlinear many-body phenomena, gaining a microscopic insight into its possible quantum many-body correlation has been prevented by the complex nonlinear behavior seen in transport experiments. In this study, we shed light on the breakdown state by measuring noise characteristics and resistively-detected nuclear magnetic resonance (NMR) in addition to standard dc transport characteristics. We focus on a local $\nu_{\rm local} = 1$ QH state formed in a point-like constriction of a bulk $\nu_{\rm bulk} = 2$ QH system (Fig. 1). While a previous experiment performed in a similar setup found contradictory results for shot noise and NMR when analyzed within a non-interacting Landauer-Büttiker model [1], we show that our results can be understood coherently by taking a many-body effect into account.

We first prepare a local $\nu_{\rm local} = 1$ state in equilibrium, which is confirmed by the quantized conductance e^2/h through the constriction, absence of shot noise, and a full NMR Knight shift. When a finite bias $V_{\rm in}$ is applied, the conductance plateau breaks down ($|V_{\rm in}| > 0.25$ mV, Fig. 2a), while the longitudinal conductance in the bulk remains zero. This ensures that dissipative transport occurs only near the constriction, indicating the breakdown of the $\nu_{\rm local} = 1$ state. The breakdown is accompanied by the emergence of finite excess noise (Fig.2b) and a decrease in the Knight shift. If we assume that these are caused by stochastic scattering of spin-up and -down electrons, the spin polarization in the non-equilibrium $\nu_{\rm local} = 1$ state can be independently determined from both of the shot noise and Knight shift [1]. However, in this assumption the two experiments give different polarization values; at $V_{\rm in} \cong 1.0$ mV, for example, spin polarization $P \cong 0.92$ is estimated from the noise while $P \cong 0.45$ from the Knight shift. This discrepancy can be solved by considering shot-noise reduction due to many-body correlation. We compare the excess-noise data with theoretical shot-noise curves calculated assuming effective charges $e^* = e$ and $e/3$ of tunneling quasiparticles, with the transmission probabilities of spin-up and -down charges estimated from NMR. At high bias ($|V_{\rm in}| > 0.5$ mV), the excess noise follows the curve assuming $e^* = e/3$. Interestingly, the data in this regime closely resemble those reported for tunneling experiments in fractional QH systems [2,3], where the shot noise takes non-trivial fractional values reflecting the fractional charge of quasiparticle excitations and/or correlation between tunneling events due to the Luttinger-liquid nature of fractional edge states. Our result is thus a strong indication of quantum many-body physics that is absent in the original integer QH state.

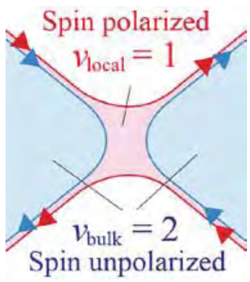

Fig. 1 QH states near constriction.

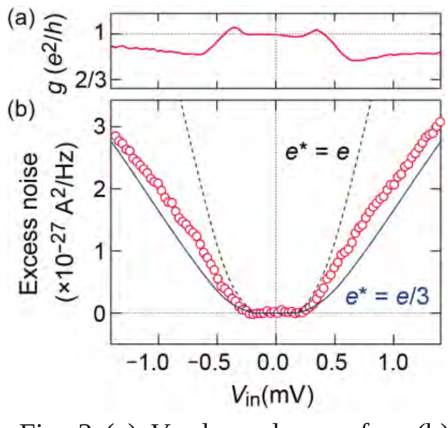

Fig. 2 (a) $V_{\rm in}$ dependence of g. (b) Measured excess noise. Dashed and solid lines are shot-noise curves for $e^* = e$ and $e/3$, respectively.

This work was supported by KAKENHI JP15H05854, JP26247051, JP16H06009, and Nanotechnology Platform Program (Tokyo Tech.).

[1] K. Chida *et al.*, Phys. Rev. B **85**, 041309(R) (2012).
[2] M. Hashisaka *et al.*, Phys. Rev. Lett. **114**, 056802 (2015). [3] M. Heiblum, arXiv: 0912. 4868.

Transport and optical properties of nanostructures / Dynamics and c
Spintronics and spin related transport / Quantum Hall systems / Nan
Micro and nanomechanical system / Micro and nanomechanical syst
Quantum computation and information processing / Hybrid quantum
Nanolithography and self-assembling / Quantum Hall systems / Nan
Mesoscopic superconductivity / Micro and nanomechanical system /
quantum system / Nanoprobing and nanoscale characterizati
coherent control of quantum systems / Spintronics an
Metal Dichalcogenide (TMDC) materials / N
/ Hybrid quantum syst

Abstract program PDF download from here.

ISNTT2017
International School and Symposium on Nanoscale Transport and phoTonics
http://www.brl.ntt.co.jp/event/isntt2017/